

UNIVERSITY OF LJUBLJANA

Faculty of Mechanical Engineering

**Improvement of thermal comfort and efficient
energy use in buildings based on active-passive
systems for overheating reduction**

Doctoral dissertation

Submitted to the Faculty of Mechanical Engineering, University of Ljubljana
to be granted a scientific title of the Doctor of Philosophy

Eva Zavrl

Ljubljana, October 2023

UNIVERSITY OF LJUBLJANA

Faculty of Mechanical Engineering

**Improvement of thermal comfort and efficient
energy use in buildings based on active-passive
systems for overheating reduction**

Doctoral dissertation

Submitted to the Faculty of Mechanical Engineering, University of Ljubljana
to be granted a scientific title of the Doctor of Philosophy

Eva Zavrl

Mentor: Assoc. Prof. PhD. Uroš Stritih, univ. dipl. inž. str.
Co-mentor: Assoc. Prof. PhD. Mateja Dovjak, univ. dipl. san. inž.

Ljubljana, October 2023



Tekoča številka: Dr III/209
Datum: 3. 2. 2020

Na osnovi sklepa 23. seje Komisije za doktorski študij, Univerze v Ljubljani z dne 14. 1. 2020 po pooblastilu 30. seje Senata UL, z dne 20. 1. 2009, izdajam naslednjo

ODLOČBO

Komisija za doktorski študij, Univerze v Ljubljani je na svoji 23. seji, dne 14. 1. 2020 kandidatki

Evi Zavrl

1. sprejela temo doktorske disertacije z naslovom:
Izboljšanje toplotnega ugodja in učinkovite rabe energije v stavbah na podlagi uvajanja aktivno-pasivnih sistemov za zmanjšanje pregrevanja
2. imenovala mentorja: *izr. prof. dr. Uroš Stritih*
3. in somentorico: *doc. dr. Mateja Dovjak*
4. ter odobrila pisanje doktorske disertacije **v angleškem jeziku**

V skladu s 45. členom Pravilnika o doktorskem študiju Univerze v Ljubljani mora kandidatka za pridobitev doktorata znanosti najpozneje **v štirih letih**, od potrditve teme na Senatu UL, predložiti članici univerze izdelano doktorsko disertacijo.

Pravni pouk:

Zoper to odločbo je dopusten ugovor na Senat Univerze v Ljubljani v roku 15 dni od prejema odločbe.

Current number: Dr III/209

Date: 3 February 2020

On the basis of the decision taken at the 23th Meeting of the Commission for Doctoral Studies on 14 January 2020 by authority of the 30th Meeting of the Senate of the University of Ljubljana on 20 January 2009, I am delivering the following

DECISION

At the 23th Meeting of the Commission for Doctoral Studies, University of Ljubljana on 14 January 2020 candidate

Eva Zavrl

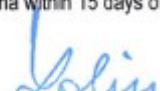
1. was approved the topic of the dissertation entitled
Improvement of thermal comfort and efficient energy use in buildings based on active-passive systems for overheating reduction
2. appointed as mentor: *Assoc. Prof. Dr. Uroš Stritih*
3. as co-mentor: *Asst. Prof. Dr. Mateja Dovjak*
4. approved the writing of the dissertation **in English**

In accordance with Article 45 of the Rules on Doctoral Studies at the University of Ljubljana, the candidate must produce the final version of the dissertation within **four years** from the date of approval of the dissertation topic.

Legal instruction:

Against this decision an appeal may be laid at the Senate of the University of Ljubljana within 15 days of the receipt of the Decision.




Prof. Dr. Mitjan Kalin,
Dekan/ Dean

Acknowledgement

First and foremost, I would like to express my sincere gratitude to my mentor Assoc. Prof. PhD. Uroš Stritih and co-mentor Assoc. Prof. PhD. Mateja Dovjak for all the guidance, support and outstanding feedback on my work.

I must thank my PhD commission members president Prof. PhD. Božidar Šarler, Assoc. Prof. PhD. Rok Fink and Prof. PhD. Mohamed El Mankibi for his unlimited support and unconditional guidance on the PhD research during my exchange in Lyon, France at ENTPE.

I would also like to extend my thanks to Assist. PhD. Urban Tomc for his unfailing dedication, constant availability, wisdom and encouragement and other professionals Prof. PhD. Simon Muhič and PhD. Zlatko Rek for advising me on numerical modeling within computational fluid dynamics (CFD).

A special thanks goes to bachelor and master students Gašper Zupanc, Davor Švajger, David Hriberšek, Salma Ifkirne and Loubna Fartal for showing interest in my work and helping me develop it.

I want to thank my coworkers from the Laboratory for Heating, Sanitary, Solar and Air Conditioning Engineering LOSK Rok Koželj, Žiga Lampret, Assist. Urška Mlakar, Assist. PhD. Rok Stropnik and Assist. PhD. Eneja Osterman for their collegiality and professional advices.

In addition, I would like to mention my coworkers from ENPTE Yousra Laaroussi, Myriam Bahrar, Mike Eliot, Gabriel Remion and Aiman Reza for help with my experiment and emotional support.

I am thanking the team from IRI UL for making the work environment in my last months of thesis preparation patient, supportive and understanding.

Finally, but the most importantly, I would like to thank my family Liza, Marjana and Tomaž and my partner Dejan for the love, patience and interest they showed over my PhD period.

Nevertheless, I am grateful to my friends who listened to my thoughts in my best and worst moments and always believably cheered for me.

My PhD project was financed by European Commission Horizon 2020 (project HEART, grant agreement N°768921), Erasmus+ academic staff exchange programme, Campus France with high level scientific research scholarship and Region Auvergne-Rhône-Alpes.

Izboljšanje toplotnega ugodja in učinkovite rabe energije v stavbah na podlagi uvajanja aktivno-pasivnih sistemov za zmanjšanje pregrevanja

Eva Zavrl

Ključne besede: fazno spremenljive snovi
reševanje pregrevanja
zalogovnik toplote
toplotno ugodje v prostoru
hlajenje stavb
prezračevana rega

Zaradi globalnega segrevanja se povečuje potreba po energiji za hlajenje stavb. Raziskan je bil aktivno-pasivni sistem (APS) s fazno spremenljivimi snovmi (PCM) integriranimi v podkonstrukcijo notranje stene in stropa za hlajenje stavb. Za zagotavljanje zadostnega hladilnega učinka sistema v dnevnem ciklu, se mora PCM v nočnem ciklu popolnoma strditi. Za izboljšanje prenosa toplote v PCM ponoči je bila za stensko in stropno podkonstrukcijo PCM nameščena prezračevana zračna rega namnjena hlajenju PCM z nekondicioniranim zrakom. APS je bil raziskan in zasnovan na podlagi sistematičnega pregleda literature, nestacionarne numerične simulacije na nivoju stavbe, eksperimentalne raziskave, parametrične analize izvedene z numeričnim modelom na mikro-skali z računalniško analizo dinamike tekočin ter izračuna energetske učinkovitosti in obratovalnih stroškov APS. V sklopu prvega tipa scenarijev je bil eksperimentalno raziskan hladilni učinek PCM v dnevnem ciklu. Slednji je bil določen s temperaturno razliko med celico brez in celico s PCM. Z drugim tipom scenarijev je bil eksperimentano in numerično ugotavljan čas strjevanja PCM v nočnem ciklu. Z aplikacijo APS se je notranja temperatura zraka znižala do 4,5 °C. Rezultati so pokazali, da se lahko PCM v APS strdi z vstopno temperaturo 17 °C. Sistem APS ima nižje obratovalne stroške kot klimatska naprava razreda G.

Abstract

UDC 697.1:628.8:620.9(043.3)

No.: DR III/209

Improvement of thermal comfort and efficient energy use in buildings based on active-passive systems for overheating reduction

Eva Zavrl

Key words: phase change material
 overheating reduction
 thermal energy storage
 indoor thermal comfort
 cooling of buildings
 ventilated air gap

As a consequence of global warming, the energy demand for cooling is increasing. A novel active-passive system (APS) with phase change material (PCM) integrated into the substructure of the internal walls and ceiling for cooling is introduced. To ensure sufficient cooling effect of the system during the daytime cycle, the system must solidify completely during the nighttime cycle. To improve the heat transfer of the PCM, a ventilated air gap was placed behind PCM wall and ceiling substructure for free cooling. APS was investigated and designed based on literature review, unstationary full-scale numerical simulation (building level), experimental investigation, parametric study performed with micro-scale numerical model in CFD and calculation of energy performance and operation cost. First type of scenarios experimentally tested the cooling effect of the PCM during the daytime cycle, determined by the temperature difference between the cell-without and cell-PCM. Second type of scenarios experimentally and numerically tested the PCM solidification time during the nighttime cycle. APS decreased the indoor temperatures for by 4.5 °C. The results showed that with the current configuration, the PCM can be sufficiently solidified at inlet temperature of 17 °C. APS system has lower operating costs than G class AC device.

List of Contents

1. Introduction	1
1.1. Energy use scenarios	1
1.2. Heat storage systems	3
1.3. Building-integrated phase change materials.....	4
1.4. Doctoral dissertation formulation.....	5
2. Theoretical Background.....	7
2.1. Heat transfer mechanisms through the building envelope	8
2.2. Indoor thermal requirements	9
2.3. Phase change materials - presentation of concept.....	12
Numerical modelling of.....	14
2.4. heat transfer PCM – air gap: nighttime solidification	14
2.4.1. Assumptions	14
2.4.2. Conservation laws – air	15
2.4.2.1. Mass conservation.....	15
2.4.2.2. Momentum conservation.....	15
2.4.2.3. Conservation of energy	16
2.4.3. Conservation laws – PCM	17
2.4.3.1. Conservation of energy	17
2.4.4. Finite volume method	17
2.4.5. Specifics in numerical modelling	18
2.5. Ventilation heat losses	19
3. Literature review	21
3.1. Enhancing the heat transfer to improve the PCM energy performance..	21
3.1.1. Addition of metal structures	21
3.1.2. Water-based systems	22
3.1.3. Summer overhang	22
3.1.4. Air discharge concepts.....	22
3.2. Nighttime ventilation.....	23
3.2.1. Natural nighttime ventilation.....	24
3.2.2. Natural and mechanical nighttime ventilation	25
3.2.3. Mechanical nighttime ventilation	26

3.3.	Ventilated building elements	29
3.3.1.	PCM-improved ventilated Roofs.....	29
3.3.2.	PCM improved ventilated ceilings	31
3.3.3.	PCM improved ventilated floor.....	37
3.3.4.	PCM improved ventilated internal walls.....	39
3.3.5.	PCM improved ventilated façades.....	40
3.3.6.	PCM improved ventilated glazing elements.....	47
3.3.7.	PCM improved ventilated walls with BiPV	49
4.	Purpose and aim of doctoral dissertation	51
4.1.	Problem description	51
4.2.	Hypotheses and objectives	52
4.3.	Workflow.....	55
4.4.	Publications.....	57
5.	Preliminary investigation	61
5.1.	Full-scale numerical model.....	61
5.1.1.	Method.....	61
5.1.2.	Results	64
5.1.2.1.	Parametric study of PCM characteristics in Ljubljana.....	64
5.1.2.2.	Parametric study of PCM characteristics in EU countries	66
5.1.3.	Conclusions	68
5.2.	Pre-Experimental investigation	69
5.2.1.	Method.....	69
5.2.1.1.	Air preparation and ventilation unit.....	69
5.2.1.2.	Heat storage	70
5.2.1.3.	Measuring equipment and measuring points	71
5.2.2.	Results	74
5.2.3.	Conclusions	75
5.3.	Pre-numerical simulation with ANSYS.....	75
5.3.1.	Method.....	76
5.3.1.1.	Geometry selection.....	76
5.3.1.2.	Grid and time step	76
5.3.1.3.	Material properties	78
5.3.1.4.	Parametric analysis.....	80
5.3.1.5.	Initial and boundary conditions and calculation model	81
5.3.1.6.	Model Validation	81
5.3.2.	Results	82
5.3.2.1.	Outlet air temperatures obtained under constant conditions	82
5.3.2.2.	Outlet air temperatures obtained under transient conditions.....	85

5.3.2.3.	Heat released during the solidification period	85
5.3.3.	Conclusions.....	86
5.4.	Discussion of literature review	87
5.4.1.	Discussion on total volume nighttime ventilation	87
5.4.1.1.	Melting temperature and location in the structural complex.....	87
5.4.1.2.	Material thicknesses.....	88
5.4.1.3.	Effect of system on energy performance and indoor thermal conditions.....	88
5.4.1.4.	General findings on total volume nighttime ventilation	89
5.4.2.	Discussion on Ventilated building elements.....	89
5.4.2.1.	Ventilated building elements with the list of investigated PCM melting temperatures.....	89
5.4.2.2.	General findings on local nighttime ventilation	90
5.5.	Selection of the phase change material characteristics	91
6.	Experimental investigation	93
6.1.	Method.....	93
6.1.1.	The operation principle of active-passive system.....	93
6.1.2.	Phase change material properties.....	94
6.1.3.	The description of the APS system test cell and features	95
6.1.4.	Measuring equipment and measuring point locations	99
6.1.5.	Description of the experimental protocol	101
6.2.	Experimental results	105
6.2.1.	Daily PCM melting cycle performance	105
6.2.2.	Nighttime PCM solidification cycle performance	107
6.3.	Discussion of the experimental results.....	109
7.	Numerical model and parametric study	115
7.1.	Method.....	115
7.1.1.	Geometry selection	115
7.1.2.	Grid and time step.....	116
7.1.3.	Calculation model.....	117
7.1.4.	Initial and boundary conditions	117
7.1.5.	Material properties.....	118
7.1.6.	Parametric study	119
7.1.7.	Validation	122
7.1.8.	Energy storage by PCM.....	124
7.1.9.	Energy Performance and operation costs	124
7.2.	Numerical results.....	125
7.2.1.	Thermal response in adiabatic conditions.....	125

7.2.2. Thermal response in each inlet temperature scenario.....	126
7.2.3. Energy released from PCM in adiabatic conditions	128
7.2.4. Energy use and operation costs of APS operation.....	128
7.3. Discussion.....	129
7.3.1. Discussion on the simulated results.....	129
7.3.2. Result comparison to other studies.....	131
7.3.2.1. Thermal performance	131
7.3.2.2. Energy performance	133
8. Conclusions	137
8.1. Hypotheses	137
8.2. Scientific contribution.....	140
8.3. General conclusions.....	141
8.4. Advantages, disadvantages and limitations	142
8.4.1. Active passive system.....	142
8.4.2. Preliminary research.....	143
8.4.3. Experimental investigation.....	143
8.4.4. Numerical model	143
8.5. Future work	144
9. Literature	145
Appendix A: Remaining literature review analysis	157
Appendix B: Remaining full-scale numerical model results ...	169
Appendix C: Detailed sketch of pre-experimental set-up	171
Appendix D: ANSYS Fluent calculation parameters	173
Curriculum Vitae	185
10. Povzetek v slovenščini.....	189

List of Figures

Figure 1.1: The classification of the most common phase change materials in building elements [33].	4
Figure 2.1: Scheme of room locations and corresponding theoretical background.	7
Figure 2.2: Heat transfer mechanisms in the building envelope (left— non-transparent structural complex, middle— non-transparent structural complex with air gap and right transparent structural complex with air gap) [38].	8
Figure 2.3: T_{rm} – outdoor running temperature and T_{op} – operative temperature.	11
Figure 2.4: Phase change diagram (temperature and heat stored) [34].	12
Figure 2.5: Phase change hysteresis process represented as a function of temperature [44].	13
Figure 2.6: Partial enthalpy in relation to temperature for PCM type RT24 [45].	14
Figure 2.7: Space discretization in FVM [51].	17
Figure 2.8: The numerical simulation principle sketch of the air and PCM layer.	18
Figure 3.1: PCM (orange) and load-bearing wall (white) with air discharge concepts: 1) total volume nighttime ventilation, 2) ventilated air gap, and 3) free cooling active thermal energy storage unit.	22
Figure 3.2: Total volume nighttime ventilation principles with location of PCM in building elements.	23
Figure 3.3: The window-based cooling unit a) nighttime and b) daytime [92].	26
Figure 3.4: Ventilated building elements with PCM.	29
Figure 3.5: Composite phase change ventilated roof [108].	30
Figure 3.6: Ventilated roof composed with multiple phase change material (VR-MPCM) [109].	30
Figure 3.7: Ceiling ventilation system enhanced by solar photovoltaic thermal collectors and phase change materials [111].	31
Figure 3.8: PCM based storage system integrated with ceiling fan ventilation [112].	31
Figure 3.9: Ventilated slab with the addition of PCM modules [113].	32
Figure 3.10: night ventilation with PCM packed bed storage [114].	32
Figure 3.11: Schematic of proposed heat pipe/PCM installation [115].	33
Figure 3.12: PCM implementation alternatives [116].	33
Figure 3.13: A ventilated cooling ceiling with integrated latent heat storage [117].	34
Figure 3.14: The simplified ventilated PCM ceiling [118].	34
Figure 3.15: Night ventilated hollow core slabs cast with micro-encapsulated PCM concrete [119].	35
Figure 3.16: Pipe-embedded ventilation roof with outer-layer shape-stabilized PCM in different climate zones [120].	35
Figure 3.17: An active PCM-heat exchanger ceiling [121].	36
Figure 3.18: Cooling PCM ceiling for peak shaving control [122].	36
Figure 3.19: Ceiling panel made out of PCM composite [123].	37
Figure 3.20: Floor supply air conditioning system using granular phase change material [124].	38
Figure 3.21: The Magic Box prototype [125].	38
Figure 3.22: Ventilated wall cavity [126].	39

Figure 3.23: The PCM wall consisting out of 5 layers of shape-stabilized PCM panels [127].	40
Figure 3.24: Ventilated facade with PCM for cooling applications [130].	41
Figure 3.25: The ventilation tubes in integrated in blocks with PCM [134].	42
Figure 3.26: A ventilated active façade including phase change materials [136].	42
Figure 3.27: A new ventilated Trombe wall with PCM and active cooling/heating [137].	43
Figure 3.28: Phase change materials integrated renewable systems with hybrid ventilation and active cooling [138].	44
Figure 3.29: Description of the innovative E2VENT system [140].	45
Figure 3.30: Modified solar phase change material storage wall system [141].	45
Figure 3.31: PCM improved Trombe wall [142].	46
Figure 3.32: Solar PCM wall [143].	46
Figure 3.33: Integrated PCM blind system for double skin façade buildings [144].	47
Figure 3.34: A ventilated window with PCM heat exchanger [145].	48
Figure 3.35: A ventilated window with PCM heat exchanger improved with internal shading and window glazing characteristics [146].	48
Figure 3.36: BiPV façade system enhanced with PCM [147].	49
Figure 3.37: Ventilated PCM wall with BIPV [148].	49
Figure 4.1: PhD. project workflow diagram.	55
Figure 4.2: Timeline with task durations and milestones.	57
Figure 5.1: Single-family building (front).	62
Figure 5.2: Structural complex (SC) of heavyweight load-bearing structure.	63
Figure 5.3: Structural complex (SC) of lightweight load-bearing structure.	63
Figure 5.4: Structural complex (SC) of lightweight load-bearing structure with macroencapsulated BioPCM™ layer.	63
Figure 5.5: Structural complex (SC) of lightweight load-bearing structure with microencapsulated PCM gypsum board.	63
Figure 5.6: Systematic scheme of variations investigated under three different climate types Ljubljana, Copenhagen and Rome.	64
Figure 5.7: Outside dry-bulb temperature, operative temperatures obtained with heavyweight and lightweight load-bearing structure and thermal comfort limits for III Category of EN 16798:2019 [37].	64
Figure 5.8: Operative temperatures obtained with lightweight load-bearing structure, microencapsulated gypsum boards and thermal comfort limits for III Category of EN 16798:2019 [37].	65
Figure 5.9: Operative temperatures obtained with lightweight load-bearing structure, macroencapsulated BioPCM™ and thermal comfort limits for III Category of EN 16798:2019 [37].	65
Figure 5.10: Operative temperatures obtained with lightweight load-bearing structure, macroencapsulated BioPCM™ with melting point of 24 °C and thermal comfort limits for III Category of EN 16798:2019 [37].	66
Figure 5.11: Operative temperatures obtained with BioPCM™ in Ljubljana with thermal comfort limits for III Category of EN 16798:2019 [37].	67
Figure 5.12: Operative temperatures obtained with BioPCM™ in Copenhagen with thermal comfort limits for III Category of EN 16798:2019 [37].	67

Figure 5.13: Operative temperatures obtained with BioPCM™ in Rome with thermal comfort limits for III Category of EN 16798:2019 [37].	68
Figure 5.14: Testing station with air preparation unit and PCM heat storage.	69
Figure 5.15: Electric heater.	70
Figure 5.16: Ventilator.	70
Figure 5.17: PCM heat storage - ventilated channel with PCM plates.	70
Figure 5.18: DSC diagram of Rubitherm RT22HC [154].	71
Figure 5.19: Agilent 34970A.	71
Figure 5.20: Vane anemometer.	71
Figure 5.21: Locations of thermocouples for PCM plate surface temperature measurements.	72
Figure 5.22: Locations of thermocouples for air temperature measurements.	72
Figure 5.23: Air temperature profile on outlet measured with thermocouples.	73
Figure 5.24: Scheme of experimental cases.	73
Figure 5.25: Temperatures obtained during the solidification of PCM in case VIII.	74
Figure 5.26: Air temperatures at the outlet temperature profile.	75
Figure 5.27: Sketch of model's geometry.	76
Figure 5.28: Time step independence test.	77
Figure 5.29: Grid independence test.	77
Figure 5.30: The selected grid with element size of 5 mm.	77
Figure 5.31: Partial enthalpy in relation to temperature for PCM type RT22HC [144].	78
Figure 5.32: Partial enthalpy in relation to temperature for PCM type RT24 [146].	79
Figure 5.33: Partial enthalpy in relation to temperature for PCM type SP24E [155].	79
Figure 5.34: Partial enthalpy in relation to temperature for PCM type SP252E [156].	79
Figure 5.35: Scheme of cases in parametric study.	80
Figure 5.36: The outdoor air temperatures of the coldest night (1.-2.8.2022) and the hotter night (3.-4.8.2022).	81
Figure 5.37: Simulated and experimentally measured outlet air temperatures for model validation.	82
Figure 5.38: Example of solidification with inlet air temperature of 15 °C and air velocity of 0.1 m/s PCM RT24.	82
Figure 5.39: Outlet air temperatures obtained with PCM RT22HC under constant inlet air temperature.	83
Figure 5.40: Outlet air temperatures obtained with PCM RT24 under constant inlet air temperature.	83
Figure 5.41: Outlet air temperatures obtained with PCM SP24E under constant inlet air temperature.	84
Figure 5.42: Outlet air temperatures obtained with PCM SP252E under constant inlet air temperature.	84
Figure 5.43: Outlet air temperatures obtained under transient inlet air temperature.	85
Figure 6.1: The operating principle of the active-passive system for cooling application.	93
Figure 6.2: DSC diagram Rubitherm SP24E [155].	94
Figure 6.3: PCM SP24E plates opened and melted.	94
Figure 6.4: Initial state of test chamber in Lyon, France.	95

Figure 6.5: Wooden frame structure for PCM plates integration onto the internal wall and ceiling.	96
Figure 6.6: Experimental facility (left) and PCM modified cell - wall and ceiling (right).....	96
Figure 6.7: The air gap division in 5 identical channels with air streams.	97
Figure 6.8: The sketch of experimental features and location of measuring points.	98
Figure 6.9: Experimental features: inlet fan, outlet fan, spiral heating coil and cell heater.	98
Figure 6.10: Experimentail features: cooling coil.....	99
Figure 6.11: PCM modified cell with T_a and T_{mr} measuring locations.	100
Figure 6.12: Locations of the measuring points in PCM wall (up) and ceiling (down).	101
Figure 6.13: Diagram of the daily meting and nighttime solidification cycle cases, where the diagram of daily meting cases (left) refers to the set point air temperatures in Cell B.	102
Figure 6.14: The sketch of ventilation operation in case with constant temperature of 30 °C in cell B and additional background ventilation.	103
Figure 6.15: Outdoor and indoor air temperatures for TRY and OH case simulated during the hottest day of the year in Ljubljana.....	104
Figure 6.16: Cell air temperatures obtained during the daytime melting cycle in cell A and cell B - constant cases.	105
Figure 6.17: Cell air temperatures obtained during the daytime melting cycle in cell A and cell B - constant case with background ventilation.	106
Figure 6.18: Cell air temperatures obtained during the daytime melting cycle in cell A and cell B – transient cases.....	107
Figure 6.19: The average PCM surface temperatures and inlet air temperatures obtained during the case solidified with average inlet air temperature of 15 °C.....	108
Figure 6.20: The average PCM surface temperatures and inlet air temperatures obtained during the case solidified with average inlet air temperature of 16 °C.....	108
Figure 6.21: The average PCM surface temperatures and inlet air temperatures obtained during the case solidified with average inlet air temperature of 17 °C.....	109
Figure 6.22: PCM leakage due to volume expansion dropping from the ceiling on the floor.	113
Figure 7.1: Sketch of the 2D model geometry with simplifications.....	115
Figure 7.2: Grid and time step independence test of Outlet air temperatures T_{ao} during 25 h of operation (note: the lines from 2 mm (10 s) to 10 mm (30 s) are overlapping).....	116
Figure 7.3: Grid and time step independence test of PCM surface temperatures $T_{PCM_back, avg}$ during 25 h of operation (note: the lines from 2 mm (10 s) to 10 mm (30 s) are overlapping).....	116
Figure 7.4: The selected grid with element size of 5 mm.	117
Figure 7.5: DSC diagram Rubitherm SP24E [155].....	118
Figure 7.6: Partial enthalpy in corelation with temperatures - numerical model input	119
Figure 7.7: Temperatures obtained during the reference experimental case in the cooling cycle. .	120
Figure 7.8: The estimated cell air temperatures during two solidification periods for the determination of PCM wall boundary condition.	121
Figure 7.9: Experimental cases showing the characteristic temperature difference between $T_{PCM_front, avg}$ and $T_{a, cell}$	122
Figure 7.10: The first validation case (melting/solidification) based on the outlet air temperuress.	122
Figure 7.11: The second validation case (solidification) – based on the outlet air temperatures and average surface PCM temperature (back).	123

Figure 7.12: Outlet air temperatures obtained in adiabatic conditions for different inlet air temperature scenarios.	125
Figure 7.13: The results obtained at inlet air temperature of 15 °C.	126
Figure 7.14: The results obtained at inlet air temperature of 16 °C.	127
Figure 7.15: The results obtained at air inlet temperature of 17 °C.	127
Figure 7.16: Electrical energy use to produce 6.34 kWh of cooling energy of the best case (A+++ class) and the worst case (G class) air conditioner in comparison to the proposed APS.	128
Figure 7.17: The cost of consumed electrical energy per day of operation to produce 6.34 kWh of cooling energy of the best case (A+++ class) and the worst case (G class) air conditioner in comparison to the proposed APS.	129
Figure 7.18: The area-weighted average outlet air temperatures simulated within corresponding inlet temperature scenario.	130
Figure 7.19: The area-weighted average back surface PCM temperatures simulated within corresponding scenario.	130
Figure 0.1: PCM with melting temperature of 23 °C.	169
Figure 0.2: PCM with melting temperature of 25 °C.	170
Figure 0.3: Average daily temperatures subtracted from the upper limit of thermal comfort 26 °C.	170

List of Tables

Table 2.1: The values for A value in correspondence with the room air velocities v [41].	10
Table 2.2: Examples of recommended design values of the indoor temperature for design of buildings and HVAC systems [37].	10
Table 2.3: Maximum and minimum limit temperature of indoor operative temperatures [37].	11
Table 2.4: Thermal state of the body as a whole [37].	11
Table 2.5: Basic required ventilation rates for diluting emissions (bio effluents) from people for different categories [37].	19
Table 4.1: Hypothesis with corresponding objectives.	54
Table 5.1: Simulation conditions.	62
Table 5.2: Heat transfer coefficients U [$W/(m^2 K)$] of the designed building envelope structural complexes.	63
Table 5.3: The list of PCM types and their thermal characteristics.	78
Table 5.4: Heat released during the temperature stabilization period with constant inlet air temperature conditions.	85
Table 5.5: Heat released during the solidification period with transient inlet air temperature conditions.	86
Table 5.6: Location of the PCM in the structural complex according to the selected PCM temperature.	87
Table 5.7: Cooling effect of the system on the energy performance and indoor thermal conditions.	89
Table 5.8: Ventilated building elements with the list of investigated PCM melting temperatures.	90
Table 6.1: Temperature difference between the maximum daily air temperature in summer in Ljubljana based on the period (1981-2010) and periods (2011-2040, 2041-2070 and 2071-2100) of RCP4.5 and RCP8.5 scenarios [159].	103
Table 6.2: Thermal comfort assessment.	110
Table 7.1: The estimated cell air temperature differences during two solidification periods for the determination of PCM wall boundary condition.	120
Table 7.2: Calculated energy released from the plates Q_{dis} and the error from the theoretical value of Q .	128
Table 0.1: Ventilation rates and duration period of the nighttime ventilation cycle.	158
Table 0.2: The research summary of the nighttime ventilation studies.	161
Table 0.3: The research summary of the ventilated building element studies.	164

Nomenclature

Symbol	Unit	Definition
A	/	velocity/temperature coefficient
\vec{A}	/	surface
a	m	plate thicknesses
$A_{\text{air gap}}$	m ²	area of the air gap
\vec{A}_f	/	area of surface f
$c_{p,a}$	J/(kg K)	specific heat capacity of air
c_p	J/(kg K)	specific heat capacity of the material
$c_{p,PCM}$	J/(kg K)	specific heat capacity of PCM
$c_{p,s}$	J/(kg K)	specific heat capacity of the solid material
$c_{p,l}$	J/(kg K)	specific heat capacity of the liquid material
total c_p	J/(kg K)	total heat capacity of PCM in the range presented by the producer
d_p	m	pipe/duct diameter
$f(T)$	/	liquid fraction as a function of temperature, 0-1
F_i	/	geometry factor of radiation exchange between surface I in the environment and the surface of the building
F_{sky}	/	geometry factor of radiation exchange between the sky and the surface the building
\emptyset_f	/	value of \emptyset brough across surface f
g	/	total solar energy transmittance
\vec{g}	/	acceleration due to gravity
g_x	m/s ²	component of acceleration due to gravity in direction x
g_y	m/s ²	component of acceleration due to gravity in direction y
$G_{\text{glob},\beta}$	W/m ²	total/global solar radiation on the external surface of the building
I	clo	clothing insulation
i	/	counter of surfaces in the surrounding (the sum equals n), $i=1\dots n$
k	m ² /s ²	turbulence kinetic energy
l	J/kg	mass specific latent heat
M	met	metabolic rate
\dot{m}	kg/s	mass flow rate
m	kg	mass
m_a	kg	mass of air that has moved out of the building
\vec{n}	/	normal on the interface between air and PCM layer
n_{faces}	/	number of areas
$\Delta T_{(\text{TRY-OH})}$	°C	temperature difference between outdoor air temperatures obtained with preliminary investigation simulated with test reference year (hottest day of the year in Ljubljana) and outdoor air temperatures estimated for the summer heatwave
$\Delta T_{(\text{Tai-Tao})}$	°C	temperature difference between indoor and outdoor air temperatures obtained with preliminary investigation

		simulated with test reference year (hottest day of the year in Ljubljana) from 10:00 to 20:00
P	W	power
P_k	m^2/s^2	production of turbulent kinetic energy
p	Pa	pressure
PMV	/	predicted mean vote
PPD	%	predicted percentage of dissatisfied
RH	%	relative humidity
S_ϕ	W/m^3	source or sink per unit of surface
S_h	W/m^3	volumetric heat sources and heat generation from chemical reactions
T_a	$^\circ C$	air temperature or room air temperature
$T_{a, cell}$	$^\circ C$	mean air temperature measured in the centre of the cell
$\Delta T_{a, cell} (0-5 h)$	$^\circ C$	temperature difference between the mean air temperature measured in the centre of the cell at the beginning and after 5 hours of the case
$\Delta T_{a, cell} (6-30 h)$	$^\circ C$	temperature difference between the mean air temperature measured in the centre of the cell after 6 hours and after 30 hours of the case
T_{ai}	$^\circ C$	inlet air temperature
T_{ao}	$^\circ C$	outlet air temperature
$T_{ao1} \dots T_{ao6}$	$^\circ C$	outlet air temperature measured in points 1-6
T_e	$^\circ C$	final temperature of the material, air temperature in the surrounding
T_{ekv}	$^\circ C$	equivalent temperature
T_i	$^\circ C$	the temperature of surface i in the environment
T_{in}	$^\circ C$	initial material temperature
$T_{l, max}$	$^\circ C$	maximum limit temperature of indoor operative temperature
$T_{l, min}$	$^\circ C$	minimum limit temperature of indoor operative temperature
T_{rm}	$^\circ C$	outdoor running temperature
$T_{a, room}$	$^\circ C$	room air temperature
T_m	$^\circ C$	melting temperature
T_{mr}	$^\circ C$	mean radiant temperature
T_{op}	$^\circ C$	operative temperature
T_{PCM}	$^\circ C$	PCM temperature
T_{PCM_front}	$^\circ C$	surface temperature measured on the front of the PCM plate
T_{PCM_back}	$^\circ C$	surface temperature measured on the back of the PCM plate
$T_{PCM_back, avg}$	$^\circ C$	average value of surface temperatures measured on the back of the PCM plate
T_{rm}	$^\circ C$	outdoor running temperature
T_s	$^\circ C$	surface temperature measured on the primary wall and ceiling
T_{se}	$^\circ C$	surface temperature of the building
T_{set}	$^\circ C$	set point temperature
T_{set_B}	$^\circ C$	set point air temperature in cell B

T_{sky}	°C	temperature of sky
t_i	h	time at the beginning of the nighttime cycle (0 h)
t_e	h	time at the end of the nighttime cycle
U_w	W/(m ² K)	thermal transmittance of the windows
V	m ³	volume
\dot{V}	m ³ /s	volumetric flow rate
v	m/s	air velocity
\vec{v}	/	velocity vector
\vec{v}_a	/	air velocity vector
\vec{v}_f	/	flow velocity
v_x	m/s	velocity of the air in x-direction
v_y	m/s	velocity of the air in y-direction
v_{ar}	m/s	room air velocities
Q	J, Wh	heat stored in material
Q_{dis}	J, Wh	heat released from material
Q_v	J, Wh	ventilation heat losses
q_{conv}	W/m ²	convective heat flux
q_{rads}	W/m ²	shortwave radiation heat flux
q_{radl}	W/m ²	longwave radiation heat flux
q_{cond}	W/m ²	conduction heat flux
α	/	turbulent model coefficient
$\alpha_{s,e}$	/	absorption of shortwave solar radiation
$\alpha_{k,e}$	W/(m ² K)	convective heat transfer coefficient between the external surface of the building and environment
β	/	turbulent model coefficient
β^*	/	turbulent model coefficient
β_T	/	thermal volume expansion coefficient
Γ_{\emptyset}	m ² /s	diffusion coefficient for \emptyset
∇_{\emptyset}	/	gradient \emptyset
$\nabla_{\emptyset f}$	/	gradient \emptyset on the surface f
$\varepsilon_{\text{IR},i}$	/	longwave heat radiation emissivity
$\varepsilon_{\text{IR},\text{sky}}$	/	emissivity of longwave heat radiation from the sky
$\varepsilon_{\text{IR},se}$	/	emissivity of longwave heat radiation from the surface of the buildings
λ	W/(m K)	thermal conductivity
λ_a	W/(m K)	thermal conductivity of air
λ_{PCM}	W/(m K)	thermal conductivity of PCM
μ	kg/(m s)	dynamic viscosity
μ_{eff}	kg/(m s)	effective dynamic viscosity
μ_{turb}	kg/(m s)	turbulent viscosity
ρ	kg/m ³	density
ρ_a	kg/m ³	density of air
ρ_{PCM}	kg/m ³	density of PCM
ρ_f	kg/m ³	density of the flow
$\rho_{\text{(solid-liquid)}}$	kg/l	average density of PCM between solid and liquid state
$\sum_f^{n_{\text{faces}}} \rho_f \vec{v}_f \vec{A}_f$	kg/m ³	mass flow rate across the surface

σ	W/(m ² K ⁴)	Stefan-Boltzmann constant ($5.67 \cdot 10^{-8}$ W/(m ² K ⁴))
σ_k	/	turbulent model coefficient
σ_ω	/	turbulent model coefficient
ω	m ² /s ³	specific dissipation rate

Index

CELL_A	measuring location in the centre of test cell A (PCM modified cell)
CELL_B	measuring location in the centre of test cell B (reference cell, without PCM)
15-20 °C	values measured at inlet temperature scenario of 15-20 °C
1-13	values measured in PCM surface measuring points numbered 1-13
1-6	values measured in air gap measuring points numbered 1-6
y, y and z	global cartesian coordinates

List of acronyms

Acronym	Definition
AC	Air-Conditioning
ACH	Air Change per Hour
APS	Active-Passive System
CSM	Compact Storage Module
DSC	Differential Scanning Calorimetry
DSY	Design Summer Year
CIBSE	Chartered Institution of Building Services Engineers
ENTPE	National School of State Public Works
EPBD	European Directive on Energy Performance of Buildings
EPS	Expanded PolyStyrene
H1-6	Hypothesis from number 1 to number 6
HVAC	Heating, Ventilation and Air-Conditioning
HW	Heavyweight
IEA	International Energy Agency
IPCC	International Panel for Climate Change
ISO	International Standard Organisation
LW	Lightweight
LW _{PCM.a}	Lightweight with microencapsulated BioPCM™
LW _{PCM.b}	Lightweight with microencapsulated PCM gypsum boards
OH	Overheating
OH LJ	Test Reference Year of Ljubljana, Slovenia modified for the Overheating period
PCM	Phase Change Material
PID	Proportional Integral Derivative
RANS	Reynolds-averaged Navier-Stokes
TRNSYS	Transient System Simulation Tool
TRY	Test Reference Year
TRY LJ	Test Reference Year of Ljubljana, Slovenia
TRY RO	Test Reference Year of Rome, Italy
SC	Structural Complex
UDF	User Defined Function

1. Introduction

1.1. Energy use scenarios

The building sector accounts for 40 % of the final energy used for heating and cooling. In Europe, this sector is one of the largest energy consumers, producing more than one-third of the EU's emissions [1].

Eurostat and the Intergovernmental Panel on Climate Change (IPCC) confirmed that one of the consequences of global warming is increased outdoor air temperatures in summertime [2], [3]. According to the Eurostat 2020 analysis, space heating remains the largest energy-consuming activity, especially in the residential sector (European domestic average 68 %) [4]. However, the energy demand for cooling is increasing. The International Energy Agency (IEA) estimated that about 20 % of the total electrical energy in buildings is consumed for cooling and that the electrical energy demand tripled between 1990 and 2018 [5]. The projections show that the energy demand for heating will increase until 2030 and afterwards stabilise. They also show that by 2060 the energy demand for cooling will overtake the demand for heating [6]. Over the last 10 years in Europe, the number of heating days in buildings decreased by 13 % [7]. It is predicted that by 2030 the energy consumed for cooling will increase by 72 %. Simultaneously, the energy needed for heating will drop by 30 % [8]. The increasing energy use for cooling is related to generally increased outdoor temperatures throughout the year (1.5°C global warming), changes in the dynamics of the daily heatwaves (very sudden and unpredictable peaks), and higher demand for indoor thermal comfort.

According to the EPBD directive, the EU aims to be climate neutral by 2050 [9]. This is achievable only by following the *Responsible Policy Scenario*, which follows the EU's latest strategy to boost building renovation – the Renovation Wave [1], [10], which requires changes in current construction and renovation practices while aiming for strong efficiency measures. Currently, most of the EU building stock is energy inefficient (75 %), and in 2050, 90 % of the buildings will remain in use [11]. Also, it specifies that the current annual deep renovation rate has to rise from 0.2 % to 2-3 %. Furthermore, this is also a strongly emphasised issue promoted in the European Green Deal initiative (launched in 2020) [12].

Especially in these times of increasing costs of energy sources, the renovation motivation is often challenged due to energy or fuel poverty which is defined as a situation where low-income households are not able to adequately provide basic energy services in their homes and for their transport at affordable cost [13].

The deep energy renovation should aim for both main objectives: decreasing the carbon footprint and establishing healthy living and working environments for building occupants. Inadequate thermal conditions in the living and working environment (too hot/too cold) are one of the important risk factors for building occupants' health. The occupant's thermal comfort, health, wellbeing, and productivity are affected by high indoor temperatures and may also cause sleep deprivation [14], [15]. Because their effects are not immediately perceived, heatwaves are often neglected when assessing natural hazards. Between 1998 and 2017, heatwaves in Europe claimed over 166 000 victims, of which about 70 000 were in 2003 [16].

In addition, heatwaves in 2019 broke the records in many European locations [17]. Concerning climate change, it is predicted that such events will occur more frequently [18]. The 3 °C average global warming scenario shows that by the end of this century, the number of EU and UK citizens exposed to heatwaves will increase from 10 million/year (average in years 1981-2010) to about 300 million/year [17]. However, the predicted mortality rate in the 1.5 °C average global warming scenario is limited to 2 hemispheres. 30 000 fatalities/year with the highest impact in southern Europe. The exposure and extreme cold (and its related mortality) will be reduced by milder winters.

The current regulatory framework does not sufficiently address the potential risk of overheating in buildings [14], [19]. If the risk is not brought to the attention of policymakers soon, the usage of the mechanical cooling systems, such as air conditioning and fans, will increase and reverse the progress attained in reducing the energy consumed in buildings. However, the Chartered Institution of Building Services Engineers (CIBSE) prepared some guidelines in which they adopted the adaptive thermal model to define thermal comfort and design overheating criteria (TM52), published a design methodology for the assessment of overheating risk in homes (TM59), provided the industry with a consistent methodology for assessing thermal comfort at the design stage, and recommended the use of future weather files (TM48 and TM49) that capture future projections of climate changes when assessing overheating risk and mitigation options at design stage [14], [20], [21].

Nowadays, lightweight buildings (skeleton structure and low-density thermal insulation as the prevailing material in wall composition) and buildings with large windows are popular structural concepts. Within construction industry, the use of modular architecture and prefabricated housing construction principles has experienced an increase in recent years [22], [23]. The transformation was influenced due to growing significance on overall prerequisites of lightweight construction over conventional buildings such as reduced solid waste generation in landfills, improved construction process, reduced construction time, reduced environmental impact and improved cost-effectiveness.

The Forestry Commission reported that in the United Kingdom, 25 % of all new housing uses timber frame construction. Also, in Scotland 75-85 % of new housing consist of timber frame construction. Similarly, this trend is also growing in Ireland where the timber

frame homes account for 25 % of newly build homes [24]. Traditionally, the percentage of timber frame buildings has been large in North America and it is also increasing in Central Europe, especially in France, Germany, Switzerland and Austria, Sweden, Japan and China. In Sweden, there are over 20 000 apartments in timber buildings as well as one in five new apartment buildings is being built using timber [25]. Since 2007, the light timber structures production has increased for 15 % is expected to grow further in double digits in the coming years [26].

Current trend of thermal renovation measures is focused on improvement of the thermal resistance of the building envelope by increasing the thickness of thermal insulation without increasing the buildings' thermal accumulation properties. In the heating season, the indoor spaces are kept warm due to a high amount of thermal insulation in the building envelope. Over the years, improved knowledge led to a considerable drop in energy use for heating. However, the energy efficiency of building heating technology can still be improved. In the cooling season, such buildings are easily overheated due to the high thermal response of the building (low in thermal accumulation); they need to be cooled instantly to sustain a comfortable living environment [27]–[29]. Therefore, such buildings need to be renovated to keep the indoor temperatures over the summer low (i.e., within the thermal comfort ranges).

Generally speaking, the buildings can be heated or cooled by bioclimatic architectural design, passive or active systems [30]. Passive building systems are systems that do not require a drive power, moving parts and controls for their function and require relatively little maintenance [31]. Active building systems include mechanical systems for heating, cooling and ventilation (HVAC), illumination, and control systems.

1.2. Heat storage systems

Heat may be stored physically or chemically. Physical systems have high heat accumulation abilities and store the excess heat by changing their temperature (sensible heat) or changing their phase (latent heat).

The most frequent example of sensible heat storage in a building component is a Trombe-Michel wall [32]. The system is used for heating and cooling application and may be used as a retrofitting alternative. The mass wall (brick or concrete) is on the external side covered by glass, forming a ventilation gap. The sun heats the brick wall, which establishes the buoyancy-driven upward airflow in the ventilation gap. To provide heating in winter, the cooler air from the indoor space is sucked from the opening in the lower part of the brick wall and exhausted through the gap into the upper opening of the wall and taken into space. To provide cooling in summer, the procedure is the same, but the air is exhausted through the air gap into the upper opening in the glass and taken outside.

However, sensible heat storage systems consume a large amount of space, affect a building's appearance, are not suitable for office buildings, and are normally not used to renovate a single unit (room/office/zone) in a building.

1.3. Building-integrated phase change materials

Change Material (PCM), which has a high heat-storing capacity at a selected phase-changing temperature. PCM may be integrated into the units of the mechanical cooling systems to improve their energy efficiency, such as water-based heat storages, PCM heat exchangers etc. (active systems), or it may present a layer in a structural complex of the building component (wall, ceiling, floor etc.; passive systems): building-integrated PCM.

Building-integrated PCM can be used for heating and/or cooling. Chemically, they are divided into groups of organic materials (paraffines), inorganic materials (salt hydrates) and eutectics (Figure 1.1).

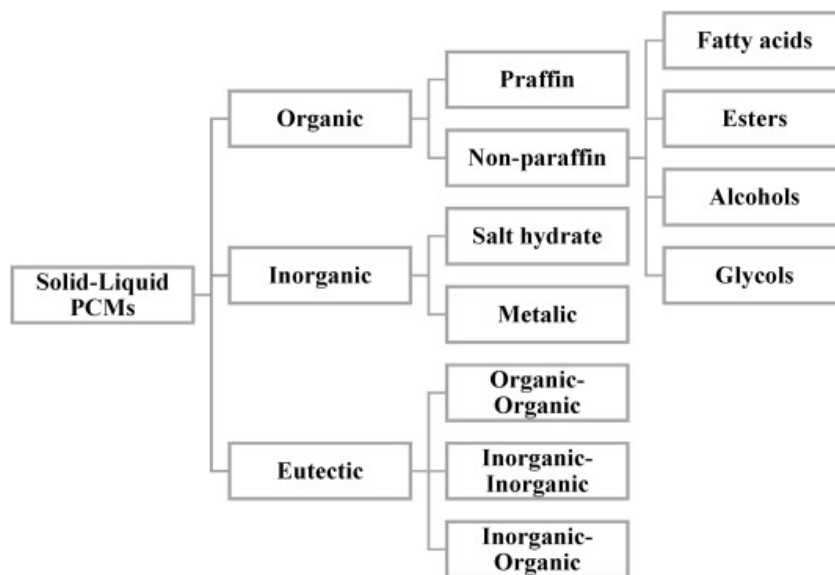


Figure 1.1: The classification of the most common phase change materials in building elements [33].

While the main advantages of organic PCMs are availability in a large temperature range, high heat of fusion, no super-cooling, chemical stability and recyclability and high compatibility with other materials, the disadvantages are considerable changes in volume, low thermal conductivity (0.2 W/(m K)), and flammability [34]. Inorganic PCMs have favourably high heat of fusion, high thermal conductivity (0.5 W/(m K)), low volume change and cost-availability properties. However, their performance suffers from super-cooling and corrosion. Nevertheless, eutectics may provide very targeted melting temperature and high volumetric thermal storage density while only little-tested thermophysical properties are available.

When PCM are integrated into building elements (defined by International Standard Organisation (ISO) standard 6946:2017 building elements is a major part of a building such as wall, floor or roof [35]) they should meet the following criteria [34]: thermodynamic properties (melting temperature in desired range, high latent heat of fusion

per unit volume, high thermal conductivity, high specific heat and high density, small volume changes on phase transformation and small vapour pressure at operating temperatures to reduce the containment problems and congruent melting), kinetic properties (high nucleation rate to avoid super-cooling and high rate of crystal growth to meet demands of heat recovery from the storage system), chemical properties (complete reversible freezing/melting cycle, chemical stability, no degradation after a large number of freezing/melting cycle, no corrosiveness and no toxic, no flammable and no explosive material) and economic properties (effective cost and large-scale availabilities).

PCM are incorporated in the building components as independent layers in the structural complex; PCM is poured into large capsules (e.g., plate case) (macro-encapsulation), PCM as a dispersion mixed into the composites assembling the structural complex (micro-encapsulation) [36], by impregnating the elements of the structural complex (impregnation) or in the form of shape stabilized PCM in which PCM is poured into the shaping matrix. The phase change temperature range of building-integrated PCM normally varies between 18 and 30 °C, depending on the type of the targeted yearly period (heating/cooling/seasonal), position in the structural complex, weather conditions and are related to the indoor thermal comfort criteria [34], [37].

1.4. Doctoral dissertation formulation

- **Basis:** Based on the energy use scenarios it is possible to conclude that the energy use needs to be minimized by decreasing the number of active systems and improving their energy efficiency. The opposite of active systems are passive systems (e.g. PCM) consuming no electricity for their operation. PCM serves as an alternative for cooling system and can be implemented in active mechanical building systems or in building components where they cool the buildings passively.
- **Problem:** In recent years the research showed that during the day PCM have high cooling potential. However, during the night they have a difficulty to solidify completely due to low material density (the material insulates itself along the thickness of its layer) and material heat release indoors. Therefore, PCM needs to be solidified by active means (e.g. improved heat transfer by air).
- **Aim:** Within this doctoral dissertation an active-passive system is designed to cool the indoor building spaces passively, during the summer days and actively, during the nights when material in the system is regenerated. The system is optimised experimentally and numerically to ensure the optimal performance under South-Easter European summer climate conditions. Afterwards, the systems energy performance and operational costs are compared to the conventional cooling systems.

2. Theoretical Background

In this chapter theoretical background of the PhD. project is presented. Figure 2.1 shows the locations in the structural scheme and are described in the following subchapters:

- Heat transfer mechanisms through the building envelope (window in blue) (1)
- Radiation, convection and conduction of the indoor space with thermal comfort requirements (2)
- Heat transfer in phase change material (PCM) (3)
- Heat transfer from PCM to the air gap forced convection (4)
- Heat losses with ventilation system (5)

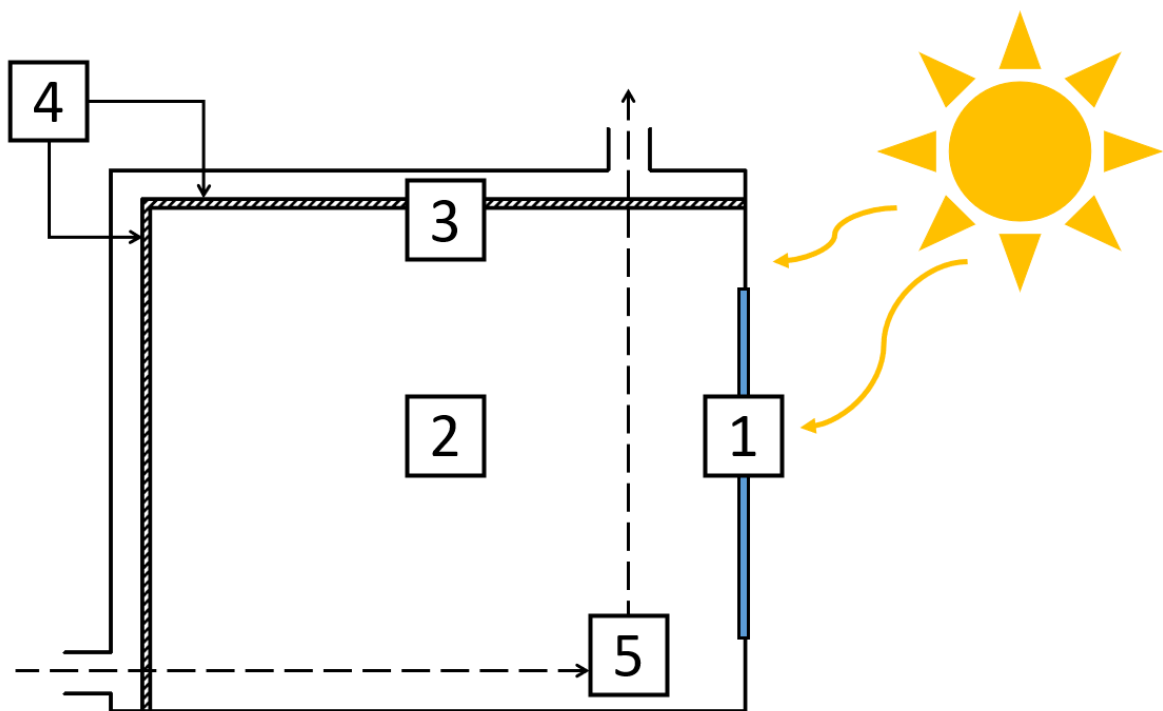


Figure 2.1: Scheme of room locations and corresponding theoretical background.

2.1. Heat transfer mechanisms through the building envelope

This chapter presents the mechanisms of heat transfer through the building envelope. In buildings, the heat can be transferred through transparent and non-transparent, and ventilated and non-ventilated parts of the building envelope. In summer months, when the outdoor solar radiation is the strongest of the entire year, large and sudden amounts of heat are transferred indoors resulting in high indoor temperatures and overheating of a building.

Basic heat transfer mechanisms in building envelope are divided in conduction (q_{cond}), convection (q_{conv}) and radiation (short: q_{rads} and long: q_{radl}) [38]. Figure 2.2 shows the three examples of structural complexes of a building envelope, where the first two cases are non-transparent (1st non-ventilated and 2nd ventilated; the first layer of the loadbearing structure is dark grey, the second layer of the loadbearing structure is light grey and the white layer presents the air gap) and the third one transparent (the transparent layers (glass) are presented in light blue and the air gap layer with white). The figure shows the heat transfer in building envelope with the outdoor and indoor environmental effect.

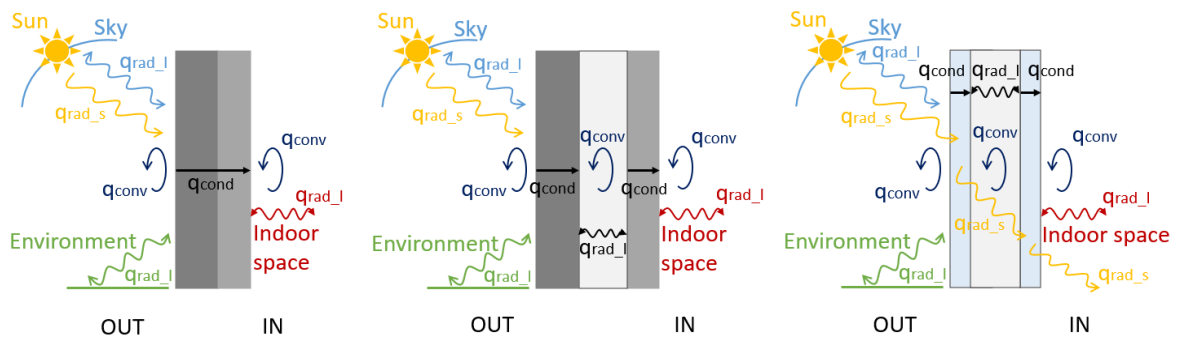


Figure 2.2: Heat transfer mechanisms in the building envelope (left— non-transparent structural complex, middle— non-transparent structural complex with air gap and right transparent structural complex with air gap) [38].

The influence of heat flows affecting the building can be summarized and presented by the equivalent temperature (T_{ekv}) [38]. The equivalent temperature captures: fluctuating outdoor surface temperature of a building envelope (changing solar radiation, inconstant building envelope surface temperature during the heat absorption), absorbed and emitted longwave radiation from the surrounding environment and convection. Equation 2.1 shows the formula for determination of (T_{ekv}).

$$T_{\text{ekv}} = T_e + \frac{\overbrace{\alpha_{s,e} \cdot G_{\text{glob},\beta}}^{\text{absorbed solar radiation}} + \overbrace{\frac{\sum_{i=1}^n (\varepsilon_{\text{IR},i} \cdot \sigma \cdot F_i \cdot T_i^4)}{\alpha_{k,e}}}_{\text{longwave radiation flux from surrounding surfaces}}}{\underbrace{\frac{\varepsilon_{\text{IR,sky}} \cdot F_{\text{sky}} \cdot \sigma \cdot T_{\text{sky}}^4}_{\text{longwave radiation flux from skydolgvalmi}} - \frac{\varepsilon_{\text{IR,se}} \cdot \sigma \cdot T_{\text{se}}^4}_{\text{longwave radiation flux from buildings structure}}}}_{\alpha_{k,e}}} + \quad (2.1)$$

, where T_e – air temperature in the surrounding, $\alpha_{k,e}$ – convective heat transfer coefficient between the external surface of the building and environment, absorbed solar radiation: $\alpha_{s,e}$ – absorption of shortwave solar radiation, $G_{glob,\beta}$ – total/global solar radiation on the external surface of the building, longwave radiation flux of surrounding surfaces: $i, i=1\dots n$ – counter of surfaces in the surrounding (the sum equals n), ε_{IRi} – longwave heat radiation emissivity, σ – Stefan-Boltzmann constant ($5.67 \cdot 10^{-8} \text{ W}/(\text{m}^2 \text{ K}^4)$), FI_i – geometry factor of radiation exchange between surface i in the environment and the surface of the building (for horizontal surfaces $I = 0$), T_i – the temperature of surface i in the environment, longwave radiation flux from the sky: $\varepsilon_{IR,sky}$ – emissivity of longwave heat radiation from the sky, F_{sky} – geometry factor of radiation exchange between the sky and the surface the building, T_{sky} – temperature of sky, longwave radiation flux emitted by the building: $\varepsilon_{IR,se}$ – emissivity of longwave heat radiation from the surface of the building and T_{se} – surface temperature of the building.

A building is a complex thermodynamic body with constantly changing energy flows between the outside environment and different thermal zones within the building. To holistically determine the annual energy performance of a building, all influential factors need to be considered under unsteady conditions.

This can be achieved by using unsteady state building energy simulation tool for modelling building, heating, cooling, ventilation, lighting, and other energy flows, for example DesignBuilder (EnergyPlus) [39], [40]. Two main groups of the building energy simulation model are building elements (with equipment and occupants), and mechanical components (e.g. HVAC). The simulation tool comes with a graphical user interface (GUI).

2.2. Indoor thermal requirements

The main goal of this investigation is to improve the indoor thermal comfort in the building's indoor spaces. Therefore, this chapter is focused on presenting the indoor thermal requirements which are the key to evaluating the operation performance of the proposed system considering the effect on indoor conditions.

First, room air temperature (T_a) and room air velocity (v_{ar}) can be measured by various types of thermometers and anemometers. Second, mean radiant temperature (T_{mr}) is an average radiant temperature of all surrounding room surfaces and can be measured with black-globe and infrared thermometers. These quantities directly affect thermal comfort of the building user. However, their effect may be captured with only one quantity explaining the main temperature that building user experiences. This temperature is called operative temperature (T_{op}) and is defined in Equation 2.2 and Table 2.1 [41]. The A values are specified in Table 2.1.

$$T_{op} = A \cdot T_a + (1 - A) \cdot T_{mr} \quad (2.2)$$

Table 2.1: The values for A value in correspondence with the room air velocities v [41].

v [m/s]	< 0.2	0.2 to 0.6	0.6 to 1.0
A [/]	0.5	0.6	0.7

Furthermore, Table 2.2 specifies two types of the building, category with corresponding minimum and maximum operative temperatures recommended during the heating and cooling season indoors, respectively [37].

Table 2.2: Examples of recommended design values of the indoor temperature for design of buildings and HVAC systems [37].

Type of building	Category	Operative temperature [°C]	
		Minimum for heating (winter season), 1.0 clo	Minimum for cooling (summer season), 0.5 clo
Residential buildings: living spaces, sede-tary - 1.2 met	I	21.0	25.5
	II	20.0	26.0
	III	18.0	27.0
	IV	16.0	28.0
Single office (cellular office), sede-tary - 1.2 met	I	21.0	25.5
	II	20.0	26.0
	III	19.0	27.0
	IV	18.0	28.0

During the day, the system proposed within this study decreases the indoor air temperatures passively (nonmechanically) and thus, cools the indoor space. Figure 2.3 and Table 2.3 introduce 3 categories (I, II, III and IV) of the adaptive thermal comfort concept for nonmechanically cooled buildings shown with the regression of operative temperature (T_{op}) and the external running mean temperature (T_{rm}). For summer comfort range, the concept allows the inclusion of controlled air speed increases [37].

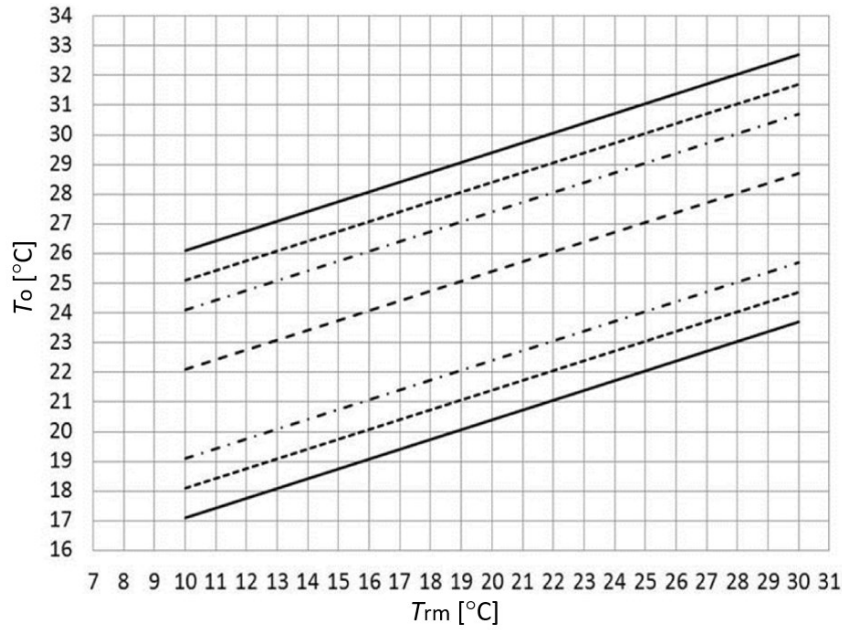


Figure 2.3: T_{rm} – outdoor running temperature and T_{op} – operative temperature.

Table 2.3: Maximum and minimum limit temperature of indoor operative temperatures [37].

Category I	upper limit:	$T_{l,max} = 0.33 \cdot T_{rm} + 18.8 + 2$
	lower limit:	$T_{l,min} = 0.33 \cdot T_{rm} + 18.8 - 2$
Category II	upper limit:	$T_{l,max} = 0.33 \cdot T_{rm} + 18.8 + 3$
	lower limit:	$T_{l,min} = 0.33 \cdot T_{rm} + 18.8 - 3$
Category III	upper limit:	$T_{l,max} = 0.33 \cdot T_{rm} + 18.8 + 4$
	lower limit:	$T_{l,min} = 0.33 \cdot T_{rm} + 18.8 - 4$

, where $T_{l,max}$ and $T_{l,min}$ are max and min limit temperature of indoor operative temperature.

Table 2.4 shows Predicted Mean Vote (PMV) and Predicted Percentage of Dissatisfied (PPD) [%] assessing thermal state of the body as a whole [37] in relation to the categories.

Table 2.4: Thermal state of the body as a whole [37].

Category	Thermal state of the body as a whole	
	PMV [I]	PPD [%]
I	$-0.2 < PMV < + 0.2$	< 6
II	$-0.5 < PMV < + 0.5$	< 10
III	$-0.7 < PMV < + 0.7$	< 15
IV	$-1.0 < PMV < + 1.0$	< 25

2.3. Phase change materials - presentation of concept

This chapter addresses the thermal behaviour of Phase Change Material (PCM). Figure 2.4 presents a theoretical diagram for pure substance/material without hysteresis and temperature interval of heat stored in material in dependence of its temperature during different states of matter. It can be observed, that while the reference material line doesn't change its inclination the PCM line becomes horizontal in the range of phase change. In the range of phase change, bonds between the material's molecules are changing and the PCM stores the latent heat.

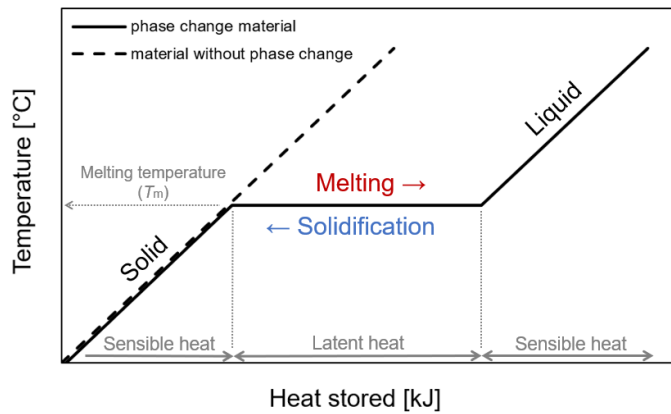


Figure 2.4: Phase change diagram (temperature and heat stored) [34].

The following Equation 2.3 shows the heat stored in the material (Q) during the solid phase.

$$Q = m \int_{T_{in}}^{T_m} c_p(T) dT \quad (2.3)$$

The following Equation 2.4 shows the heat stored in the material (Q) considering also the latent heat.

$$\frac{Q}{m} = \int_{T_{in}}^{T_m} c_{p,s}(T) dT + l \cdot f(T) + \int_{T_m}^{T_e} c_{p,l}(T) dT \quad (2.4)$$

, where m – mass of the material [kg], c_p – specific heat capacity of the material [J/(kg K)], $c_{p,s}$ – specific heat capacity of solid material [J/(kg K)], $c_{p,l}$ – specific heat capacity of liquid material [J/(kg K)], l – mass specific latent heat [J/kg], $f(T)$ – liquid fraction as a function of temperature (0-1) [/], T_{in} – initial material temperature [°C], T_m – melting temperature of the material [°C] and T_e – final temperature of the material [°C].

The phase change problem can be solved by different methods [43]. For example, it can be solved analytically with Stefan's problem with the temperature distribution in the homogenous substance. With enthalpy method there is no explicit phase change boundary defined, only the percentage of solidified substance. Also, the phase change can be covered in the specific heat of the material meaning that the phase change will be increased by the

latent heat of this same substance in a certain interval. Finally, the total enthalpy can be divided into specific heat and latent heat, while including the latter as a source or heat sink.

However, the melting and solidification of the PCM often doesn't occur at the exact same or only one single temperature as shown in Figure 2.4. This is due to two phenomena – hysteresis and mixing of more pure materials into one homogenous mixture of PCM to obtain the preferred thermal characteristics.

The hysteresis may be explained as the dependence of the state of a system on its history or the lagging of an effect behind the cause of this state [44]. Normally, the effect of hysteresis is shown by two curves which describe the course of the same phenomena (Figure 2.5). When modelling the hysteresis, two different functions which describe the material enthalpy within the phase change range need to be used.

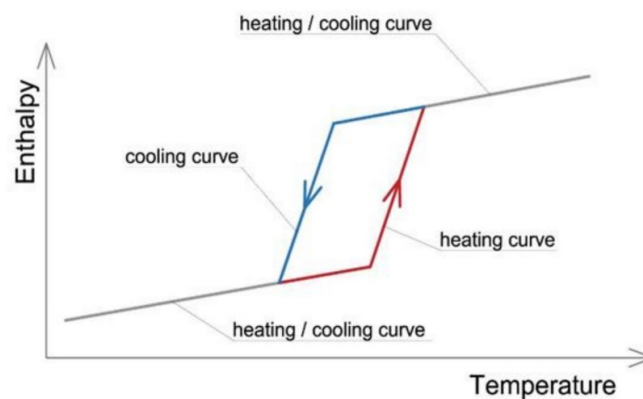


Figure 2.5: Phase change hysteresis process represented as a function of temperature [44].

Pure materials with different melting temperatures are often mixed into one homogenous material with the aim to obtain the thermal characteristics for a preferred application. An example of different melting temperatures is shown in Figure 2.6. It has to be noted, that the term 'Partial enthalpy' is used by the Rubitherm company and is not a commonly used term. Normally, the expert users would name it 'Heat stored in a temperature interval' or scientific users 'Enthalpy difference'.

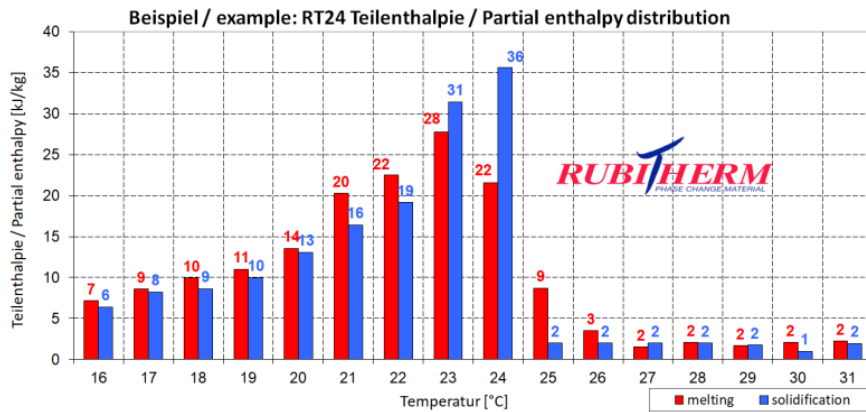


Figure 2.6: Partial enthalpy in relation to temperature for PCM type RT24 [45].

2.4. Numerical modelling of heat transfer PCM – air gap: nighttime solidification

This chapter elaborates the heat transfer from PCM to air in the air gap. Since this investigation was performed not only experimentally but also numerically with Computer Fluid Dynamics (CFD), the chapter presents the governing equations and principals met during the numerical modelling assumed in both numerical models (preliminary research in chapter 5.3 and numerical model in chapter 7) calculated with ANSYS Fluent [43], [46]. Further specifics of each model are presented separately in corresponding chapters.

2.4.1. Assumptions

Geometrical assumptions:

- The air flow in the air gap is parallel to the edge of the PCM plates. This leads to the first assumption: the changes in z-axis may be neglected.
- The second assumption: the airflow distribution in the channel is uniform. The air gap is divided into 5 geometrically equal channels and the simulation plane is in the middle of the channel.

Calculation model assumptions:

- **Air:**
 - The flow is defined incompressible (low airflow velocities) [46].
 - The flow is transient/time dependant [47].
 - In the models, laminar and turbulent flows were simulated, depending on the simulation model's geometry and airflow velocities [48].
 - Air is defined as Newtonian fluid with constant density (except at fluids with volume force $\rho \vec{g}$ – Boussinesq approximation), specific heat, thermal conductivity and viscosity [47].

- **PCM:**
 - Heat transfer is obtained only by means of conduction [49].
 - Latent heat is released or absorbed in the temperature range of the phase change [47].
 - Phase change temperature is fixed, and it is the material property [49].
 - In the models, hysteresis was considered – only the characteristics of solidification part of the DSC diagram were used [43].
 - The material is homogeneous and isotropic [49].
 - The material properties such as density and thermal conductivity are the same for the solid and liquid phase [47].

2.4.2. Conservation laws – air

The conservation laws state that a certain physical property does not change in the course of time within an isolated physical system. Therefore, for the air movement in the air gap the law of mass conservation, momentum conservation and conservation of energy apply.

Mass conservation equation and momentum conservation equation are presented for the stationary condition. However, because the heat transfer is non-stationary, the conservation of energy equation is presented with time dependency.

2.4.2.1. Mass conservation

For two-dimensional steady flow (velocity deviations in z-direction are negligible) and incompressible fluids (density deviation equals 0), the conservation of mass equation predicts that the rate of increase of mass in fluid element equals the net rate of flow of mass into element (Equation 2.5), where v_x – velocity of the air in x-direction [m/s] and v_y – velocity of the air in y-direction [m/s].

$$\frac{\partial v_x}{\partial x} + \frac{\partial v_y}{\partial y} = 0 \quad (2.5)$$

2.4.2.2. Momentum conservation

Newton's second law states that the rate of change of momentum equals sum of forces. Surface forces such as pressure and viscous forces.

Body forces, which act on a volume, such as gravity, centrifugal, or electromagnetic forces (Equations 2.6-2.13), where ρ – air density [kg/m^3], p – pressure [Pa], μ – dynamic viscosity [$\text{kg}/(\text{m s})$], μ_{turb} – turbulent viscosity [$\text{kg}/(\text{m s})$], μ_{eff} – effective dynamic viscosity [$\text{kg}/(\text{m s})$], g_x and g_y – components of acceleration due to gravity in directions x and y [m/s^2] and β_T – thermal volume expansion coefficient [1].

- **Laminar flow**

$$\frac{\partial \rho v_x}{\partial t} + \rho \left(v_x \frac{\partial v_x}{\partial x} + v_y \frac{\partial v_x}{\partial y} \right) = -\frac{\partial p}{\partial x} + \mu \left(\frac{\partial^2 v_x}{\partial x^2} + \frac{\partial^2 v_x}{\partial y^2} \right) + \rho(1 - \beta_T T_a) g_x \quad (2.6)$$

$$\frac{\partial \rho v_y}{\partial t} + \rho \left(v_x \frac{\partial v_y}{\partial x} + v_y \frac{\partial v_y}{\partial y} \right) = -\frac{\partial p}{\partial y} + \mu \left(\frac{\partial^2 v_y}{\partial x^2} + \frac{\partial^2 v_y}{\partial y^2} \right) + \rho(1 - \beta_T T_a) g_y \quad (2.7)$$

- **Turbulent flow**

$$\frac{\partial \rho v_x}{\partial t} + \rho \left(v_x \frac{\partial v_x}{\partial x} + v_y \frac{\partial v_x}{\partial y} \right) = -\frac{\partial p}{\partial x} + \mu_{\text{eff}} \left(\frac{\partial^2 v_x}{\partial x^2} + \frac{\partial^2 v_x}{\partial y^2} \right) + \rho(1 - \beta_T T) g_x \quad (2.8)$$

$$\frac{\partial \rho v_y}{\partial t} + \rho \left(v_x \frac{\partial v_y}{\partial x} + v_y \frac{\partial v_y}{\partial y} \right) = -\frac{\partial p}{\partial y} + \mu_{\text{eff}} \left(\frac{\partial^2 v_y}{\partial x^2} + \frac{\partial^2 v_y}{\partial y^2} \right) + \rho(1 - \beta_T T) g_y \quad (2.9)$$

$$\mu_{\text{eff}} = \mu + \mu_{\text{turb}} \quad (2.10)$$

$$\mu_{\text{turb}} = f(k, \omega) \quad (2.11)$$

Transport equations for the standard k - ω model based on Reynold average Navier-Stokes (RANS) equations follow bellow (Equations 2.12-13), where k – turbulence kinetic energy [m^2/s^2], ω – specific dissipation rate [m^2/s^3], P_k – generation of turbulent kinetic energy [m^2/s^2] and α , β , β^* , σ_k and σ_ω – turbulent model coefficients [50].

$$\begin{aligned} \rho \frac{\partial k}{\partial t} + \rho \left(v_x \frac{\partial k}{\partial x} + v_y \frac{\partial k}{\partial y} \right) &= P_k - \rho \beta^* k \omega + \frac{\partial}{\partial x} \left[\left(\mu + \frac{\mu_{\text{turb}}}{\sigma_k} \right) \frac{\partial k}{\partial x} \right] \\ &+ \frac{\partial}{\partial y} \left[\left(\mu + \frac{\mu_{\text{turb}}}{\sigma_k} \right) \frac{\partial k}{\partial y} \right] \end{aligned} \quad (2.12)$$

$$\begin{aligned} \rho \frac{\partial \omega}{\partial t} + \rho \left(v_x \frac{\partial \omega}{\partial x} + v_y \frac{\partial \omega}{\partial y} \right) &= \alpha P_k \frac{\omega}{k} - \beta \omega^2 + \frac{\partial}{\partial x} \left[\left(\mu + \frac{\mu_{\text{turb}}}{\sigma_\omega} \right) \frac{\partial \omega}{\partial x} \right] \\ &+ \frac{\partial}{\partial y} \left[\left(\mu + \frac{\mu_{\text{turb}}}{\sigma_\omega} \right) \frac{\partial \omega}{\partial y} \right] \end{aligned} \quad (2.13)$$

Wilcox standard k - ω model assumes the following k - ω model constants to be: $\alpha = 0.52$, $\beta^* = 0.09$, $\beta = 0.072$ and $\sigma_k = \sigma_\omega = 2$.

2.4.2.3. Conservation of energy

The first law of thermodynamics states that the rate of change of energy of a fluid particle is equal to the rate of heat addition plus the rate of work done (Equation 2.14), where \vec{v}_a – air velocity vector [m/s], T_a – air temperature [$^\circ\text{C}$] and λ_a – thermal conductivity of air [$\text{W}/(\text{m K})$]. Radiation and internal heat gains (chemical reactions) are neglected, two-dimensional flow and constant air properties are considered.

$$\rho_a \cdot c_{p,a} \left(\frac{\partial T_a}{\partial t} \right) + \rho_a \left(v_{ax} \frac{\partial T_a}{\partial x} + v_{ay} \frac{\partial T_a}{\partial y} \right) = \lambda_a \left(\frac{\partial^2 T_a}{\partial x^2} + \frac{\partial^2 T_a}{\partial y^2} \right) \quad (2.14)$$

2.4.3. Conservation laws – PCM

Since, the convection in PCM is not present, the use of mass conservation equation and momentum conservation equation are not required. For the calculation of heat transfer in PCM only the application of non-stationary conservation of energy equation is needed.

2.4.3.1. Conservation of energy

As the material is not moving – solidus state, for PCM only the equation of conservation of energy applies (Equations 2.15 and 2.16), where ρ_{PCM} – density of PCM [kg/m^3], $c_{p,\text{PCM}}$ – specific heat capacity of PCM [$\text{J}/(\text{kg K})$], T_{PCM} – PCM temperature [$^{\circ}\text{C}$] and λ_{PCM} – thermal conductivity of PCM [$\text{W}/(\text{m K})$]. The phase change is included in the quasi-specific heat and the volumetric heat sources and heat generation from chemical reactions are not included ($S_h = 0$). Equation 2.16 is further explained with Figure 2.8 and Equation 2.9.

$$\rho_{\text{PCM}} \left(\frac{\partial c_{p,\text{PCM}} T_{\text{PCM}}}{\partial t} \right) = \lambda_{\text{PCM}} \left(\frac{\partial^2 T_{\text{PCM}}}{\partial x^2} + \frac{\partial^2 T_{\text{PCM}}}{\partial y^2} \right) \quad (2.15)$$

$$c_{p,\text{PCM}} = f(T_{\text{PCM}}) \quad (2.16)$$

2.4.4. Finite volume method

The Finite Volume Method (FVM) is a discretization technique used in CFD. First the domain is divided into a number of control volumes (cells) with the target variable located in the centroid of the control volume (control volume formulation of analytical fluid dynamics) - Figure 2.7 [51], [52]. Afterwards, the differential form of the governing equations is integrated over each control volume. Then, the interpolation profiles are assumed to describe the variation of the concerned variable between cell centroids. The final equation is called discretization equation and it expresses the conservation principle for the variable inside the control volume.

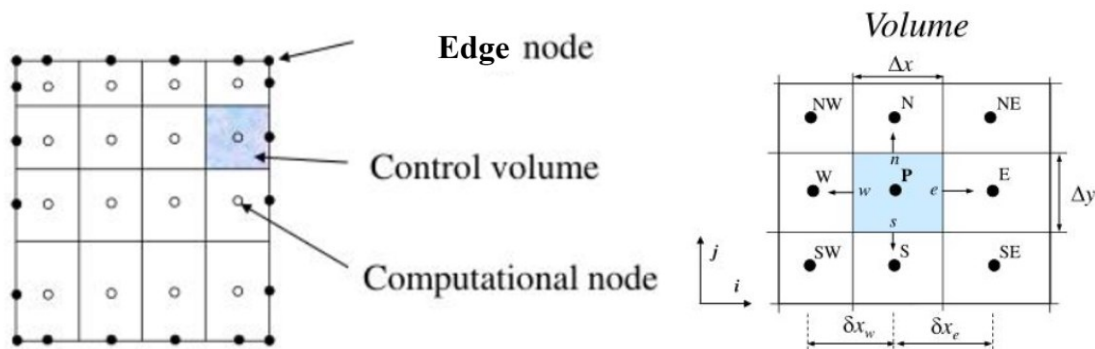


Figure 2.7: Space discretization in FVM [51].

Equation 2.17 presents the transport equation translated to algebraical form for numerical solving [43], [53].

$$\int_V \frac{\partial \rho \phi}{\partial t} dV + \oint \rho \phi \vec{v} d\vec{A} = \oint \Gamma_\phi \nabla_\phi d\vec{A} + \int_V S_\phi dV \quad (2.17)$$

Where ϕ - constant characteristic of a solvent, ρ - density [kg/m³], \vec{v} - velocity vector [/], \vec{A} - surface [/], Γ_ϕ - diffusion coefficient for ϕ [m²/s], ∇_ϕ - gradient ϕ [/], and S_ϕ - source or sink per unit of surface [W/m³].

By dividing the domain into control volumes and integrating the transport equation for each control volume separately, a system of linear equations that describe the conservation laws based on the individual control volume was obtained. This procedure is called discretization. Equation 2.18 presents the discrete form of equation.

$$\frac{\partial \rho_f \phi_f}{\partial t} V + \sum_f^{n_{faces}} \rho_f \vec{v}_f \phi_f \vec{A}_f = \sum_f^{n_{faces}} \Gamma_\phi \nabla_{\phi_f} \vec{A}_f + S_\phi V \quad (2.18)$$

n_{faces} - number of areas [/], $\sum_f^{n_{faces}} \rho_f \vec{v}_f \vec{A}_f$ - mass flow rate across the surface [kg/m³], ϕ_f - value of ϕ brought across surface f [/], \vec{A}_f - area of surface f [/], ∇_{ϕ_f} - gradient ϕ on the surface f [/] and V - volume [m³].

2.4.5. Specifics in numerical modelling

- Boundary layer – air-PCM

The plate was formed by the aluminium case encapsulating the PCM. The thickness of the aluminium layer (red line) in contact with the ventilated air gap was 1 mm and it was neglected in the geometric model as shown in Figure 2.8. In ANSYS Fluent model this boundary condition was automatically generated as ‘Coupled’.



Figure 2.8: The numerical simulation principle sketch of the air and PCM layer.

The calculation principle is shown in Equation 2.19, where \vec{n} is the normal on the interface between air and PCM layer.

$$\lambda_{PCM} \frac{\partial T}{\partial n} = \lambda_a \frac{\partial T}{\partial n}, T_{PCM} = T_a \quad (2.19)$$

- Simulation parameters

The rest of simulation parameters are shown in Appendix D.

- Simulation equipment

The meshing and simulations were carried out on ASUS VivoBookPro on 6 cores of Intel i7 central processor unit with NVIDA graphic processor unit.

2.5. Ventilation heat losses

The following chapter presents the recommended and determination of heat losses through ventilation for indoor air quality.

The recommended ventilation rates for 4 categories based on the expected percentage of dissatisfied in relation to airflow per person are presented in Table 2.5 [37].

Table 2.5: Basic required ventilation rates for diluting emissions (bio effluents) from people for different categories [37].

Category	Expected Percentage Dissatisfied [%]	Airflow per person [l/s/pers]
I	15	20
II	20	14
III	30	8
IV	>30	<5.5

Ventilation heat losses (Q_v) are determined based on the Equation 2.20, where $c_{p,a}$ – specific heat of air, m_a – mass of air that has moved out of the building, T_{ai} – inlet air temperature and T_{ao} – outlet air temperature.

$$Q_v = c_{p,a} \cdot m_a \cdot (T_{ao} - T_{ai}) \quad (2.20)$$

3. Literature review

3.1. Enhancing the heat transfer to improve the PCM energy performance

Low thermal conductivities of PCM prolong the charging and discharging cycles [34]. Therefore, one of the main challenges of PCM integrated into building elements (building element is major part of a building such as a wall, floor or roof) is heat transfer enhancement [35]. It has been shown that building-integrated PCM have high benefits for passive winter use [54]. Meanwhile, many studies showed [55] that problems occur on summer nights when PCM does not solidify completely. The thick layers of thermal insulation prevent the heat losses from the building, and the heat stored in the PCM is discharged indoors. The incomplete solidification prevents the material from using its entire melting capacity during the daytime, which results in the decreased cooling capacity of a passive system, increased use of energy by active systems for cooling and lower energy-saving potential [56].

Therefore, it is important to investigate the techniques to enhance their solidification cycle and improve their performance. The improvement can be achieved either by improving the material properties or physically improving the heat transfer enhancement approach.

3.1.1. Addition of metal structures

Numerous studies have investigated the addition of metal (high-conductivity) particles into PCM materials structure. For example, metal additives may be added to the paraffin wax [57]. Positive results were found by investigating the metal foams and cascaded metal foams with nanoparticles [58], [59]. To the bio-based PCM was added recycled graphite [60], [61]. Several studies explored nano-technological benefits with metal additives with PCM-infused graphite with the addition of aluminium nanoparticles [62] or CuO nano-additives [63]. Nevertheless, PCM may be nano-encapsulated and added highly conducted expanded graphite nanosheets [64].

3.1.2. Water-based systems

Studies have frequently investigated the PCM structural components improved with water systems. For example, numerous studies coupled the floor heating systems imbedded in PCM-improved floor material resulting in decreased energy use for space heating [65]–[67]. In addition, Sinka et al. experimentally tested the phase change material chilled ceiling in a warm-summer humid continental climate and showed that the highest efficiency of PCM was obtained when it was used in conjunction with capillary ceiling cooling; it decreased the indoor temperature by 3–4 °C during the day [54]. Furthermore, similar PCM cooling ceilings were investigated by Weinläder et al. and Yasin et al., who showed highly beneficial results reflected in the good regeneration behaviour of two PCM cooling ceiling constructions [68], [69].

3.1.3. Summer overhang

Taking advantage of the bioclimatic design coupled with the smart geometrical shaping of external building elements, in 2012, Arce et al. attempted to overcome the issue of nighttime solidification by decreasing the effect of solar radiation with the addition of awnings [70]. They experimentally tested and discussed the effect of microencapsulated PCM integrated into the concrete walls of a cubicle positioned Spain (Lleida) and showed that the peak temperatures could be reduced by about 6 %, and the PCM activeness was prolonged by 4 % of the time or longer.

3.1.4. Air discharge concepts

Finally, performance may also be improved by discharging PCM with air (Figure 3.1). On the one hand, the heat from the PCM can be released by means of total volume nighttime ventilation (1); on the other, the PCM solidification can be accelerated locally by ventilating the layers in structural complexes adjacent to the PCM layer (2) or to join the building element with a free cooling active thermal energy storage unit (3).

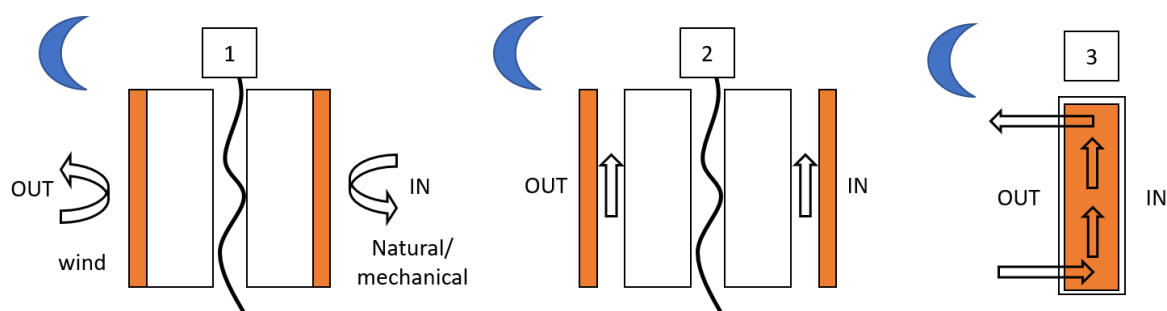


Figure 3.1: PCM (orange) and load-bearing wall (white) with air discharge concepts: 1) total volume nighttime ventilation, 2) ventilated air gap, and 3) free cooling active thermal energy storage unit.

While other related reviews are focused on broader or different sets of topics, the main advantage of this review is presenting only the research on the topic of PCM for cooling application improved by air discharge concepts integrated into the building elements and not as a self-standing storage unit [71]. For example, Arce et al. focus only on microencapsulated PCM, not other forms [70], Soares et al., Akeiber et al. and Saffari et al. only review passive systems and not active [72]–[74], Iten et al. focus also on heating technologies and re not focused only on PCM integrated in the building elements [75], Oró et al., Souayfane et al., Osterman et al. and Alizadeh and Sadrameli not focused only on the building integrated systems for cooling [76]–[79], Zhou et al., Faraj et al. and Zhang et al. have different focus and also include water-based systems and radiant ceilings [80]–[82], Bastani et al. focus on numerical simulation of wallboards with no specific local ventilation systems [83] and Solgi et al. review only total volume night ventilation strategies where the focus is not on PCM [84].

3.2. Nighttime ventilation

The PCM for the passive cooling of the buildings are normally positioned in the external or internal layers of the building envelope (Figure 3.2). The externally positioned PCM are placed in the roof or in the facades and have higher melting-point temperatures than internally positioned PCM in ceilings, walls, or floors. Due to improved indoor air mixing, the total volume ventilation may enhance the PCM performance during the daytime. However, it is even more crucial during the night when, with the increased airflow rates of cool outdoor air mechanically or naturally removes the excess heat, preventing the complete solidification of PCM.

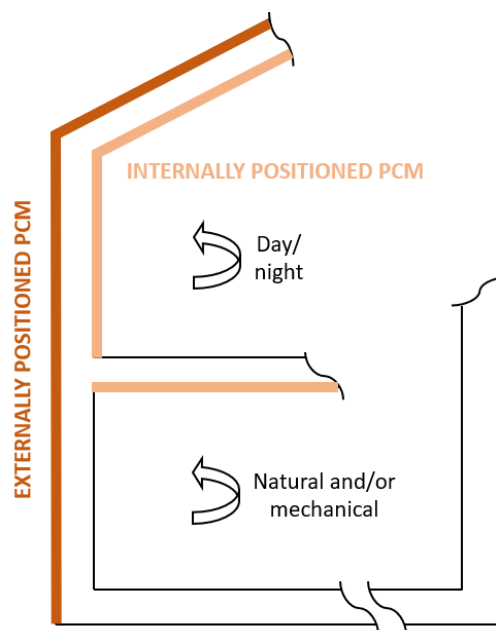


Figure 3.2: Total volume nighttime ventilation principles with location of PCM in building elements.

3.2.1. Natural nighttime ventilation

The passive solidification enhancement of the macro-encapsulated PCM (Rubitherm RT24 - 15 mm thick) was numerically investigated by Prabhakar et al. with natural nighttime ventilation in the office building [56]. Two control strategies for windows were tested; in the first one, the windows were 50 % open from 24:00 to 6:00, and in the second one, the window was open up to 50 % when the outdoor dry bulb temperature was lower than the zone temperature and thermostat setpoint temperature (by 3 °C). After testing 15 different locations around the world. With the addition of nighttime ventilation, the daily PCM effectiveness increased from 3.32 % to 25.62 %.

Furthermore, an experimental and numerical study of the effect of the individual (summer) and combined (autumn) operation of passive PCM systems was carried out in Tehran by Memarian et al. [85]. They tested DuPont Energain (5 mm thick PCM panel) and numerically BioPCM (21 °C, 23 °C, 25 °C, 27 °C and 29 °C) at natural ventilation rates of 0 air change per hour (ACH), 1 ACH, 3 ACH, 5 ACH, 7 ACH and 10 ACH. The PCM with a melting point of 29 °C coupled with natural nighttime ventilation at 5 ACH reduced the yearly energy use by 15 % and the daily PCM cooling by 20 % period-to-period. In spring, the PCM with melting temperature of 25 °C.

In four Italian cities (Palermo, Naples, Rome and Milan), Piselli et al. simulated the control of the natural ventilation [86]. Depending on the location, they optimized the melting temperature of Knauf PCM Smartboard (1.25 cm thick, 30 %wt microencapsulated PCM) and tested different natural ventilation control strategies. They learned that PCM can reduce the annual cooling load by 300 kWh/year in milder climates, and while all nighttime ventilation strategies improved the PCM discharge cycle, the control by indoor/outdoor temperature difference shows the highest energy cooling reduction in all studied locations.

In western China, Liu et al. numerically investigated the effect of natural night-time ventilation (NV) in 10 cities (from very cold to very hot) by changing the melting point of BioPCM in thickness of 20 mm from 19-33 °C [87]. They separately simulated the reference case and the cases in the presence of only NV, only PCM and both, NV and PCM. Finally, they compared the presence of PCM with NV to NV alone and concluded that the PCM had a greater effect in transition periods than in hot summer periods. In Turpan, Nanning, Hechi, and Chongqing, the discomfort hours were reduced by 16 %, 19 %, 28 %, and 48 %, respectively, while in hot summer only from 0-11 %.

Six different cities in Kazakhstan (Nur Sultan, Karaganda, Kokshetau, Almaty, Aktobe and Atyrau; extremely hot to cold) were selected to simulate the effect of cooling by nighttime ventilation in combination with PCM (5 mm thick) with melting temperatures of 26 °C, 28 °C, 30 °C and 32 °C placed on the inner side of the roof [88]. Adilkhanova et al. scheduled the natural ventilation at 8 ACH from 19:00 until 07:00 operating only when the temperature difference between the indoor air temperature was 2 °C or higher from the outdoor. Over the more extended time, the nighttime ventilation with PCM generally resulted in maximum operative temperature reduction up to 5 °C (the best results were reached in Almaty and Aktobe with PCM 28 + night ventilation).

Jamil et al. investigated the application of a 0.02 m thick layer of BioPCM25 to the ceiling and/or wall of the rooms under the Melbourne (Australia) climate conditions [89]. The

window was opened to 20 % of the total window area from 19:00 to 07:00 when the outdoor air temperature was lower than 22 °C. With the addition of night ventilation without mixing, the maximum daily temperature was reduced by over 2 °C.

3.2.2. Natural and mechanical nighttime ventilation

Under Lativan summer conditions, Sinka et al. [54] tested the performance of two PCM (DuPont Energain and BioPCMQ25M51) materials integrated into five different test buildings (made out of different materials) coupled with various HVAC systems. In the nighttime, the mechanical ventilation rate (0.76 ACH) was increased, and the windows opened (19:00–07:00). Over the night, this strategy could completely solidify BioPCM, which ensured the improved indoor thermal environment (by around 2 °C) during the day.

From July to October in Toronto (Canada), Berardi and Soudian studied the effectiveness of PCM in retrofitting high-rise apartment buildings with high window to wall ratios (80 %) [90]. BioPCM (25 °C) and DuPont Energain were placed in the walls and ceiling of one test cell while the other cell was not PCM-modified. In summer, they numerically investigated the night ventilation rates of 1 m³/s (2 ACH), 0.16 m³/s (3 ACH), 0.26 m³/s (5 ACH), 0.37 m³/s (7 ACH) and 0.53 m³/s (10 ACH) in operation from 00:00 to 07:00. The performance of controlled mechanical ventilation was more accurate compared to the natural and decreased the number of discomfort hours when the operative temperatures were higher than 26 °C or lower than 21 °C. Generally, the PCM system could lower the peak indoor and surface temperatures by up to 6 °C.

In Auckland, New Zealand, Bai et al. numerically investigated the PCM PureTemp20 applied to the floor, ceiling and internal walls and tested its cooling performance combined with natural and mechanical ventilation (set point temperature, $T_{\text{set}} = 26$ °C) [91]. Natural ventilation was tested between 2 ACH and 10 ACH; 10 ACH increased its heat transferability to 46 W/K, and the maximum room temperature drop by 2.1 °C. Furthermore, the mechanical ventilation was tested with flow rates up to 40 ACH; at 20 ACH, the maximum room temperature was decreased by 2.8 °C.

Xiang and Zhou [92] introduced a novel window-based cooling unit filled with PCM. During the night (21:00–04:00), the unit is shut down, and the PCM releases heat by means of natural ventilation (wind) (Figure 3.3 a). In the daytime, the unit is lifted, and the fans actively melt the PCM and cool the indoor air (b). According to the Beijing (China) summer weather data, the inlet velocities of the main wind direction are 0.5 m/s, 1 m/s, 2 m/s. The optimum thickness of the PCM slab where the PCM solidified completely was 5 mm. With the unit, the indoor temperatures dropped by 3.3 °C.

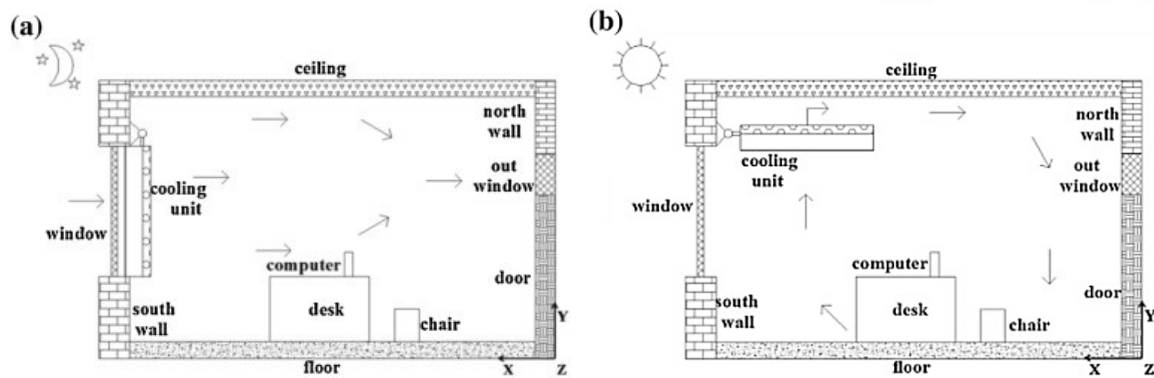


Figure 3.3: The window-based cooling unit a) nighttime and b) daytime [92].

Mechouet et al. placed the 6 mm, 18 mm, and 30 mm PCM layer in multilayer nylon/PE foil pouches between the brick layers [93]. They numerically investigated it in six different Moroccan cities (Agadir, Marrakech, Tangier, Fes, Ifrane and Errachidia). In the nighttime (21:00–6:00), they added the effect of natural ventilation by keeping the window opened at 50 % of their surface at all times; in other cases, they added the effect of mechanical ventilation at 0.5 ACH, 1.5 ACH, 3 ACH and 6 ACH (19:00–24:00) when the outside temperature did not exceed 26 °C. The results showed that with 18 mm thick PCM layer and mechanical ventilation of 3 ACH compared to natural ventilation, only the indoor temperatures and the cooling energy use dropped by 1.92–2.33 °C and 19.5–62.9 %, respectively.

3.2.3. Mechanical nighttime ventilation

In Auckland, New Zealand, Barzin et al. [94] tested the performance of nighttime ventilation in two identical wooden huts, where one was improved with 13 mm thick PCM-impregnated gypsum boards (Pure Temp20). During the day, the PCM system was combined with AC to additionally decrease the indoor temperatures to in thermal comfort standards recommended indoor summer temperatures (24–26 °C). The effect of night-time ventilation was tested at a nominal flow rate of 300 m³/h (21:00–07:00) with a 20 W fan. By using nighttime ventilation, the weekly electricity use for AC dropped by 73 %.

Evola et al. used the 2 cm thick Micronal23® board from BASF applied to three internal partition walls while the external wall was covered by the large glazed surface [95]. The daily ventilation rate is kept constant (0.5 ACH), and in the night from 21:00 to 06:00, it was tested for higher ventilation rates (2–8 ACH). The results showed that night ventilation of 4 ACH enabled the PCM daily activation to 80 % in both Chambery and Catania.

A similar numerical study by Costanzo et al. investigated the effect of the position and thickness (1.95 mm and 3.57 mm for M27 and M51, respectively) of the PCM layer in the drywall partition systems of lightweight office buildings in summer [96]. The building was simulated with EnergyPlus on three different European locations Rome, Italy, Vienna, Austria, and London, UK. During the night, the building was mechanically ventilated with

a rate of 2–4 ACH (from 21 to 7 h). The PCM system reduced the peak cooling load by 10 %-15 %.

In addition, Pajek et al. carried out numerical analysis of the energy use and thermal response of the buildings placed in Helsinki, Finland, Vienna, Austria, and Madrid, Spain [97]. Several types of external walls were studied in a single-family house in which some were added 25 mm thick PCM a gypsum PCM board. Normally, the ventilation rate was fixed to 0.7 ACH during the daily and nighttime cycles. However, to analyse the intense ventilation during the night and certain overheated periods over the day (air temperature over 23 °C), they increased the ventilation rate to 1.5 ACH, 3 ACH, ACH, 7 ACH, and 14 ACH. In all investigated cases, the increase in ventilation had a favourable effect on PCM operation; consequently, the air temperature in the room dropped up to 3.8 °C.

A survey by Solgi et al. with a numerical model located in Yazd, Iran shows that the combination of cooling with natural night ventilation (24:00 pm to 7:00 am) with untreated air can reduce the use of electricity by as much as 47 % (with 15 ACH and its temperature below 30 °C) and that the southern, eastern, and western walls and ceilings were appropriate for the installation of 1 cm thick PCM with a melting point at 27 °C [98]. Interestingly, the floor embedded in PCM increased the energy needed for cooling.

Ascione et al. in the five different Mediterranean climates (Ankara, Turkey, Athens, Greece, Naples, Italy, Marseille, France, and Seville, Spain) tested the effect of the night ventilation from 19:00 to 7:00 at 3 ACH on the solidification of 3 cm PCM plaster layer (constant daytime rate 0.5 ACH) [99]. In Ankara, the PCM with a melting temperature of 29 °C, the energy need for cooling was reduced by 7.2 % and by up to 3.0 % in Seville and Naples. The number of occupied hours in the comfort zone increase from 11.2 % to 21.9 % in Athens and from 32.9 % to 51.0 % in Marseille.

In Athens, Thessaloniki, and Heraklion, Greece, Karaoulis investigated the addition of the PCM (thickness 0.03 m) with a melting temperature of 29 °C in an external wall, internal wall, or ceiling with Design Builder software [100]. The night discharge mechanical ventilation rate was set to 1.5 ACH from 18:00 to 8:00. The study underlined that the greatest effect was obtained when PCM was applied to the ceiling and that the cooling savings due to night ventilation increased by 5-7 times.

Nazi et al. numerically analysed a high-rise office building located in Putrajaya, Malaysia with BioPCM (melting temperature of 29 °C) applied in the ceiling [101]. Mechanical ventilation was turned on after office hours between 17:00 and 07:00. When the daily cooling set point was set to 26 °C, PCM alone reduced only 22.18 % of the cooling load and with nighttime ventilation present up to 49.21 %.

Zhou et al. numerically investigated 20 mm thick shape-stabilized PCM placed on the ceiling and four walls of the office building under climatic conditions of Beijing, China [102]. During the day, the rooms were ventilated between 8:00 and 18:00 at 2 ACH and the rest was the night ventilation. The results for the 2 cm thick board with melting temperature of 26 °C and max ventilation rate tested 40 ACH (among other tested 0 ACH, 10 ACH, 20 ACH and 30 ACH) revealed that, due to night ventilation, the plates could decrease the daily maximum temperature by up to 2 °C. Two years later, they also

determined the energy performance of PCM layer (0.5 cm) while adding an active daily cool-supply system activated between 8:00 and 18:00 to maintain the maximum indoor air temperature below 28 °C [103]. Compared to the case without solutions, the addition of night ventilation (40 ACH) accounts for a 76 % reduction in daytime energy consumed for cooling and with ventilation alone by 66.4 %. The coefficients of performance (COPs) of night ventilation for cases with and without PCM are 7.5 and 6.5, respectively.

Soudian and Berardi [104] placed PCM in building wall and ceiling as joint layers of DuPont Energain and BioPCM25 and tested its cooling performance in the climates of Toronto, Canada and New York, U.S.A. They investigated different melting periods (3 h, 5 h, 7 h and 9 h). However, only a small energy saving of 1.6 % was observed when doubling the ventilation flow rate from 5 ACH to 10 ACH (7 h period). In New York, the ventilation flow rate of 10 ACH increased the solidification rate for 45 % compared to the best-case scenario of T_{set} variation.

In Seoul, South Korea, Seong et al. numerically analysed the addition of 0.64 cm thick layer of paraffin-based PCM (hexadecane, heptadecane, dodecanol, and octadecane with melting points of 20 °C, 21 °C, 24 °C, and 29 °C, respectively) on the inner side of the external wall [105]. The effect of night ventilation on cooling was considered determined by scheduling the ventilation between 00:00 and 07:00, when the outdoor air temperature is 2 °C lower than indoor. The daily cooling setpoint (T_{set}) was set to 26 °C. Under these conditions, the night ventilation decreased the annual load by 7.94 % (dodecanol) and the peak load by 10.15 % with the highest indoor temperature drop at 0.19 °C (octadecane).

Qu et al. [106] investigated four types of PCM positioned in the ceiling, floor and wall under six different Chinese climate conditions (Lijiang, Weifang, Wuhan, Hohhot, Yan'an, and Guangzhou). There were four different PCM layer configurations (outside, middle, middle and inside, and inside the envelope) with thicknesses of 1 cm, 3 cm, 5 cm, and 7 cm, respectively. The night ventilation operated at 3 ACH between 21:00 and 07:00. The results showed that the most important influential parameter was PCM envelope type (Wall and Ceiling), PCM layer layout (inner layer) and PCM type (BioPCMTM23) and the PCM layer thickness (7 cm). Doing so, they obtained considerable energy-saving effects (the energy-saving rate is 4.8–34.8 %).

The performance of original PCM Infinite-RTM- R29 with a melting temperature of 29 °C was tested for three further melting temperature variations ($T_m = 27$ °C, 28 °C, and 30 °C) and numerically investigated in Penang Island, Malaysia by Al-Absi et al. [107]. The thickness of the PCM layer was adapted to 6 mm, 12 mm, and 18 mm and combined with night ventilation at 8 ACH. The presence of night ventilation in combination with 18 mm PCM ($T_m = 27$ °C) reduced the maximum daily indoor temperature peaks by up to 4.78 °C and monthly mean temperatures in the range between 3.43 °C and 1.53 °C.

3.3. Ventilated building elements

Since the total volume ventilation does not supply the air (with high velocities) directly to the PCM panels, large amounts of air must be provided for any considerable discharge effect. However, the primary task of ventilation is to supply people with clean air; therefore, it is also difficult to meet the needs of enhancing the PCM solidification simultaneously. Thus, the total volume ventilation method can also be energy consuming. For this purpose, the following description presents the ventilated building elements. Within this chapter, the elements ventilated by ceiling fans, naturally or mechanically ventilated air gaps in the vicinity of the PCM layer and thermal storage incorporated into the building elements suitable for cooling are presented. Figure 3.4 shows the conceptual groups of ventilated building elements improved with PCM for cooling application (building-integrated photovoltaic (BiPV)).

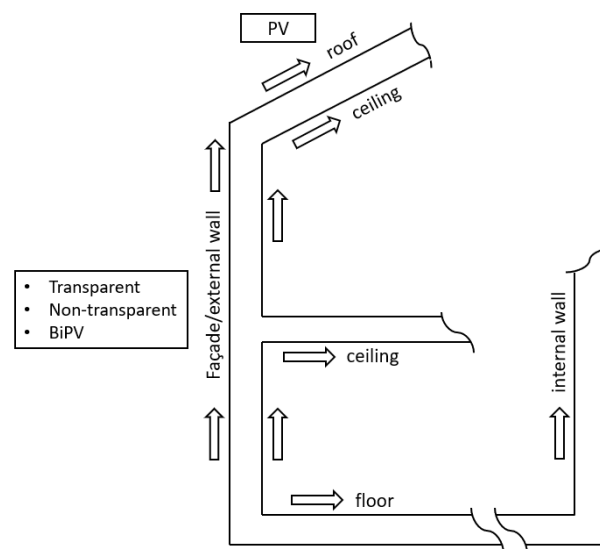


Figure 3.4: Ventilated building elements with PCM.

3.3.1. PCM-improved ventilated Roofs

PCM are often placed in the building envelope roof or facade because these parts are in direct contact with solar radiation. For instance, in Tianjin, China, Hou et al. and Li et al. experimentally tested the thermal performance of a composite phase change ventilated roof [108], [109]. The roof has two layers of PCM mixed into the concrete (Figure 3.5 and Figure 3.6). The first layer is in contact with the exterior environment covering the load-bearing roof (melting temperature, $T_m = 32.55\text{ }^\circ\text{C}$). Beneath, there is an air layer (20 cm) that is ventilated by natural means (wind) at night, and the second layer of PCM also helps to discharge the heat. The second layer is in contact with the interior environment ($T_m = 24.12\text{ }^\circ\text{C}$) and has embedded cooling water pipes. Among the studied cases, in comparison to the outdoor air temperature, the system reduced the indoor air temperatures by 34.4–

47.0 % (3.74–8.2 °C), which results in a very high potential energy-saving rate of 89.6–113.2 %.

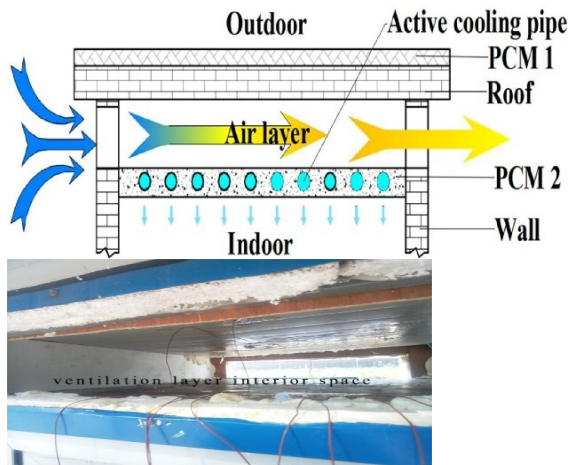


Figure 3.5: Composite phase change ventilated roof [108].

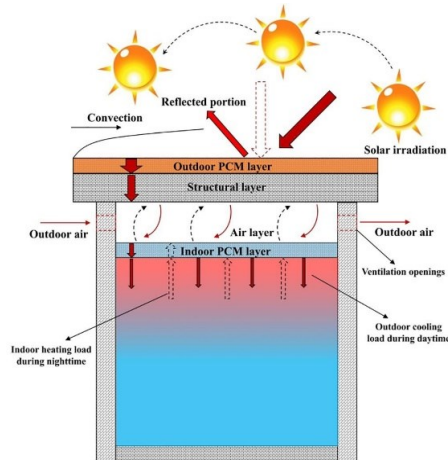


Figure 3.6: Ventilated roof composed with multiple phase change material (VR-MPCM) [109].

PCM are known to improve the electricity production of PV by accumulating some of its heat, even when they are not ventilated [110]. However, Lin et al. in Wollongong (Australia) numerically investigated (TRNSYS) an inclined roof ceiling ventilation system enhanced by solar photovoltaic (PV) thermal collectors and PCM for heating and cooling applied to a timber single-family building in Sydney [111]. The roof consists out of two PCM layers and two ventilated layers, as shown in Figure 3.7. The PV layer is in contact with the exterior environment, and its performance is enhanced by the ventilated layer (*PVT air channel*). The ventilated layer is followed by the thermal insulation and, afterwards, by a sequence of two more layers of PCM divided by the mechanically ventilated air layer. Both PCM layers consist of PCM bricks ($T_m = 24\text{ °C}$) with a thickness of 1 cm. The system was investigated for summer and winter conditions; the results indicated that the design is more suitable for winter usage. The coefficients of thermal comfort enhancement increased from zero to max. 0.9921 and max. 0.7876 in winter and summer, respectively.

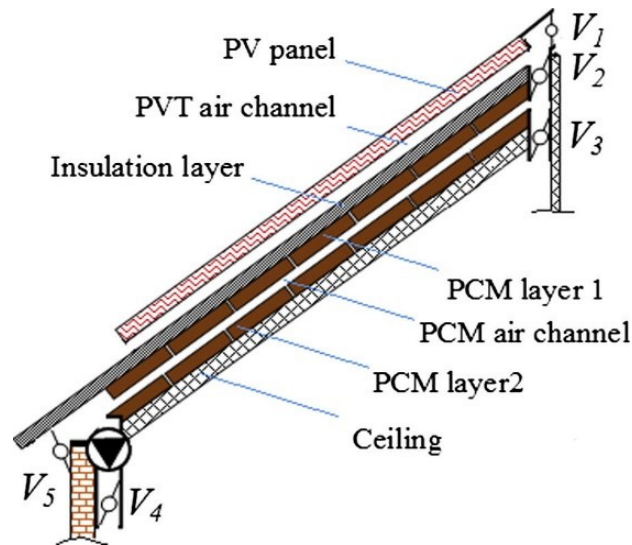


Figure 3.7: Ceiling ventilation system enhanced by solar photovoltaic thermal collectors and phase change materials [111].

3.3.2. PCM improved ventilated ceilings

Because the warm air in an indoor space dilutes upwards, the application of the PCM to the ceiling is very common. For example, Alizadeh and Sandrameli experimentally investigated the indoor thermal comfort of a PCM-based storage system integrated with ceiling fan ventilation [112]. The experiment was performed in summer and winter in Teheran (Iran), where the ceiling fan of the test cell was thermally improved with PCM ($T_m = 27\text{ }^\circ\text{C}$), as shown in Figure 3.8. The experimental results were validated with DesignExpert® 7.0.0 to determine optimum experimental condition parameters: inlet air temperature and humidity, fan rotating speed, fan distance from ceiling surface and PCM slab thickness. The results show that the peak indoor temperatures in the summer with the addition of PCM decreased by $2.5\text{ }^\circ\text{C}$.

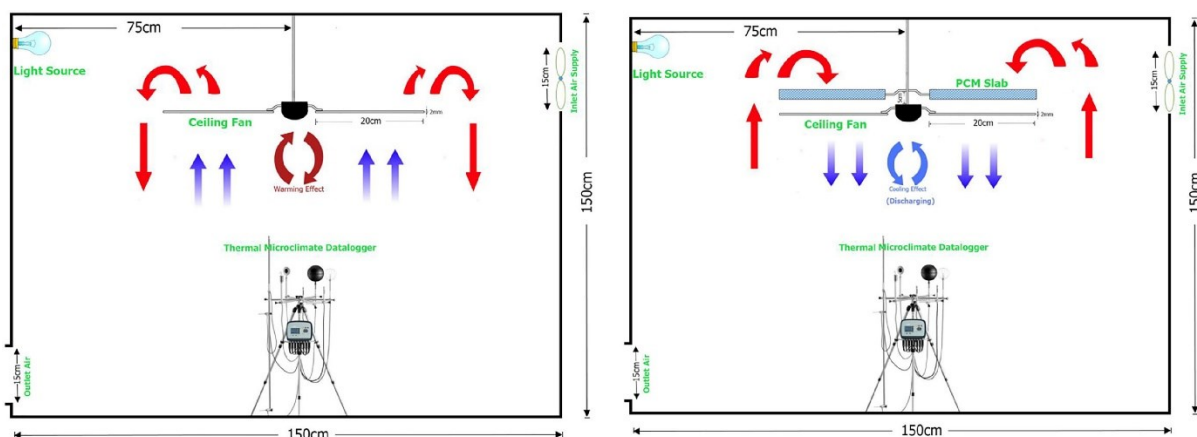


Figure 3.8: PCM based storage system integrated with ceiling fan ventilation [112].

In Lleida, Spain, PCM may be used as a heating technique in winter in combination with a solar collector. In 2016, Navarro et al. proposed an innovative system integrating PCM inside the horizontal structural building component (i.e., a slab) (Figure 3.9) [113]. During the day, heated air from the solar collector was blown through the slab, where melted the macro-encapsulated PCM modules. During the night, the air from the indoor space was blown through the slab, where it is heated by the PCM plates and afterwards recirculated back into space. On the coldest days, such a system represented energy savings of 21 %.

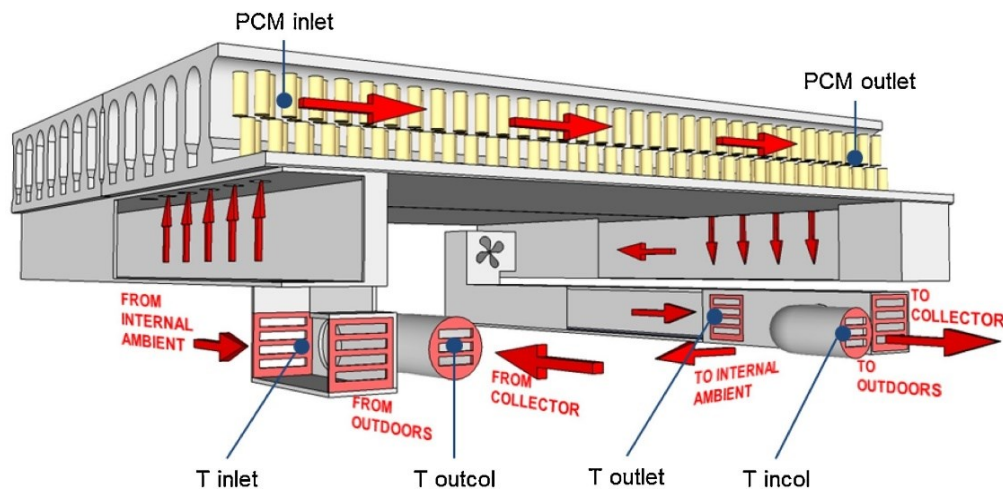


Figure 3.9: Ventilated slab with the addition of PCM modules [113].

The PCM Night Ventilation with PCM Packed Bed Storage (NVP) was investigated in Beijing, China, by Yanbig et al. [114]. The PCM melting temperature range between 22 °C and 26 °C with a peak at 25 °C and the 150 kg of the material in flat-plate capsules (Figure 3.10) were attached to the ceiling and solidified during the night with cool outdoor air. During the day, they were in direct contact and melted by the heated indoor environment. Tested in four rooms (experimental, meeting and two office rooms), the indoor air temperatures did not exceed 28 °C for 62 %, 39 %, 16 %, and 0 %, respectively.

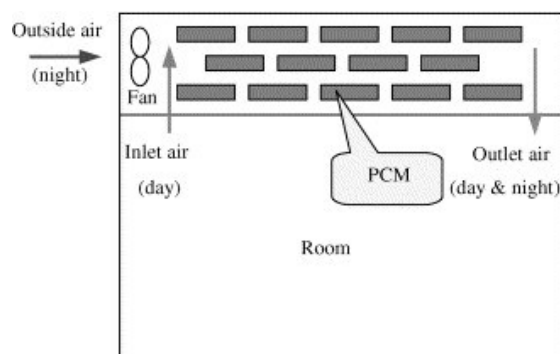


Figure 3.10: night ventilation with PCM packed bed storage [114].

A pipe-embedded PCM ceiling unit for cooling was mounted on the ceiling by Turnpenny et al. [115]. The test unit was sized by the 1D mathematical model describing the heat transfer from air to PCM (Figure 3.11). With the 5 °C temperature difference between PCM and the air, the PCM was melted for 19 h with a heat transfer flow rate of 40 W.

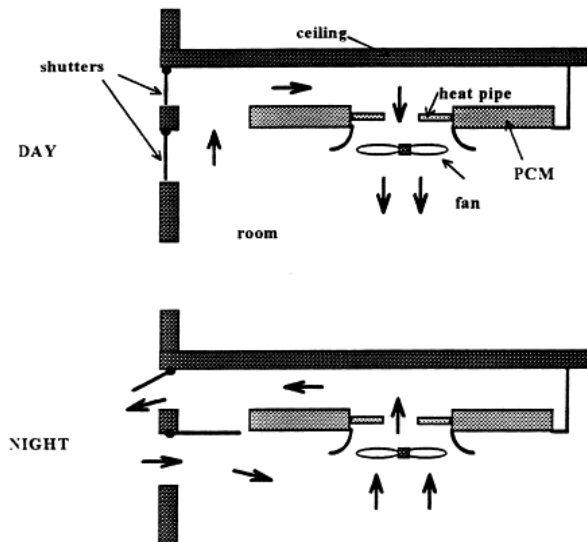


Figure 3.11: Schematic of proposed heat pipe/PCM installation [115].

The PCM implementation alternatives in the ceiling combined with ventilation were investigated and compared by Lizana et al. [116]. In Figure 3.12, three investigated cases are presented: reference scenario without PCM application, conventionally installed PCM as a passive alternative in direct contact with indoor space and active PCM layer insulated from indoor space and ventilated (indirect contact with indoor space). The study indicated that TES cannot completely regenerate without night ventilation and that the indirect solution without AC system addition decreased the discomfort hours by 65 % and discomfort period by 83 %.

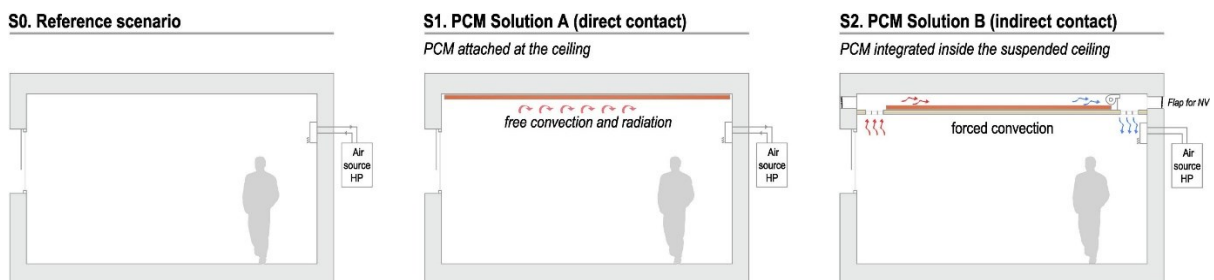


Figure 3.12: PCM implementation alternatives [116].

In the summer of 2009 and 2010, Weinläder et al. monitored a ventilated cooling ceiling with integrated with PCM plates ($T_m = 24$ °C) in two offices and a conference room (Figure 3.13) [117]. The air gap in the ceiling was mechanically ventilated with cool outdoor air during the night. The results showed that the maximum operative room

temperature was decreased by as much as 2 K. The cooling power of the system was determined to be 30 W/m² at operative room temperature of 28 °C and volumetric flow rate of 300 m³/h.

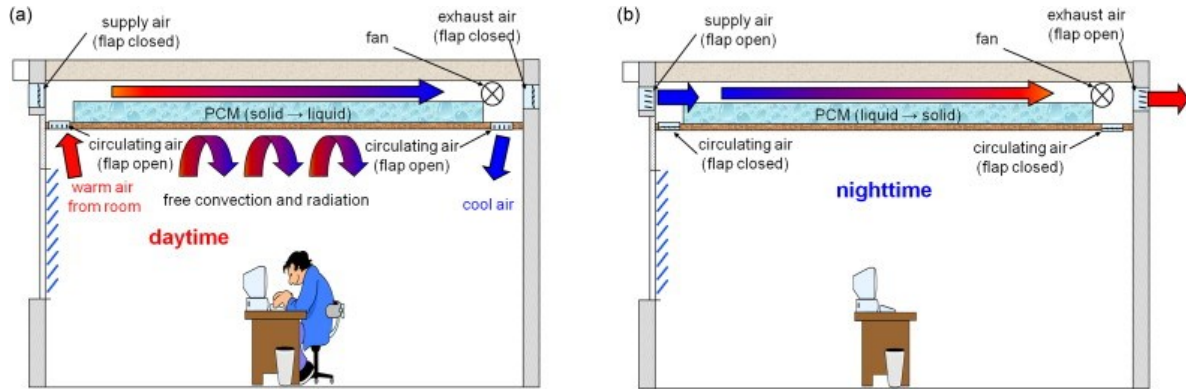


Figure 3.13: A ventilated cooling ceiling with integrated latent heat storage [117].

The simplified ventilated PCM ceiling shown in Figure 3.14 was investigated by Jiao and Xu with EnergyPlus energy simulation software [118]. Three different melting temperatures ($T_m = 26\text{ °C}$, 27 °C and 28 °C), ventilation rates (night ventilation rates: 5–20 ACH and window opening ventilation rates: 3–8 ACH, thermal conductivity coefficient ($0.5\text{--}0.8\text{ W}/(\text{m}^2\text{ K})$), and PCM thicknesses (2, 4, 6, and 8 cm) were investigated. The results showed that single layer PCM ceiling has a stronger effect compared to multi-layer ceilings and that the melting temperature of 27 °C keeps the indoor temperatures in the most comfortable summer range.

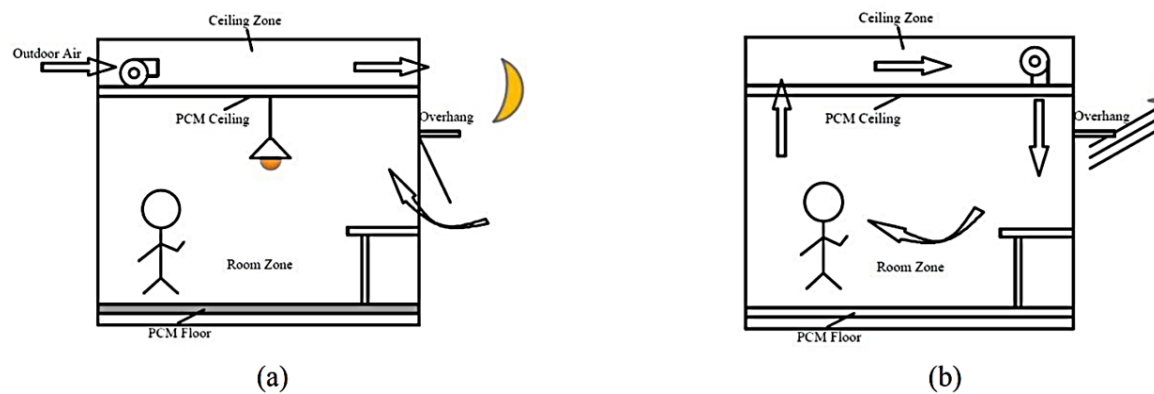


Figure 3.14: The simplified ventilated PCM ceiling [118].

The thermal performance of night-ventilated hollow-core slabs improved with microencapsulated PCM concrete were investigated numerically by Faheem et al. [119] (Figure 3.15). The reference for their research was PCM PureTemp 23, which they derived for different melting temperatures (18 °C , 19 °C , 20 °C , and 21 °C) and different amounts of PCM content in the concrete mixture (0–20 % of mass weight PCM). The best

performing design in the low thermal mass building case depends on the ventilation rate and the selected PCM melting point. The optimal results were met with a PCM melting point of 20 °C and 19 °C with an inlet velocity of ≤ 2 m/s and 5 m/s, respectively.

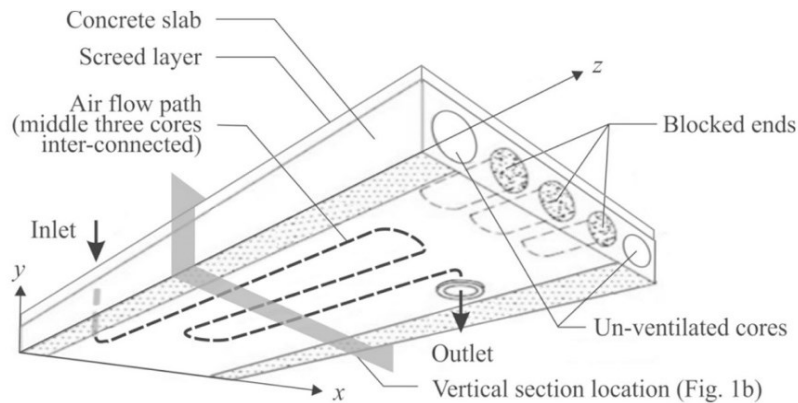


Figure 3.15: Night ventilated hollow core slabs cast with micro-encapsulated PCM concrete [119].

In comparison to the previous study, the study by Yu et al. presents a ventilated concrete roof with shape-stabilized PCM as its external layer (Figure 3.16) [120]. Under the different Chinese climate zones, from severe cold to hot summer, the melting point temperatures vary from 29 °C to 36 °C, its thicknesses from 20 mm to 30 mm and velocities from 1.4 m/s to 2.5 m/s.

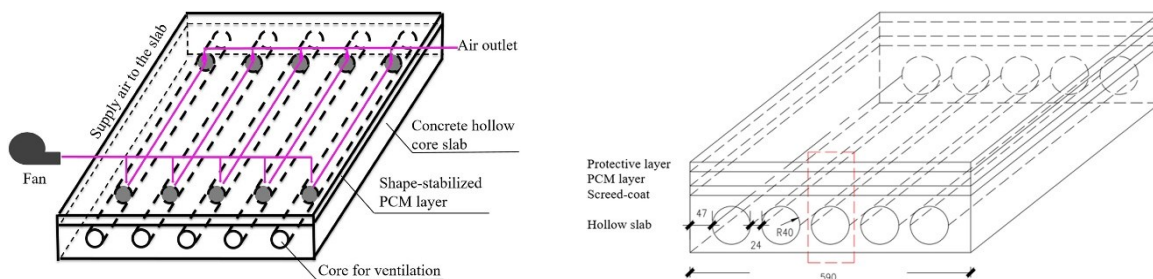


Figure 3.16: Pipe-embedded ventilation roof with outer-layer shape-stabilized PCM in different climate zones [120].

Ceiling-integrated PCM may be melted only by active means. Morovat et al. introduced an active PCM-air heat exchanger installed on the ceiling. [121] (Figure 3.17). The system's numerical model was validated and calculated using Python 3.6. Eight rows of DuPont Energain™ were ventilated along the 2.4 m long heat exchanger, and the number of air channels was adapted (1-6). During the daytime cycle, the PCM was actively melted by the heated indoor air; during the nighttime, it was actively solidified by the cool outdoor air. It was determined that with one channel the PCM needed 7.25 h and 8.56 h and with six channels 2.58 h and 3.10 h to 90 % solidify and 90 % melt. Overall, the system with 1000 W and 3000 W heaters in the room reduces the peak load duration by 82 % and 31 % and daytime mean power load duration load by 31 % and 22 %, respectively.

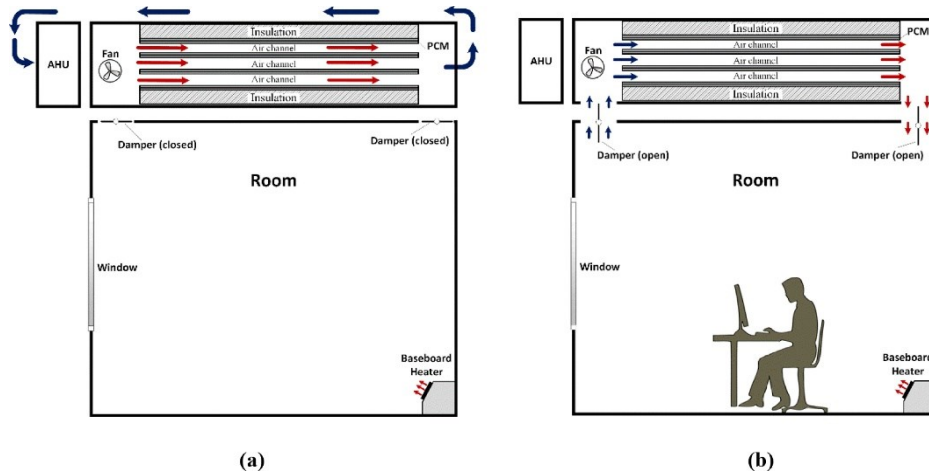


Figure 3.17: An active PCM-heat exchanger ceiling [121].

Kodo and Ibamoto investigated the microencapsulate PCM ceiling boards (25 °C) coupled with air-conditioning systems in an office building to overcome the energy peak demands [122]. Figure 3.18a shows the system in which the PCM plates in the ceiling chamber space are cooled at night by the cool air from the air handling unit (AHU) using low-rate electricity. During normal daily operation (i.e., cooling), the air cooled by the AHU is supplied to the room (Figure 3.18b). During the daily peak saving period (peak load), the air on its way back to the AHU also passes the cooling ceiling chamber space. This results in precooling the warm room air on the way back to the AHU (Figure 3.18c).

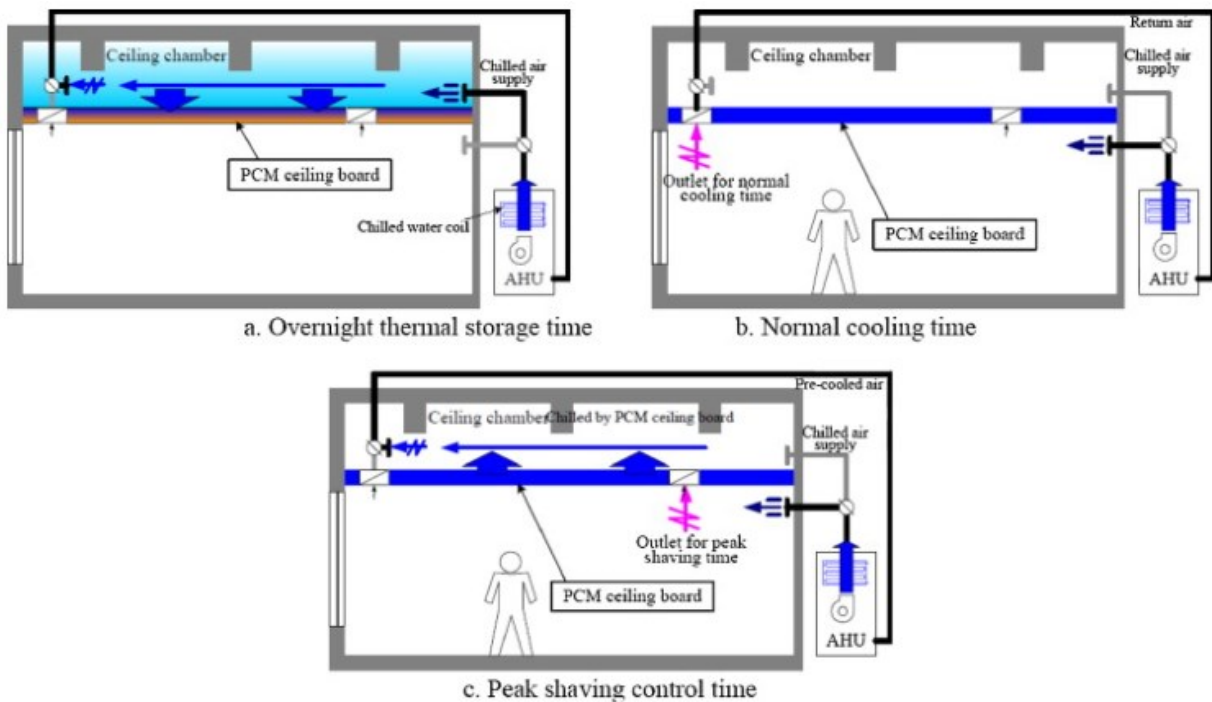


Figure 3.18: Cooling PCM ceiling for peak shaving control [122].

Under central Poland weather conditions, Jaworski experimentally tested the heat-exchanging ventilated ceiling panel unit made out of PCM gypsum composite (BASF Micronal™) presented in Figure 3.19 [123]. Under the steady-state experimental conditions (8 h), inlet and outlet air temperatures of 29.5 °C and 23-24 °C and the air velocity of 2 m/s, the unit could accumulate 1.14 MJ/m² of heat (and at 3 m/s - 1.86 MJ/m²).

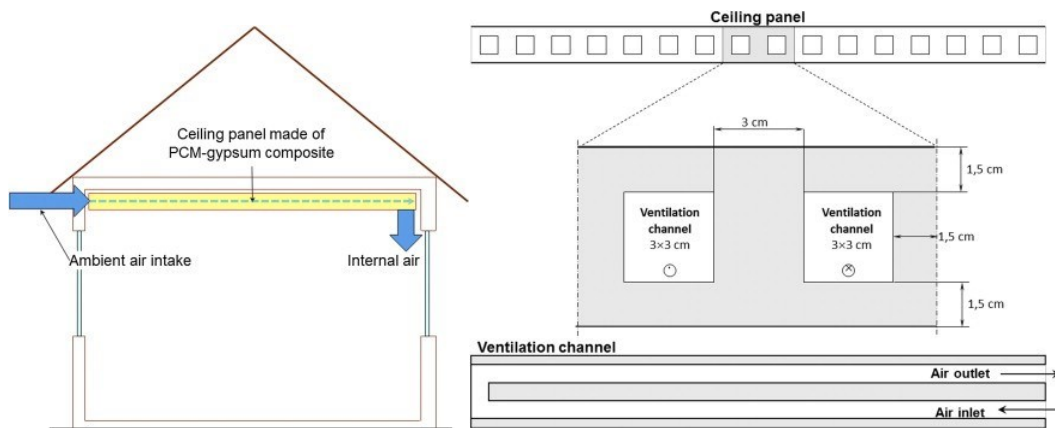


Figure 3.19: Ceiling panel made out of PCM composite [123].

3.3.3. PCM improved ventilated floor

PCM for cooling application is usually not placed into the floor, because the warm air is diluted upwards toward the ceiling. However, the heat response of an active floor supply air-conditioning system was tested and improved with an embedded granular phase change material to increase a building mass thermal storage by Nagano et al. [124]. The arrows in Figure 3.20 show the air circulation during the day (white arrows) and during the night cycle (black arrows). Over the night, when the air was exhausted to the room, the system could store 1.79 MJ/m². During the day, the air conditioning was in use for 3 h.

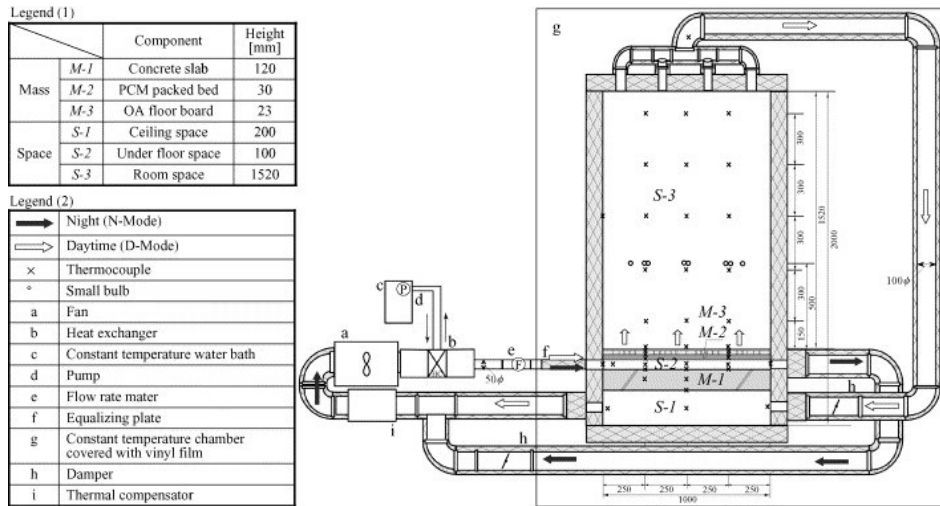


Figure 3.20: Floor supply air conditioning system using granular phase change material [124].

In contrast to the previous study, González et al. experimentally tested a passive approach of the PCM for energy storage in architecture combined with the Magic Box prototype in Madrid, Spain, Washington, U.S.A., and Beijing, China [125]. The PCM ($T_m = 23\text{ }^\circ\text{C}$) was placed into the floor where the performance was investigated during heating and cooling periods combined with natural ventilation. The upper two figures (Figure 3.21) show the nightly summer solidification and daily melting cycles, and the lower two figures show the winter daily melting cycle and nightly solidification cycles.

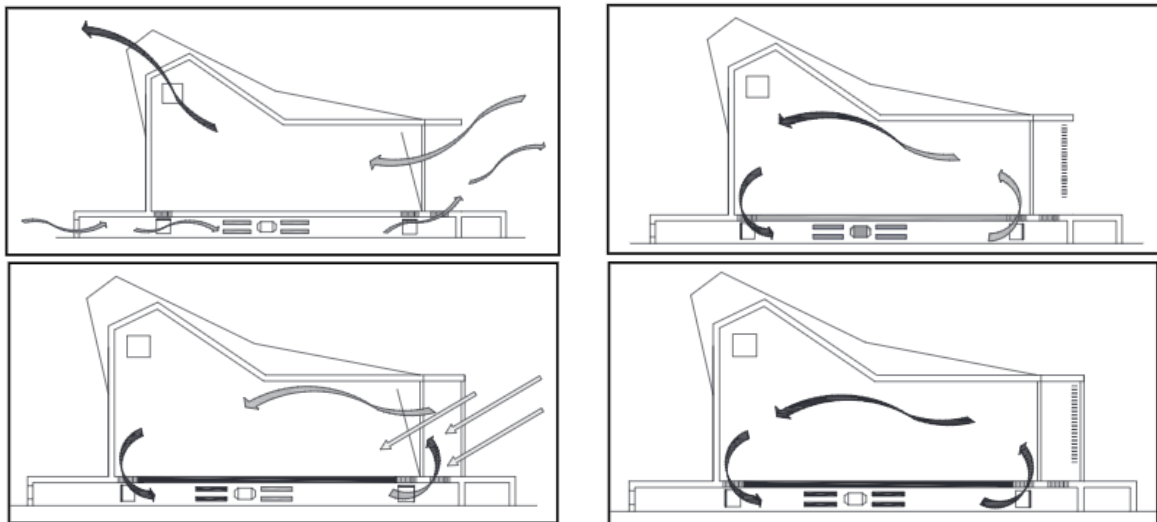


Figure 3.21: The Magic Box prototype [125].

3.3.4. PCM improved ventilated internal walls

In some cases, PCM are applied to the internal walls of the building. For example, Evola et al. numerically investigated an effect of a ventilated wall cavity on the overheating reduction with a mathematical determination of heat transfer coefficients on a micro level and EnergyPlus 7.0 on a building level [126]. The characteristics of the PCM wall were adapted to a micro-encapsulated board with a peak melting temperature at 27.6 °C. The presence of the ventilated cavity promoted the PCM storage efficiency during the day (Figure 3.22). For the given configuration in Catania, Italy, the presence of the ventilated cavity in the east wall increased the energy storage efficiency from 48.5 Wh /(m^2 day) to 100.4 Wh /(m^2 day) or the daily PCM storage efficiency from 42.4 % to 78.2 %.

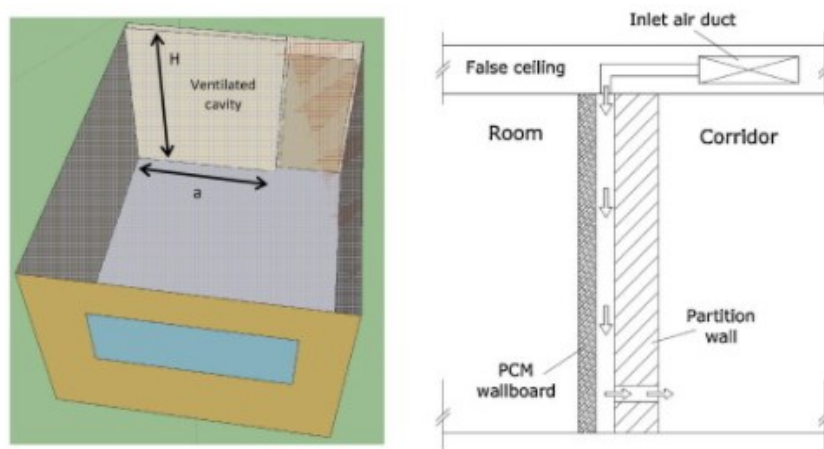


Figure 3.22: Ventilated wall cavity [126].

Additionally, an active PCM thermal energy storage wall was modelled and experimentally investigated by Dermadiros et al. [127], [128]. The PCM wall consisted of five layers of shape-stabilized PCM panels with a ventilated gap between the 3rd and the 4th layers (Figure 3.23). During the charging cycle, the panels were melted with an inlet air temperature of 28 °C and discharged with an inlet temperature of 13 °C. The panels could store 2.63 kWh of energy and needed 8.9 h and 14.6 h to be fully charged and discharged, respectively.

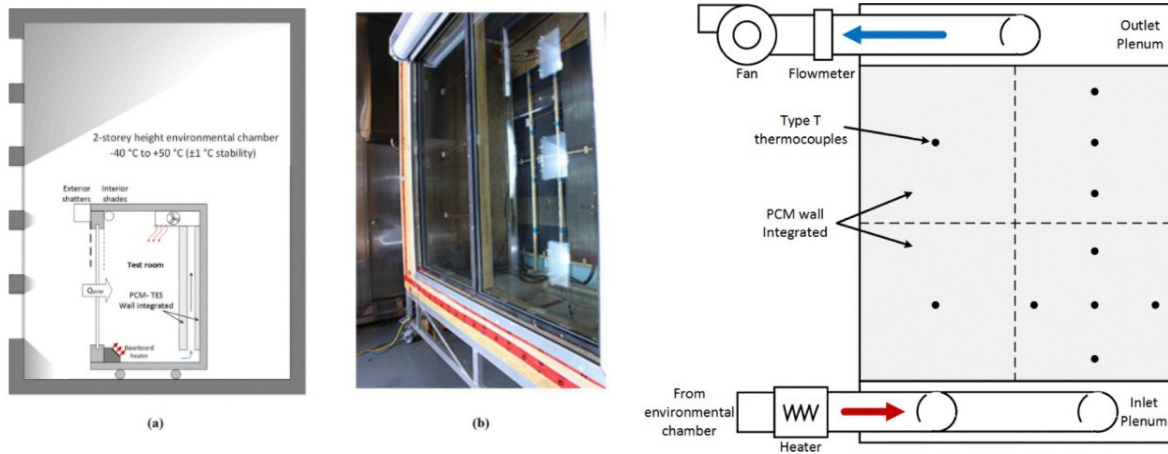


Figure 3.23: The PCM wall consisting out of 5 layers of shape-stabilized PCM panels [127].

3.3.5. PCM improved ventilated façades

Similar to PCM applied in the roof layers, a very common application of PCM for cooling application is in its external walls. For instance, in Chengdu, China, Wang et al. prepared a mathematical model of a lightweight building for natural disasters that was validated using EnergyPlus [129]. First, 16 different designs were tested, and the one with the highest number of thermally acceptable hours was selected and further optimized for the PCM thickness. The selected thickness was 2 cm, because higher thicknesses did not considerably improve the performance. PCM was positioned on the inner side of the wall/roof or the outer side of the wall/roof with the addition of a 20 cm air gap. Walls were modified for different orientations and, in some cases, theoretically repositioned from the internal side to the external during the nighttime. The selected case was a non-ventilated PCM on the west wall during daytime but moved outside during the nighttime.

In summer, Gracia et al. tested a ventilated active façade in an experimental cubical in Lleida, Spain [130]. The microencapsulated PCM plates (peak melting point temperature of 22 °C) were installed in the centre of the façade wall, where they were ventilated with a fan or naturally (depending on the scenario) with an airflow of 0.9 and 0.6 m³/s, respectively. They investigated four periods shown in Figure 3.24: PCM solidification period (a), PCM melting period (b), overheating prevention period (c) -after the PCM is completely melted, the buoyancy flow takes and releases the air flow into the outdoor environment and night ventilation (d) after the PCM are solidified the free cooling period starts. The results showed that among the five different experiments performed in the study, the system could provide 34.9 MJ/day and 42.8 MJ/day in hot and mild summer conditions, respectively. On this same experimental set up, the same group also investigated the reinforcement learning techniques [131].

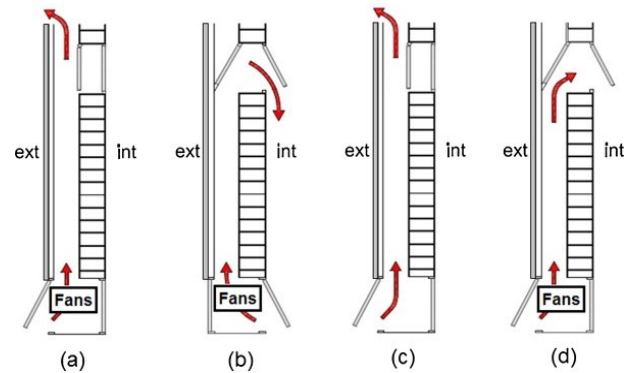


Figure 3.24: Ventilated facade with PCM for cooling applications [130].

The present configuration with this same PCM system was calculated using a finite control volume method and weather data from EnergyPlus for 21 locations in the world – tropical climates: Brasilia (Aw), Kuala Lumpur (Af), Singapore (Af), dry climates: Abu Dhabi (BWh), Antofagasta (BWk), Albuquerque (BsK), New Delhi (Bsh), temperate climates: Brisbane (Cfa), Tokyo (Cfa), Auckland (Cfb), Quito (Cfb), Berlin (Cfb), Madrid (Csa), San Francisco (Csb), Mexico (Csa), Johannesburg (Cwb), continental climates: Chicago (Dfa), Beijing (Dwa), Montreal (Dfb), Stockholm (Dfb) and Moscow (Dfb) [132]. The warm temperate and snow climates have high free cooling potential. Meanwhile, arid and equatorial areas have limited potential for such system operation. The most important factors for calculation were the vertical solar irradiance and the heat gains of the structure. The system may supply up to 12 MJ/day of cold (for 3-4 h).

Furthermore, this ventilated façade system was used to study the effect of different control strategies on its performance [133]. Under the above listed different climatic conditions, three different control strategies based on cost savings, energy reduction, and CO₂ mitigation were investigated. The results revealed that the average energy savings by changing the manual operation to automatic reached 4.3 %. Energy control and cost savings control reached similar average savings of 7.8 %. The average CO₂ mitigation control strategy savings were 16.7 %.

The thermal performance of building elements may be improved by ventilating the tubes in integrated into blocks with PCM in a concrete block frame (Figure 3.25) [134]. The system was investigated by Laouatni et al. on a component level experimentally and afterwards numerically with COMSOL. The selected melting point was rather high (27 °C) to eliminate the additional melting due to the laboratory conditions. The results showed that the measured temperature on the lateral surface of the concrete block with the addition of PCM (open or closed tubes) dropped between 3.2 °C and 4.0 °C and by ventilation the tubes for each additional 1 °C.

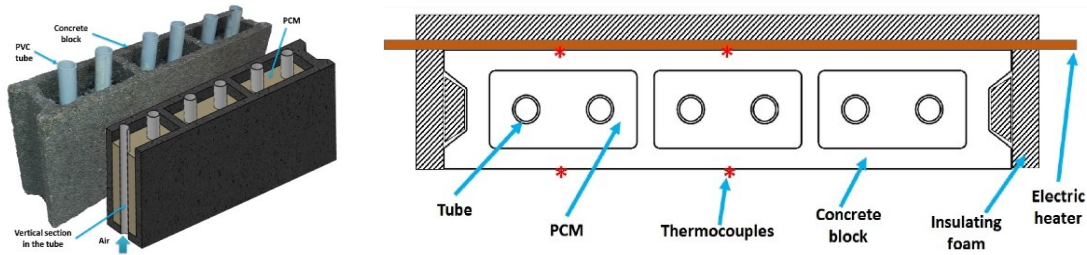


Figure 3.25: The ventilation tubes in integrated in blocks with PCM [134].

A ventilated active façade with PCM on its external side was investigated experimentally and numerically by Diarce et al. [135], [136]. Although the system was investigated for the winter period, it may also be used during the summer to reduce the overheating of the building by improving the PCM solidification over the night. The air gap next to the PCM layer (peak melting temperature of 35 °C) was ventilated upwards by an ancillary fan placed on the roof (Figure 3.26). The thermal performance of the façade was compared to the performance of four other traditional external walls assemblies (masonry and face brick). The experiment was performed in March for 14 days; during this period, the indoor air temperatures indoors increased by 2 °C. Compared to the traditional assemblies, the investigated system increased the indoor temperatures up to 2 °C. The air in the airgap was heated up to 12 °C during the day and for 2.5 h after the end of solar radiation still heated up by 2 °C. The energy efficiency of the façade during the testing period is attributable to the 10–12 % of the total energy efficiency of incident radiation gains.

The same system was afterwards also investigated with an ANSYS Fluent numerical model [136]. Within the model, three turbulence and two radiation models were applied. The results showed that an RNG k- ϵ model was more accurate for higher airflow rates and SST and Standard k- ω for lower flow rates. For the given air gap dimensions, the airflow in October (77 l/s) was turbulent and March (27 l/s) transitional.

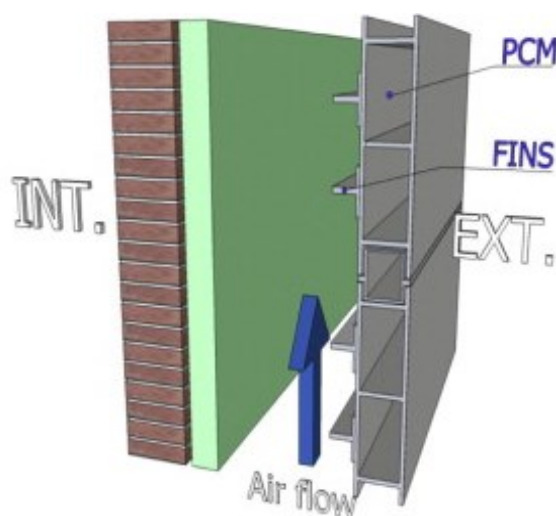


Figure 3.26: A ventilated active façade including phase change materials [136].

A heat-transfer mechanism of ventilated Trombe wall for active cooling and heating was proposed and numerically investigated by Zhout et al. [137]. Figure 3.27 shows the layer of glazing and naturally ventilated air gap followed by the exterior layer of PCM (melting temperature of 26 °C and optimum thickness of 8 mm) covered by a high absorptivity/reflective coating. On the interior side of the load-bearing structure, there is another layer of PCM wallboards (melting temperature of 22 °C and optimum thickness of 28 mm) in which the phase change was activated by heated or cooled water pipes during the heating and cooling peaks. In summer, the exterior PCM is solidified by the cool night air in the ventilated air gap (storing cold). The cooled water runs through the interior PCM during the night and is stopped during the day. In winter, the exterior PCM is melted by the hot air in the closed air gap (storing heat). The hot water melts the inner PCM during the day, and it is stopped during the night. The study determined that maximum energy storage and release efficiency for interior and exterior PCM in winter were 23 % and 18.2 % and 16.8 % and 18.9 %, in summer, respectively.

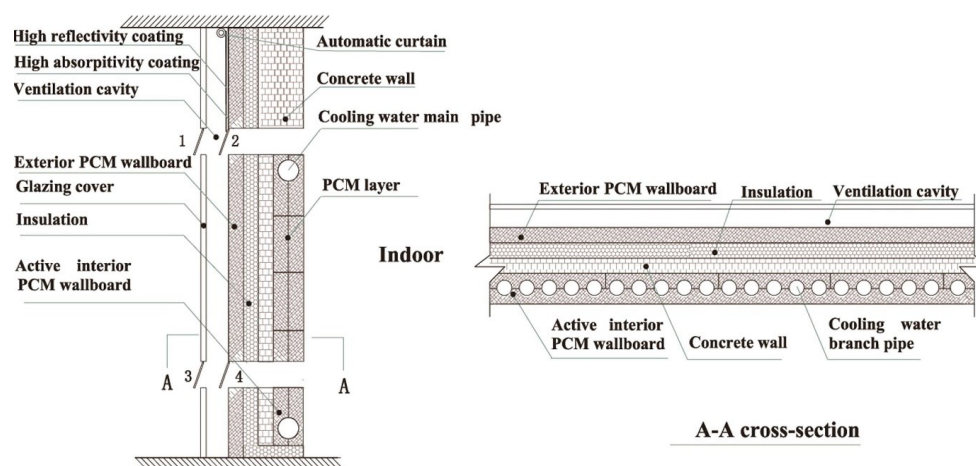


Figure 3.27: A new ventilated Trombe wall with PCM and active cooling/heating [137].

The authors from the previous study [137] upgraded the system from the façade also to the roof with solar electrical power-generating cells and active water pipes embedded in the PCM layer - PV/T-PCM (as shown in Figure 3.28) [138]. By combining the air vents' opening combinations, the daytime overheating of the system was avoided by opening the air vents 1, 2, 4, and 5. The nighttime natural cooling for energy storage was obtained when only air vents 2 and 6 are open, and the fan is turned on. The air is let into the indoor space due to the control regime and stable thermal comfort. The nighttime natural cooling for energy release mode was set by opening only air vents 3 and 6 and turning the fan on (the recirculation of the indoor air). The results showed that such a system can increase the performance of the PV cells by reducing its temperature with PCM and active cooling water (from 70.9 °C to 32.8 °C). The flow rate of the water was optimised to 0.24 kg/s and the correct melting point temperature to 30 °C. The thermal energy gain from the PV/T-PCM system increased from 63.01 in January to 157.67 MJ/m² in July. The annual net electricity efficiency of pumps and fans was 12.56 %.

In a further study, Zhou and Zheng also performed a multi-level uncertainty-based analysis and optimisation of the renewable system for the cooling period [139], which were

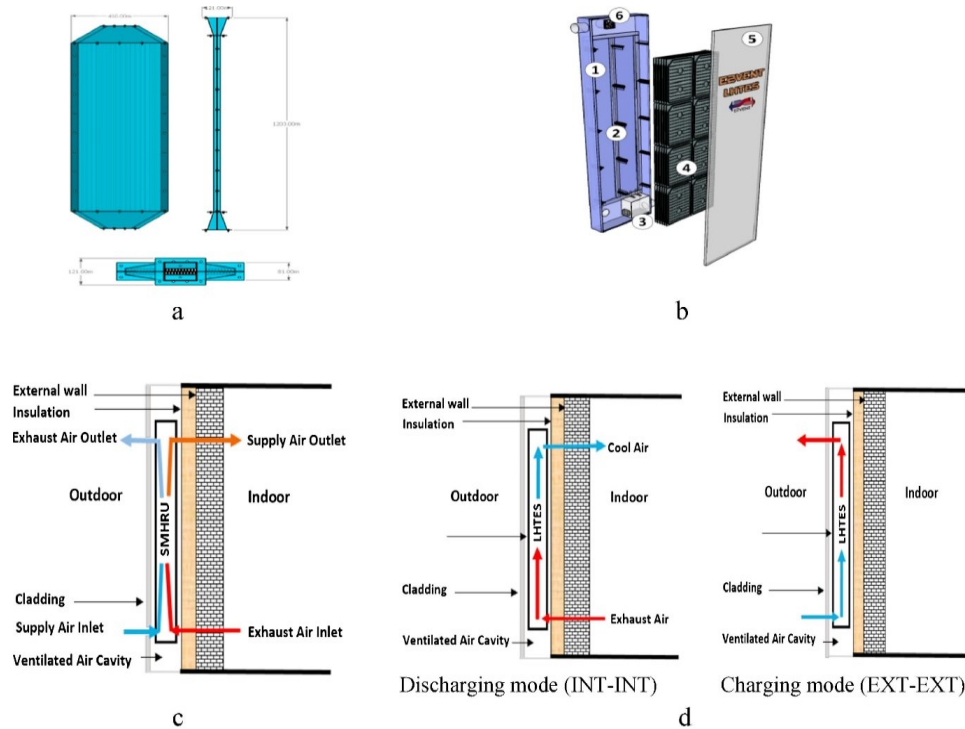


Figure 3.29: Description of the innovative E2VENT system [140].

A ventilated solar PCM wall system was experimentally investigated by Luo et al. in hot summer and cold winter periods in Hefei (China) [141]. Figure 3.30 shows the system's configuration. In summer, during the daily heat insulation mode, indoor and middle layer upper and lower vents are closed, and the outdoors opened. During the nightly passive cooling mode, the indoor upper and lower vents are shut, and the middle layer and outdoor ones kept open. In winter, during the daily solar passive heating function, the exterior upper and lower vents of the system are closed, the middle layer ones opened, and the interior ones can remain opened/closed. During the nightly heat preservation function, the indoor, outdoor, and middle layer upper and lower vents are all closed. The experimental analysis showed that the system could prevent the overheating problem in summer and efficiently contribute to heating the indoor environment in winter.

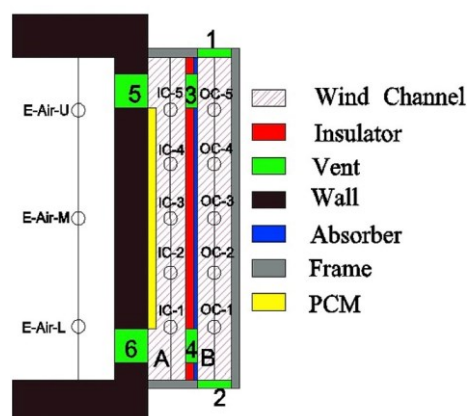


Figure 3.30: Modified solar phase change material storage wall system [141].

A traditional Trombe Wall was improved with the layers of PCM wallboard with different melting point temperatures by Zhu et al. [142]. The system's performance was investigated with TRNSYS in the summer and winter periods in Wuhan, China (Figure 3.31). The exterior and interior PCM melting temperatures were 30 °C and 18 °C, respectively. With the system's function compared to the reference building, the peak heating and cooling load were reduced by 9 % and 15 %, respectively; in summer, the indoor temperature in the PCM room was on average 3.28 °C lower.

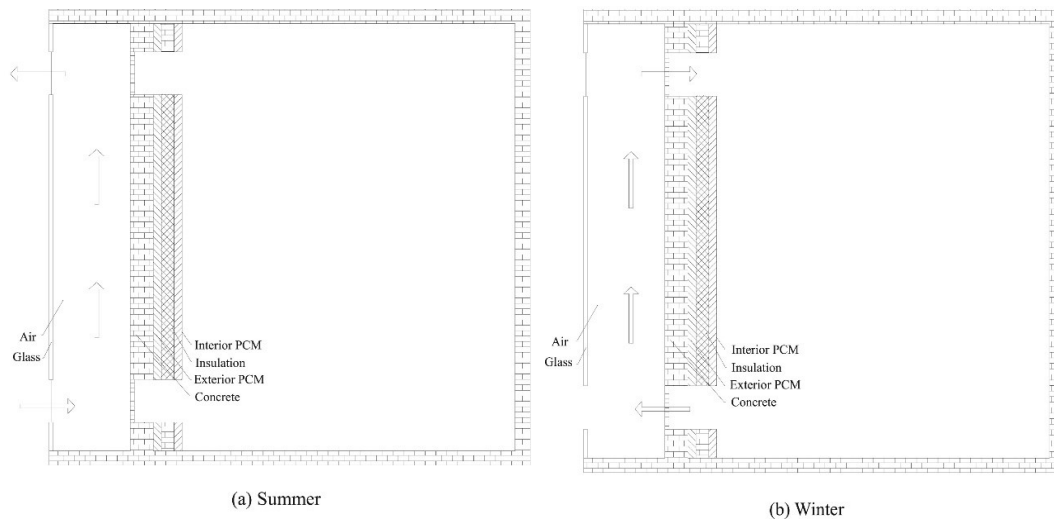


Figure 3.31: PCM improved Trombe wall [142].

Stritih presented a numerical model prepared with FORTRAN of the heat transport in heat storage of the paraffin (RUBITHERM RT30) PCM wall [143]. Figure 3.32 shows the PCM captured into the fins for enhancement of heat transfer (layers 1-2: glass with transparent insulation material (TIM), layer 3: black paraffin wax, layer 4: the air for the house ventilation is heated in the air channel exhausted indoors, layer 5: insulation and layer 6: plaster). The results showed that the distance between the fins is the most influential parameter, while the effect of the thickness of the fins was insignificant.

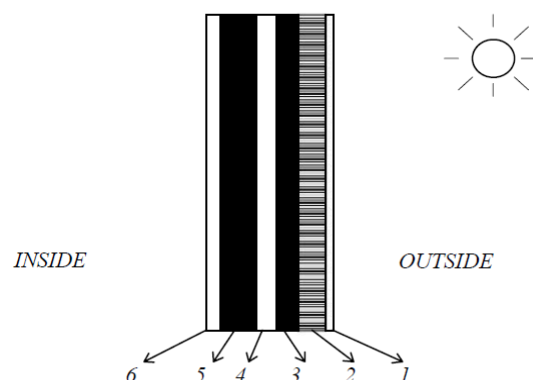


Figure 3.32: Solar PCM wall [143].

3.3.6. PCM improved ventilated glazing elements

PCM was integrated into a blind system for a double-skin façade (DSF) buildings and experimentally and numerically tested [144]. In this way, the design helps to reduce the overheating of DSF in summer (Figure 3.33). The researchers prepared several PCM composite mixtures and selected microencapsulated PCM PX35 powder mixed with an epoxy resin material (75 %wt PCM), which was afterwards placed on the blade. The investigation showed promising results where the air temperature in the DSF test cell did not exceed 39 °C. Comparing the thermal performance of PCM blinds to traditional aluminium blinds, it was possible to observe the reduction of average air temperature in the cavity of 2.2 °C (5.5 %).

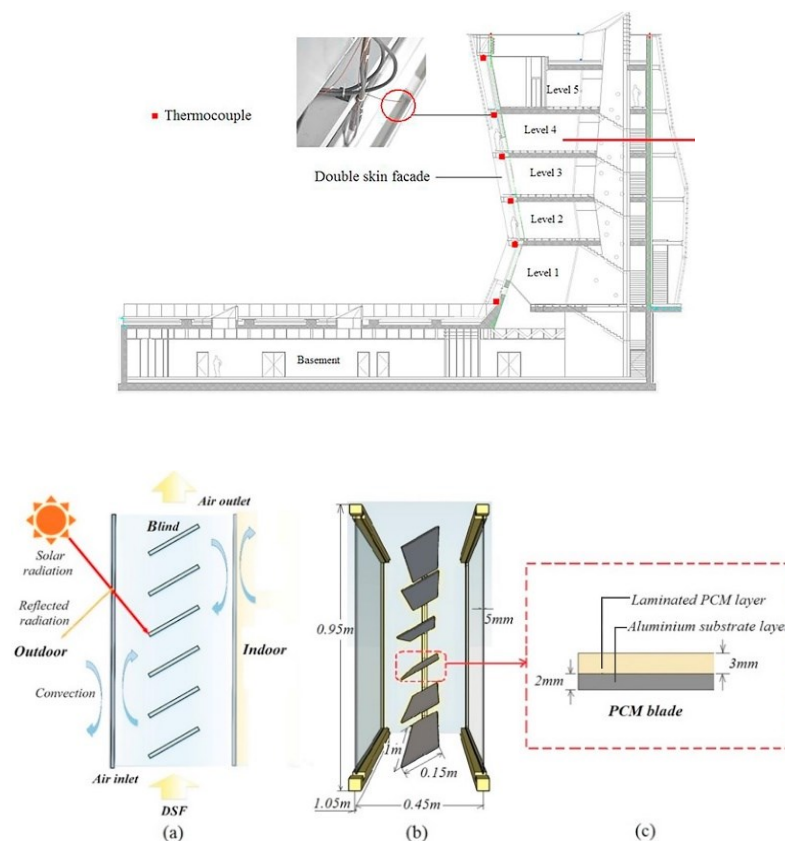


Figure 3.33: Integrated PCM blind system for double skin façade buildings [144].

The performance and the design of a new ventilated window with a PCM heat exchanger were optimised experimentally (the cool and hot box) and numerically (COMSOL Multiphysics) by Hu and Heiselberg [145]. The proposed system was investigated for three summer control operation modes (Figure 3.34). During the night ventilation mode (a), the heat from the PCM heat exchanger is released outdoors. If ventilation indoors is needed, the night free cooling mode and the cold air is blown indoors (b). The PCM is melted during the daytime within ventilation pre-cooling mode (c), where the outdoor air is pre-cooled, and the system is covered with the shading device. The system could cool down the ventilated air by 6.5 °C on average with a 3.9 h pre-cooling effective time, which resulted in an energy saving of 3.19 MJ/day.

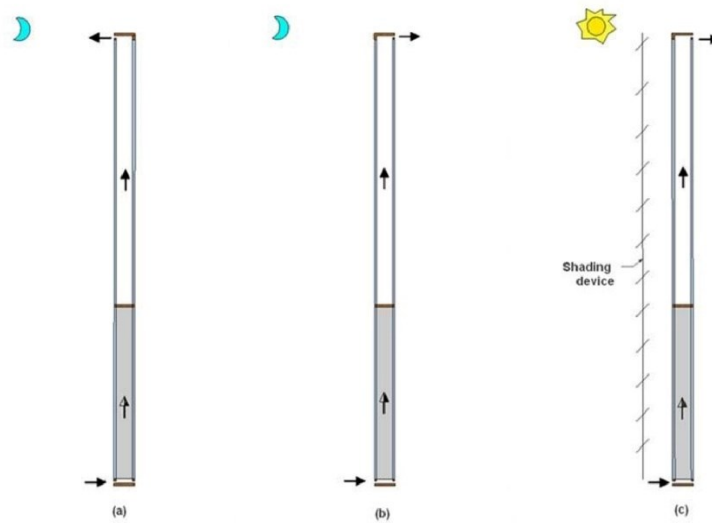


Figure 3.34: A ventilated window with PCM heat exchanger [145].

This concept was additionally researched with EnergyPlus software in the summer and winter periods by Hu et al. [146]. As visible in Figure 3.35, the system was slightly modified with the adaptation of the window glazing and the addition of internal shading. With improved system and exploitation of its external shading control, the analysis emphasised 62.3 % of building energy savings in summer and 9.4 % in winter.

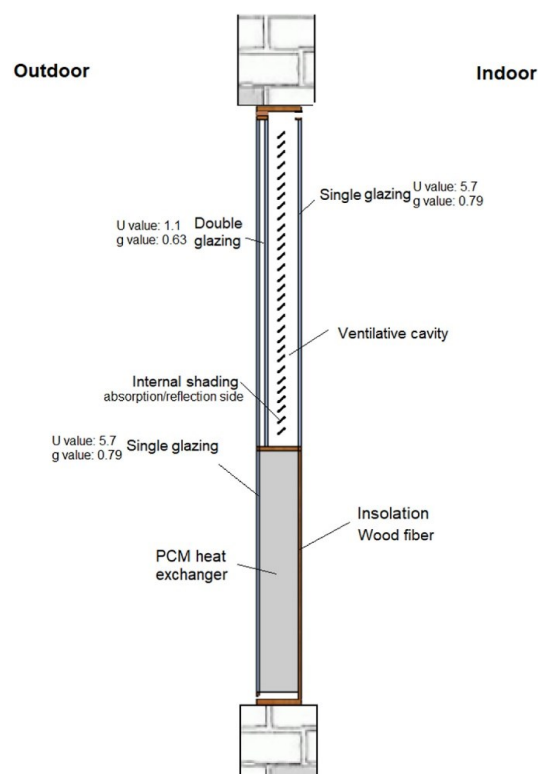


Figure 3.35: A ventilated window with PCM heat exchanger improved with internal shading and window glazing characteristics [146].

3.3.7. PCM improved ventilated walls with BiPV

Two similar systems with building-integrated photovoltaic (BiPV) improved by the ventilated PCM layer are presented. The primary goal is to improve the PV module performance (electricity generation). It is believed that secondarily they also improve indoor thermal comfort by accumulating the excess heat from daily solar radiation. Both studies place the BiPV in the façade, where the PCM layer is positioned directly after the PV layer. The ventilated air gap separates the PCM from the load-bearing structure. The first study was performed by Čurpek and Čekon and investigated the climate response of a BiPV façade system enhanced with PCM (Figure 3.36) in Brno, Czech Republic [147]. It was concluded that BiPV/PCM adequately performed when the outdoor air temperatures were lower than 30 °C.

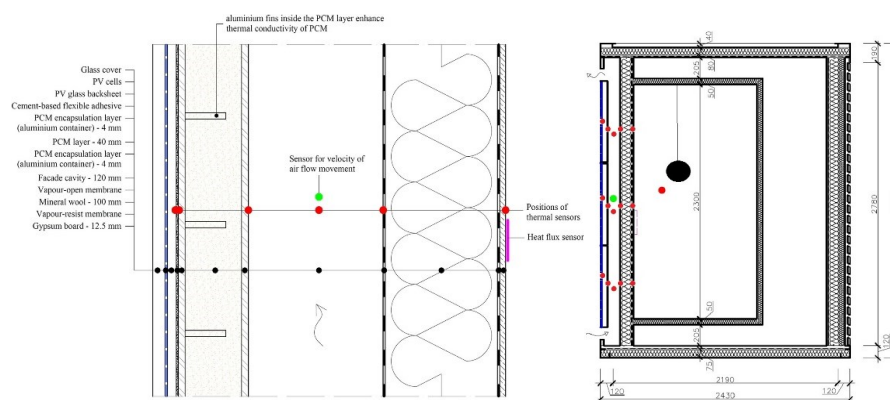


Figure 3.36: BiPV façade system enhanced with PCM [147].

Furthermore, Kant et al. ventilated the PCM wall with a BIPV system to improve the performance of the PV system [148]. Three PCMs (RT-25–26.6 °C, n-octadecane–28.2 °C and capric acid 32.3 °C) were tested (Figure 3.37). Under the mass flow rate of 0.091 kg/s and 0.08 m air gap, the maximum values of outlet air temperatures and maximum extracted heat by air were obtained: 37.82 °C, 37.54 °C, and 37.52 °C and the 18 500 kJ, 17 170 kJ, and 16 250 kJ for RT-25, n-octadecane and capric acid, respectively.

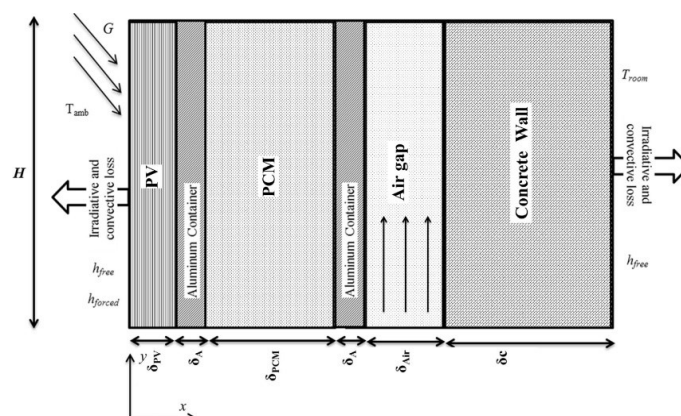


Figure 3.37: Ventilated PCM wall with BIPV [148].

4. Purpose and aim of doctoral dissertation

4.1. Problem description

In summer, lightweight buildings (low building thermal mass and large window area) are often overheated due to rapid heat loads which cannot be accumulated in the building's thermal mass. Therefore, the conventional cooling systems such as air conditioning devices consuming electrical energy at higher daily electricity tariffs are used. On the global scale (city) this such behaviour resents high daily energy demand peaks where office buildings play a crucial role.

Therefore, this research is focused on the renovation method for the existing lightweight office buildings with large window area in its building envelopes. The research proposes a passive method for overheating reduction in the daytime by increasing the buildings thermal mass and heat accumulation properties. The phase change material (PCM) accumulates the excess heat from the indoor spaces during the daytime cycle by melting. However, in recent years the studies showed that because itself insulates itself (low material density) and discharges the heat indoors, it cannot solidify completely during the nighttime cycle. The unsolidified material cannot accumulate the heat and cool the indoor space which results in deteriorated cooling performance.

Transparent building envelopes are hardly modified, so the proposed PCM system isn't affecting the building's exterior appearance. Office buildings are usually equipped with ventilation systems which are during the day used for improving the indoor air quality (IAQ). In the nighttime, this ventilation system will be coupled with the PCM system. The ventilation system will run over the night when the electricity tariffs are lower, in order to complete solidification of the PCM systems in the required nighttime cycle. PCM systems may be solidified also with the water-based systems, which are less practical to modify. On the global scale (city) in the nighttime, there is a surplus of electrical energy. The PCM system may be ventilated with room ventilation or with locally supplied ventilation. Compared to the effectiveness of locally applied air for PCM heat transfer enhancement, the main limitation of nighttime total volume ventilation (either natural or mechanical) is the decreased contact of the PCM surface and heat removing air. Therefore, higher

amounts of air need to be delivered into the room to reach the solidification effect with higher energy consumption and operation costs.

The advantages of such PCM system are lower renovation costs and increased energy efficiency of the system because the system is placed only offices with critical need for indoor thermal comfort improvement (overheating reduction) and the system's characteristics (e.g. melting point and thickness of the PCM plates) may be accurately optimised based on the individual office conditions and requirements.

Many studies focus on this problem by performing a full-scale building unsteady state simulation for energy performance of buildings such as ID Design Builder. On the positive side, such simulations may provide yearly energy performance results of the simulated building. On the negative side, they are less accurate or unable to simulate ventilated air gaps. As the results are indoor temperature fluctuations or energy use, the phase change state of PCM during daily or nighttime cycles is unknown. An internal ventilated PCM wall was investigated by Evola et al. with EnergyPlus software however there is no experimental investigation of such ventilated wall available. Weinlader et al. experimentally investigated a ventilated PCM ceiling by monitoring the indoor temperatures in the offices (uncontrolled experimental conditions) during their use. Building element integrated PCM systems are often tested under real outdoor conditions and in some cases even without a simultaneously measured control cell without PCM.

The cooling effect and thermal performance of the PCM under different outdoor conditions from investigated aren't known. Furthermore, such experimental conditions aren't appropriate to test any other outdoor conditions (e.g. different test reference year (TRY) or heatwaves). Also, the cooling effect of the PCM under an individual temperature condition (constant reference cell temperature set point) is unknown because the outdoor temperatures fluctuate. Often when the heat transfer is investigated with a micro-scale numerical model simulations only a section of the system's temperature distribution is investigated. Rarely the model consists out of the entire building element system. In studies where the model is validated with the experiment affected by the system's surrounding thermal environment there is normally no parametric analysis available.

4.2. Hypotheses and objectives

This chapter presents the research hypothesis and objectives, based on the reviewed literature and specified knowledge gap.

The main objectives of the research are:

- O1: to investigate the cooling effect of the APS (experiment)
- O2: to determine the effect of different air gap inlet air temperatures on the nighttime solidification of the PCM (experiment and numerical model)
- O3: to determine the highest air gap inlet air temperature for a complete PCM solidification in the selected nighttime period (12 h) (experiment and numerical model)
- O4: to evaluate the energy performance of the APS during the cooling season (experiment, numerical model and calculation model)

The initial research hypotheses are listed below:

- H1: The PCM panels will fully solidify in the night cycle of discharge and completely melt in the daily charge cycle.
- H2: The results of a parametric operation test show that optimal thermal comfort (local operating temperature) is provided with 2 cm thick panels, with a melting point of 24°C panels and a melting point of 25 °C ceiling panels at a distance of 5 cm from the wall. The optimum direction of air ventilation is the wall-ceiling direction with a volumetric flow of 150 m³/h. The shape of the diffuser is mixing.
- H3: The best local thermal comfort (the chosen criterion of thermal comfort) will be compared to the passive system, the ventilated wall without ceiling, the ventilated ceiling without a wall, the APS system.
- H4: By considering the local thermal comfort, the best thermal comfort (the lowest daily temperature in the room) will be symmetrically close to the PCM wall and will decrease depending on the radiation level of the radiation surface opposite the PCM wall.
- H5: The energy use for cooling of the APS with the selected heating, cooling and ventilation system will be lower than the energy use for cooling of passive system alone, where the panels are not ventilated at night.
- H6: The energy use for cooling will be lower in the chosen heating, cooling and ventilation system in the APS (walls and ceiling), as in the case with ventilated single element - ventilated ceiling without ceiling or ventilated ceiling without wall.

To address the proposed hypothesis, the main objectives need to be reached with experimental, numerical and calculation methods. First, the daily and nocturnal performance of the APS is applied in the experimental chamber tested experimentally under various controlled experimental conditions. To further optimise the APS, the simulation with validated micro-scale numerical model of the air gap (without the chamber zone) is performed to investigate the performance of the system in the nocturnal cycle under different air gap inlet air temperatures. Finally, the energy stored in PCM (energy saving potential of the APS) during different experimental and numerical cycles was determined with manual calculations. Based on energy performance results the feasibility of the APS is assessed. Table 4.1 shows how each individual hypothesis is answered with proposed objectives.

Table 4.1: Hypothesis with corresponding objectives.

Hypothesis	Objectives	Explanation
H1	O1 and O3	The complete melting of the PCM will be shown by the experimental results (cell air temperatures and temperature distribution along the PCM of the APS). The complete solidification of the PCM will be shown with experimental and numerical results (air gap inlet air temperatures and temperature distribution along the PCM of the APS).
H2	O1, O2 and O3	The configuration of the APS is based on the characteristics found during the literature review, preliminary investigation, experimental and numerical results.
H3	O1	The best local thermal comfort in relation to the APS geometry configuration variations will be assessed based on the experimental results where measurements of the temperature fluctuations in the chamber are available.
H4	O1	The local thermal comfort related to the location in cell with the APS will be assessed experimentally where measurements of the temperature fluctuations in the chamber are available.
H5	O2 and O3	The cooling potential of the APS where PCM is nocturnally ventilated compared to the regular passive system without nocturnally ventilating the PCM through the air gap will be assessed based on the amount of solidified PCM after the nighttime solidification period. The unsolidified material cannot melt and store heat during the daytime cycle. The energy use of the APS for daily cooling operation will increase with smaller amount of PCM. The amount of PCM available will be calculated based on the numerical simulation results where the amount of remaining energy in the PCM is clear.
H6	O1 and O4	The cooling potential of the APS differs when the amount and location of the PCM material is changed. The effect of the PCM location (wall or ceiling) will be determined within the experiment where measurements of the temperature fluctuations in the chamber are available. With lower amount of PCM its cooling effect decreases, and the energy need for cooling increases.

Based on the research deficiencies presented in Chapter 4.1 the novelty and scientific contributions of the present research are:

- The investigated system combines a ventilated internal PCM wall and ceiling (APS).
- APS is investigated experimentally in controlled experimental conditions where APS is measured simultaneously with the reference cell without APS. Such experimental facilities enable APS investigation under constant thermal conditions, optional transient thermal conditions (selected day of the test reference year or summer heatwave scenarios) and adding ventilation for improving the indoor air quality in the test cells for building users. In this way, the effect of the individual influential parameter under investigation can be distinguished.

- The micro-scale numerical simulation is calculated and validated with geometry of the entire PCM ceiling and wall.
- Numerical simulation on a micro scale considers the boundary condition of the temperature change in the test cell during the ventilation of the PCM curing air during the night (the effect of system's surrounding thermal environment). Considering such boundary conditions, a parametric analysis is performed based on changing the temperature of the inlet air in the air gap. The solidification time is determined, and the maximum inlet air temperature is determined for sufficient operation of the APS system – optimization of the system.

4.3. Workflow

This chapter presents the PhD. project workflow and describes how the main project tasks are structured in the chapters of the present manuscript.

Figure 4.1 shows the PhD. project workflow diagram and explains how the tasks are connected. Also, the number before each task name specifies in which chapters the individual task is discussed.

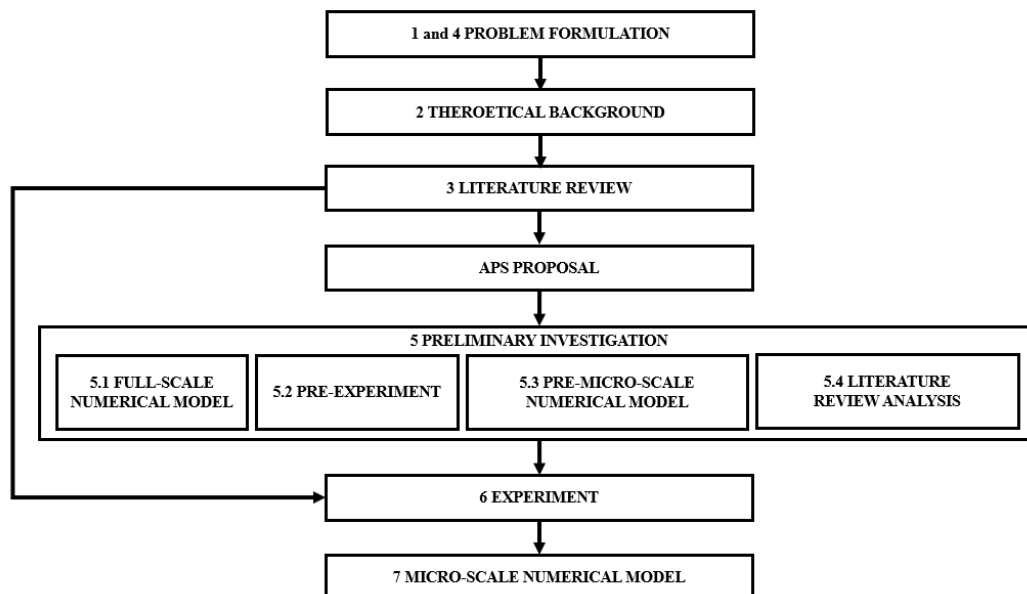


Figure 4.1: PhD. project workflow diagram.

- The formulation of the problem is presented in chapters '1 Introduction' and '4 Purpose and Aim of Doctoral Dissertation' of this manuscript. The Introduction addresses global world-scale challenges such as global warming and high energy use for cooling and the 'Purpose and aim of doctoral dissertation' focuses on specific challenges based on the presented knowledge gap of the field.
- The literature review presents the state-of-the-art of the research from the scope of the building element integrated PCM materials with nocturnal free cooling.

- The solution to the challenges and the proposed active-passive system (APS) development was influenced following the literature review.
- The purpose of the preliminary investigation was to gain knowledge on the problem and find design characteristics for the proposed APS system. The preliminary research was performed with three different methods: full-scale energy performance numerical model of the system, small-scale pre-experiment and micro-scale numerical model of the heat transfer from PCM to air.
 - Full-scale energy performance of a single-family building with application of phase change materials (PCM) with DesignBuilder v3.4 software tool for unsteady state building simulation [39]. The main drawback is that the software cannot calculate air gaps. In investigated climates of Rome and Ljubljana with hot summer periods, the lesson learned was that among other investigated products and melting temperatures (T_m) the PCM with T_m of 24 °C showed the best results in decreasing the daily indoor temperatures of the hottest day of TRY within the recommended values of indoor thermal comfort standards (EN 16798-1:2019) [37].
 - In the pre-experiment a small-scale test of a section of an APS ceiling was tested. The test consisted of a sequence of PCM plates with T_m of 22 °C positioned on the bottom of the rectangular ventilated Expanded PolyStyrene (EPS) channel. Based on the performed measurements, key characteristics of PCM phase change were obtained and measuring technique learned.
 - Micro-scale numerical model of the pre-experimental set-up was performed with ANSYS Fluent v19.1 software [149]. The model was validated with the pre-experiment. The main purpose was to learn how to model a PCM with heat transfer to air and simulate PCM with different melting points to examine the phase change dynamics. The results showed that to fully complete PCM solidification cycle in the determined nighttime period (12 h) a suitable temperature difference between the initial PCM material temperature and air gap inlet air temperature needs to be established.
- The experiment was performed at National School of State Public Works (ENTPE) in Vaulx-en-Velin, France. The experimental chamber had to be completely re-built and equipped with some new equipment to be able to provide the required experimental conditions. The experiment was configured with knowledge obtained from the literature review and preliminary investigation (e.g. selection of the melting points, air flow characteristics).
- Another micro-scale numerical model was established simulating the APS system. It was validated with the results from the experimental measurements and its key objective was to simulate the effect of different air gap inlet air temperatures and to define the highest inlet air temperature for the complete nighttime solidification of the PCM. Within the micro-scale numerical model also the energy performance and operation costs were calculated based on the numerical results. Based on the final energy analysis, the potential of the APS system is assessed and discussed with comparison to conventional cooling systems.

Figure 4.2 shows the timeline with task durations and milestones.

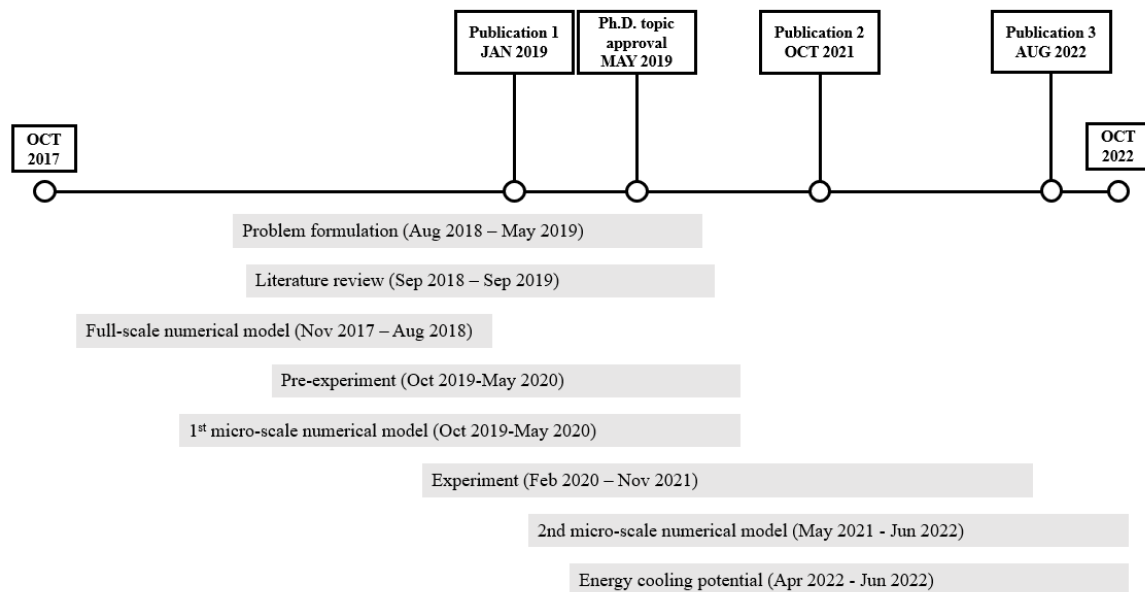


Figure 4.2: Timeline with task durations and milestones.

4.4. Publications

The results of this PhD project were published as original scientific journal articles:

1. **ZAVRL, Eva**, ZUPANC, Gašper, STRITIH, Uroš, DOVJAK, Mateja. Overheating reduction in lightweight framed buildings with application of phase change materials. *Strojniški vestnik*. Jan. 2020, vol. 66, no. 1, str. 3-14, si 3, ilustr. ISSN 0039-2480. <https://www.sv-jme.eu/article/overheating-reduction-in-lightweight-framed-buildings-with-application-of-phase-change-materials/>, DOI: 10.5545/sv-jme.2019.6244. [COBISS.SI-ID 17015835], [JCR, SNIP, WoS]
2. **ZAVRL, Eva**, EL MANKIBI, Mohamed, DOVJAK, Mateja, STRITIH, Uroš. Enhancing performance of building elements with phase change materials for cooling with air-based systems. *Journal of energy storage*. [Print ed.]. Jul. 2022, vol. 51, str. 1-32, ilustr. ISSN 2352-152X. <https://www.sciencedirect.com/science/article/pii/S2352152X22004832>, DOI: 10.1016/j.est.2022.104461. [COBISS.SI-ID 102719491], [JCR, SNIP, Scopus]
3. **ZAVRL, Eva**, EL MANKIBI, Mohamed, DOVJAK, Mateja, STRITIH, Uroš. Experimental investigation of air-based active-passive system for cooling application in buildings. *Sustainable cities and society*. [Spletna izd.]. 2022, str. 1-13, ilustr. ISSN 2210-6715.

<https://www.sciencedirect.com/science/article/pii/S2210670722003511>, DOI: 10.1016/j.scs.2022.104031. [COBISS.SI-ID 117204483], [JCR, SNIP, Scopus]

The results were also presented at international conferences:

4. **ZAVRL, Eva**, EL MANKIBI, Mohamed, DOVJAK, Mateja, STRITIH, Uroš. Experimental investigation of PCM system improved with nighttime ventilation for enhanced solidification. V: Clima 2022 : REHVA 14th HVAC World Congress, 22nd-25th May, Rotterdam, Netherlands : eye on 2030 : towards digitalized, healthy, circular and energy efficient HVAC : proceedings. [Delft]: TU Delft Open, 2022. Str. 1-7, ilustr. <https://proceedings.open.tudelft.nl/clima2022/article/view/249>, DOI: 10.34641/clima.2022.249. [COBISS.SI-ID 110501123]

5. **ZAVRL, Eva**, ZUPANC, Gašper, STRITIH, Uroš, DOVJAK, Mateja. Application of PCM in building's envelope of lightweight prefabricated houses as an addition to a PV driven renovation cooling system by EU project HEART. V: HÄBERLE, Andreas (ur.). EuroSun2018 : proceedings of the ISES EuroSun 2018 Conference. 12th International Conference on Solar Energy for Buildings and Industry, September 10-13, 2018, Rapperswil, Switzerland. Freiburg: International Solar Energy Society, cop. 2018. F. [1-9], ilustr. ISBN 978-3-9820408-0-6. <http://proceedings.ises.org/?doi=eurosun2018.04.02>, DOI: 10.18086/eurosun2018.04.02. [COBISS.SI-ID 16505371], [WoS]

6. **ZAVRL, Eva**, STROPNIK, Rok, KOŽELJ, Rok, STRITIH, Uroš, DOVJAK, Mateja. Application of macro-encapsulated PCM in light-weight building structure for reduction of cooling energy use. V: RISTIĆ, Alenka (ur.), STRITIH, Uroš (ur.). Enerstock 2021 : 15th International Virtual Conference on Energy Storage : June 9-11, 2021, Ljubljana, Slovenia : book of abstracts. 15th International Virtual Conference on Energy Storage, June 9-11, 2021, Ljubljana, Slovenia. [Ljubljana]: National Institute of Chemistry, Department of Inorganic Chemistry and Technology: Faculty of Mechanical Engineering, 2021. Str. 65. ISBN 978-961-6104-49-4. <https://www.enerstock2021.org/>. [COBISS.SI-ID 67214339]

7. **ZAVRL, Eva**, TOMC, Urban, EL MANKIBI, Mohamed, STRITIH, Uroš, DOVJAK, Mateja. Parametric study of the PCM system for space cooling improved with the nighttime ventilation for the enhanced solidification. V: RISTIĆ, Alenka (ur.), STRITIH, Uroš (ur.). Enerstock 2021 : 15th International Virtual Conference on Energy Storage : June 9-11, 2021, Ljubljana, Slovenia : book of abstracts. 15th International Virtual Conference on Energy Storage, June 9-11, 2021, Ljubljana, Slovenia. [Ljubljana]: National Institute of Chemistry, Department of Inorganic Chemistry and Technology: Faculty of Mechanical Engineering, 2021. Str. 182. ISBN 978-961-6104-49-4. <https://www.enerstock2021.org/>. [COBISS.SI-ID 67216899]

8. **ZAVRL, Eva**, KOŽELJ, Rok, STRITIH, Uroš, ZUPANC, Gašper, DOVJAK, Mateja. Uporaba PCM-ja v lahkih montažnih stavbah kot dopolnilo k prenovi hlajenja s fotovoltaike : EU projekt Heart. V: Akademija strojništva 2018 : povezovanje in mreženje. 7. mednarodna konferenca strojnih inženirjev 2018, Ljubljana, Cankarjev dom, 25. oktober 2018. Ljubljana: Zveza strojnih inženirjev Slovenije, 2018. Letn. 7, št. 3/4, str. 42, ilustr. Svet strojništva, Letn. 7, št. 3/4. ISSN 1855-6493. [COBISS.SI-ID 16309275]

9. STROPNIK, Rok, **ZAVRL, Eva**, STRITIH, Uroš. Improved thermal comfort of light weight structure with macro-encapsulated PCM : presentation at X IAQVEC 2019, 10th

International conference on indoor air quality, ventilation and energy conservation in buildings, 5-7th September 2019, Bari, Italy. [COBISS.SI-ID 59654915]

5. Preliminary investigation

This chapter aims to present the preliminary investigation which is the base for the selection of PCM material and product type. The preliminary investigation consists out of four parts, each presenting an individual investigation:

- Full-scale numerical model
- Pre-Experimental investigation
- Pre-micro-scale numerical model
- Discussion and analysis of literature review

5.1. Full-scale numerical model

The purpose of the full-scale numerical model investigation is to determine thermal and energy performance of the PCM during the cooling season. DesignBuilder Software Ltd is an advanced unsteady state building performance simulation tool that helps the designer to quickly assess the environmental performance of new and existing buildings [39].

5.1.1. Method

An energy performance of a single-family house with floor area of 177.45 m², located in moderate climate of Ljubljana, Slovenia was simulated with DesignBuilder™ v3.4 software (Figure 5.1). Although the system is primarily purposed for office buildings, the preliminary investigation was carried out on a simpler less complex single-family building. A lightweight wooden frame structure was added PCM on the inner side of the building envelope. Different melting points ($T_m = 23\text{ °C}$, 24 °C , 25 °C , 26 °C and 27 °C) and heat storage capacities (M182, M91 M51, M27) of macroencapsulated BioPCM™ layer were investigated [150]–[152]. Since, BioPCM™ is commercially available only in $T_m = 23\text{ °C}$, 25 °C and 27 °C , materials with $T_m = 24\text{ °C}$ and 26 °C are fictive and their thermal characteristics are determined based on the interpolation between the existing materials' characteristics. Microencapsulated PCM gypsum board was investigated for ($T_m = 23\text{ °C}$ and 25 °C) and at $T_m = 23\text{ °C}$ for two thicknesses (1.25 cm and 2.50 cm) [153].



Figure 5.1: Single-family building (front).

The simulation conditions are presented in Table 5.1.

Table 5.1: Simulation conditions.

Fixed input data	Value
Clothing insulation	0.5 clo
CO ₂ emissions	(The amount was defined based on the function of the space)
Occupancy rate	/
Internal heat gains	/
Air leakage of all SC*	0.7 ACH, constant
Thermal transmittance of the windows	1.058 W/(m ² K)
Total solar energy transmittance	0.579
Shading type	blinds outside
Light gains	n.a.
Ventilation type	hybrid ventilation; (1 ACH**)
Air conditioning	The inclusion point was set when the internal air temperature exceeded 26 °C and the coefficient of cooling efficiency was 3.2
Season	Summer (1.8. to 7.8.2002)*** and whole year 2002
Location	Ljubljana, Slovenia; Rome, Italy and Copenhagen, Denmark
PCM melting point (initial)****	25 °C

*Structural complex (SC), **Air change per hour (ACH), ***The hottest week in 2002, for 5 days the outdoor temperature exceeded 30 °C, ****Phase change materials (PCM)

The structural complexes of the building envelope and their U values are presented in Table 5.2.

Table 5.2: Heat transfer coefficients U [$W/(m^2 K)$] of the designed building envelope structural complexes.

U [$W/(m^2 K)$]	HW	LW	LWPCM.a	LWPCM.b
Exterior wall	0.201	0.139	0.130	0.138
Roof	0.182	0.111	0.111	0.111
Floor	0.260	0.260	0.260	0.260

Figure 5.2-Figure 5.5 show the structural complexes (SCs) of the investigated external walls (heavyweight (HW), lightweight (LW), lightweight with microencapsulated BioPCM™ (LW_{PCM.a}) and lightweight with microencapsulated PCM gypsum boards (LW_{PCM.b})).

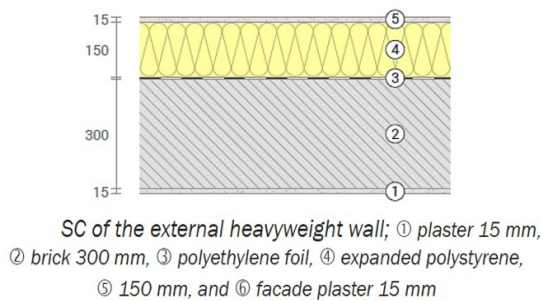


Figure 5.2: Structural complex (SC) of heavyweight load-bearing structure.

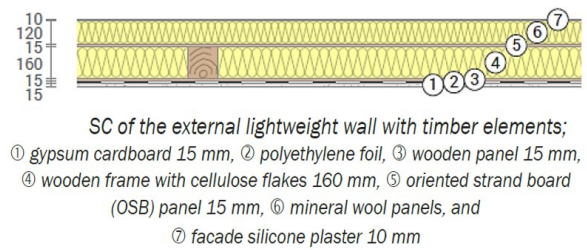


Figure 5.3: Structural complex (SC) of lightweight load-bearing structure.

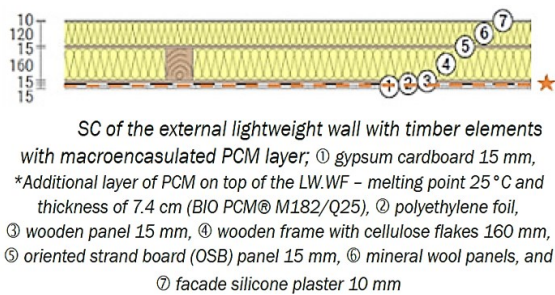


Figure 5.4: Structural complex (SC) of lightweight load-bearing structure with macroencapsulated BioPCM™ layer.

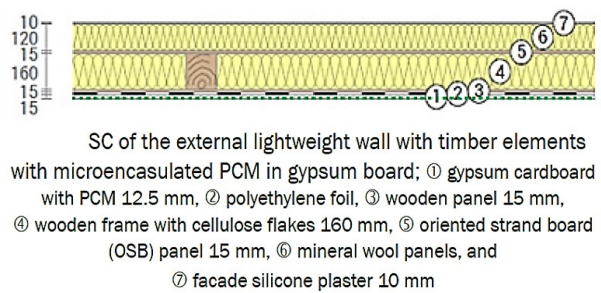


Figure 5.5: Structural complex (SC) of lightweight load-bearing structure with microencapsulated PCM gypsum board.

Figure 5.6 shows the systematic scheme of variations investigated under three different climate types of Ljubljana, Copenhagen and Rome.

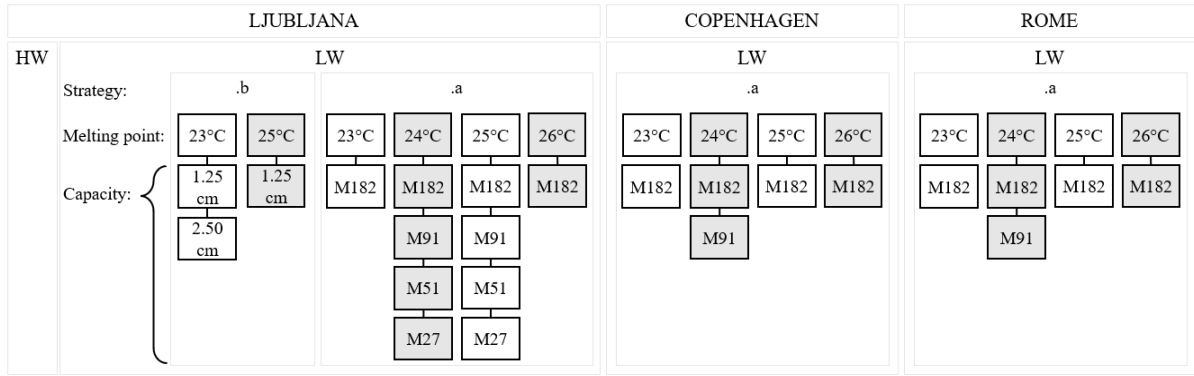


Figure 5.6: Systematic scheme of variations investigated under three different climate types Ljubljana, Copenhagen and Rome.

5.1.2. Results

5.1.2.1. Parametric study of PCM characteristics in Ljubljana

Figure 5.7 shows the Outside-dry bulb temperatures obtained operative temperatures obtained with heavyweight and lightweight load-bearing structure and thermal comfort limits for III Category of EN 16798:2019 [37]. Operative temperatures obtained with lightweight structure on the hottest day of the year exceed the recommended indoor temperature for 2 °C.

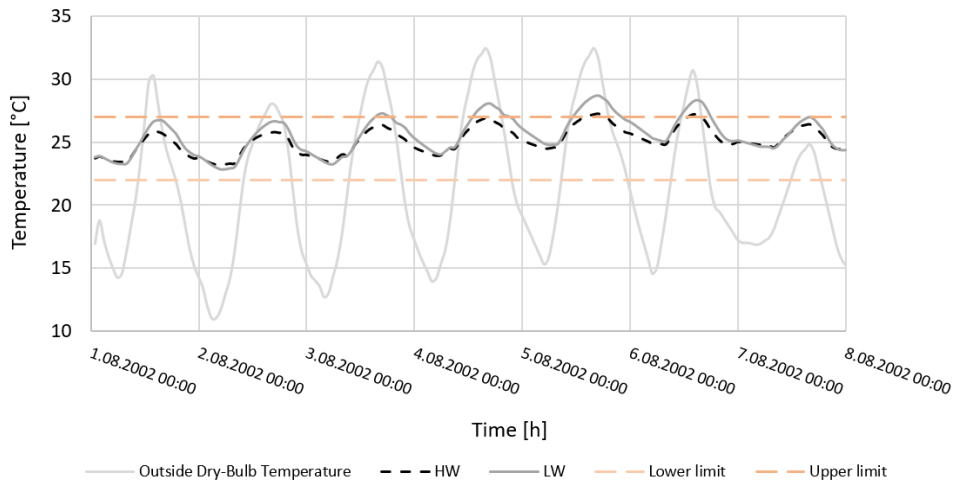


Figure 5.7: Outside dry-bulb temperature, operative temperatures obtained with heavyweight and lightweight load-bearing structure and thermal comfort limits for III Category of EN 16798:2019 [37].

Figure 5.8 shows the operative temperatures obtained with lightweight load-bearing structure, microencapsulated gypsum boards of two melting temperatures ($T_m = 23\text{ °C}$ and 25 °C) and at $T_m = 23\text{ °C}$ for two thicknesses (1.25 cm and 2.50 cm) and thermal comfort

limits for III Category of EN 16798:2019 [37]. Microencapsulated gypsum boards have very little cooling effect. However, the product with $T_m = 25\text{ }^\circ\text{C}$ has slightly higher cooling effect compared to the product with $T_m = 23\text{ }^\circ\text{C}$.

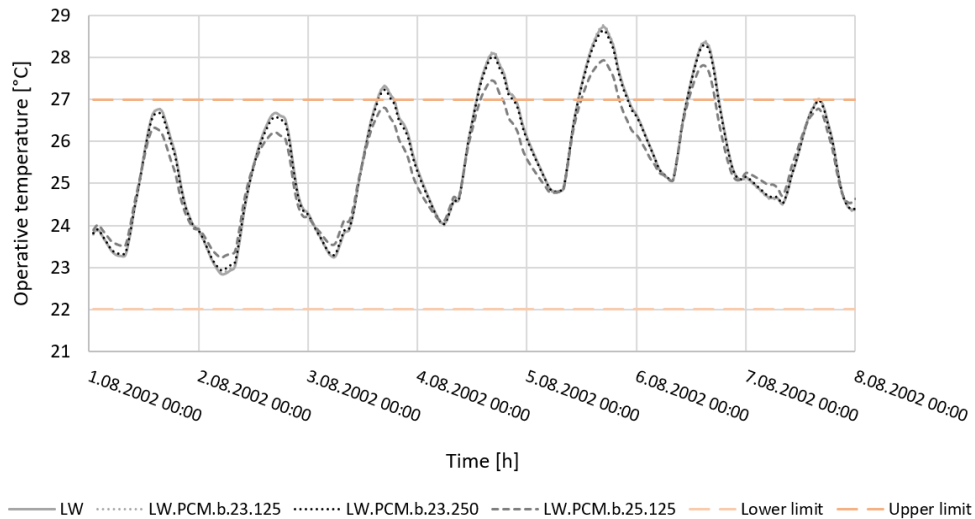


Figure 5.8: Operative temperatures obtained with lightweight load-bearing structure, microencapsulated gypsum boards and thermal comfort limits for III Category of EN 16798:2019 [37].

Figure 5.9 shows the operative temperatures obtained with lightweight load-bearing structure, macroencapsulated BioPCM™ with 5 different melting temperatures ($T_m = 23\text{ }^\circ\text{C}$, $24\text{ }^\circ\text{C}$, $25\text{ }^\circ\text{C}$, $26\text{ }^\circ\text{C}$ and $27\text{ }^\circ\text{C}$) and thermal comfort limits for III Category of EN 16798:2019 [37]. The highest cooling effect has PCM with $T_m = 24\text{ }^\circ\text{C}$. Almost during the entire week, PCMs with $T_m = 25\text{ }^\circ\text{C}$ and $25\text{ }^\circ\text{C}$ can keep the operative temperatures within the recommended temperatures. PCM with $T_m = 23\text{ }^\circ\text{C}$ has no cooling effect.

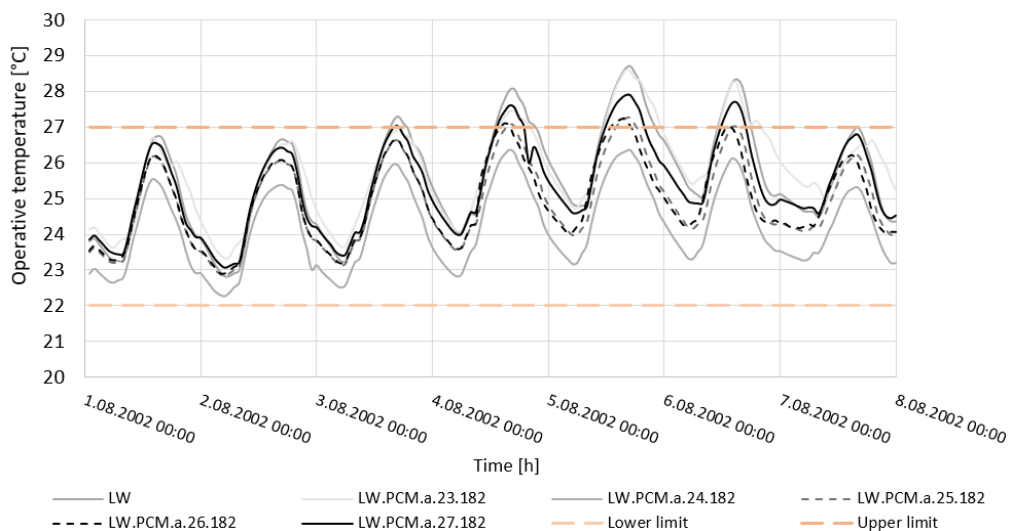


Figure 5.9: Operative temperatures obtained with lightweight load-bearing structure, macroencapsulated BioPCM™ and thermal comfort limits for III Category of EN 16798:2019 [37].

Figure 5.10 shows the operative temperatures obtained with lightweight load-bearing structure, macroencapsulated BioPCM™ with melting point of 24 °C and 4 different material amounts - thermal capacities (M182, M91, M51 and M27) and thermal comfort limits for III Category of EN 16798:2019 [37].

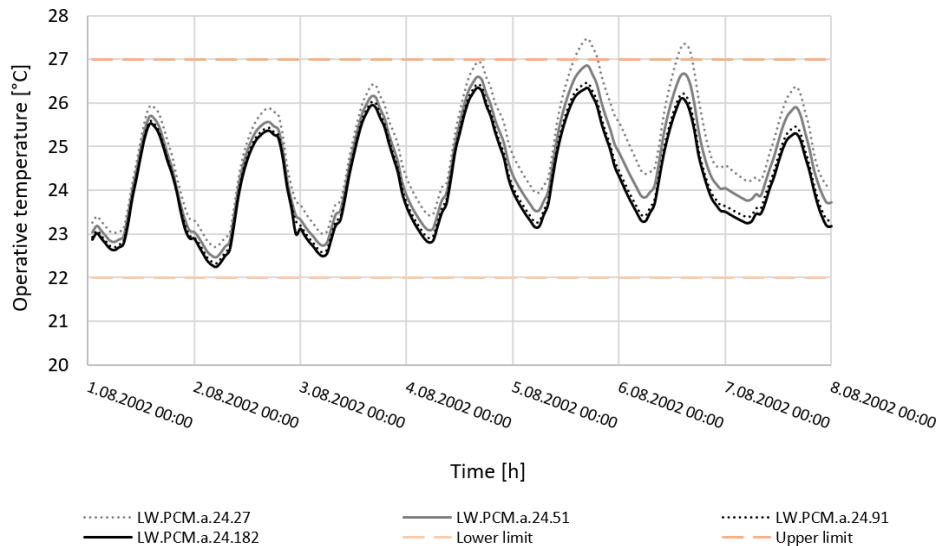


Figure 5.10: Operative temperatures obtained with lightweight load-bearing structure, macroencapsulated BioPCM™ with melting point of 24 °C and thermal comfort limits for III Category of EN 16798:2019 [37].

Therefore, it may be concluded that PCM with $T_m = 24$ °C shows the highest cooling effect even at lower amounts of material (lower thermal capacities). Higher or lower melting temperatures do not perform as efficiently or have almost no effect.

5.1.2.2. Parametric study of PCM characteristics in EU countries

As visible from previous chapter, the microencapsulated PCM gypsum boards didn't provide much cooling effect so in this chapter the focus is given only on macroencapsulated BioPCM™ with effective melting temperatures. All investigated cases Ljubljana, Copenhagen and Rome are tested with 3 different melting temperatures ($T_m = 23$ °C, 24 °C and 25 °C) of BioPCM™ and PCM with $T_m = 24$ °C is tested for two different capacities (M182 and M91).

Figure 5.11 shows operative temperatures obtained with BioPCM™ in Ljubljana with thermal comfort limits for III Category of EN 16798:2019 [37]. From the figure it is visible, that for both thicknesses of PCM ($T_m = 24$ °C), the cooling effect is the strongest. Since there is no difference in the temperatures obtain under different thicknesses, the LW.PCM.24.91 has enough PCM material to cool the building space effectively. In the hottest days, PCM ($T_m = 25$ °C) can keep the operative temperatures below the recommended upper limit of thermal comfort. Melting temperature of 23 °C is too low, to cool the building space.

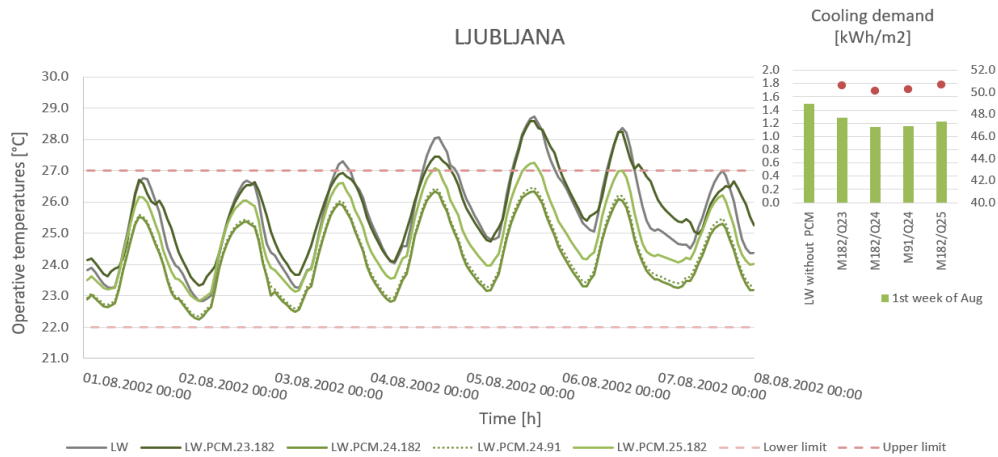


Figure 5.11: Operative temperatures obtained with BioPCM™ in Ljubljana with thermal comfort limits for III Category of EN 16798:2019 [37].

Figure 5.12 shows operative temperatures obtained with BioPCM™ in Copenhagen with thermal comfort limits for III Category of EN 16798:2019 [37]. In all investigated cases, the operative temperatures are kept within the recommended values. Therefore, the application of PCM in Copenhagen is not needed. The rest of the results can be found in Appendix B.

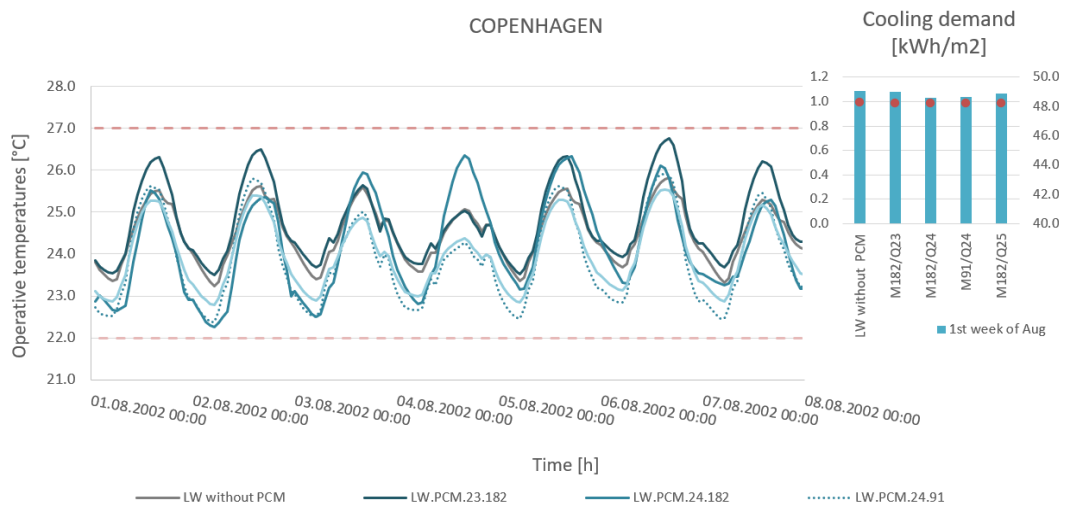


Figure 5.12: Operative temperatures obtained with BioPCM™ in Copenhagen with thermal comfort limits for III Category of EN 16798:2019 [37].

Figure 5.13 shows operative temperatures obtained with BioPCM™ in Rome with thermal comfort limits for III Category of EN 16798:2019 [37]. In Rome, most of the investigated PCM cases keep the operative temperatures within the recommended values. Even the LW structure without PCM isn't overheated. However, it may be observed, that PCM ($T_m = 23\text{ }^\circ\text{C}$) even deteriorates the thermal environment, as it stores the excess heat due to low temperature differences between PCM material and ambient air which result in unsolidified material.

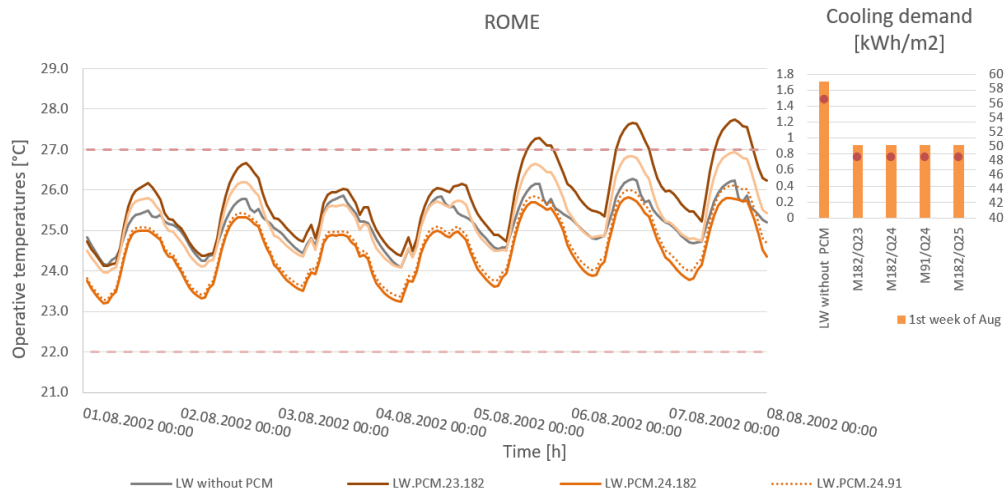


Figure 5.13: Operative temperatures obtained with BioPCM™ in Rome with thermal comfort limits for III Category of EN 16798:2019 [37].

5.1.3. Conclusions

With full-scale building model simulation, the following conclusions may be drawn.

- Based on the results it can be concluded that melting temperature is the most important PCM thermal characteristic for optimal performance.
- The amount of PCM in the building must be high enough to provide cooling, but not too high that it remains unused.
- In Ljubljana and Rome, PCM with $T_m = 24$ °C provides the highest cooling effect. In both cases, the optimal performance was obtained even when its amount was reduced by half.
- Even though ID Design Builder provides a user-friendly interface for a holistic determination of thermal and energy performance of the building, some questions, such as level of phase change, remain unanswered. Since many environmental, geometric and system parameters strongly effect the results, an effect of a detailed thermal characteristic of PCM cannot be distinguished. As well, the software is less convenient for optimisation of the PCM thicknesses.
- To fully understand heat transfer dynamics in PCM, furthermore detailed analysis on a component level need to be performed.

5.2. Pre-Experimental investigation

The purpose of this experiment is to investigate the heat transfer from the PCM plates to air, to investigate the section of the final APS (section of the ceiling) and to learn how to use the measuring equipment to obtain correct measuring results.

5.2.1. Method

In the Laboratory for Heating, Sanitary, Solar and Air conditioning Engineering (LOSK) at University of Ljubljana, the experiment was performed. The testing station consisted out of the air-preparation /ventilation unit and PCM heat storage - ventilated channel with PCM plates (section of the PCM suspended ceiling with ventilated air gap) as visible from Figure 5.14.

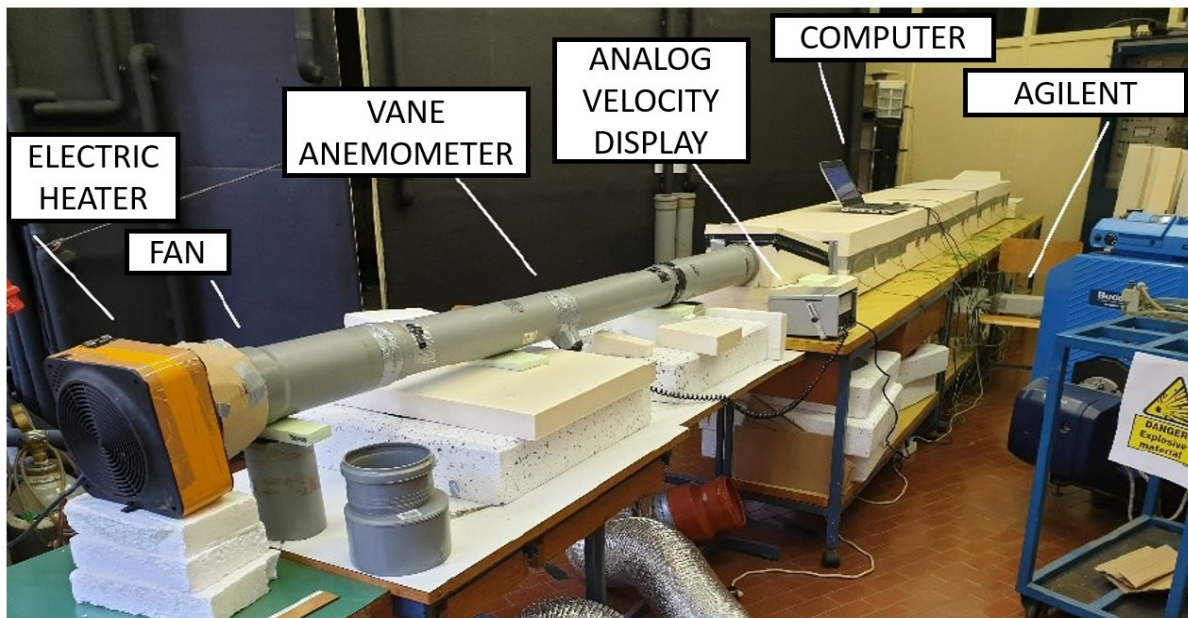


Figure 5.14: Testing station with air preparation unit and PCM heat storage.

5.2.1.1. Air preparation and ventilation unit

The PVC ducts (2 m long; Ø 10 cm and Ø 12 cm) distributed the air from the electric heater to the heat storage opening. In the ducts, there is a still honeycomb which improves the airstream direction. The purpose of electric heater (Figure 5.15) was to heat the air before it entered the ventilator and PVC ducts. There are two power settings available, $P = 1118 \text{ W}$ or $P = 2200 \text{ W}$. As the heater's ventilator wasn't strong enough to deliver the air to the PCM heat storage at required flow rates, an additional ventilator for airflow acceleration was placed afterwards (Figure 5.16). In cases of solidification, an aluminium

duct was connected to the ventilator instead of the heater and the duct end was positioned through the window, to provide the storage with cold outdoor air.

The airflow in the duct was monitored by the vane anemometer.



Figure 5.15: Electric heater.



Figure 5.16: Ventilator.

5.2.1.2. Heat storage

The heat storage - ventilated channel with PCM plates was constructed out of 10 cm thick expanded polystyrene (EPS) plates (Figure 5.17). There are 8 PCM plates (Rubitherm RT22HC) positioned in the channel [154].

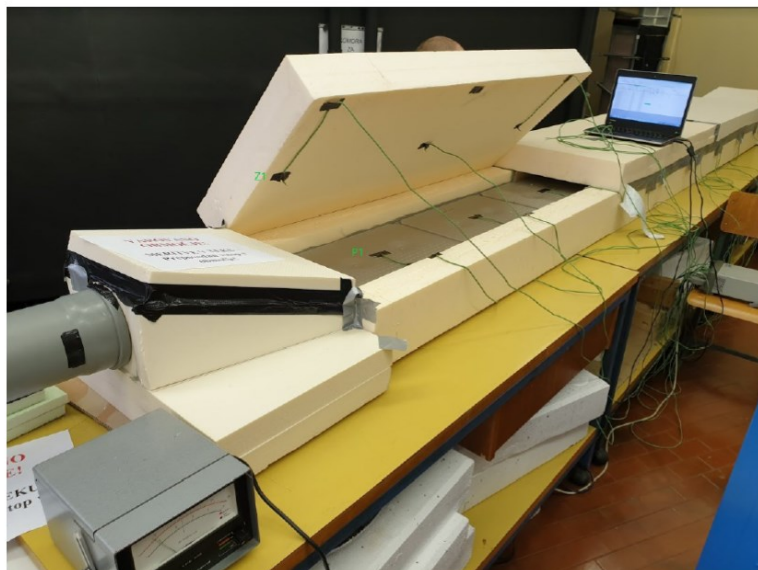


Figure 5.17: PCM heat storage - ventilated channel with PCM plates.

The peak melting temperature of the PCM is 22 °C. The CSM plate (45 cm x 30 cm x 1.5 cm) weights 1.5 kg, with the aluminium case mass of 363 g and PCM mass of 1140 g. The DSC diagram of the PCM is presented in Figure 5.18. The total heat storage capacity is 190 kJ/kg.

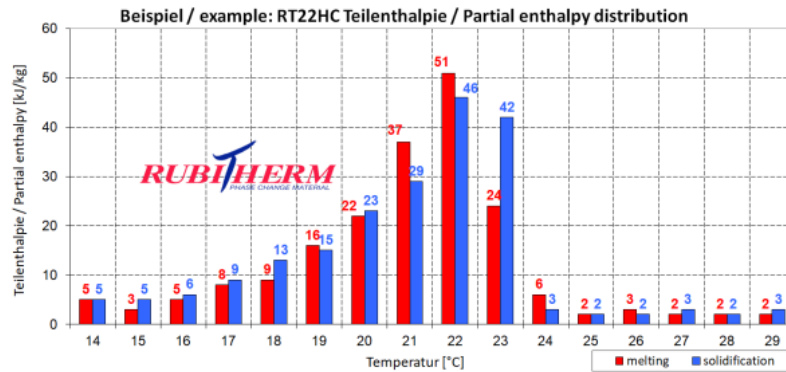


Figure 5.18: DSC diagram of Rubitherm RT22HC [154].

5.2.1.3. Measuring equipment and measuring points

Thermocouples were made from NiCr-Ni and covered in PVC (Measuring range: -50 °C do 200 °C; Accuracy: A: $\pm (0,15 + 0,002|t|)$ °C). They were connected to Agilent 34970A data acquisition (Figure 5.19). The measuring time step of 10 s was logged into BenchLink Data Logger 3 software. Figure 5.20 shows the vane anemometer (\varnothing 10 cm) was positioned in the middle of the PVC ducts. The analog data display showed velocities in [m/s] (at 20 °C, the accuracy in a low velocity range: ± 2.5 % and the accuracy in a high velocity range: ± 1 %; Temperature range: 10-70 °C; Pressure range: 500 mb-2 bar).



Figure 5.19: Agilent 34970A.



Figure 5.20: Vane anemometer.

The thermocouples were positioned in the top/middle (air side) of the PCM plates and sealed with plastic tape. Two thermocouples were positioned also at the bottom/middle (EPS wall side) of the first and the last PCM plate (Figure 5.21).

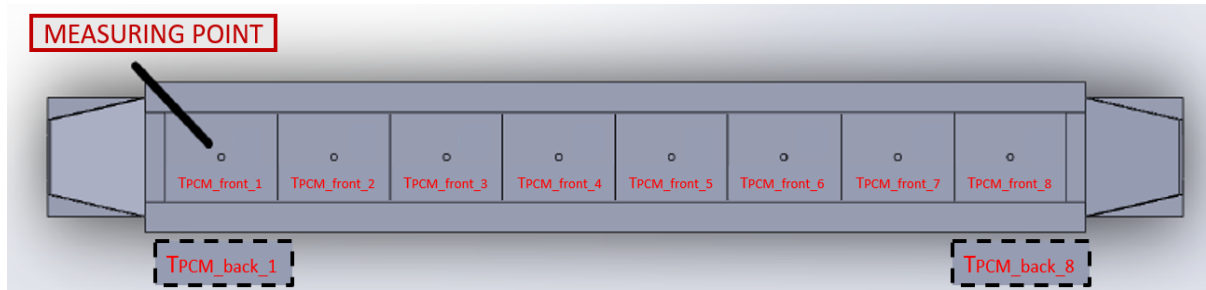


Figure 5.21: Locations of thermocouples for PCM plate surface temperature measurements.

The rest of the thermocouples were positioned at the air inlet and outlet and in the centre of air channel above each PCM plate (Figure 5.22). More detailed sketches with dimensions in Appendix C.



Figure 5.22: Locations of thermocouples for air temperature measurements.

At first, many different air velocity and air temperature cases were predicted. However, due to the impossibility of inlet air temperature regulation, the inlet air temperatures depended on the environment (laboratory or outdoor air temperatures). Therefore, none of the results are comparable. Also, this was the first experiment performed within this project and therefore, the method for measuring protocol was incorrect. Most of the cases were stopped before the phase change was finalized. This is due to the fact that instead of observing air temperatures and waiting that T_{a_8} reaches T_{a_1} , the case was stopped when the PCM surface temperature on the bottom of the plate ($T_{PCM_back_8}$) reached $21\text{ }^{\circ}\text{C}$ ($1\text{ }^{\circ}\text{C}$ less than peak melting temperature of the PCM). This misconception occurred because before the experiment the first numerical model analysis with ANSYS Fluent were performed (Figure 5.38) and the temperature drop of the PCM material (as well as the phase change) appeared sequentially along the channel [149].

Finally, also the temperature profile at the outlet was measured with thermocouples (Figure 5.23).

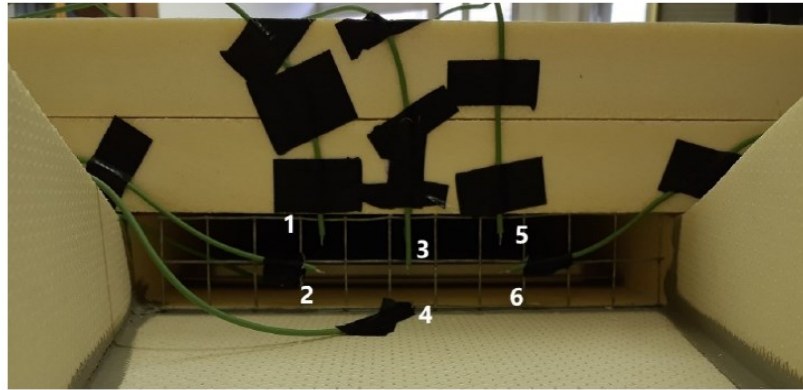


Figure 5.23: Air temperature profile on outlet measured with thermocouples.

Due to the little experiences with this sort of measurements and the learning process, the measuring scheme among all the cases only one case (VIII) wasn't stopped prior to the end of the phase change (Figure 5.24).

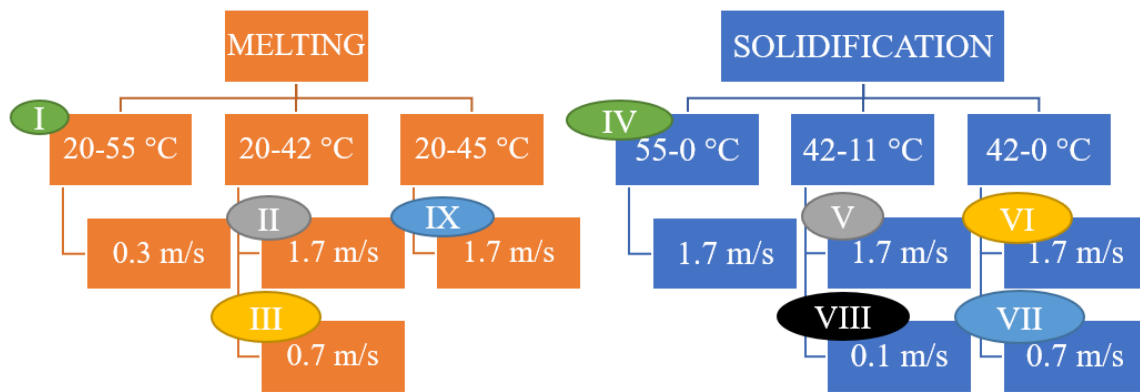


Figure 5.24: Scheme of experimental cases.

At the end, energy stored in PCM plates was calculated based on the volumetric flow rate (\dot{V}) as shown in Equation 5.1:

$$\dot{V} = \frac{\pi \cdot d_p^2}{4} \cdot v \cdot 3600 \quad (5.1)$$

, where d_p is pipe/duct diameter and v velocity. The mass flow rate (\dot{m}) was determined considering the air density ($\rho_a = 1.118 \text{ kg/m}^3$) presented in Equation 5.2:

$$\dot{m} = \dot{V} \cdot \rho_a \quad (5.2)$$

Equation 5.3 shows the power (P) determined considering the specific heat capacity of air ($c_{p,a} = 1.007 \text{ kJ/(kg K)}$) and temperature difference between the inlet and outlet air temperature (ΔT):

$$P = \dot{m} \cdot c_{p,a} \cdot \Delta T \quad (5.3)$$

Equation 5.4 presents the final heat storage determined based on the measuring time step (10 s):

$$Q_{\text{dis}} = P \cdot (10/3600) \quad (5.4)$$

5.2.2. Results

The graph in Figure 5.25 shows the solidification period during the case VIII. At air velocity of 0.1 m/s, the airflow rate was 0.79 l/s (2.844 m³/h). The preheated PCM plates were cooled from 42 °C with inlet air temperature of 11 °C. As this is the only finalized case, it is used for the validation of the experiment with micro-level numerical model in ANSYS Fluent.

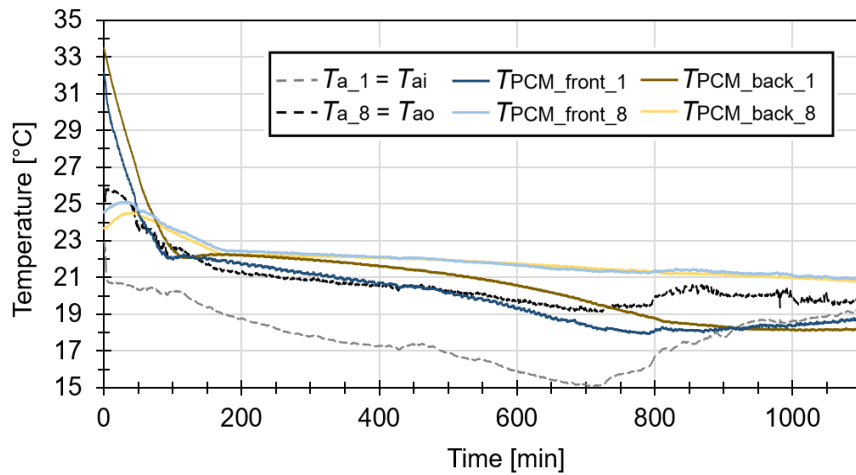


Figure 5.25: Temperatures obtained during the solidification of PCM in case VIII.

The temperatures profile obtained on the outlet are presented in Figure 5.26.

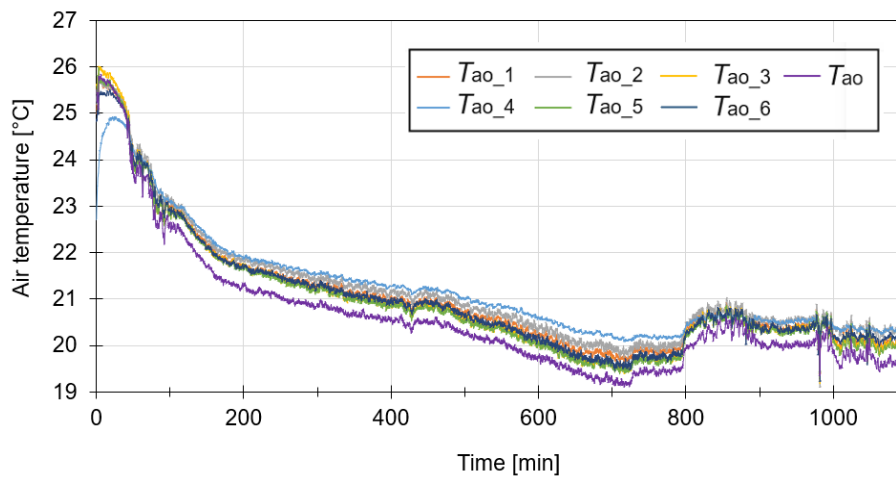


Figure 5.26: Air temperatures at the outlet temperature profile.

The measured and afterwards calculated energy stored in plates was in size of 433.6 kWh which was 49.8 Wh lower from the theoretically determined energy storage of the plates 483.4 Wh (range 14-29 °C).

5.2.3. Conclusions

Therefore, the pre-experimental results were used for understanding the measuring approach, melting and solidification dynamics, and validation of pre-numerical simulation with ANSYS. In conclusion, the lessons learned are:

- The melting of PCM in plates was not directly sequential along the entire channel length, like it was in ANSYS software (Figure 5.38). It is assumed, that the solidification started occurring in each plate from the beginning to the end of the plate in relation to the temperature of the incoming air stream.
- The measurements of PCM plate surface temperatures with selected thermocouples were not a reliable method for the determination of phase change end.
- Compared to the previous statement, the outlet air temperatures are more reliable method.
- The energy analysis showed that due to the high temperature differences between the PCM and the environment (laboratory air) there was a lot of heat losses through the EPS walls to the environment.

5.3. Pre-numerical simulation with ANSYS

The purpose of the pre-micro scale numerical simulation with ANSYS Fluent is to simulate the effect of different PCM materials with different melting temperatures and heat storage capacities [149].

5.3.1. Method

In this chapter, the specifics of the present preliminary numerical simulation model are specified. The rest of the method is set out in chapter 2.4.

5.3.1.1. Geometry selection

The two-dimensional geometry is constructed out of two adjacent zones, liquid air and solid PCM zone. The first PCM analysed (RT22HC) was the same as chosen in the pre-experiment described in the previous chapter '5.2 Pre-Experimental investigation'. The length of the system is 360 cm and the thickness of air layer is 4 cm (Figure 5.27). The thickness of PCM layer was determined based on the mass (8x1140 g), surface of the plates (8x30x360 cm²) and density (700 kg/m³) of PCM (RT22HC) and should be 1.2 cm, but was due to improved meshing characteristics simplified to 1 cm. The purpose of this investigation is finding the required solidification time in relation to the inlet air temperature and velocity. Therefore, only the solidification cycle of the system with PCM was investigated.

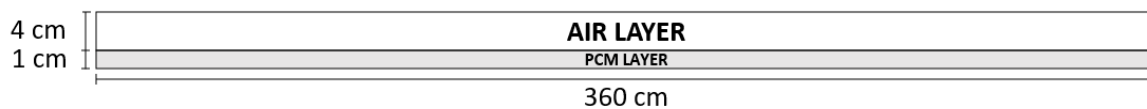


Figure 5.27: Sketch of model's geometry.

5.3.1.2. Grid and time step

The sensitivity of the model to grid size and calculation time step was investigated and the results are shown in Figure 5.28 and Figure 5.29. The tested grids consisted out of square elements with element size between 1 mm and 50 mm. Based on the results, the model was calculated using square 5 mm grid (7200 elements) and the time step set to 120 s. The simulation duration depended on the investigation case. The nighttime solidification case simulated the 12 h cycle (1440 time steps) and the other cases simulated the time required for the material to reach the inlet temperature (up to 26400 time steps).

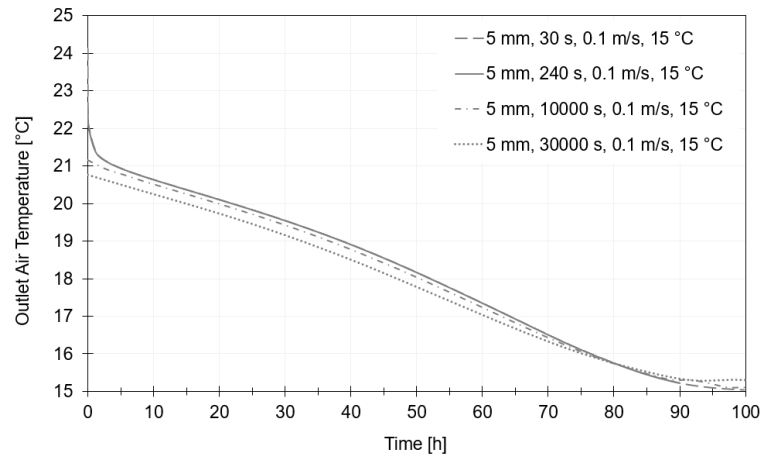


Figure 5.28: Time step independence test.

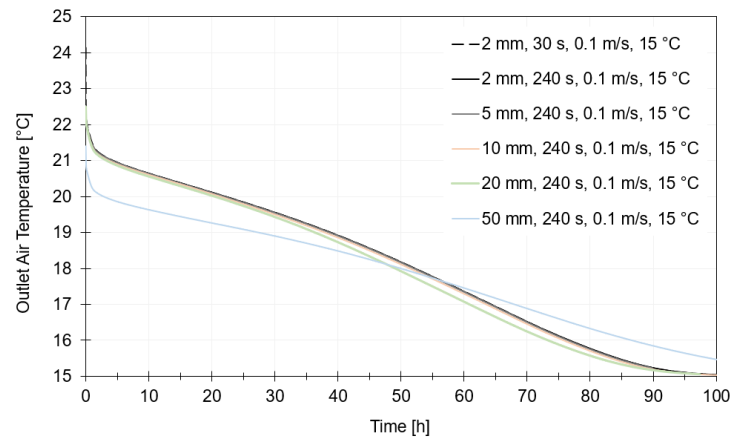


Figure 5.29: Grid independence test.

Figure 5.30 shows the selected grid with element size of 5 mm.



Figure 5.30: The selected grid with element size of 5 mm.

5.3.1.3. Material properties

Different types of PCM material with different melting temperatures and heat storage capacities were chosen based on encapsulation method (macroencapsulation in the aluminium CSM plate). The melting temperatures of PCM were selected to target the recommended indoor temperatures in summer (24 – 26 °C).

The phase change materials were simulated as solid domain. Their heat capacity was modified with piece-wise linear input of solidification cycle by inserting temperatures from the Differential Scanning Calorimetry (DSC) diagram with corresponding partial enthalpies. Table 5.3 presents four phase change materials with their thermal characteristics tested: PCM RT-line – organic phase change materials and PCM SP-line inorganic phase change materials. From RT line, besides RT22HC (Figure 5.31) also RT24 (Figure 5.32) was tested and from SP line, SP24E (Figure 5.33) and SP25E2 (Figure 5.34) were investigated.

Table 5.3: The list of PCM types and their thermal characteristics.

	RT22HC	RT24	SP24E	SP25E2
T_m [°C]	20-23 °C	21-25 °C	24-25 °C	24-26 °C
Total c_p	190 kJ/kg	160 kJ/kg	180 kJ/kg	180 kJ/kg
ρ (solid-liquid) [kg/l]	0.76-0.7 kg/l	0.88–0.77 kg/l	1.6–1.5 kg/l	1.6–1.5 kg/l
a [cm]	1.01 cm	0.9 cm	0.96 cm	0.96 cm

Despite the fact, that the PCM plates were determined different plate thicknesses (a), the model was simplified by setting a single thickness of 1 cm and air gap height of 4 cm for all simulated materials.

Figures Figure 5.31-Figure 5.34 show the DSC diagrams for all four materials tested.

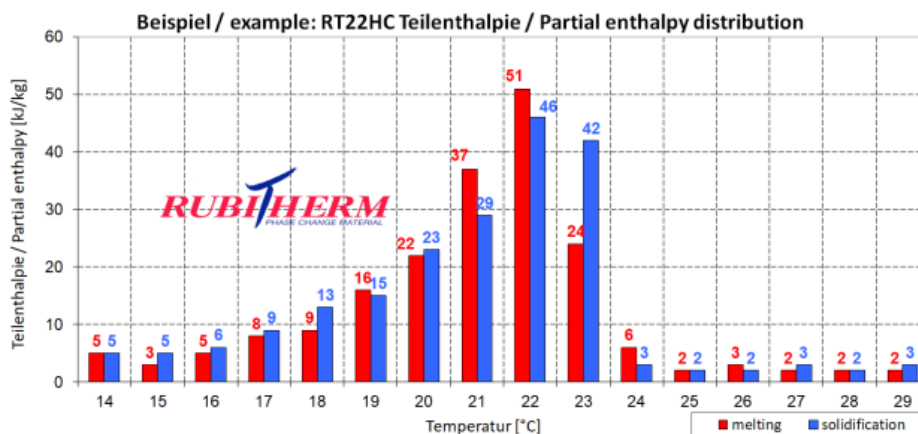


Figure 5.31: Partial enthalpy in relation to temperature for PCM type RT22HC [144].

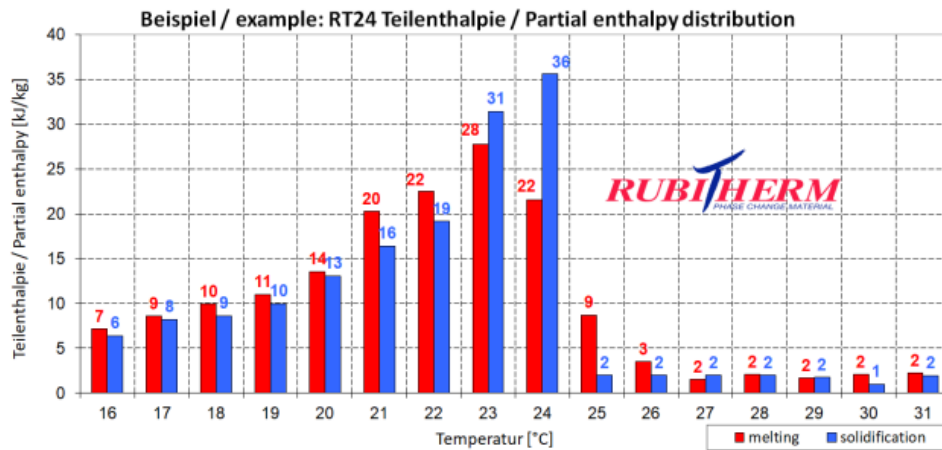


Figure 5.32: Partial enthalpy in relation to temperature for PCM type RT24 [146].

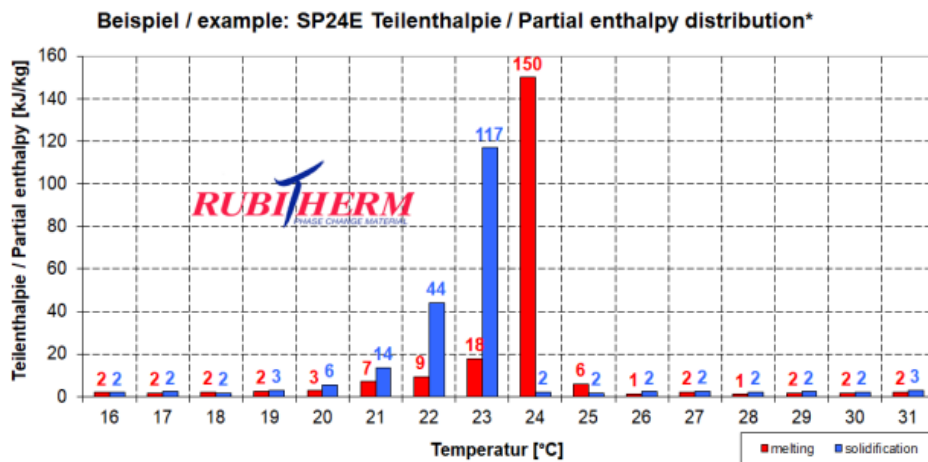


Figure 5.33: Partial enthalpy in relation to temperature for PCM type SP24E [155].

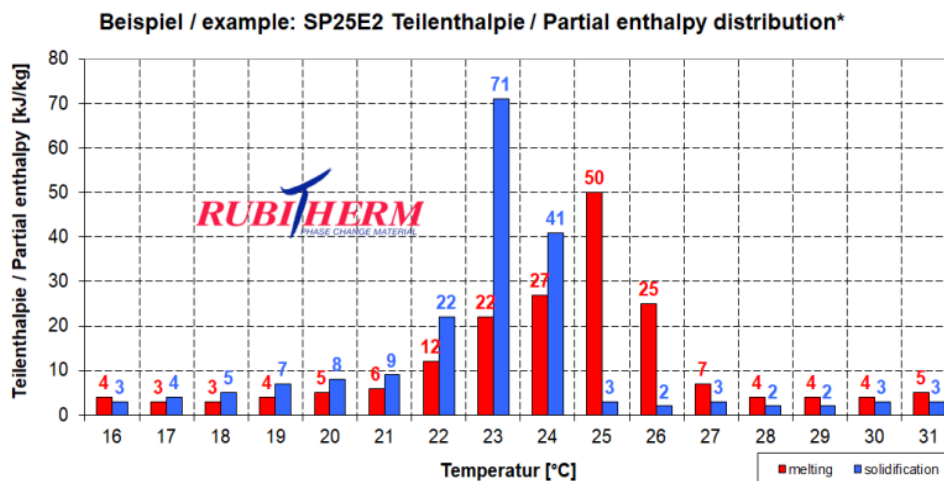


Figure 5.34: Partial enthalpy in relation to temperature for PCM type SP25E2 [156].

Finally, the energy released from the PCM was calculated following Equations 5.1-5.4.

5.3.1.4. Parametric analysis

Figure 5.35 shows the scheme of cases in parametric study. The system was ventilated with two types of inlet conditions, constant and transient. The cases with constant inlet air temperatures were ventilated with air temperatures of 15 °C, 17 °C and 20 °C, which are considered as the outdoor air temperatures during the summer in south-central Europe. There were two scenarios in case of transient cases where the inlet air temperatures presented two nights in the hottest week of the test reference year (TRY).

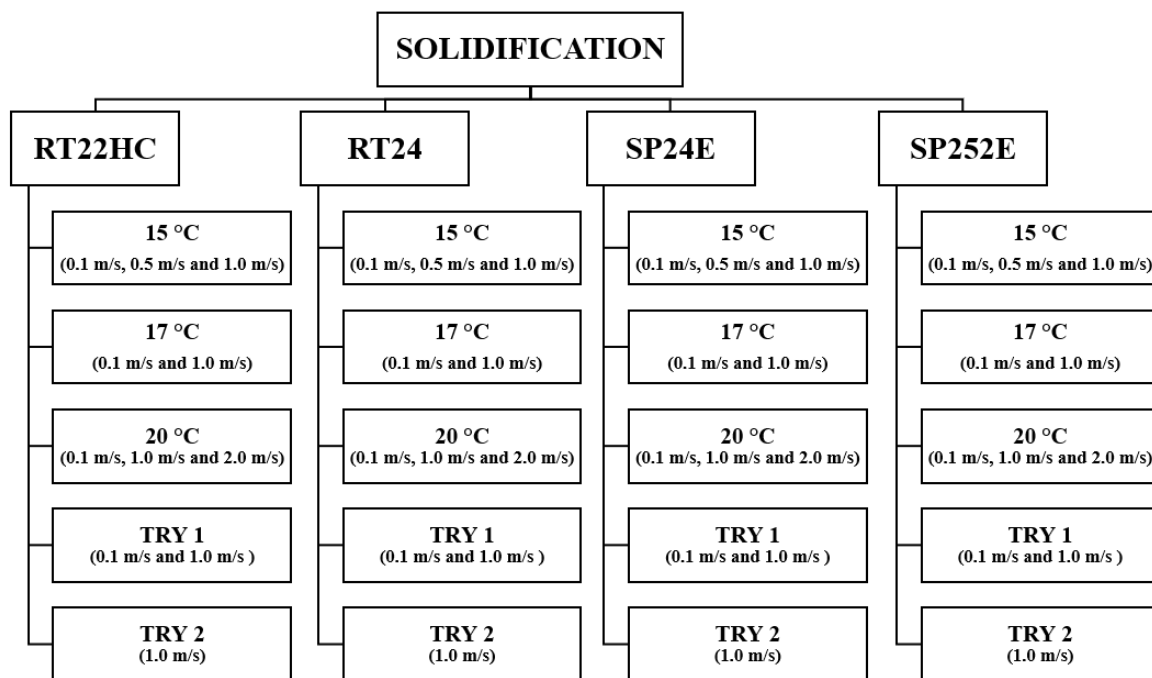


Figure 5.35: Scheme of cases in parametric study.

The outdoor air temperatures of the coldest night (1.-2.8.2022) and the hotter night (3.-4.8.2022) are shown in Figure 5.36. The average inlet air temperature (T_{ai}) of TRY 1 and TRY 2 are 14.3 °C and 17.33 °C, respectively.

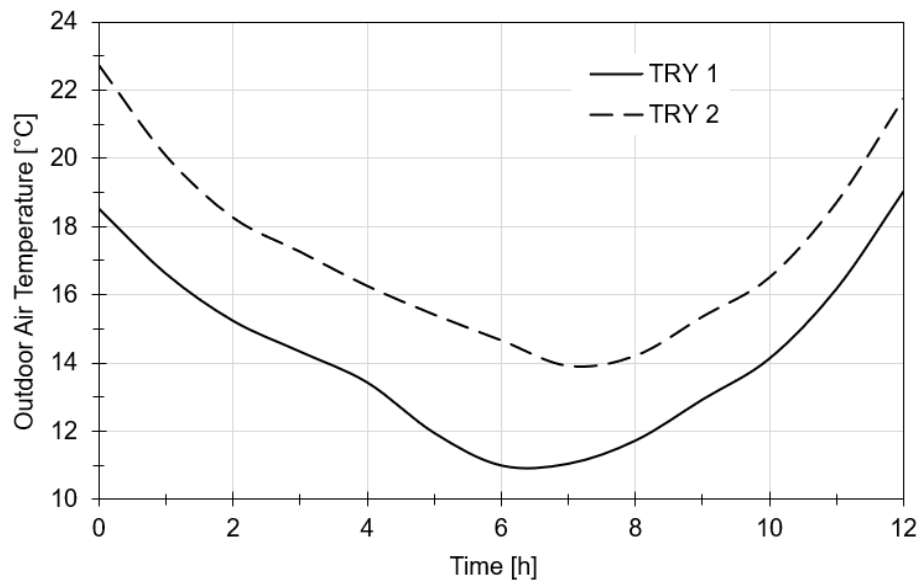


Figure 5.36: The outdoor air temperatures of the coldest night (1.-2.8.2022) and the hotter night (3.-4.8.2022).

5.3.1.5. Initial and boundary conditions and calculation model

The initial temperature of the PCM materials was set to 25 °C. The top edge of the air layer and bottom edge of the PCM layer were set as adiabatic boundary conditions.

The calculation with inlet air velocity of 0.1 m/s ($Re = 808.5$) was performed using laminar model and with higher inlet air velocities of 0.5 m/s, 1.0 m/s and 2.0 m/s ($Re = 4042.6$, 8085.1 and 16170.2, respectively) the model was calculated using k- ω (k- ω) model.

The heat transfer in air gap – fluid domain was simulated using default material properties of fluid air with only one modification: setting the air density to Boussinesq (1.18 kg/m³).

The rest of numerical model parameters are specified in Appendix D.

5.3.1.6. Model Validation

The model was validated by comparing the outlet air temperatures simulated with ANSYS Fluent to the experimentally measured temperatures. The results of validation are shown in Figure 5.37.

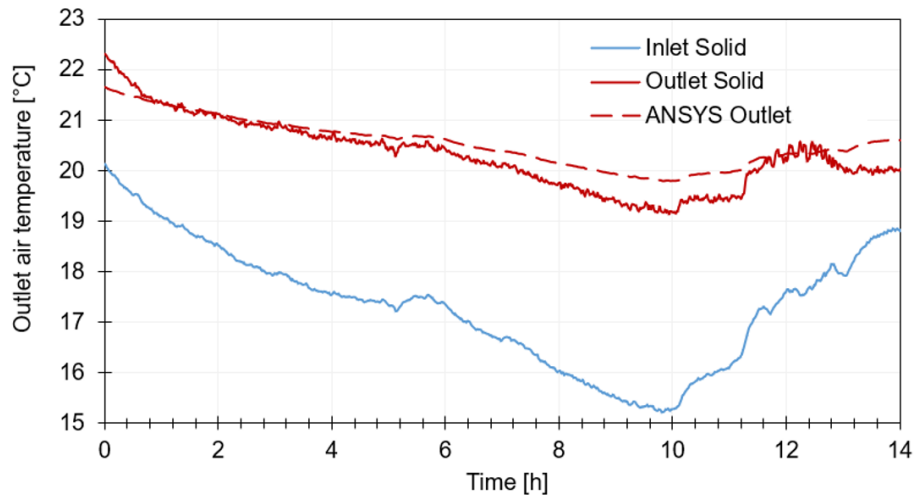


Figure 5.37: Simulated and experimentally measured outlet air temperatures for model validation.

5.3.2. Results

5.3.2.1. Outlet air temperatures obtained under constant conditions

Figure 5.38 presents the example of solidification of PCM RT24 with inlet air temperature of 15 °C and air velocity of 0.1 m/s.

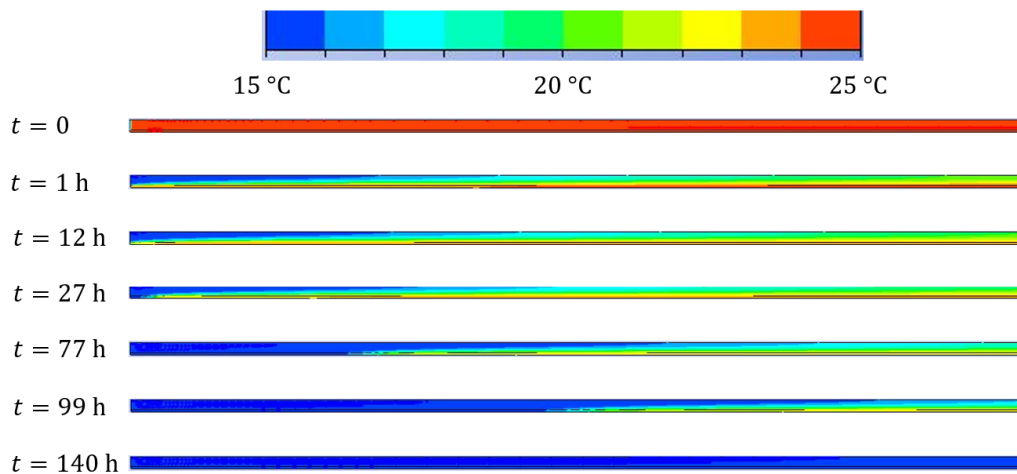


Figure 5.38: Example of solidification with inlet air temperature of 15 °C and air velocity of 0.1 m/s PCM RT24.

The rest of the results are presented in the following Figure 5.39-Figure 5.42 where each graph presents its own material tested under different constant inlet air temperature and velocity conditions of 0.1 m/s, 0.5 m/s, 1.0 m/s and 2.0 m/s.

In all investigated cases, the fastest temperature stabilization time is reached with inlet air temperature of 15 °C and 1.0 m/s and the longest at inlet air temperature of 20 °C and 0.1 m/s.

Figure 5.39 shows the outlet air temperatures obtained with PCM RT22HC.

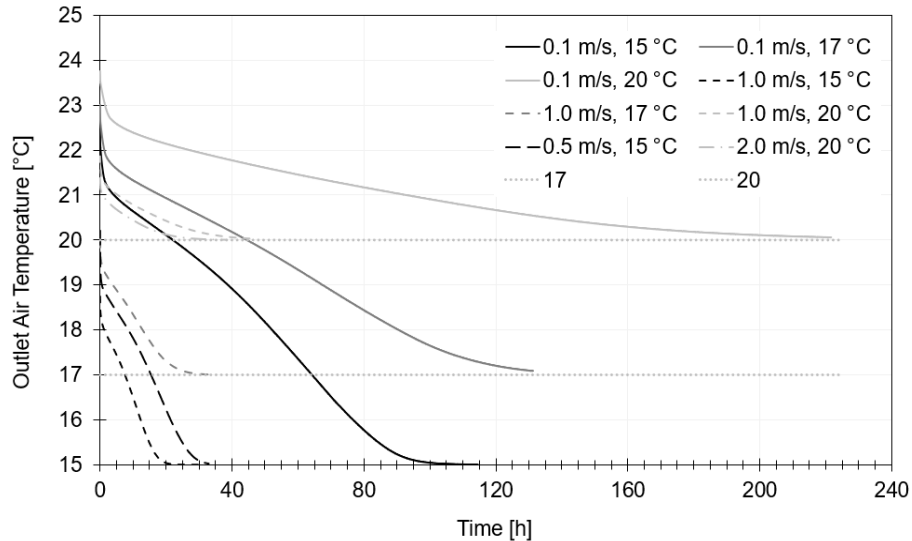


Figure 5.39: Outlet air temperatures obtained with PCM RT22HC under constant inlet air temperature.

Figure 5.40 shows the outlet air temperatures obtained with PCM RT24.

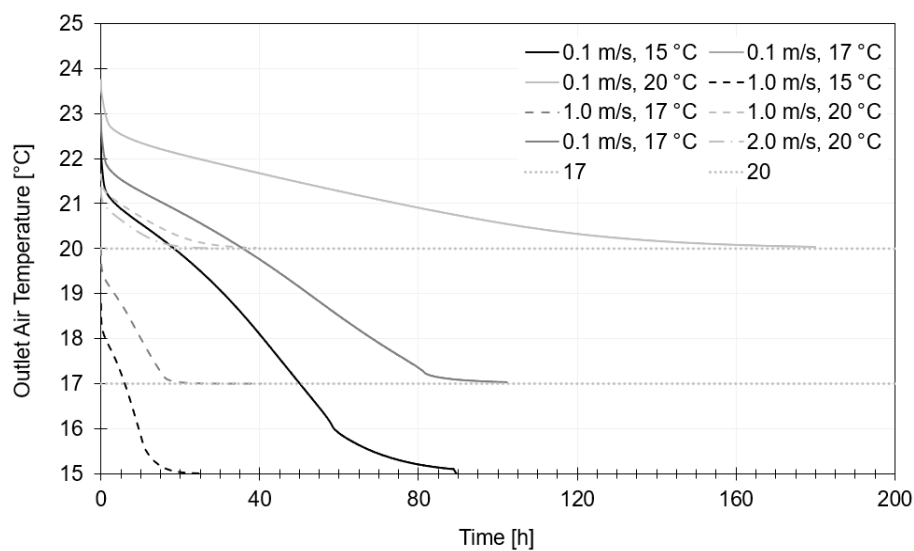


Figure 5.40: Outlet air temperatures obtained with PCM RT24 under constant inlet air temperature.

Figure 5.41 shows the outlet air temperatures obtained with PCM SP24E.

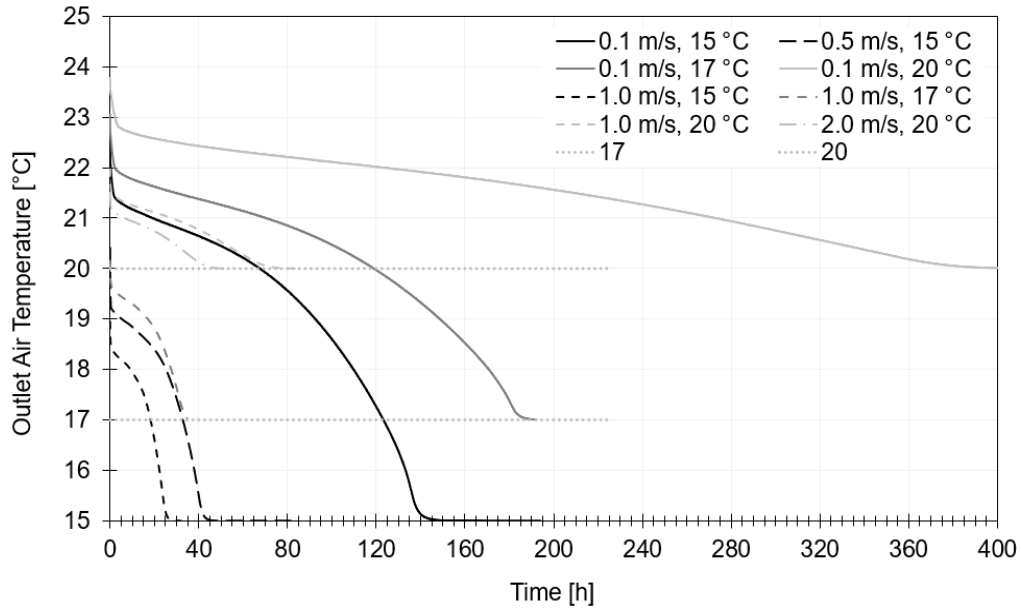


Figure 5.41: Outlet air temperatures obtained with PCM SP24E under constant inlet air temperature.

Figure 5.42 shows the outlet air temperatures obtained with PCM SP252E.

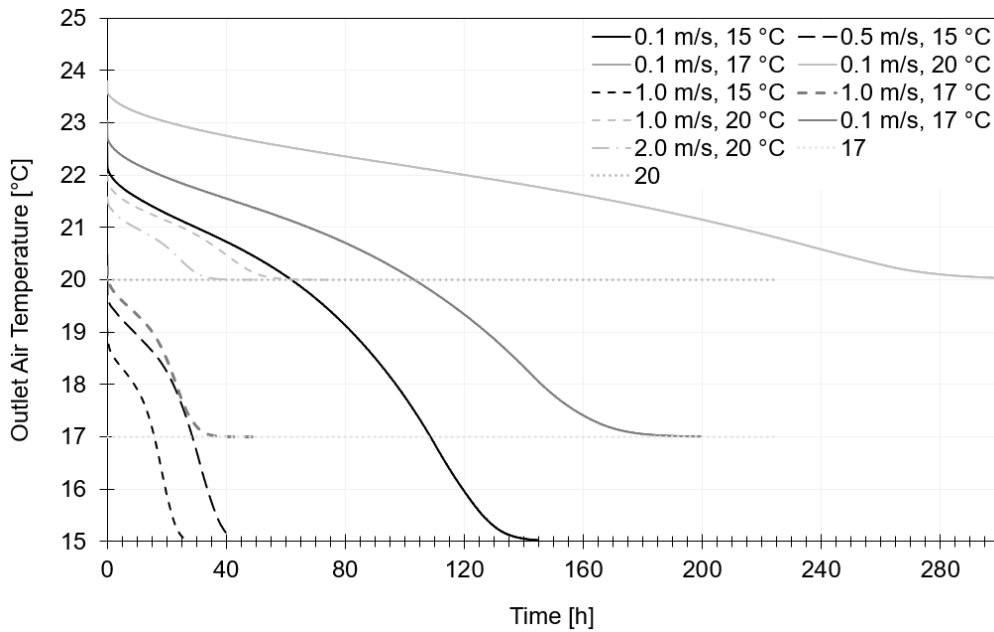


Figure 5.42: Outlet air temperatures obtained with PCM SP252E under constant inlet air temperature.

5.3.2.2. Outlet air temperatures obtained under transient conditions

Figure 5.43 shows the outlet air temperatures obtained under transient inlet air temperatures and inlet velocities of 0.1 m/s and 1.0 m/s for all four PCM materials tested.

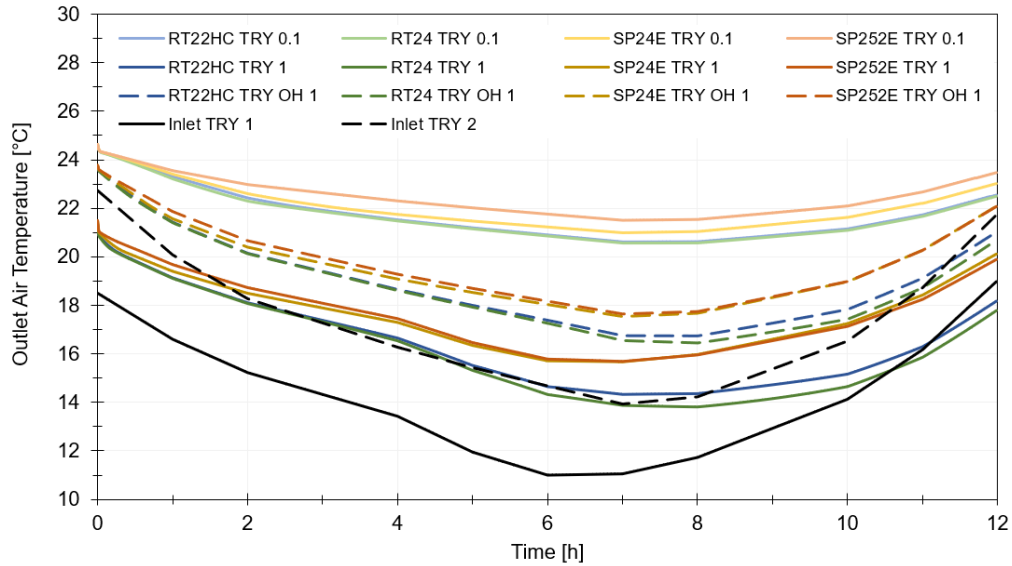


Figure 5.43: Outlet air temperatures obtained under transient inlet air temperature.

5.3.2.3. Heat released during the solidification period

Table 5.4 shows the heat released during the temperature stabilization period with constant inlet air temperature conditions. The results serve as a sort of model validation, where each type of PCM material was tested and the heat released from the PCM determined. The error was calculated to be between -12.75% and 16.76 %.

Table 5.4: Heat released during the temperature stabilization period with constant inlet air temperature conditions.

Case 15 °C, 0.1 m/s	RT22HC	RT24	SP24E	SP25E2
Q_{dis} [kWh]	0.54	0.35	0.67	0.73
Q [kWh]	0.48	0.36	0.80	0.80
Error (Q_{dis}, Q) [%]	-12.57	2.70	16.76	8.43

Table 5.5 shows the heat released during the solidification period with transient inlet air temperature conditions. From the table it is possible to observe that none of the PCMs could solidify completely with air velocities of 0.1 m/s and inlet temperatures set in TRY 1. The highest solidification rate was obtained with RT22HC (70 %) and the lowest with SP24E (16.4 %).

With the same inlet air temperature conditions (TRY 1) and air velocities of 1.0 m/s RT22HC and RT24 almost completely solidified (92.34 % and 95.68 %, respectively). PCMs SP24E and SP252E reached 71.93 % and 73.13 % solidification, respectively.

By changing the inlet air temperature conditions to TRY 2 and keeping the inlet velocity of 1.0 m/s, the percentage of solidification dropped to 71.19 % for RT22HC, to 75.83 % for RT24, to 50.95 % for SP24E and to 53.58 % for SP252E.

Table 5.5: Heat released during the solidification period with transient inlet air temperature conditions.

Case TRY 1	RT22HC 0.1 m/s	RT24 0.1 m/s	SP24E 0.1 m/s	SP25E2 0.1 m/s
Q_{dis} [kWh]	0.13	0.13	0.13	0.14
Q [kWh]	0.42	0.36	0.80	0.80
Percentage of solidification [%]	70.00	35.16	16.38	17.29
Case TRY 1	RT22HC 1.0 m/s	RT24 1.0 m/s	SP24E 1.0 m/s	SP25E2 1.0 m/s
Q_{dis} [kWh]	0.39	0.34	0.58	0.59
Q [kWh]	0.42	0.36	0.80	0.80
Percentage of solidification [%]	92.34	95.68	71.93	73.13
Case TRY 2	RT22HC 1.0 m/s	RT24 1.0 m/s	SP24E 1.0 m/s	SP25E2 1.0 m/s
Q_{dis} [kWh]	0.30	0.27	0.41	0.43
Q [kWh]	0.42	0.36	0.80	0.80
Percentage of solidification [%]	71.19	75.83	50.95	53.58

Due to higher density and PCMs SP24E and SP252E cannot fully solidify in any of the tested TRY cases. Higher temperature differences between the inlet air temperature and PCM melting temperature in case TRY 1 show the highest percentage of solidification.

5.3.3. Conclusions

- Temperature difference high enough between inlet temperature and PCM material temperature need to be ensured, for sufficient temperature stabilization.
- The time needed for outlet air temperature curve to drop to the level of inlet curve is even in the best performing case (15 °C and 1.0 m/s) longer than the nighttime cycle (12 h). However, the solidification is already completed before the outlet curve completely drops.
- Due to low thermal capacity, the fastest temperature stabilization was observed with RT24 at inlet temperature of 15 °C and velocity of 1.0 m/s (under 20 h). Interestingly,

the duration for the outlet temperature stabilization at SP24E and SP252E at the same conditions last 3 h longer or in case of inlet air of 0.1 m/s and 15 °C 40 h longer (28 % slower compared to RT-lines).

- The fact is, that RT22HC and RT24 have around 50 % lower density compared to the SP-lines. However, in 12h cycle in combination with TRY 1 and TRY 2, their released heat wasn't 50 % higher compared to the SP-lines (Case TRY 2 and 1.0 m/s: ~73 % for RT-line and ~72 % for SP-line).
- SP24E and SP252E have high potential to solidify completely at higher inlet temperatures (etc. 17, 18 °C), because they have no heat capacity at material temperature of 21 °C or lower.
- However, SP24E and SP252E have one-time higher density compared to PCMS RT22HC and RT24. Consequently, to ensure a complete solidification over the nighttime cycle, the ventilation flow rates in the air gap need to be increased.

5.4. Discussion of literature review

5.4.1. Discussion on total volume nighttime ventilation

5.4.1.1. Melting temperature and location in the structural complex

All analysed studies using the total volume nighttime ventilation for enhancement of PCM performance during the day investigated the PCM layers positioned in the internal side of the building components, internal/external walls, roof/ceilings and floor in order to establish a sufficient contact of the PCM with the heated indoor environment. Therefore, the melting temperature of the PCM didn't differ regarding to the position in the building element. However, it was determined based on the climate type of the case studied. Table 5.6 shows the prevailing melting temperature selected according to the indoor temperature requirements 22-26 °C. However, the highest melting point analysed ranged up to 30 °C. Most of the materials are organic and fatty-acid based with exception of PCM product Infinite-R™ [93],[107] which is inorganic. The enthalpy of the selected materials normally varies between 70 – 250 kJ/kg but is on average selected to be around 170 kJ/kg.

Table 5.6: Location of the PCM in the structural complex according to the selected PCM temperature.

NATURAL VENTILATION	NATURAL AND MECHANICAL	MECHANICAL
<ul style="list-style-type: none"> • Rubitherm RT24 (24 °C) – other locations optimisation (22-26 °C): interior walls, internal partition walls and ceiling [56], • DuPont Energain (21.4 °C) and numerically BioPCM (21 °C, 23 °C, 25 °C, 27 °C and 29 °C): internal layer of roof, floor and wall [85] 	<ul style="list-style-type: none"> • DuPont Energain and BioPCM Q25M51: the inner surface of the walls and ceiling [54], • BioPCM (25 °C) and DuPont Energain: the walls and ceiling [90], • PureTemp20 applied to the floor, ceiling and internal walls [91], • Self-prepared (22–24 °C): 	<ul style="list-style-type: none"> • PureTemp20: internal wall [94], • Micronal23® board from BASF: three internal partition walls [95], • BioPCM M27 and M51: drywall partition systems [96], • Gypsum PCM board and

<ul style="list-style-type: none"> • Knauf PCM Smartboard (1.25 cm thick, 30 %wt microencapsulated PCM) integrated in the roof and the external walls [86] • BioPCM (19-33 °C): the inner side of building envelopes (external walls, interior walls and ceilings [87] • Fictive PCM 26 °C, 28 °C, 30 °C and 32 °C and Rubitherm RT21, RT24, RT26, RT28 and RT31: inner layer of wall and roof [88], BioPCM25 to the ceiling and/or wall [89] 	<p>external wall over the window [92],</p> <ul style="list-style-type: none"> • Infinite R™ (18-29 °C) [93] 	<p>clay PCM board (23 °C, 25 °C and 27 °C): on the internal side of the external walls [97],</p> <ul style="list-style-type: none"> • PCM (27°C): internal side of wall ceiling and floor [98], • PCM plaster (26-29 °C): inner faces of external building envelope -wall [99], • PCM (29 °C): in an external wall, internal wall or ceiling [100], • BioPCM M182/Q29 (25-29 °C): applied in the ceiling [101], • shape stabilized PCM (24 °C, 26 °C and 28 °C): placed on the ceiling and four walls [102] and [103], • DuPont Energain and BioPCMQ25: building wall and ceiling as joint layers [104], • Paraffin-based PCM (hexadecane, heptadecane, dodecanol, and octadecane with melting points of 20°C, 21 °C, 24 °C and 29 °C): on the inner side of the external wall [105], • DuPont Energain, BioPCMTM23, Natural TCM Energy Saver® and Paraffin/LDPE/EVA : positioned in the inner layer of the ceiling, floor and wall [106], • PCM Infinite-R™- R29 (variations 27-30 °C): placed below the internal finishing layer of all the external and internal walls [107]
--	--	--

5.4.1.2. Material thicknesses

The material thicknesses range between 0.5 cm and 7 cm, depending on the product and PCM encapsulation method. However, normally the thickness varies between 1 cm to 3 cm.

5.4.1.3. Effect of system on energy performance and indoor thermal conditions

Furthermore, Table 5.7 lists the studies according to the cooling effect of the system on the energy performance and indoor thermal conditions. Three cooling effect impact levels are established evaluating the studies according to general percentage of cooling energy reduction and decreased daily indoor temperatures. It should be noted that each study is unique, it reports the system performance results with different indicators and under its individual conditions. Thus, the results cannot be directly compared. Generally, the daily temperature reduction of 3 °C or higher is considered as high-level effect, 3-1.5 °C medium-level effect and lower than 1.5 °C low-level effect.

Table 5.7: Cooling effect of the system on the energy performance and indoor thermal conditions.

Impact	References
High	[86], [88], [90], [92], [94], [97], [98], [99], [100], [101], [103] and [107]
Medium	[56], [85], [87], [89], [54], [90], [91], [93], [95], [102] and [106]
Low	[96], [104] and [105]

5.4.1.4. General findings on total volume nighttime ventilation

The studies often establish the nighttime ventilation scenarios by opening the windows for 100 %, 50 % or 20 % in combination to the condition set by the minimum temperature difference between indoor and outdoor temperature or indoor air temperature set points. In all listed cases, the natural ventilation provided visible improvements in PCM daily operation or energy performance. However, only in one case, the cooling need reduction of 65 % was outstanding where the study emphasizes the importance of application in milder climates [86] or the daily operative temperatures with reduction up to 5 °C [89]. The main disadvantage of natural ventilation in the nighttime is insufficient mixing of the air indoor when the draft cannot be established. The flow rates are limited based on the building geometry and wind pressure. Also, another concern may be the building safety during the time when the windows are opened. The studies using a combination of natural and mechanical nighttime ventilation reached some very high indoor temperature reductions (6 °C). However, in terms of energy use there were no significant reductions. The mechanical ventilation of 40 ACH showed the highest impact on a daily energy use for cooling (76 %) [103]. The studies also highlighted the possible negative effect of PCM application. For example, in one of the cases investigated, the addition of floor embedded PCM even increased the energy needed for cooling.

The melting temperatures of PCM should be high enough to provide a necessary temperature difference between the PCM melting temperature and outdoor nighttime temperatures. The best results for daily performance were achieved with PCM application with melting temperature between 25 °C and 29 °C (depending on the location and climate type) and not higher. The optimal PCM temperature should be optimized for each location separately with regard to solar radiation, outdoor daily temperatures and internal heat gains. Based on the literature, the minimal recommended ventilation rate for nighttime ventilation is 3 ACH for at least 8 h.

5.4.2. Discussion on Ventilated building elements

5.4.2.1. Ventilated building elements with the list of investigated PCM melting temperatures

In Table 5.8 melting temperatures investigated in each study are presented and categorised under the corresponding ventilated building elements group. It can be observed, that in the

external layer of the roof should be applied higher temperatures than the internal layer of the roof. Low melting temperatures in the roof, such as 22-24 °C were found too low and inefficient. Ventilated ceiling was tested for temperatures between 18 °C and 38 °C. However, the prevailing melting temperature used was around 25 °C. Melting temperatures of PCM used in ventilated floor were generally the lowest, as the heated air is convectively moved upwards in the room. Due to application practicality, the internal walls are normally not ventilated. Two studies investigated PCM with difference in melting points of 6 °C. Ventilated façades were applied PCM in range of 22-35°C with prevailing melting temperature of PCM in the external layer of 27 °C. Melting temperatures of PCM improved ventilated glazing elements were in range of 35-21.5 °C. Furthermore, the melting temperatures of PCM improved ventilated walls with BiPV are the highest between 26.5 °C and 32 °C. Based on this table it is possible to conclude, that the melting temperature varieties according to the active system geometry, specifics and layer of the PCM in the structural complex of the element.

Table 5.8: Ventilated building elements with the list of investigated PCM melting temperatures.

#	Element	Melting temperature
1	PCM improved ventilated roofs	External layer: 32°C and internal layer: 24 °C [108], [109]; 22 °C and 24 °C [111]
2	PCM improved ventilated ceilings	27 °C [112]; 21 °C [113], 25 °C [114], 21°C [115], 26 °C [116], 24 °C [117], 25 °C, 26 °C, 27 °C and 28 °C [118], 18-21 °C and 23 °C [119], 31–33 °C, 34–36 °C, 36–38 °C, 34–36 °C and 29–31 °C [121], 24.5 °C [122], 23.5 °C [123],
3	PCM improved ventilated floor	20 °C [124], 23 °C [125] [126]
4	PCM improved ventilated internal walls	27.6 °C [126], 21.7 °C [127], [128]
5	PCM improved ventilated façades	22 °C [129], 22 °C [130], 22 °C [132], 22 °C [133], 27 °C [134], 35°C [135] [136], 22 °C and 26°C [137] [138] [139], 24 °C [140], 25°C [141], 30 °C and 18 °C [142], 27 °C [143]
6	PCM improved ventilated glazing elements	35 °C [144], 22 °C [145], 21.5 °C [146]
7	PCM improved ventilated walls with BiPV	26.5°C [147]; 26.6 °C, 28.2 °C and 32 °C [148]

5.4.2.2. General findings on local nighttime ventilation

The most popular application for ventilated elements are ventilated ceilings and ventilated facades. Due to the position of the ventilation system, the suspended ceiling is practical to ventilate. Ventilated facades may be ventilated naturally by the wind or with application of the fans incorporated in the external side of the building. The ventilated floor application is the least common, as it is impractical for application (fans are normally positioned in the ceiling) and has less contact with warm air.

The enthalpy of PCMs studied is in range of 77 kJ/kg–218 kJ/kg with prevailing value of 140 kJ/kg. Compared to total volume ventilation, where PCM types are mostly organic, the PCM type in ventilated elements is in equal share organic and inorganic. The reviewed ventilated systems were for the purpose of improved building energy performance often combined with other building systems. Such as, ceiling fans, embedded water pipes in the interlay positioned layer of PCM, combination of smart modular heat recovery unit, PV and BiPV systems for electricity production. Also in this chapter, it is difficult to compare the direct cooling effect of the individual system. Compared to the total volume ventilation cases, locally ventilated PCM elements are often accessed on the component level and the results do not show the effect on the daily or seasonal energy performance and thermal comfort in the building. However, it may be pointed out that, with application of double layer PCM integrated in the roof, the indoor temperatures dropped by 8.2 °C, which is the highest value reported in this article [108], [109].

PCM may be ventilated by the spherical hollow cores or tubes in the slab or as a wall adjacent air gap. Based on the flowrates and amount of PCM in the element it is difficult to evaluate which geometry is superior. However, the spherical hollow cores are compatible with prefabricated concrete horizontal elements in the material-reduced building structures. Based on the literature, it is recommended to apply PCM with higher melting temperatures (25-28 °C) to the external layers and lower melting temperatures (22-26 °C) to the internal layers of the building envelope. To improve the cooling effect, the internal layer may be combined with water-pipe embedded systems.

5.5. Selection of the phase change material characteristics

Within this chapter, the decision on the selected PCM product for further real-scale experimental measurements and model is presented. The PCM melting temperature (T_m) and mass selection has to meet requirements and optimal performance in each cycle, passive operation – daytime cycle where T_m mustn't exceed the indoor temperature requirements and active operation - nighttime cycle where T_m must remain high enough to ensure the complete solidification. Each preliminary research importantly contributed to the decision:

- Full-scale building model simulation:
The investigation with unsteady state building performance simulation tool in DesignBuilder showed that the optimal melting temperature in the investigated climate conditions was 24 °C. The results also showed that microencapsulated PCM doesn't have enough capacity to efficiently cool the indoor spaces.
- Pre-experimental investigation:
The results showed the importance of low and stable inlet temperatures. However, this experiment served more as a validation tool for the pre-numerical analysis with ANSYS.
- Pre-numerical simulation with ANSYS:
Based on the simulated results it is possible to conclude that SP24E and SP252E have high potential to solidify completely at higher inlet temperatures (e.g. 17, 18 °C),

because they have no heat capacity at temperature of 21 °C or lower. This is especially important during the summer heatwaves, when outdoor temperatures in the nighttime do not drop sufficiently.

- Literature review:

The results summarized from literature review show a huge variety of melting temperatures and their application. However, it can be noted that, too little PCM (e.g. microencapsulation) didn't have a strong cooling effect. Prevaillingly it seems, that interior surfaces covered in PCM didn't exceed 24 °C (rather lower melting temperatures).

Finally, the indoor operative temperatures shouldn't exceed the recommended values from Table 2.2 by PCM with $T_m = 25$ °C. Simultaneously, the T_m should be high enough to establish a sufficient temperature difference between the inlet air temperature and the PCM material melting point. As it seems, that with flow rates higher from the ones from simulation, the SP-line PCM could solidify over the 12 h nighttime cycle. Even with this thickness. At this point it is important to stress the fact, that the proposed APC system cools the room passively. Therefore, the PCM plates aren't in close ventilated contact with inlet air as for example in an enclosed heat exchanger. It is believed, that for this purpose the PCM plates shouldn't be too thin, as it could compromise their daily performance.

So, the selected PCM plates were from Rubitherm SP24E microencapsulated in aluminium CSM cases with 2 kg of PCM per plate and 1 cm thickness [155].

6. Experimental investigation

6.1. Method

6.1.1. The operation principle of active-passive system

Figure 6.1 shows the operating principle of the proposed diurnal APS system for the cooling application.

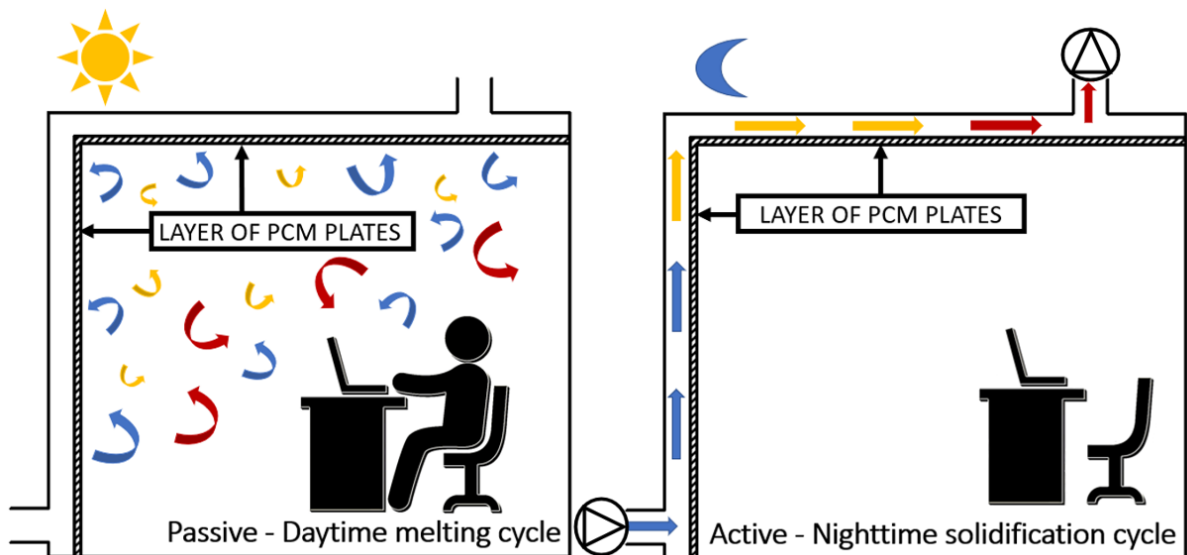


Figure 6.1: The operating principle of the active-passive system for cooling application.

The left side of the figure shows the daytime cycle, in which the PCM placed on the wall and ceiling of the room, is melted and lowers indoor temperatures by passively storing heat. The right side of the figure shows the night cycle, where PCM is actively solidified by the addition of the mechanically ventilated air gap. The cool outdoor air is supplied through the linear diffuser at the bottom of the air gap wall (air flow direction wall-ceiling) and discharged through the air gap ceiling outlet. The arrows indicate: blue - cool outside

air, yellow - slightly heated air and red - air fully heated by the panels and discharged outside.

6.1.2. Phase change material properties

The PCM material salt hydrate SP24E (Rubitherm) is encapsulated in Compact Storage Module (CSM) aluminium plates (dimensions: 40x30x15 mm and weight: 2 kg) [155]. Figure 6.2 shows the differential scanning calorimetry (DSC) diagram of the selected material with a maximum melting temperature (T_m) of 24 °C and a storage capacity of 150 kJ/kg. Solidification occurs at 22 °C and 23 °C with a storage capacity of 42 kJ/kg and 118 kJ/kg, respectively. The thermal conductivity of the material (λ) is ~ 0.5 W/(m K) and the density (ρ) of solid and liquid material is 1.5 kg/l and 1.4 kg/l, respectively. The selected melting point of the material corresponds to the thermal properties suggested for thermal comfort in hot summer periods in cooling season ($T_{a_room} = 22-26$ °C) [37].

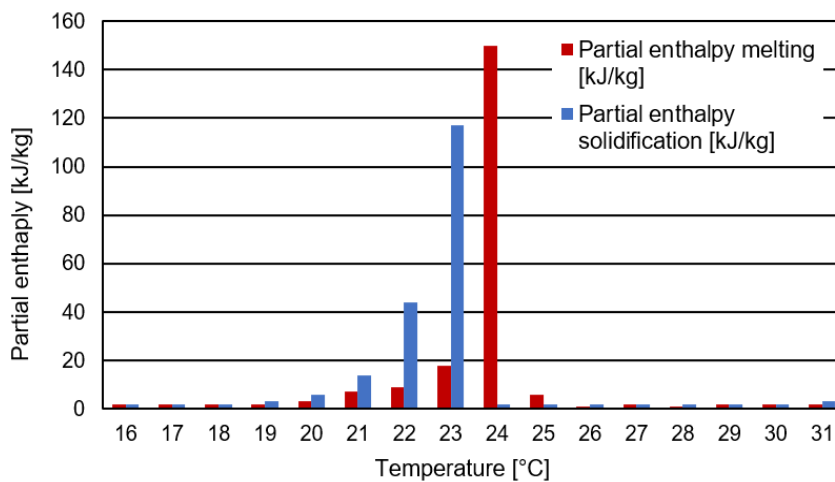


Figure 6.2: DSC diagram Rubitherm SP24E [155].

Figure 6.3 shows the opened CSM modules with the selected PCM and slightly melted.

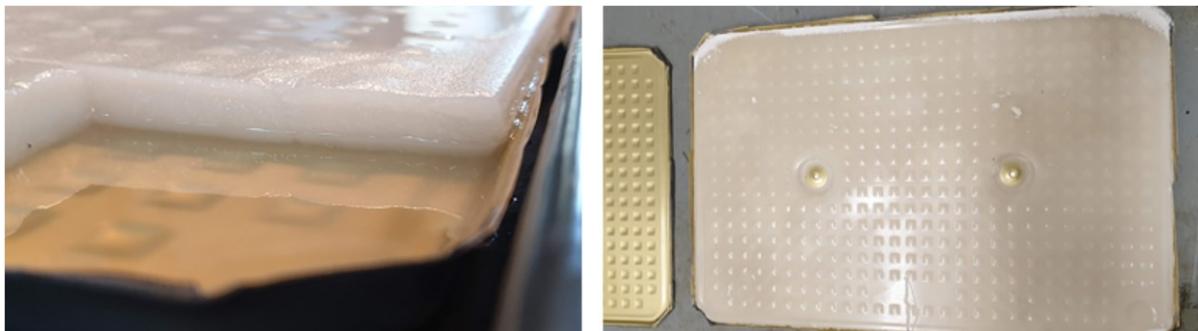


Figure 6.3: PCM SP24E plates opened and melted.

6.1.3. The description of the APS system test cell and features

The experiment with the APS system was conducted in the test chamber called Hybcell at the National School of Public Works (ENTPE) in Lyon (France).

The initial state of the test chamber is shown in Figure 6.4. The final layer of the walls and ceiling of the test chamber are made from gypsum boards and painted white and are equipped with inlet and outlet ducts. The external walls of the test chamber have double windows, which were afterwards blocked with EPS and glass wool.

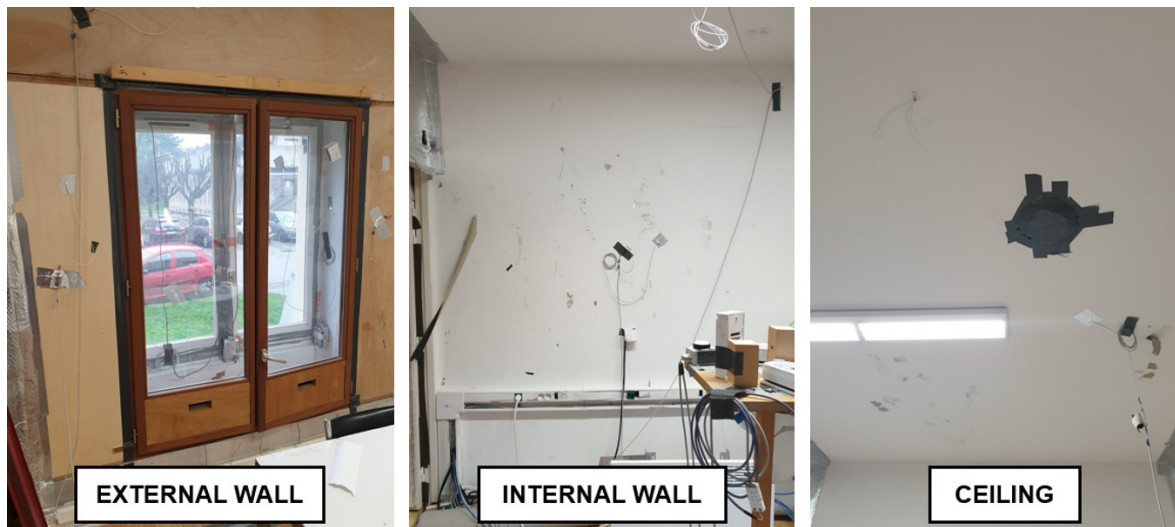


Figure 6.4: Initial state of test chamber in Lyon, France.

The electrical set-up needed to be repositioned to fit the wooden frame structure for PCM plates integration onto the internal wall and ceiling (Figure 6.5). The frame was constructed and the plates were positioned in the openings and fixed with the metal frames.

The chamber was divided into two identical test cells, cell A (PCM modified) and cell B (reference), as shown in Figure 6.6-left. All surfaces except the external wall with the window are internal.

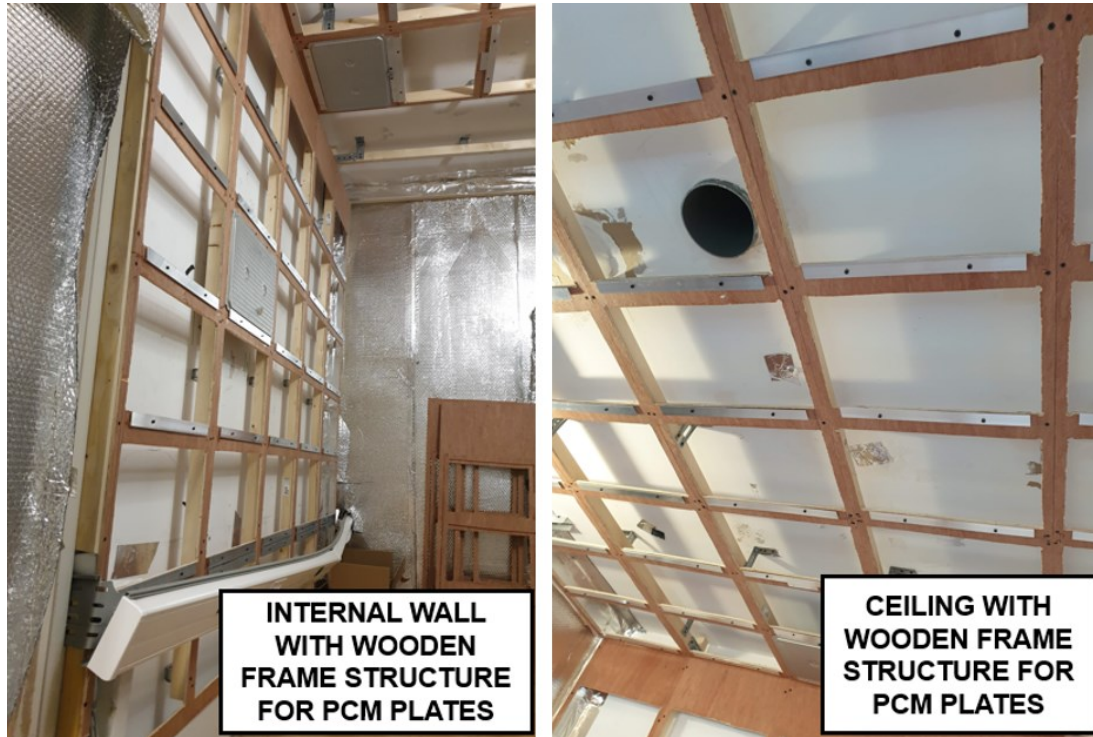


Figure 6.5: Wooden frame structure for PCM plates integration onto the internal wall and ceiling.

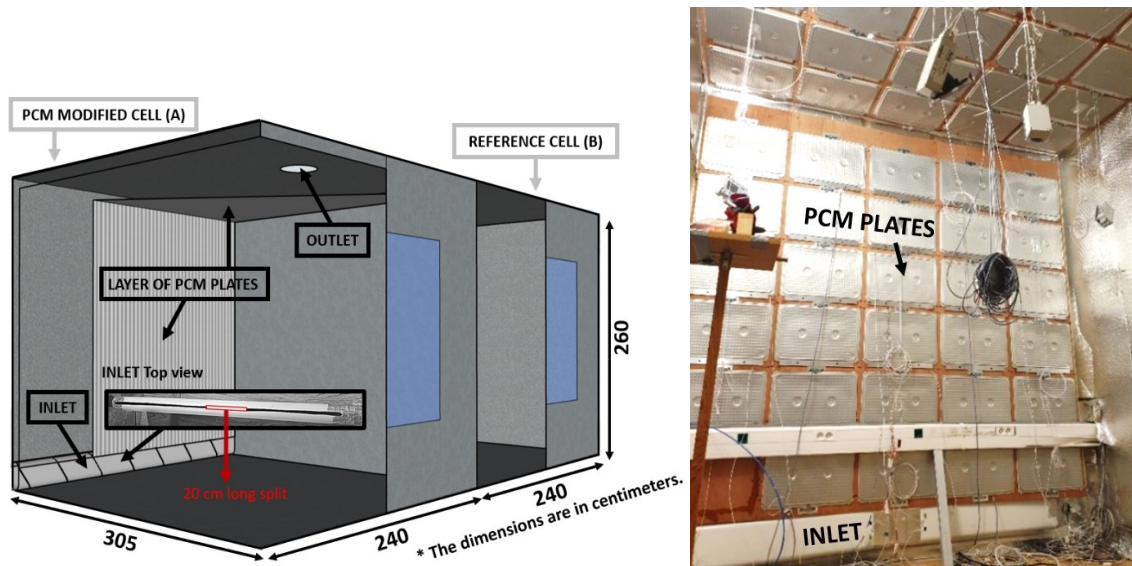


Figure 6.6: Experimental facility (left) and PCM modified cell - wall and ceiling (right).

The oval (5 cm wide) linear inlet diffuser consists of a 200 cm long duct component with a 1 cm thick opening with a 20 cm long split in the middle of the component to distribute the air along the air gap. The circular outlet opening (\varnothing 16 cm) is located in the middle of the ceiling, 117 cm from the external wall (the laboratory geometry of the Hybcell did not allow to move the outlet closer to the external wall). The metal PCM plates were positioned in the openings of the wooden frame substructure. The substructure forms an

airtight air gap with the primary wall and ceiling and it contains 29 plates in the secondary wall and 38 plates in the secondary ceiling (Figure 6.6- right).

Figure 6.7 shows that the air gap is divided into 5 identical channels - each channel is in width of a PCM plate (45 cm), with the division starting at the inlet and ending in the line of an outlet (130 cm from the external wall – green dashed line). In this way, the air can be exhausted from all the channels.

Airtightness was tested with the smoke test, where the smoke was generated before the inlet fan (the inlet fan was turned on) and the leakage was in the PCM modified test cell. During the smoke test, the exhaust fan was turned off to create overpressure in the air gap.

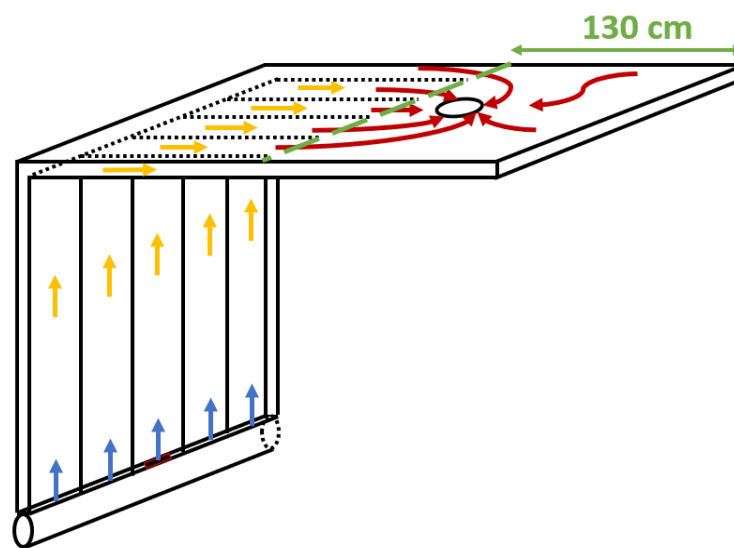


Figure 6.7: The air gap division in 5 identical channels with air streams.

In Figure 6.8, the schematic sketch (side view) of the experimental features of the APS system for setting up the experimental conditions and the location of some measuring points (T_a , T_{mr} , T_{PCM_front} , T_{PCM_back} and v) are presented.

In the nighttime solidification cycle, air was mechanically supplied into the air gap and conditioned beforehand. The supply air temperatures were first stabilised by the chiller (ThermoChill III Recirculating Chiller, operating range: 5-30 °C), which was connected to the duct before the inlet fan. Both cells were equipped with fans. Each cell had two axial fans (300-3000 m³/h, 1500 Pa, 50/60 Hz) inlet and outlet fan operating simultaneously. After the inlet fan, the cooled air was additionally heated by the spiral heating coil (Aldes BCA MONO D125 1kW). The air is then exhausted from the test cell by the outlet fan.

The air was ventilated at airflow rate of 483 m³/h. The velocity was measured in the centre of each of the five air gaps 1 m above the inlet diffuser. The airflow rate was determined with the mean average value of velocities and the area of the wall air gap.

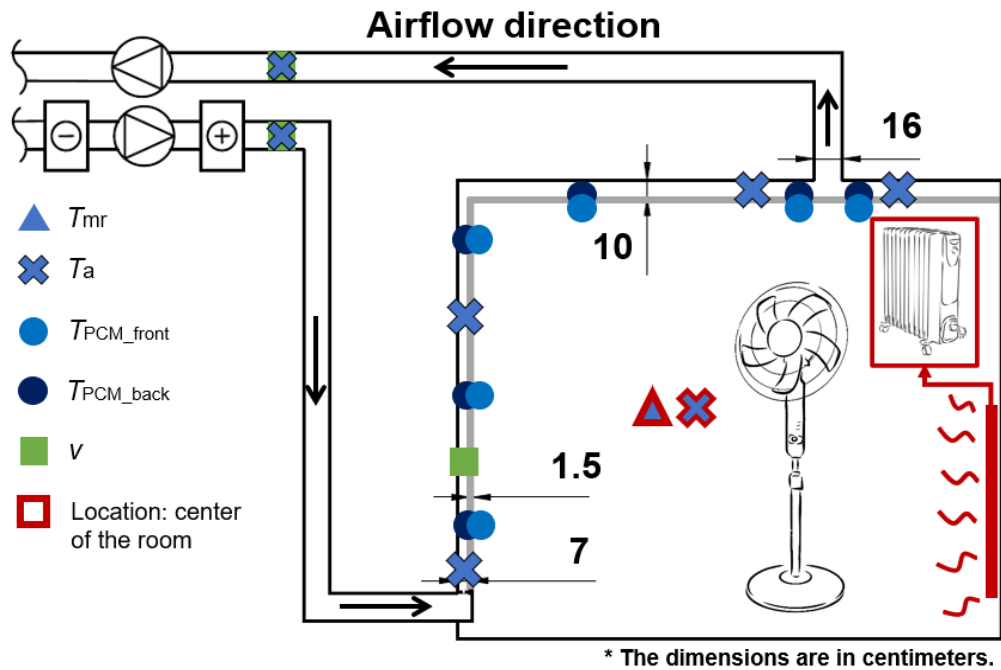


Figure 6.8: The sketch of experimental features and location of measuring points.

Both test cells were equipped with identical cell heaters (2000 W) and the windows in the external walls of both cells were blocked by the insulation (EPS block and mineral wool) to provide summer condition for the daytime melting cycle (Figure 6.9 and Figure 6.10). Each cell was equipped with room fans to ensure adequate mixing of the air in the cell.

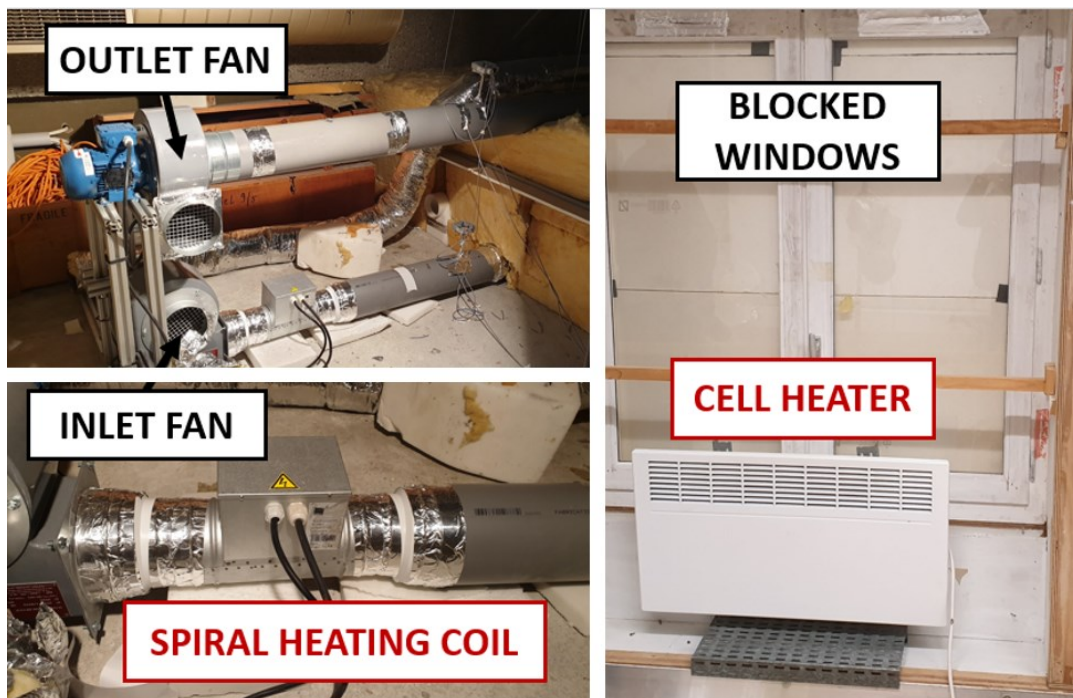


Figure 6.9: Experimental features: inlet fan, outlet fan, spiral heating coil and cell heater.



Figure 6.10: Experimental features: cooling coil.

6.1.4. Measuring equipment and measuring point locations

During the experimental cases several parameters were monitored: the air temperature in the inlet duct after the spiral heating coil, in the air gap, in front of the exhaust fan and in the centre of the cell (T_a), the mean radiant temperature (T_{mr}), the surface temperature measured on the front side of the PCM plate (T_{PCM_back}), surface temperature measured on the back side of the PCM plate (T_{PCM_front}), the surface temperature measured on the primary wall and the ceiling (T_s) and the air velocity (v).

The PCM modified cell (A) with the direction of airflow and the location of the measuring points for the air temperature (T_a) and the mean radiant temperature (T_{mr}) is shown in Figure 6.11. Air and globe thermometers (Wireless datalogging system: DeltaOHM HD_35EDG_1NB (accuracy: ± 0.2 °C, measuring range: 0-60 °C)) were located in the centre of both cells at 1.1 m height. The air temperature was measured in the air gap, with the inlet temperature, the temperature in the middle of the air gap and the outlet temperature determined with the sensor PT 100 (DeltaOHM HD_35EDWH data accusation).

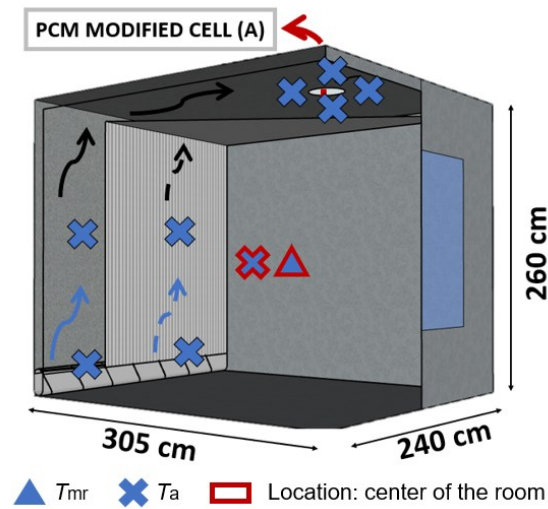


Figure 6.11: PCM modified cell with T_a and T_{mr} measuring locations.

The surface temperature of the plates was measured with RTD sensors – PT100 on the front side (cell side) and the back side (air gap side) side of the plate on the wall and on the ceiling (Figure 6.12). The sensors were protected with aluminium tape to avoid the effect of radiation. There were three measuring points at three heights on the wall and in one row on the ceiling.

The outlet was measured from four surrounding points. There was a total of 13 PCM surface (T_{PCM_back} and T_{PCM_front}) measuring points.

Air gap velocity was measured at 1.3 m height in the centre of each channel (average value of the channels is 0.9 m/s) using DeltaOHM HD403TS and DeltaOHM HD4V3TS (accuracy: ± 0.05 °C, measuring range: 0.05-25 m/s and 0-40 m/s, respectively) anemometers.

Air temperature and velocity were also monitored in the inlet (150 cm downstream of the spiral heating coil) and outlet (250 cm upstream of the outlet fan) ducts DeltaOHM HD2903TO1 anemometers. The anemometers were calibrated prior to the experiment. The surface temperature of the original wall and ceiling was measured at four locations on the wall and on the ceiling of both cells.

The humidity was stable (RH = 32 %).

The measured T_{mr} was in close agreement with the T_{ai} measured at the centre of the room. Therefore, only T_{ai} will be analysed in the following chapters.

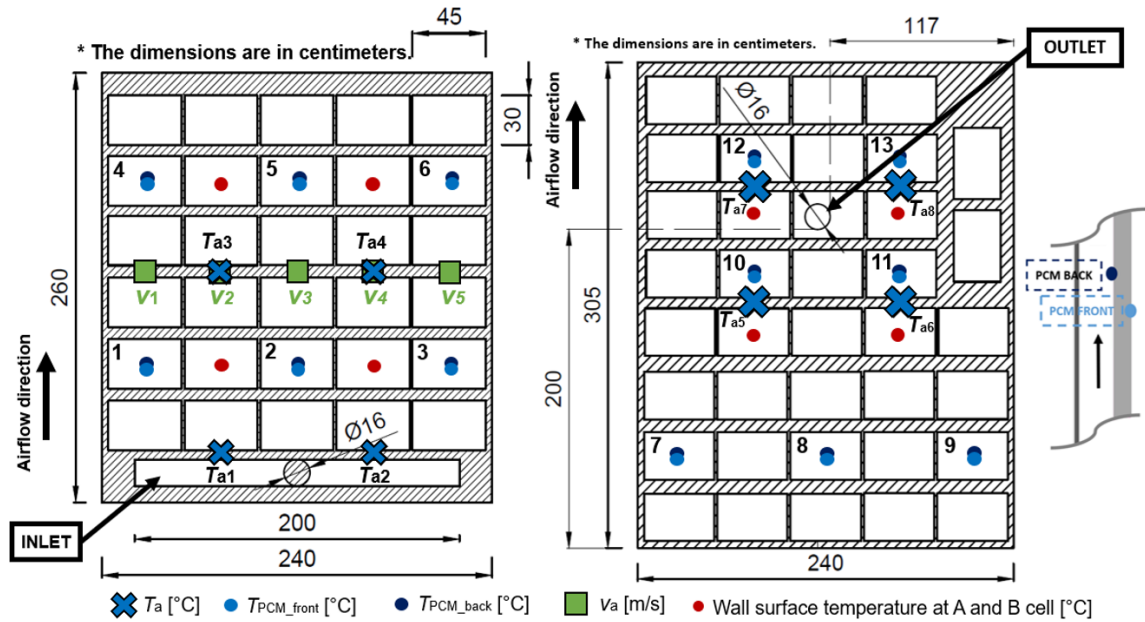


Figure 6.12: Locations of the measuring points in PCM wall (up) and ceiling (down).

6.1.5. Description of the experimental protocol

There are two different sets of experimental results obtained from September to November 2021. The purpose of the first set is to evaluate the cooling effect of the plates during the daily cycle when the PCM was melted in the plates. Through data acquisition, the sensors were detected in the LabView software. The heater in cell B was controlled to maintain the desired set point temperature of the cell based on the air temperature measured in the centre of the room. The air temperatures were selected to match the indoor conditions during the cooling season. The exact same output (amount of power) was provided by the heater in cell A. Prior to the experimental case, the plates were cooled to 20°C to ensure complete PCM solidification. The temperature difference between the measured values of air temperature in cells A and B determined the cooling effect of the PCM plates. The air temperature in cell B was maintained by a proportional integral derivative (PID) control in LabView. The room fans in cell A and B were switched ON throughout the entire test period. As part of the PCM evaluation of the cooling effect, three different groups of scenarios were tested: constant temperature, constant temperature with background ventilation and transient temperature in cell B (Figure 6.13).

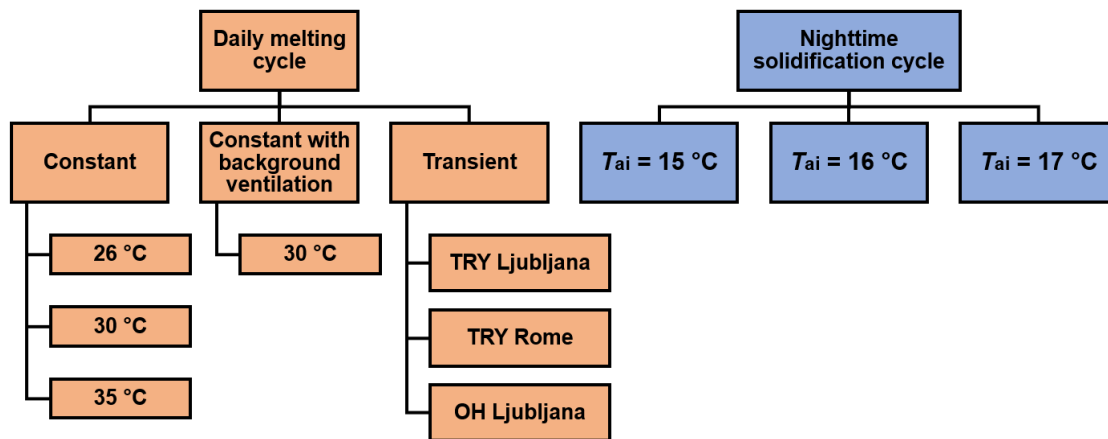


Figure 6.13: Diagram of the daily melting and nighttime solidification cycle cases, where the diagram of daily melting cases (left) refers to the set point air temperatures in Cell B.

- The constant temperature case group in cell B tests the effect of the plates by keeping the cell air temperature in cell B constant throughout the cycle. As simulated with Three different target temperatures in cell B (T_{set_B}) were tested: 26 °C, 30 °C, and 35 °C, where T_{set_B} of 26 °C refers to the highest recommended indoor operative temperature, T_{set_B} of 30 °C to a frequently appearing, and T_{set_B} of 35 °C as one of the highest indoor temperatures in summer in most of the South, West and Central European countries [157]. The case was completed when the cell air temperature in cell A reached the cell air temperature in cell B.
- The case group with constant temperature in cell B and additional background ventilation examines the drop in air temperature in cell A when background ventilation is applied for IAQ (inlet and outlet fan efficiency set to 20 %, airflow adequate for 2-3 occupants) with a supply air temperature of 21 °C in cell A throughout the 12-hour period. During the experiment, two PCM panels near the inlet on the wall and one PCM panel below the outlet on the ceiling were removed During the case 30 °C+V, the plates in front of the inlet and outlet were removed and the ventilation inlet and outlet fans switched on, so the test cell could be ventilated (Figure 6.14).

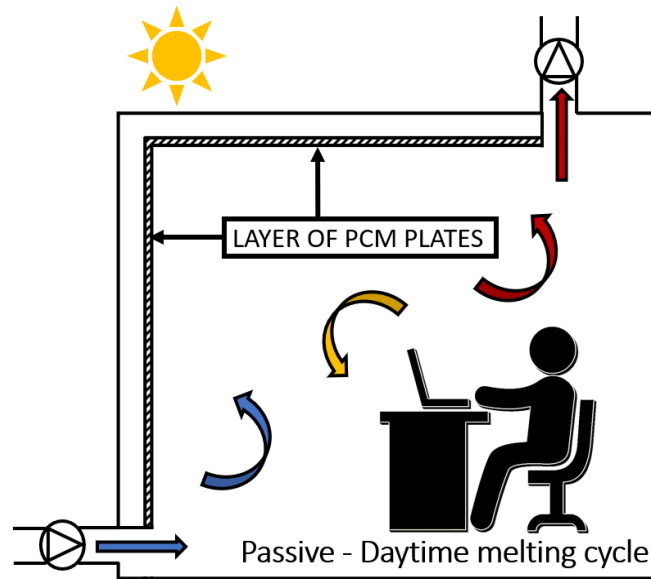


Figure 6.14: The sketch of ventilation operation in case with constant temperature of 30 °C in cell B and additional background ventilation.

- The case group with transient air temperatures in cell B was set to investigate the performance of the APS system under the daily reference fluctuations in room air temperature. The input air temperatures in cell B were obtained from the results of preliminary investigation of the lightweight building yearly thermal and energy performance simulations with Design Builder using the test reference year (TRY) for Ljubljana (Slovenia) and Rome (Italy) during the hottest day in summer [158]. In 2018, Slovenian Environmental Agency issued the projections for temperature changes in Slovenia over the 21st century [159]. Table 6.1 shows temperature difference between the maximum daily air temperature in summer in Ljubljana based on the period (1981-2010) and the periods (2011-2040, 2041-2070 and 2071-2100) of RCP4.5 and RCP8.5 scenarios with high prognosis reliability. In the moderately optimistic emission scenario (RCP4.5), it is assumed that greenhouse gas emissions will initially increase slowly, then decrease in the middle and towards the end of the 21st century but will remain relatively large. The pessimistic release scenario (RCP8.5) does not anticipate major successes in limiting emissions, so according to this scenario, emissions are increasing rapidly throughout the 21st century.

Table 6.1: Temperature difference between the maximum daily air temperature in summer in Ljubljana based on the period (1981-2010) and periods (2011-2040, 2041-2070 and 2071-2100) of RCP4.5 and RCP8.5 scenarios [159].

Scenario (max. outdoor daily temperatures)	Period (2011-2040)	Period (2041-2070)	Period (2071-2100)
RCP4.5 (summer), Ljubljana, Slovenia	0.5-1.0 °C (± 0.5 °C)	1-2 °C (± 0.5 °C)	1-2 °C (± 1.5 °C)
RCP8.5 (summer) Ljubljana, Slovenia	0.5-1.0 °C (± 0.5 °C)	1-2 °C (± 0.5 °C)	3-4 °C (± 1.5 °C)

Therefore, to test the performance of the APS system in overheated building during the heatwave in Ljubljana, the input air temperatures in cell B were obtained by linearly increasing the indoor air temperatures of the hottest day of the summer in Ljubljana obtained with TRY for 2 °C ($\Delta T_{(TRY-OH)}$) as shown in Figure 6.15. Based on the preliminary investigation during the hottest day of the year in Ljubljana (TRY Ljubljana), the indoor air temperatures compared to the outdoor air temperatures from 10:00 to 20:00 on average increased for 2.1 °C (max. $\Delta T_{(T_{ai}-T_{ao})} = 4.2$ °C). A similar temperature difference of 2 °C between the indoor and outdoor air temperatures may be observed also in present indoor air temperatures of the overheating (OH) Ljubljana case. The duration of each case is 12 hours corresponding to the duration of the daily cycle.

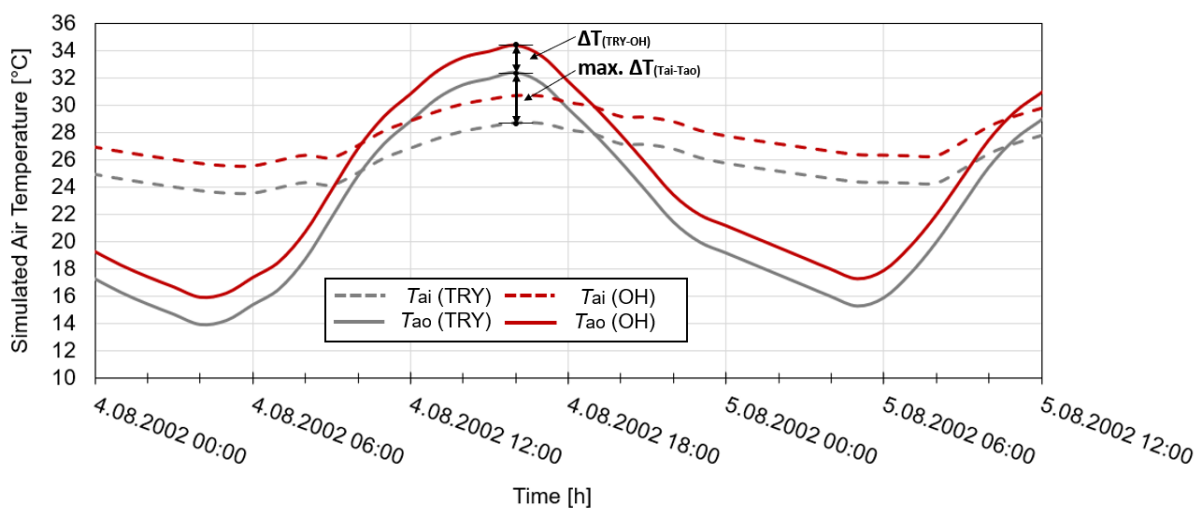


Figure 6.15: Outdoor and indoor air temperatures for TRY and OH case simulated during the hottest day of the year in Ljubljana.

The second set of experiments simulated the nighttime cycle and aimed to determine the required PCM solidification time during. Prior to the experimental case, the plates were heated to 28 °C to ensure that the PCM material was completely melted and that the predicted summer internal temperatures were achieved. The plates were then cooled using the inlet air temperature (T_{ai}), which was determined as the average of two air temperatures measured directly at the inlet linear diffuser. The inlet air temperatures studied were 15 °C, 16 °C, and 17 °C. The air temperatures were first stabilized by the cooler and then heated by the spiral heating coil. The output of the heating coil was controlled via LabView and Matlab with a fuzzy logic controller to prevent the air temperatures from exceeding the set point. The indoor temperatures were chosen based on the Central European outdoor temperatures during the cooling season. The case was closed when the average PCM surface temperatures on the front and back of the PCM panels dropped to 18 °C or less. The outlet air temperature (T_{ao}) was calculated as the average air temperature at four points near the outlet. The average surface temperature of the PCM plate measured on the front or back side of the plates is obtained by calculating the average of the PCM surface temperature at 13 measurement points on the front or back side of the PCM plates, respectively.

6.2. Experimental results

The results show the daily operation of the APS during the PCM melting cycles and its nighttime operation during the application of the ventilation for enhanced PCM solidification obtained from September to November 2021.

6.2.1. Daily PCM melting cycle performance

The results show the cooling effect of the APS system in the cases where the air temperature in cell B is constant. The effect is determined based on the air temperature drop in cell A (PCM modified cell) compared to the air temperatures in cell B (reference cell without PCM).

Figure 6.16 shows the air temperatures in cells A and B measured in three different cases with constant set points in cell B (set point temperature in cell B 26 °C – light grey line, 30 °C – dark grey line and 35 °C - black line; cell A – dashed line and cell B – solid line). All temperatures shown are air temperatures measured in the centre of cells A and B (T_a).

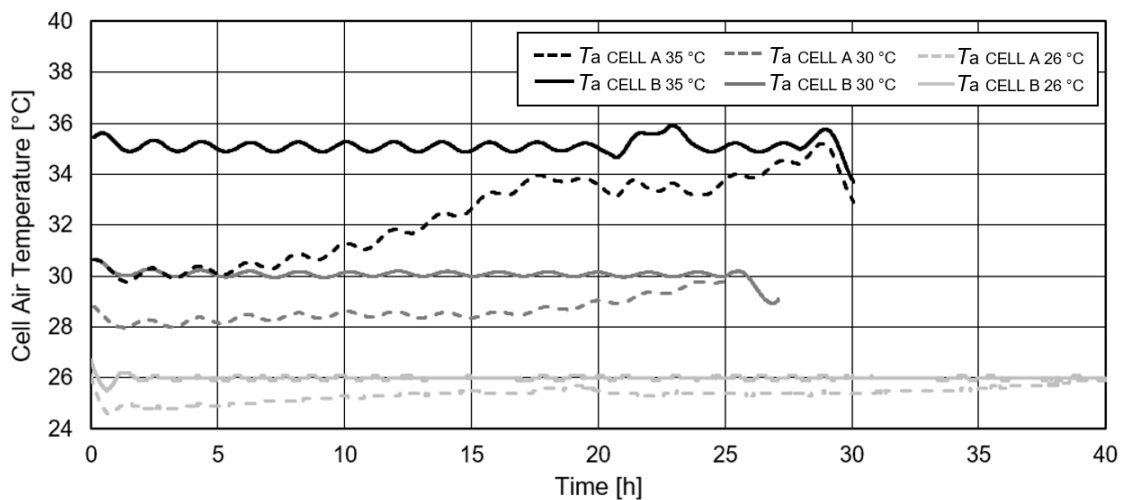


Figure 6.16: Cell air temperatures obtained during the daytime melting cycle in cell A and cell B - constant cases.

It can be concluded that in all the cases studied, the application of the APS system with PCM panels lowered the daily air temperatures. In the first case, where the target air temperature in cell B was set at 26 °C ($T_{a \text{ CELL B } 26 \text{ °C}}$), the addition of PCM plates in cell A reduced air temperatures ($T_{a \text{ CELL A } 26 \text{ °C}}$) by 1.5 °C in the first 3 h, by 1 °C between 3 h and 10 h, and from 1 to 0 °C in the last 10-40 h. In the second case, where the target air temperature in cell B was set to 30 °C ($T_{a \text{ CELL B } 30 \text{ °C}}$), the cell air temperatures in cell A ($T_{a \text{ CELL A } 30 \text{ °C}}$) differed from those of reference cell B by 2 °C in the first 15 h and by 1.5 °C to 0 °C between 15 h and 25 h. The cell air temperatures in cell B differed from those of reference cell B by 1 to 0 °C in the last 10-40 h. In the third case, when the target air

temperature in cell B was set to 35 °C ($T_{a \text{ CELL B } 35 \text{ °C}}$), cell air temperatures in cell A ($T_{a \text{ CELL A } 35 \text{ °C}}$) decreased by 5 °C in the first 5 h, from 5 to 2 °C in the next 5- 15 h, and from 2 -0 °C between 15-30 h thereafter.

Figure 6.17 shows the air temperatures in cells A and B obtained during the case with constant setpoints in cell B and the addition of background ventilation for indoor air quality (setpoint temperature in cell B: 30 °C without ventilation – black line and 30 °C with background ventilation – blue line; cell A – dashed line and cell B – solid line).

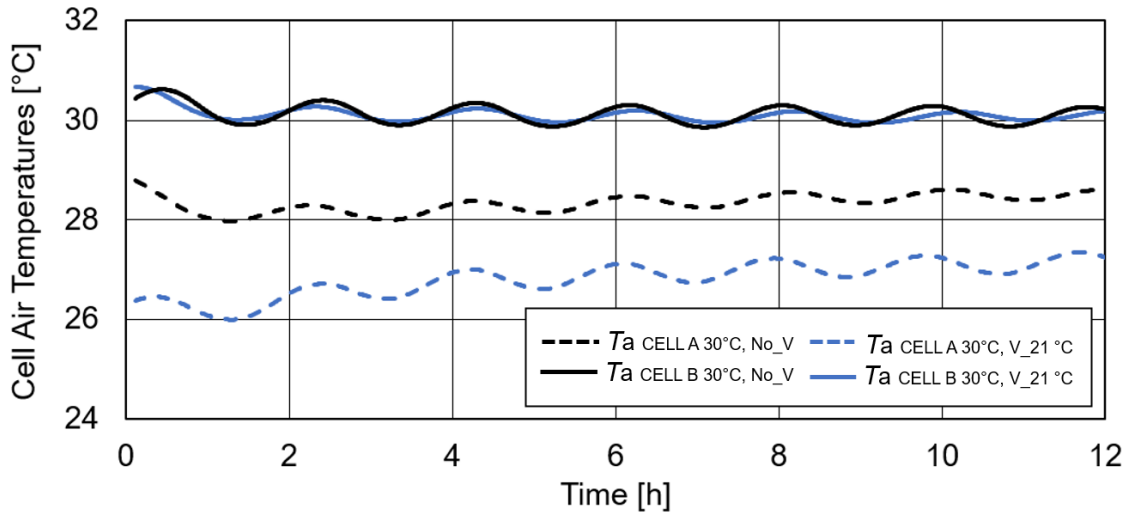


Figure 6.17: Cell air temperatures obtained during the daytime melting cycle in cell A and cell B - constant case with background ventilation.

The results from the figure show, that during the first 12 hours period with additional background ventilation supplied at 21 °C, the air temperatures in cell A ($T_{a \text{ CELL A } 30 \text{ °C, V_21 °C}}$) drop for 3.5 °C compared to the reference case ($T_{a \text{ CELL B } 30 \text{ °C, No_V}}$ or $T_{a \text{ CELL B } 30 \text{ °C, V_21 °C}}$) and by 2 °C compared to the temperatures in cell A without background ventilation ($T_{a \text{ CELL A } 30 \text{ °C, No_V}}$).

Figure 6.18 shows the air temperatures in cells A and B obtained in three different cases with transient set point scenarios in cell B (Ljubljana TRY – black line, Rome TRY - grey line and Ljubljana OH - red line; cell A – dashed line and cell B – solid line).

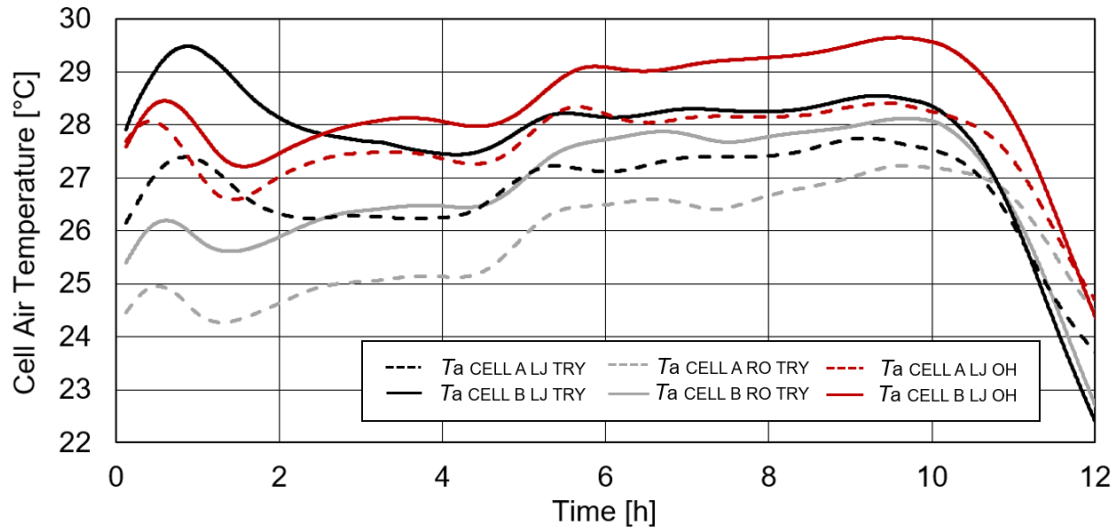


Figure 6.18: Cell air temperatures obtained during the daytime melting cycle in cell A and cell B – transient cases.

During the daily cycle period of 12 hours, the presence of the APS system lowers the air temperatures of cell A ($T_{a_CELL_A_LJ_TRY}$, $T_{a_CELL_A_RO_TRY}$ and $T_{a_CELL_A_LJ_OH}$) between 1 °C and 1.5 °C in all tested cases compared to their reference cases ($T_{a_CELL_B_LJ_TRY}$, $T_{a_CELL_B_RO_TRY}$ and $T_{a_CELL_B_LJ_OH}$).

6.2.2. Nighttime PCM solidification cycle performance

The following results aim to show the solidification behaviour of the APS system during the nighttime solidification cycle. Figures Figure 6.19-Figure 6.21 present the average surface temperatures measured at the front (cell side) surface of the PCM plate (solid line), the average surface temperatures measured at the back (air gap side) surface of the PCM plate (dashed line), and the inlet air temperature (dotted line) measured at the inlet of the air gap. The results show three different cases with average inlet air temperatures of 15 °C (light grey), 16 °C (dark grey) and 17 °C (black). Taking into account that the selected PCM material solidifies completely at 21 °C and that the non-uniform temperature distribution along the PCM wall and ceiling (± 0.5 °C), the end of the phase change is determined at 20.5 °C (blue dashed line). Strong agreement was observed between the average surface temperatures measured on the front and back surfaces of the PCM plates, indicating that the thickness of the PCM plates did not strongly influence the phase change process.

Therefore, Figure 6.19 shows the average surface temperatures on the front and back surfaces of the PCM plates (mean average of T_{PCM_front} and T_{PCM_back} measured at all 13 locations of the PCM wall and ceiling) during the solidification at an inlet air temperature (T_{ai}) of 15 °C. It can be seen, that PCM solidified completely at stable inlet temperatures in the first 5 h of the present case.

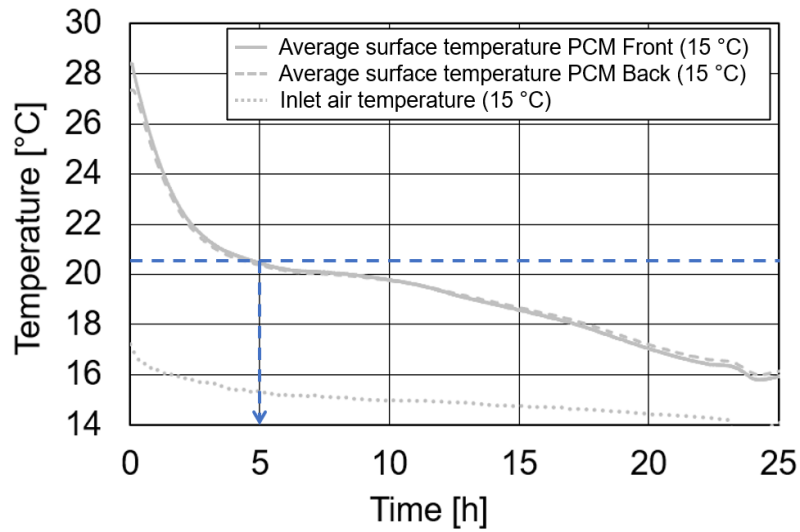


Figure 6.19: The average PCM surface temperatures and inlet air temperatures obtained during the case solidified with average inlet air temperature of 15 °C.

Figure 6.20 shows that the average surface temperature on the front and back sides of the PCM plates during solidification with an average $T_{ai} = 16$ °C. After 14 h, the PCM plates completely solidified.

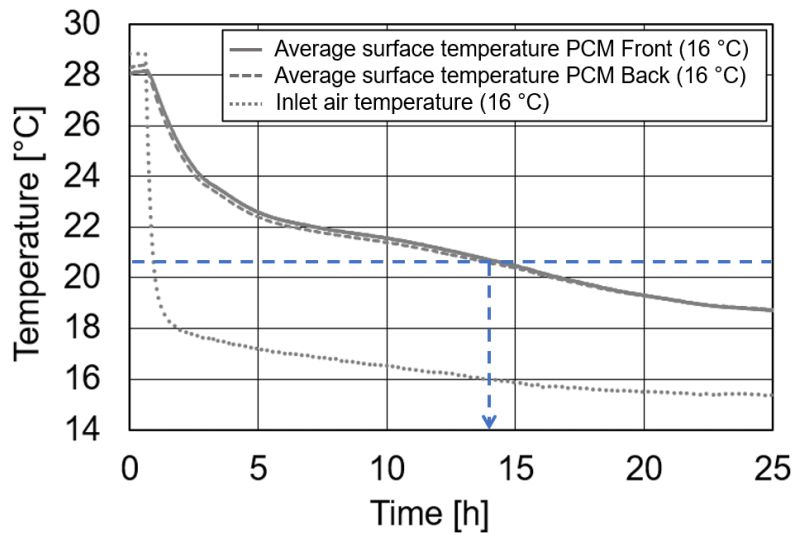


Figure 6.20: The average PCM surface temperatures and inlet air temperatures obtained during the case solidified with average inlet air temperature of 16 °C.

Figure 6.21 shows the average surface temperature on the front and back sides of the PCM plates during solidification with an average $T_{ai} = 17$ °C. The solidification of the PCM plates was completed after 16 h.

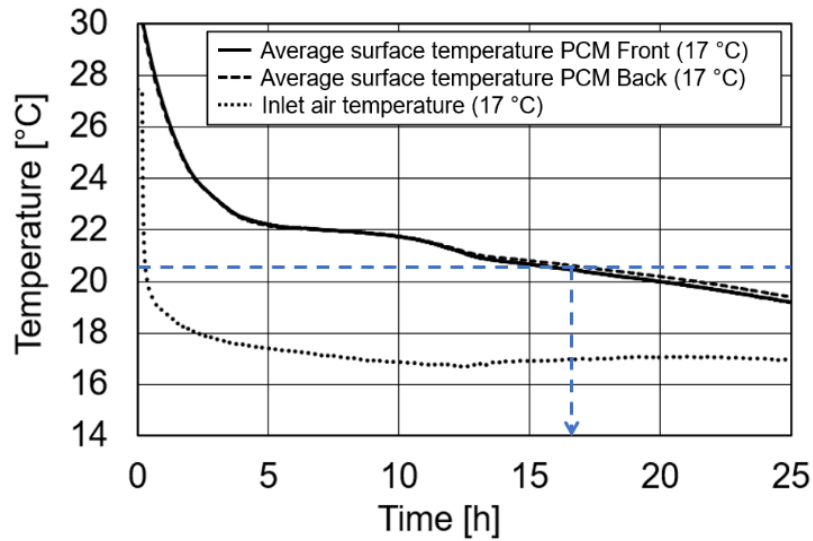


Figure 6.21: The average PCM surface temperatures and inlet air temperatures obtained during the case solidified with average inlet air temperature of 17 °C.

6.3. Discussion of the experimental results

The results show the potential of the APS system for cooling application and outline its challenges. In all the studied cases with daily melting cycle, the cooling effect of the plates is the strongest during the first hours of the experiment. For example, during the cases with constant T_{set_B} , the smallest temperature drop is observed in cell A ($T_{a \text{ CELL A}}$) compared to reference cell B ($T_{a \text{ CELL B}}$) in the case with $T_{\text{set}_B} = 26$ °C, as the smallest amount of heat is supplied to the cell. Throughout the case, the $T_{a \text{ CELL A } 26 \text{ °C}}$ is maintained at 25 °C, making it the only case that can independently (without additional space cooling systems) provide a thermally comfortable environment (recommended summer indoor air temperatures between 22 °C and 26 °C) [37]. In addition, during the entire daily cycle (12 h), the $T_{a \text{ CELL A } 30 \text{ °C}}$ was maintained at 28 °C. This case shows a slightly stronger cooling effect than the case with $T_{\text{set}_B} = 26$ °C, but under these conditions the APS system alone cannot establish provide a thermally comfortable environment. With the addition of background ventilation for indoor air quality in the present case, $T_{a \text{ CELL A } 30 \text{ °C}}, v_{21 \text{ °C}}$ reaches recommended air temperatures that are 2 °C lower (from 28 °C to 26 °C - upper limit of indoor thermal recommendations) than in the case without the ventilation $T_{a \text{ CELL A } 30 \text{ °C}}$. Such a case is realistic, as offices must be equipped with ventilation to avoid adverse health effects among occupants and provide healthy and productive living environment. The highest cooling effect among all studied cases was observed at the case with $T_{\text{set}_B} = 35$ °C. During daily operation (12 h), $T_{a \text{ CELL A } 35 \text{ °C}}$ were maintained between 30 °C and 31 °C.

The thermal comfort during the investigated daytime cycle cases is assessed based on the recommended values in Table 2.2 and Table 2.4 and presented in Table 6.2. It is assumed that due to the mixing of room air T_a is similar to T_{op} . For the calculation of PMV and PPD it was assumed that $v = 0.1$ m/s, $RH = 50$ %, $M = 1.1$ met and $I = 0.61$ clo.

Table 6.2: Thermal comfort assessment.

Case	$T_a=T_{op}^*$	PMV	PPD	Category**	Category T_{op}^{***}
$T_{a\text{ CELL A } 26\text{ }^\circ\text{C}}$	25 °C	0.08	5 %	I	I
$T_{a\text{ CELL A } 30\text{ }^\circ\text{C}}$	28 °C	1.01	27 %	IV	IV
$T_{a\text{ CELL A } 35\text{ }^\circ\text{C}}$	30 °C	1.65	59 %	IV	IV
$T_{a\text{ CELL A } 30\text{ }^\circ\text{C, V } 21}$	26.8 °C	0.64	14 %	III	III
$T_{a\text{ CELL A_LJ TRY}}$	min: 24 °C max: 27.8 °C mean: 25.9 °C	0.36	8 %	II	II
$T_{a\text{ CELL A_RO TRY}}$	min: 24.5 °C max: 27.2 °C mean: 26.8 °C	0.64	14 %	III	III
$T_{a\text{ CELL A_LJ OH}}$	min: 24.5 °C max: 28.5 °C mean: 27.6 °C	0.89	22 %	IV	IV

*mixing of room air with the fan at all times, ** Table 2.4, ***Table 2.2

The table shows that only $T_{a\text{ CELL A } 26\text{ }^\circ\text{C}}$ are in the 1st category of thermal comfort. $T_{a\text{ CELL A_LJ TRY}}$ and $T_{a\text{ CELL A } 30\text{ }^\circ\text{C, V } 21}$ are in the 2nd category (compared to $T_{a\text{ CELL A } 30\text{ }^\circ\text{C}}$ this case is due to ventilation heat losses two categories higher) and $T_{a\text{ CELL A_RO TRY}}$ in the 3rd category. The rest of the $T_{a\text{ CELL A}}$ cases are in the 4th category.

Moreover, the cases with transient T_{set_B} showed a more dynamic and realistic performance of the APS system during the day. In all the tested cases, the results showed that the indoor temperatures were very sensitive to the temperature changes around the cell, despite the PCM buffer. The temperature difference between cell A ($T_{a\text{ CELL A}}$) and the reference case ($T_{a\text{ CELL B}}$) was kept constant (between 1.0 °C and 1.5 °C).

Based on the measured results, the proposed APS system can be used almost independently only in Rome (Italy) because $T_{a\text{ CELL A_RO TRY}}$ cross the upper limit of indoor thermal requirements of 26 °C only for max. 1 °C for 6 hours. Due to the higher outdoor temperatures, during the TRY case of Ljubljana $T_{a\text{ CELL A_LJ TRY}}$ exceed the required upper indoor temperature limit during the entire daytime cycle and reach almost 28 °C. Similarly, during the OH case of Ljubljana, $T_{a\text{ CELL A_LJ OH}}$ the required upper indoor temperature limit is exceeded for the entire daytime cycle. Even though in the first half of the experiment the temperatures fluctuate slightly above 27 °C in the second half they mostly stay at 28 °C. In TRY cases of Rome and Ljubljana, the cooling effect of the plates is larger compared to the OH case of Ljubljana and it reaches a constant value of 1.5 °C and values between 0.8 °C and 1.5 °C, respectively. In OH case of Ljubljana, the cooling effect is the smallest and it reaches the values between 0.5 °C and 1 °C. The temperatures $T_{a\text{ CELL A_LJ OH}}$ correspond to the temperatures $T_{a\text{ CELL B_LJ TRY}}$ obtained without APS system.

Since in most cases of the daily melting cycle, the air temperatures in cell A do not reach the recommended values for thermal comfort, additional cooling devices such as air-conditioners are required. Considering that, unlike $T_{a\text{ CELL A } 35\text{ }^\circ\text{C}}$, where cell temperatures rise after 5 hours, cell temperatures $T_{a\text{ CELL A } 26\text{ }^\circ\text{C}}$ and $T_{a\text{ CELL A } 30\text{ }^\circ\text{C}}$ are kept constant for a very long period (longer than 12 hours), the number of PCM plates could be reduced.

The results of the present study are consistent with similar studies conducted by other researchers. For example, the cell temperatures ($T_{a \text{ CELL A } 30 \text{ }^\circ\text{C}}$) obtained in the case of a constant $T_{\text{set B}} = 30 \text{ }^\circ\text{C}$ largely correspond to the performance of salt hydrates with MP of $24 \text{ }^\circ\text{C}$ attached to the suspended nightly ventilated ceiling and tested by Weinläder et al. were able to reduce the internal temperatures to $28 \text{ }^\circ\text{C}$ (for $2 \text{ }^\circ\text{C}$) [117].

BioPCMs are a very popular technique due to their ease of use and sustainable design. Accordingly, Jamil et al. and Berardi and Soudian applied BioPCM25 ($T_m = 25 \text{ }^\circ\text{C}$) to the interior surfaces of the building and in combination with nighttime ventilation, reduced daily indoor temperatures by 2°C and even $6 \text{ }^\circ\text{C}$, respectively [90], [160].

Moreover, the combination of PCM with different MP in different layers of building elements can greatly enhance their performance. Hou et al. and Li et al. incorporated PCM into the external side of the roof ($T_m = 32 \text{ }^\circ\text{C}$) and internal side of the ceiling ($T_m = 24 \text{ }^\circ\text{C}$), lowering daily temperatures by up to $8 \text{ }^\circ\text{C}$ [108], [109].

The nighttime solidification cycles showed the influence of the inlet air temperature (T_{ai}) on the solidification time. Among the tested cases, the case with an average $T_{\text{ai}} = 15 \text{ }^\circ\text{C}$ showed the shortest solidification time, which was achieved by the highest temperature difference between the plates and the inlet air. Further optimization of the required air flow should be carried out to reduce the energy use for the operation of the fans. Nevertheless, promising results were obtained even in the case of average $T_{\text{ai}} = 16 \text{ }^\circ\text{C}$. Even if the solidification time exceeds the night cycle (14 h), a slightly improved system could complete the solidification in time. Due to the experimental conditions in the first hours of the experiment, the inlet temperature could not reach the required set point temperature and eventually exceeded $16 \text{ }^\circ\text{C}$. This anomaly had a significant effect on the solidification time. Also, in the case of $T_{\text{ai}} = 17 \text{ }^\circ\text{C}$, the initial temperature of the plate was slightly higher than in the previous two cases ($29 \text{ }^\circ\text{C}$), which could slightly increase the solidification time. In addition, stabilization of the inlet temperature from $18 \text{ }^\circ\text{C}$ to $17 \text{ }^\circ\text{C}$ took 5 hours, similar to the previous case, thus further increasing the solidification time. However, it is assumed that the solidification time would still exceed the nightly cycle limit of 12 hours regardless of the anomalies and thus the final inlet temperature ($T_{\text{ai}} = 17 \text{ }^\circ\text{C}$) is insufficient for the APS system to operate. Finally, solidification can be accelerated by increasing the air flow rate in the system. Weinläder et al. even doubled the flow rate from $300 \text{ m}^3/\text{h}$ to $600 \text{ m}^3/\text{h}$ during the experiment and reported that the fan power tripled [117]. Thus, the increased air flow rates are a compromise solution.

In general, one of the major drawbacks of using PCM in building elements remains its price. The economic feasibility of PCM is affected by the energy prices, the cost of the material PCM and the calculation of energy savings. Although the PCM price has decreased significantly in the last 5 years (from 30-50 %), PCM systems integrated in buildings are still an economically unsuitable concept according to economic feasibility studies [161], [162].

The limitations of the present experimental study are underlined in the following paragraph.

- At this stage of the APS investigation, the aim is to find the effect of IAQ ventilation on cooling of the cell and to characterise the thermal behaviour of the system by finding the required airflow rate to adequately decrease the indoor air temperatures to

the recommended indoor thermal levels. Therefore, at later stages of investigation, the inlet and room temperatures need to be adapted according to the ventilation standards which should be respected once the system is finalised.

- Overheating case of Ljubljana was determined based on the indoor and outdoor temperatures simulated with TRY and on average value of the highest daily temperature projections in Ljubljana for period (2011-2100) and scenarios RCP4.5 (mild) and RCP8.5 (pessimistic) prepared by Slovenian Environmental Agency. The temperature difference between TRY and OH is assumed based on the average of the outdoor air temperatures shown in six types of projections. Since it is linearly summed to outdoor air temperatures from TRY, the outdoor air temperatures from OH scenario does not consider any possible change in daily dynamics of outdoor air temperature fluctuations during the heatwave. Also, there are several methods that could be tested and compared with the results of other studies. For example, the Chartered Institution of Building Services Engineers (CIBSE) proposed a method of Design Summer Years (DYSs) for moderately warm summer, short intense warm spell or long, less intense warm spell scenarios [163]. The DYSs weather files are prepared based on the projections and temperature monitoring of 14 cities in United Kingdom.
- The results lack the uncertainty analysis. It must be noted that the evaluation of the system is always given with the reference to simultaneously obtained measurements from cell B. The purpose of this is to eliminate the outdoor environmental conditions error (heat losses through the walls of the test cells). Even though the indoor air temperature in the laboratory remained almost constant (20 °C) during the entire year, one insulated external wall was in contact to the outdoor environment. Although the temperature in test cells was regulated based on the cell air temperature, the effect the heat transfer through the external wall (heat losses) could affect the cell air temperature regulation dynamics (important for transient cases: TRY Ljubljana, TRY Rome and OH Ljubljana). There is repeatability on ventilation system performance, but the complete thermal environment repeatability is harder to ensure. Nevertheless, the measurements were performed in Autumn in Lyon, so the outdoor environment didn't reach very cold or hot air temperatures.
- To completely assess the APS performance, thermal comfort survey with human subjects or measurements with manikin may be performed. However, it is believed that at this stage of the research such advancements aren't feasible, since the air in the cells is mixed at all times to establish uniform conditions. Therefore, besides a valuable human subject assessment of the system performance, under present experimental conditions we do not expect any significant effect from the APS system to the occupant (e.g. local cooling of the seated person, draft etc.). Even more, the assessed thermal comfort may even be compromised by the heater on one side of the room (which is representable for the heat gains but not for the heat distribution in the office) causing human subject thermal asymmetry.
- Not only air temperature of the air constantly mixed in the room, but also mean radiant temperature was measured. However, the article focuses only on-air temperatures, because in this case it is considered that they are more representative compared to mean radiant temperatures. The heater in the room could affect the operative temperature calculations by indicating a major local discomfort as it has high surface temperatures (higher than at actual room temperature distribution of such summer case).
- One of the major problems occurring with PCM materials encapsulation is the material leakage from the encapsulated spaces into the environment. Figure 6.22 shows PCM

plates positioned and sealed into the ceiling frame structure with plates' joints marked and melted PCM leakage dripped on the cell's floor. The entire floor was dripped with PCM material.



Figure 6.22: PCM leakage due to volume expansion dropping from the ceiling on the floor.

7. Numerical model and parametric study

7.1. Method

In this chapter, the specifics of the present numerical simulation model are specified. The rest of the method is set out in chapter 2.4.

7.1.1. Geometry selection

The purpose of this model is to evaluate the nocturnal (solidification) cycle. A simplified 2D model calculated using ANSYS Fluent v19.1 is proposed to calculate the air and PCM temperatures [149]. The model is divided into two surface regions, the air gap (fluid region) and PCM (solid region). To avoid unnecessary geometric complexity and computational difficulties, the 3D model of the wall and ceiling is cut in the middle with a symmetry plane, where its intersection defines the 2D model geometry. So, the numerical outlet is positioned at the end of the air gap (Figure 7.1). Due to the building structure of the laboratory such configuration was not possible in reality.

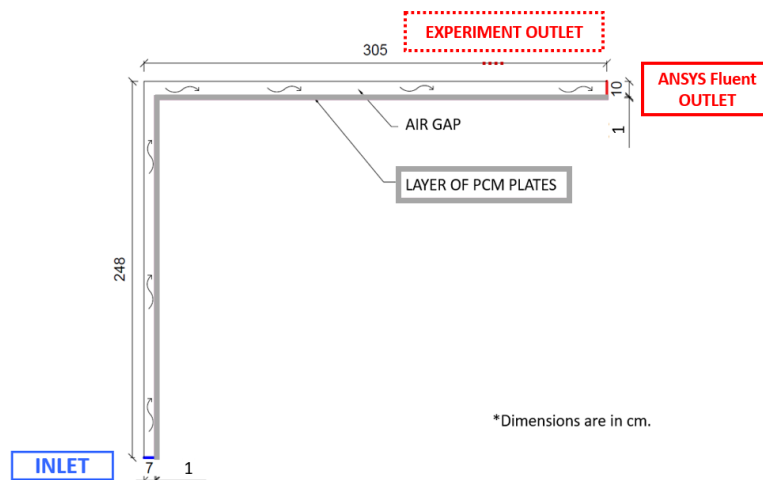


Figure 7.1: Sketch of the 2D model geometry with simplifications.

7.1.2. Grid and time step

Figure 7.2 and Figure 7.3 show the grid and time step independence test based on the outlet air temperatures (T_{ao}) and PCM surface temperatures $T_{PCM_back, avg}$ during 25 h of operation, respectively. The results are based on the tested grid size (2 mm, 5 mm, 10 mm, 15 mm and PCM /air gap: 10 mm/20 mm) and time steps 10 s, 30 s and 120 s. Some of the lines from 2 mm (10 s) to 10 mm (30 s) may be less visible, due to overlapping.

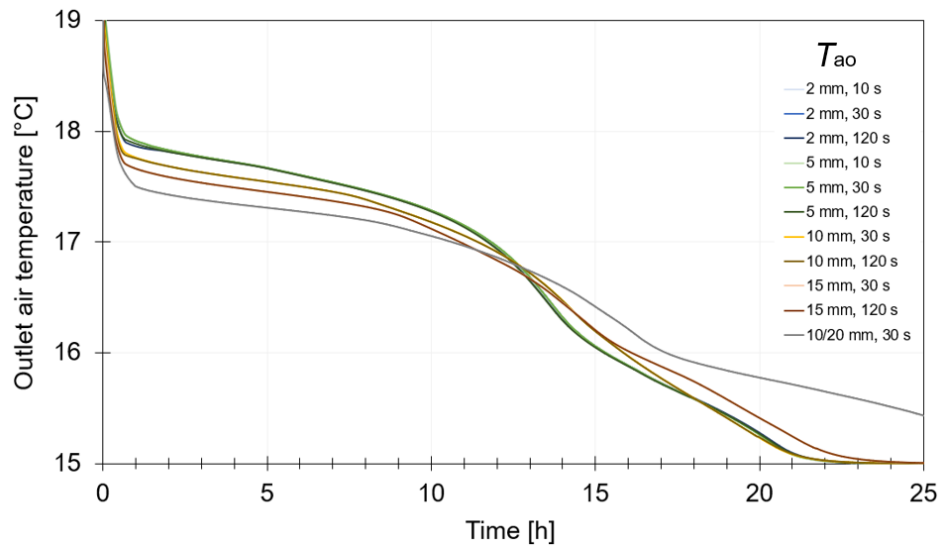


Figure 7.2: Grid and time step independence test of Outlet air temperatures T_{ao} during 25 h of operation (note: the lines from 2 mm (10 s) to 10 mm (30 s) are overlapping).

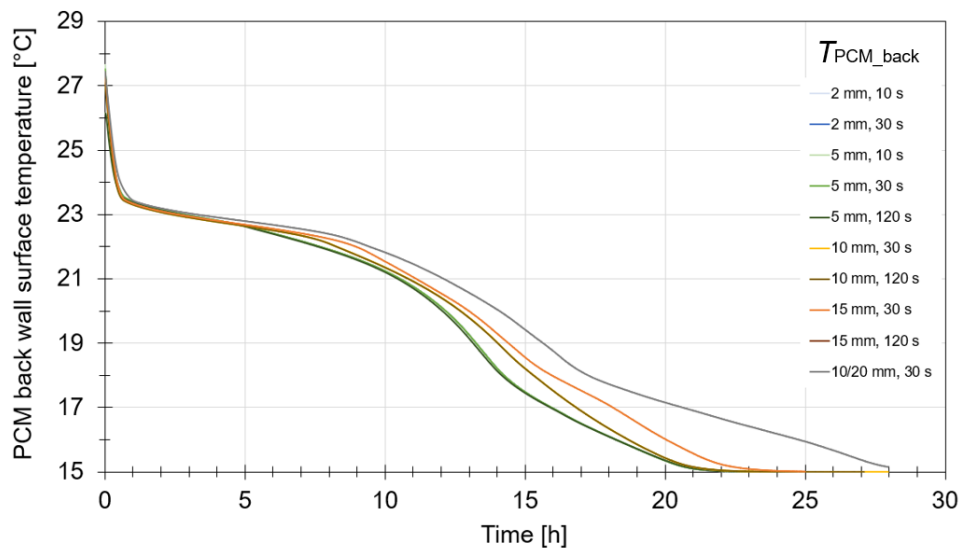


Figure 7.3: Grid and time step independence test of PCM surface temperatures $T_{PCM_back, avg}$ during 25 h of operation (note: the lines from 2 mm (10 s) to 10 mm (30 s) are overlapping)

The statistics prove that the numerical results obtained with the 10 mm grid and time step of 30 s are consistent with the 2 mm grid and time step of 10 s. The model was simulated with 5 mm grid with 21004 grid elements (Figure 7.4). The numerical validation follows the experimental results, where the sampling rate was set to 30 s. Therefore, the time step in the numerical model is fixed accordingly (30 s).

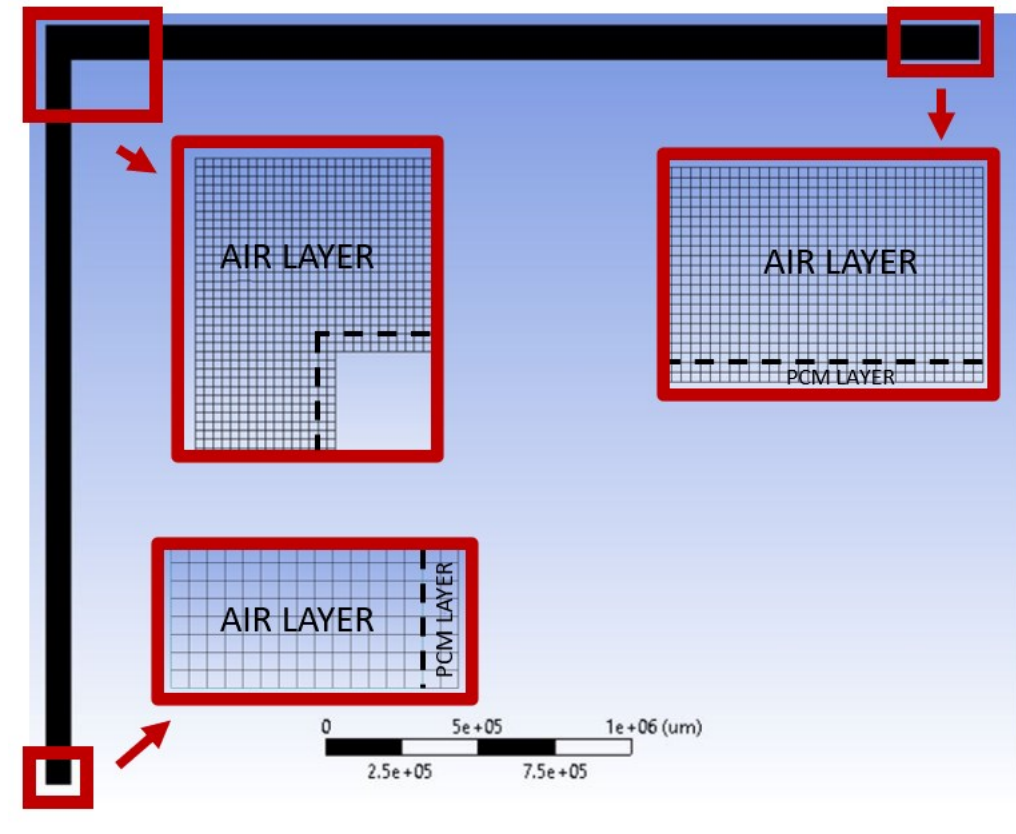


Figure 7.4: The selected grid with element size of 5 mm.

7.1.3. Calculation model

The unsteady model is calculated using ‘Energy model’ and the airflow in the air gap with standard viscous ‘model k- ω ’, which is suitable for the calculation of wall-bounded flows. K- ω was also confirmed by Diarce et al. as the best performing model for a ventilated air gap wall. The rest of numerical model parameters are specified in Appendix D.

7.1.4. Initial and boundary conditions

The model consists of the velocity inlet and outflow outlet. The primary wall has an adiabatic boundary condition and the PCM wall in contact with the indoor space (external

PCM wall) the estimated temperature according to the investigated parametric scenario. The inlet velocity was set to 0.8 m/s and the initial PCM temperature to 28 °C, as measured during the experimental reference case. The fluid material air has a Boussinesq density of 1.18 kg/m³ and a coefficient of thermal expansion of 0.00336 1/°C.

7.1.5. Material properties

The PCM material investigated in this study is manufactured by Rubitherm. The PCM plates are originally encapsulated in the aluminium CSM cases. In the model, the thickness of the aluminium plates is neglected (0.65 mm) and the plates are simulated as a single unit (surface). The properties obtained from differential scanning calorimetry (DSC) are available on the product page [164]. The salt hydrate SP24E with a melting temperature (T_m) and partial enthalpy of about 24 °C and 150 kJ/kg (Figure 7.5) [155]. Due to hysteresis, the solidification of the material occurs at 22 °C and 23 °C with partial enthalpies of 118 kJ/kg and 42 kJ/kg, respectively. The material has a thermal conductivity (λ) of ~0.5 W/(m K) and a density (ρ) of 1.5 kg/l and 1.4 kg/l in the solid and liquid states, respectively. The material was selected based on thermal properties suitable for thermal comfort during hot summer periods in the cooling season [37].

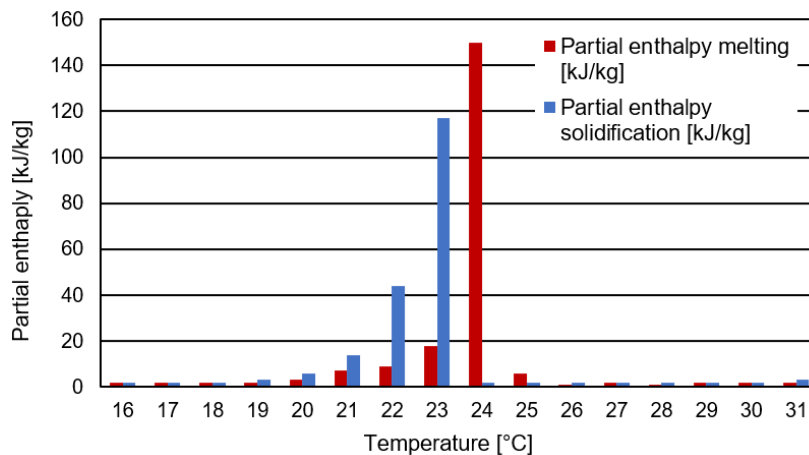


Figure 7.5: DSC diagram Rubitherm SP24E [155].

Figure 7.6 shows the material properties input inserted as a linear-piecewise partial enthalpy in dependence of 17 temperature points.

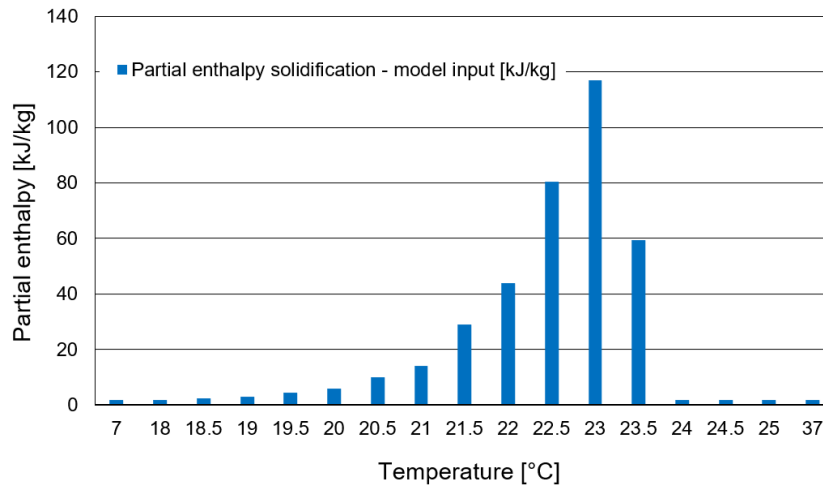


Figure 7.6: Partial enthalpy in correlation with temperatures - numerical model input

The PCM was simulated as a solid material because the PCM wall is thin compared to the size of the system and convection in the slabs is assumed to be negligible, which significantly reduces the computation time compared to the fluid input with the melting and solidification model turned on. This approach was also confirmed in study by Diarce et al. [136].

The partial heat capacity of the material was inserted according to the corresponding temperature given in the DSC of the material by piecewise-linear option available in Fluent. The thickness of the PCM layer was supposed to be 0.65 cm and was determined based on the mass weight of the PCM in the plate. However, due to an improved mesh, the thickness of the PCM layer was 1 cm and the density of the material was reduced proportionally.

The hysteresis was taken into account so that only the solidification properties of the DSC diagram were used in the material. The piecewise-linear option was also used for the density, which changed in relation to the temperature of the PCM material according to the linear fraction of its solid or liquid phase.

7.1.6. Parametric study

The parametric study examines the effects of an influential parameter - outdoor air inlet temperature (T_{ai}). Based on the outdoor air temperatures in south-central Europe, six different T_{ai} were selected (15 °C, 16 °C, 17 °C, 18 °C, 19 °C and 20 °C).

When the cooling cycle starts, the cell air is still heated and its effect on the calculation is not negligible. Two assumptions were made, one for the boundary condition temperatures at the PCM which is in contact with the cell air wall ($T_{PCM_front, avg}$), and the other for the calculation of the temperature at the PCM wall, which is in contact with the air gap ($T_{PCM_back, avg}$).

First, the boundary on the front side of the PCM wall ($T_{\text{PCM_front, avg}}$) is in constant contact with the interior environment of the cell, which has a significant effect on the solidification process. This effect was measured in the experimental studies when PCM was solidified after the heating (melting) cycles. The air temperature was measured in the centre of the cell ($T_{\text{a, cell}}$) where the air was during the experiment mixed with the room ventilators.

Based on the experimental cases, the dynamics of cell temperatures during solidification were analysed. To test different T_{ai} , the boundary condition of the cell temperature $T_{\text{a, cell}}$ was extrapolated for each of the six parametric cases according to the experimental case below, with the initial PCM temperature of 28 °C and T_{ai} of 18 – 15 °C (Figure 7.7). Similar dynamics of $T_{\text{a, cell}}$ decreases were observed in other experimental cases' measurements where the solidification cycle begins at 30 °C and are not presented within this article.

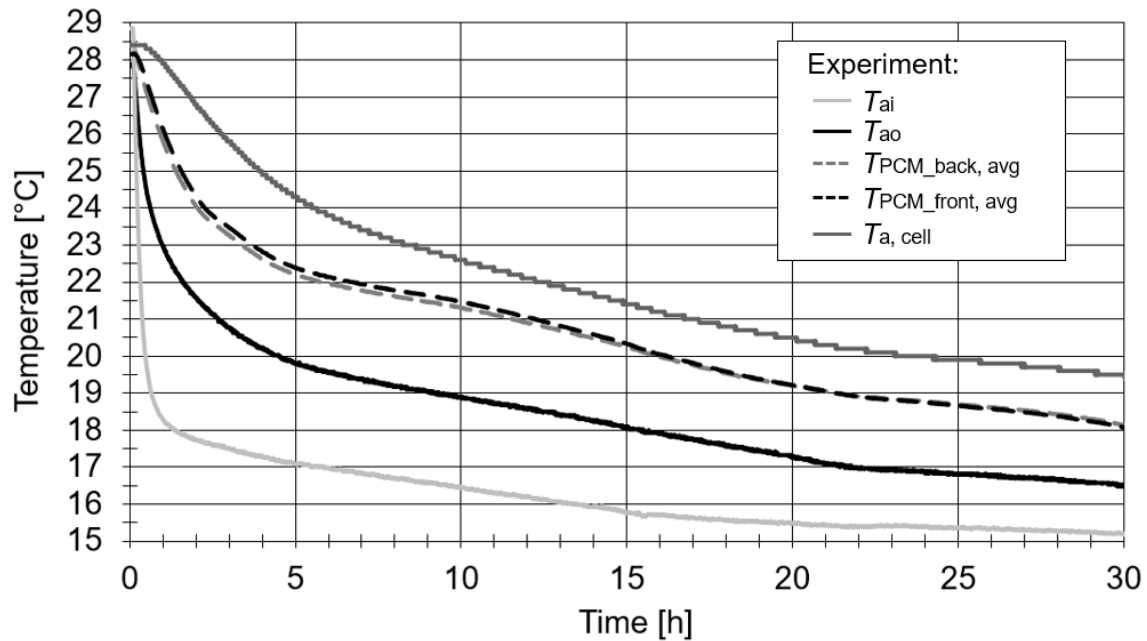


Figure 7.7: Temperatures obtained during the reference experimental case in the cooling cycle.

Table 7.1 shows the estimated air temperature differences in the cells for the corresponding constant T_{ai} scenario during two solidification periods (the first 5 h and the second 25 h).

Table 7.1: The estimated cell air temperature differences during two solidification periods for the determination of PCM wall boundary condition.

Inlet temperature scenario (T_{ai})	15 °C	16 °C	17 °C	18 °C	19 °C	20 °C
$\Delta T_{\text{a, cell}}$ (0-5 h)	3	3.5	4	4.5	5	5.5
$\Delta T_{\text{a, cell}}$ (6-30 h)	5	4.5	4	4.5	4.	3.5

The curves presented in Figure 7.8 are the estimated cell air temperatures during two solidification periods and inserted into the model via User Defined Functions (UDFs) as the PCM wall boundary condition for each case of inlet temperature (20-15 °C designated as $T_{a, cell, 20\text{ °C}} - T_{a, cell, 15\text{ °C}}$).

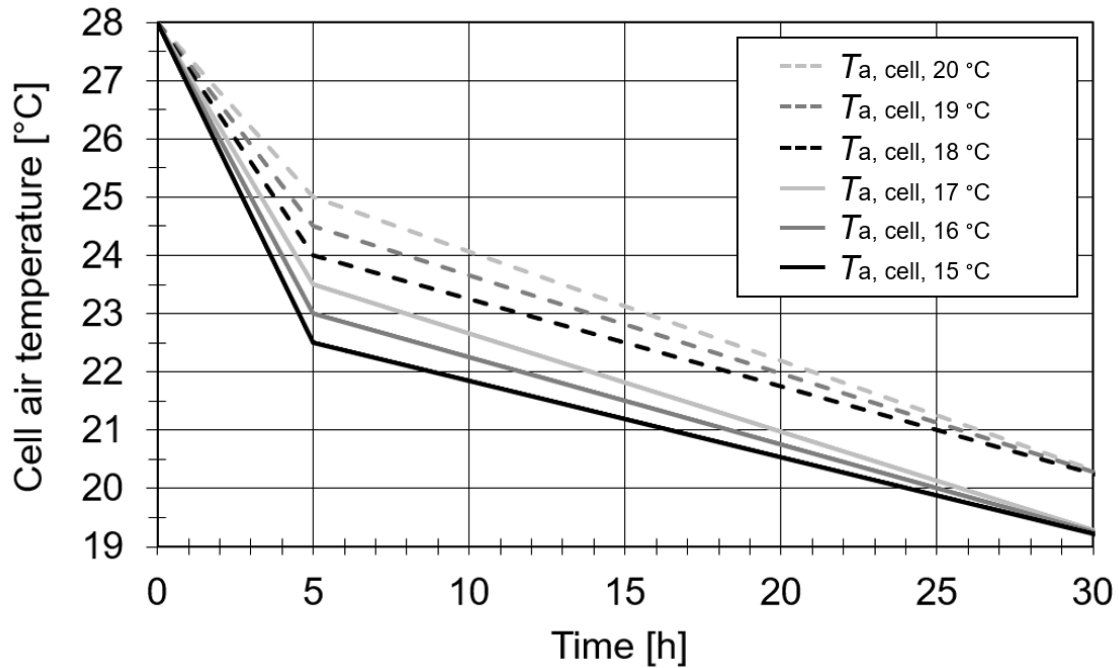


Figure 7.8: The estimated cell air temperatures during two solidification periods for the determination of PCM wall boundary condition.

Both the T_{ao} and $T_{PCM_back, avg}$ are presented as area-weighted average areas. Unfortunately, the end of the phase change cannot be determined from T_{ao} alone because high ventilation rates of the supply air in the air gap prevent a visible end of the phase change curve. Therefore, the phase change cycles can be specified using $T_{PCM_back, avg}$. So, the time required for $T_{PCM_back, avg}$ to fall to 21 °C is the solidification time for each inlet temperature scenario. From the DSC diagram (Figure 7.5), it can be seen that the PCM solidified at 21 °C.

During the validation process, the experimentally and numerically obtained $T_{PCM_back, avg}$ showed differences of more than 1 °C, which strongly affected the solidification time determination. It was concluded that the effect of the directly inserted experimentally measured $T_{a, cell}$ were not suitable for the model's $T_{PCM_front, avg}$ boundary condition. The numerical $T_{PCM_back, avg}$ values were brought closer to experimental by observing other experimental results.

As visible from Figure 7.9, the average temperature difference between $T_{PCM_front, avg}$ and $T_{a, cell}$ among four other experimental cases was 0.8 °C (± 0.4 °C). Therefore, the individual case of $T_{a, cell}$ temperatures were subtracted for 0.8 °C and inserted as boundary condition for $T_{PCM_front, avg}$.

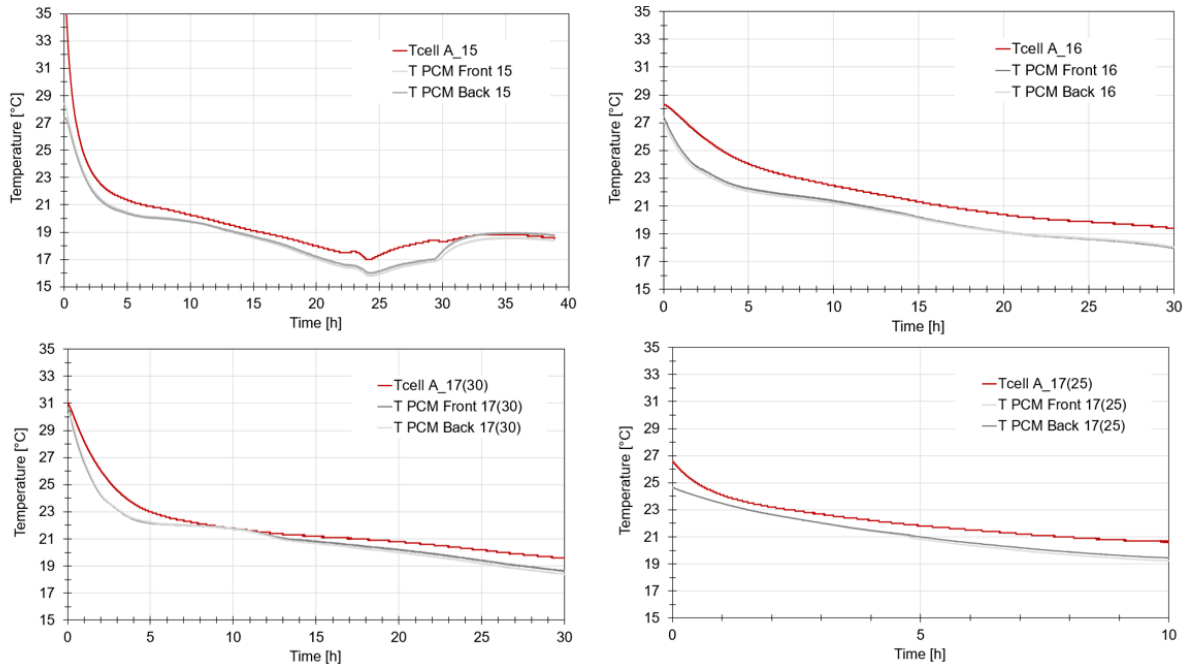


Figure 7.9: Experimental cases showing the characteristic temperature difference between $T_{PCM_front, avg}$ and $T_{a, cell}$.

7.1.7. Validation

For the purpose of validation, two cases were studied. First, a special validation case was measured in which a complete melting/solidification cycle was studied (Figure 7.10). In this case, the plates are melted and solidified only by the heated or cooled inlet air. Both phases, melting and solidification, of PCM were studied considering the hysteresis of the material (the properties of PCM (melting/solidification temperature and partial enthalpy) were adopted according to the heating or cooling period).

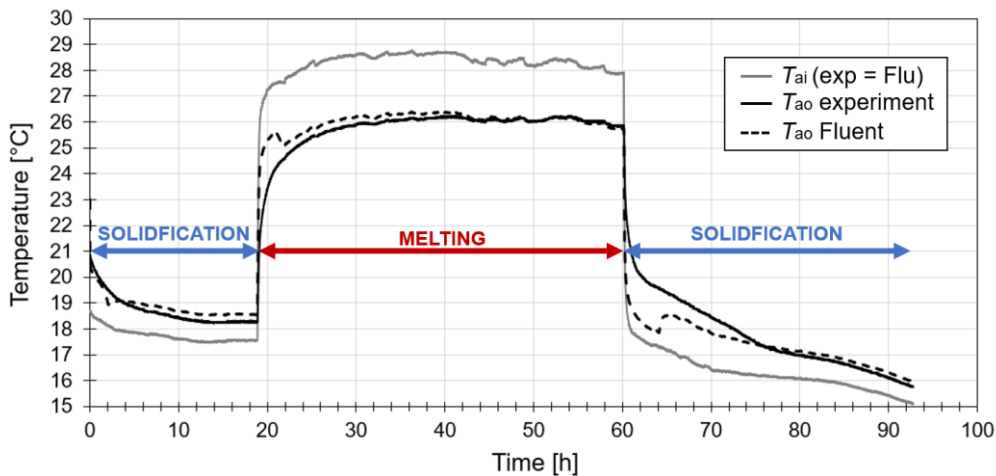


Figure 7.10: The first validation case (melting/solidification) based on the outlet air temperatures.

Second, the reference experimental solidification case was closely examined also for $T_{PCM_back, avg}$. The results show that the trend of the simulated T_{ao} and $T_{PCM_back, avg}$ temperatures drop correlate with the measured ones, even though the simulated T_{ao} and $T_{PCM_back, avg}$ temperatures deviate from the experimental values for up to 1 °C (Figure 7.11).

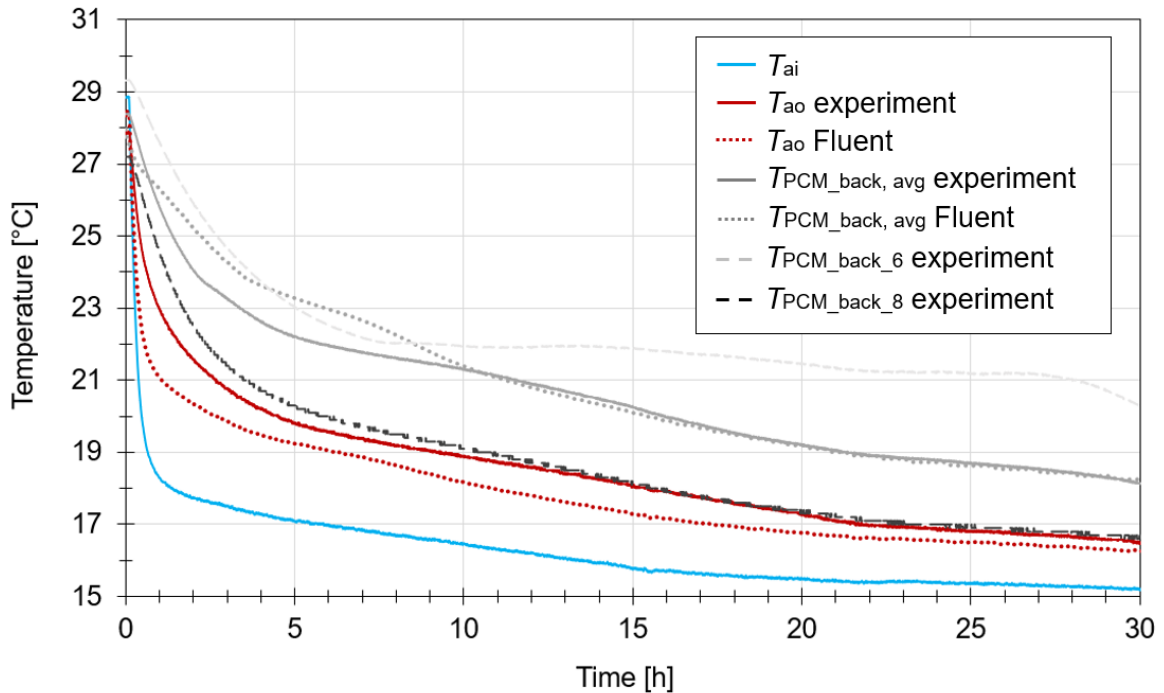


Figure 7.11: The second validation case (solidification) – based on the outlet air temperatures and average surface PCM temperature (back).

On one hand, this could be due to the experimental errors, such as the uneven phase transition along the PCM wall and ceiling and the other side was in contact with the ambient air, possible minor air leaks in the air gap and heat transfer losses through the original wall and ceiling (even though they are both insulated, in nature this is layer doesn't present and adiabatic boundary condition). Also, the air measured air velocity might still differ from the simulated one as it was determined based on the average of five measured points in the air gap. On the other hand, numerical errors may arise due to assumptions and model simplifications. For example, an effect of $T_{a, cell}$ applied to the PCM wall boundary condition could be too significant. Due to mixing of the cell air, the temperature distribution along the PCM wall and ceiling was considered uniform (in nature, the same temperature did not appear simultaneously near the wall and ceiling). Also, in the air gap no radiation calculation models were considered.

Considering the temperature differences along the PCM wall and ceiling and the scale of the experiment (room level), the temperature difference of 1-2°C between the experimental and numerical results is considered acceptable. Accordingly, also other authors also showed discrepancies between the results of experiments and numerical calculations

during nighttime solidification times in the presence of ventilation in active air-based systems with PCM for cooling application modelled at the level of a building element.

For example, Diarce et al. reported a mean temperature error between experiment and numerical calculation based on the outlet air and PCM material on the wall in front of the outlet of 1.0-2.23 °C and 1.34-2.50 °C, respectively [136]. Faheem et al. also showed a surface temperature difference at the bottom of the slab of ± 1.25 °C [119]. Hu and Heisleberg observed the outlet air temperature from experimental and numerical results and found a deviation of 2 °C between 3.5-5.5 h of ventilation period [145]. Kant et al. compared the measured and calculated PV temperatures and found a temperature difference of 2-6 °C [148]. However, Li et al. observed the profiles of the average air gap air temperature along the height of the double-glazed façade with PCM, where the simulated values differed by 1.5 °C from experimental ones [144].

7.1.8. Energy storage by PCM

In Equation 7.1, heat stored for cooling Q_{dis} is determined with area of the air gap $A_{air\ gap} = 0.168\ m^2$, density of air $\rho_a = 1.188\ \frac{kg}{m^3}$, heat capacity of air $c_{p,a} = 1.007\ \frac{kJ}{kg \cdot K}$, air velocity $v_a = 0.8\ \frac{m}{s}$, inlet air temperature T_{ao} , outlet air temperature T_{ao} , time at the beginning of the nighttime cycle $t_i = 0\ h$ and time at the end of the nighttime cycle (when the PCM is solidified) t_e :

$$Q_{dis} = A_{air\ gap} \cdot \rho_a \cdot c_{p,a} \cdot \int_{t_i}^{t_e} v_a \cdot (T_{ao} - T_{ai}) \cdot dt \quad (7.1)$$

7.1.9. Energy Performance and operation costs

As previously stated, the advantage of the proposed APS in this study is that it may be utilized in the renovation of only a single building space unit (e.g. office). However, usually a convenient, fast and relatively inexpensive approach to tackle the issues of cooling of a single space unit would be to install the air conditioning device. Therefore, a question arises whether or not the application of the proposed APS could be a viable solution in comparison to classical air conditioners. Two aspects need to be addressed, energy use as well as the operation cost of a particular cooling system.

According to Equation 7.2, the proposed APS is able to store 6.34 kWh of cooling energy, which may be utilized for cooling purposes during daytime. To store the said amount of cooling energy the ventilation has to consume 2.52 kWh of electrical energy during nighttime (two air fans EXTHCAS 200-4, each providing 101 m³/h at 0.18 kW input power [165]).

According to Commission Regulation (EU) No 626/2011 supplementing Directive 2010/30/EU of the European Parliament [166] the air conditioners with cooling capacities below 12 kW are classified in several energy efficiency classes. The Directive defines the energy classes going from A+++ (most efficient) to G (least efficient). As shown in [166]

the A+++ class should have a seasonal COP 5.1 or higher, while the G class should have the seasonal COP 1.9 or lower. In such manner and according to the following equation, we can determine how much electrical energy win would an air conditioner of a particular class need to consume to run the compressor and to produce equivalent cooling energy of 6.34 kWh:

$$W_{\text{in}} = \frac{Q}{\text{COP}} \quad (7.2)$$

7.2. Numerical results

7.2.1. Thermal response in adiabatic conditions

The purpose of calculating the solidification cycle in adiabatic conditions is to see the behaviour of the material without other boundary conditions and to further on based on the outlet air temperatures T_{ao} evaluate the energy released from the PCM during the solidification period. Figure 7.12 shows outlet air temperatures obtained in adiabatic conditions for different inlet air temperature scenarios.

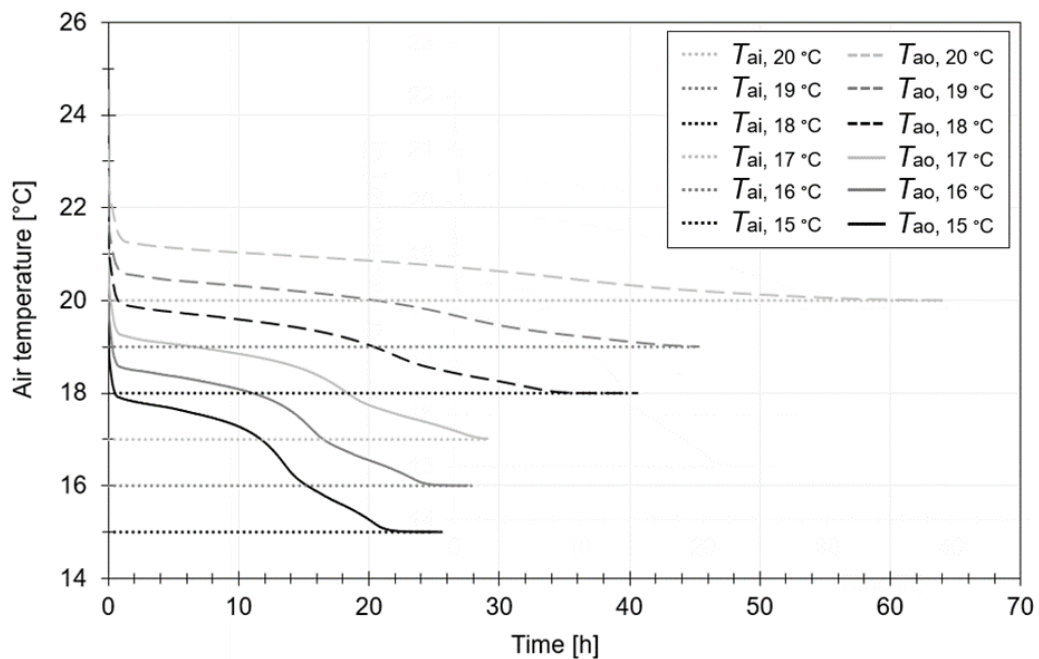


Figure 7.12: Outlet air temperatures obtained in adiabatic conditions for different inlet air temperature scenarios.

The results show, that the complete solidification with higher inlet temperatures takes up to 60 h (20 °C) and at lower (15 °C) at least 21 h.

7.2.2. Thermal response in each inlet temperature scenario

The time required for the surface temperature measured at the front of the PCM plate ($T_{\text{PCM_back, avg}}$) material temperatures to drop to 21 °C is considered the solidification time for each inlet temperature scenario. The results show the temperatures obtained during the cooling cycles for each inlet temperature scenario. The figures show that the solidification is completed in a nighttime cycle only when the inlet air is supplied at 15 °C and 16 °C and almost at 17 °C. In Figure 7.13-Figure 7.15 , the horizontal and vertical red dotted lines represent the temperature limit of 21 °C and the end of the nighttime cycle at 12 h, respectively.

Figure 7.13 shows the results obtained when the inlet air temperature (T_{ai}) was 15 °C. The average surface PCM temperatures (Back) dropped to 20 °C in the first 12 h and to 18 °C in 30 h. This shows that on average the PCM material completely solidified during the night.

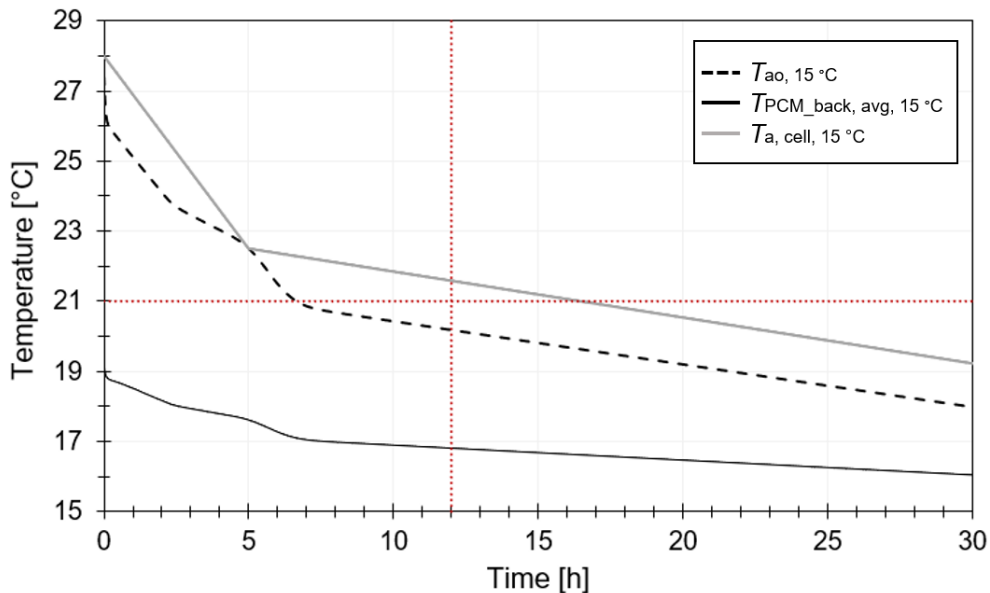


Figure 7.13: The results obtained at inlet air temperature of 15 °C.

Figure 7.14 shows the results obtained at the inlet temperature of 16 °C. The average surface PCM temperatures (Back) decreased to 20.5 °C in the first 12 h and to 18 °C during the entire simulation period (30 h).

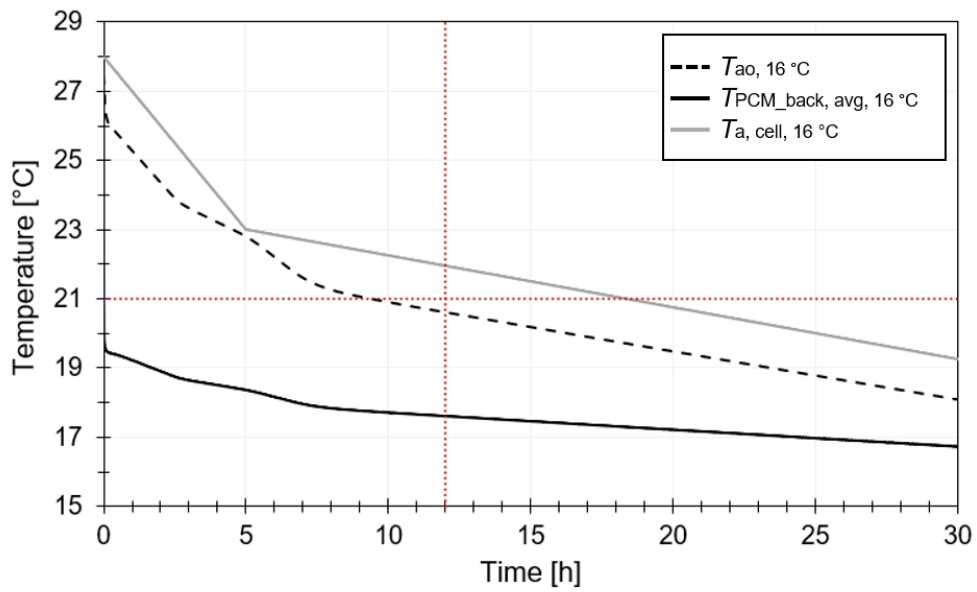


Figure 7.14: The results obtained at inlet air temperature of 16 °C.

Figure 7.15 shows that at the inlet temperature of 17 °C, the average surface PCM temperatures (Back) dropped to 21 °C in the first 12 h and to 18 °C during the entire simulation period (30 h).

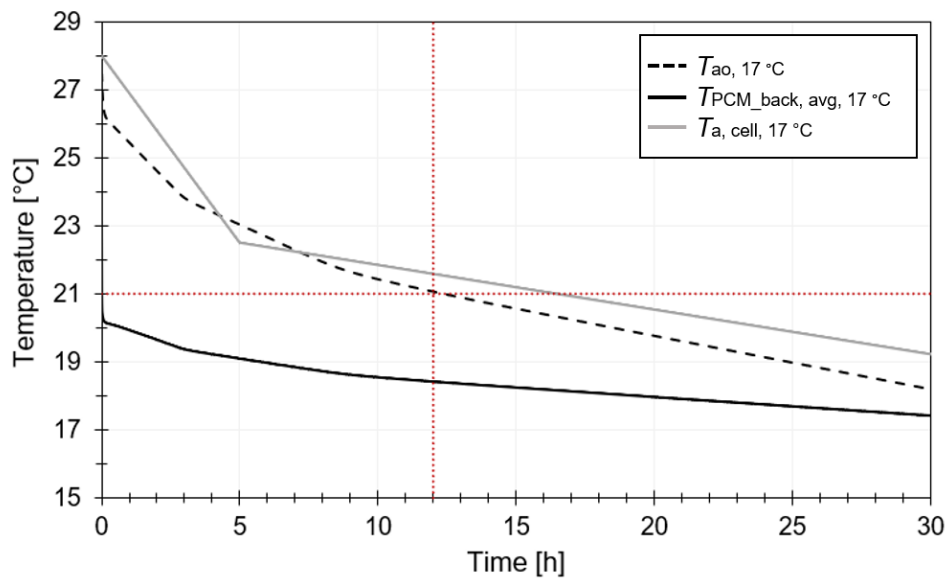


Figure 7.15: The results obtained at air inlet temperature of 17 °C.

7.2.3. Energy released from PCM in adiabatic conditions

The following chapter presents the energy released from the PCM plates (Q_s) calculated based on the outlet air temperatures obtained in adiabatic conditions for different inlet air temperature scenarios (following Equation 1) and compared to the theoretically determined total heat storage capacity of the plates in the temperature range defined in Figure 7.5. It was determined that 68 plates can store 6.53 kWh of energy. The error was calculated based on the subtraction of the of the calculated Q_s from the theoretical Q_s values, where the theoretically determined Q_s of 6.53 kWh presented 100 % of the energy and the calculated Q_s the corresponding percentage. The results are presented in Table 7.2. As visible from the table, the error increases with the inlet air temperature, as higher inlet temperatures cannot release the energy stored at lower temperatures of the PCM material.

Table 7.2: Calculated energy released from the plates Q_{dis} and the error from the theoretical value of Q .

Inlet temperature	15 °C	16 °C	17 °C	18 °C	19 °C	20 °C
Energy released Q_{dis} [kWh]	6.34	6.28	6.22	6.16	6.04	5.93
Error from theoretical value* [%]	3.0	3.8	4.8	5.7	7.5	9.2

*6.53 kWh (in the temperature range: 14-30 °C)

7.2.4. Energy use and operation costs of APS operation

As shown in Figure 7.16 the proposed APS underperforms in comparison to class A+++ and G air conditioner from energy use point of view. To produce 6.34 kWh of cooling energy the APS consumes 4.6 kWh, class G air conditioner 3.3 kWh and class A+++ air conditioner 1.2 kWh.

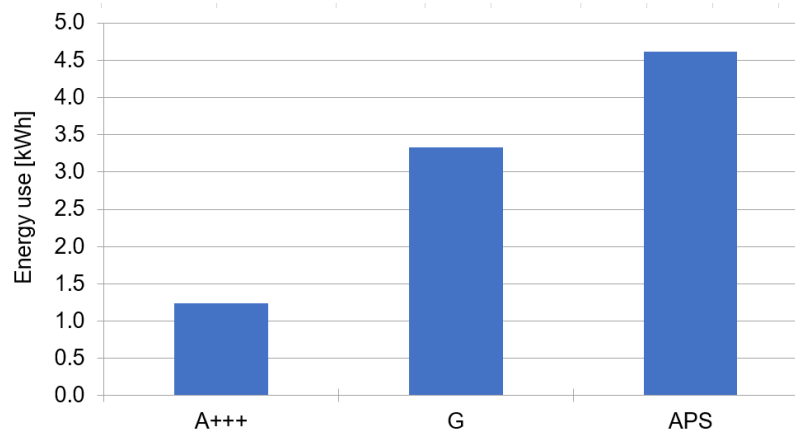


Figure 7.16: Electrical energy use to produce 6.34 kWh of cooling energy of the best case (A+++ class) and the worst case (G class) air conditioner in comparison to the proposed APS.

Furthermore, Figure 7.17 shows the cost of consumed electrical energy to produce 6.34 kWh of cooling energy for class A+++ and class G air conditioner, as well as for APS proposed in this study. The prices of electrical energy were taken after [167] and are 0.13999 €/kWh (day rate) and 0.09999 €/kWh (night rate). Both, class A+++ and G air conditioners operate in day rate, therefore, the operation cost would be approximately 0.174 €/day (class A+++), and 0.467 €/day (class G), respectively. On the other hand, APS operates in night rate, therefore, the operation cost would be 0.462 €/day.

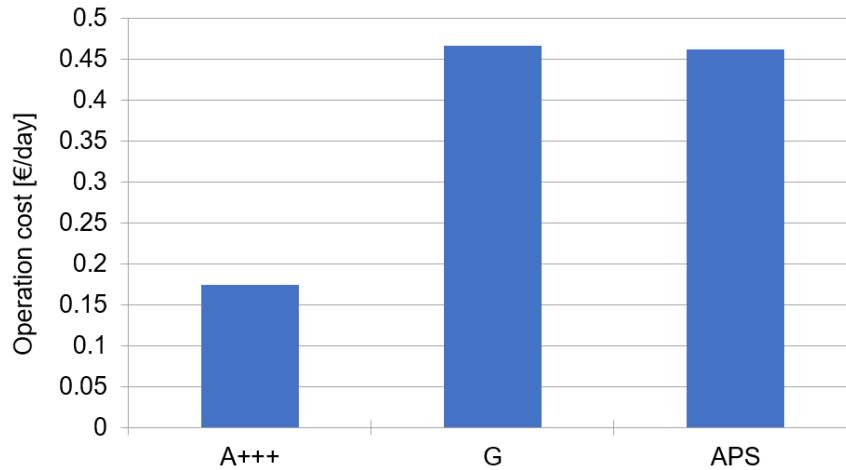


Figure 7.17: The cost of consumed electrical energy per day of operation to produce 6.34 kWh of cooling energy of the best case (A+++ class) and the worst case (G class) air conditioner in comparison to the proposed APS.

7.3. Discussion

7.3.1. Discussion on the simulated results

Complete solidification of PCM during the nighttime cycle is crucial for efficient performance and sufficient cooling effect of PCM during the day when its application is required to cool the indoor spaces. Figure 7.18 shows the outlet temperatures obtained during each of the inlet temperature scenarios. Due to the influence of the high airflow rates, inlet air velocities, and the boundary condition of cell air temperatures, the outlet air temperatures do not show a clear phase change curve. Therefore, they cannot serve as an indicator of solidification time. However, it is clear that inlet temperatures affect outlet temperatures. In Figure 7.18 and Figure 7.19, the horizontal and vertical red dotted lines represent the temperature limit of 21 °C and the end of the nighttime cycle at 12 h, respectively.

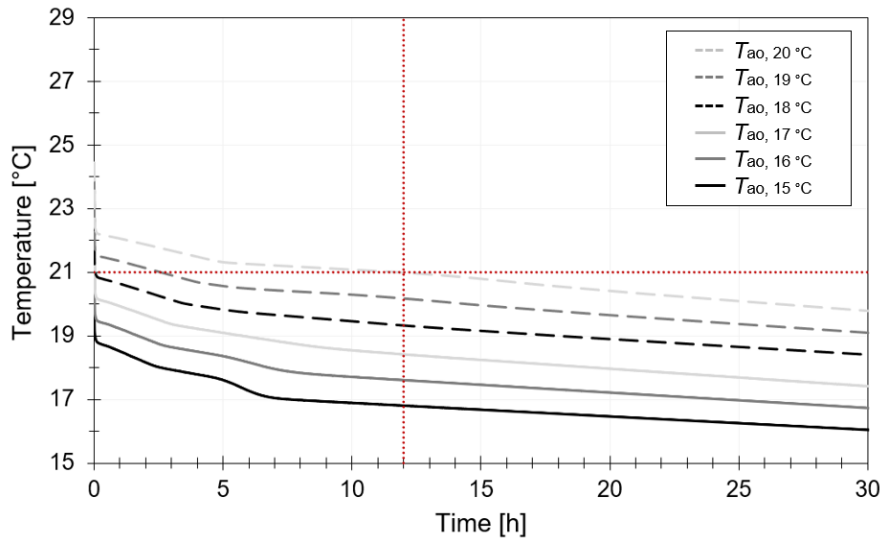


Figure 7.18: The area-weighted average outlet air temperatures simulated within corresponding inlet temperature scenario.

Compared to the outlet air temperatures (T_{ao}), the average surface temperature on the back of the PCM plates ($T_{PCM_back, avg}$) clearly shows the completed solidification time (Figure 7.19). The figure shows that solidification is completed in 7 h when the inlet air has a temperature of 15 °C. The optimum time for solidification is reached after 9 h when the inlet air has a temperature of 16 °C. The results show that, the PCM can be solidified during the night cycle after 12 h even when the air is injected into the air gap at 17 °C. The insufficient solidification time was achieved under conditions where the temperature difference between PCM and the inlet temperature is too small. For example, at inlet temperatures of 18 °C, 19 °C and 20 °C, 17 h, 19 h and 21 h, respectively, were required to complete PCM solidification.

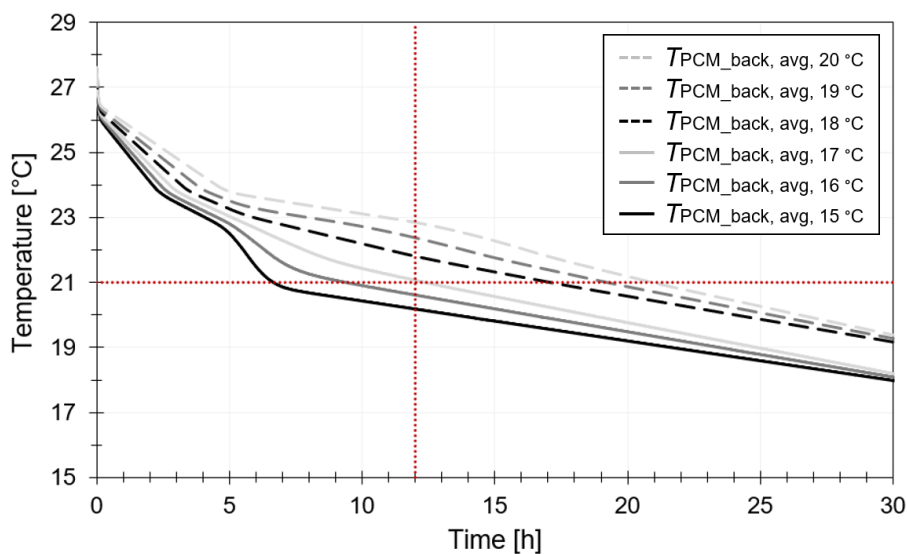


Figure 7.19: The area-weighted average back surface PCM temperatures simulated within corresponding scenario.

However, the solidification time could be drastically improved if the PCM was cooled from two sides - room side and the air gap side. This could be accomplished by opening the windows during the night or ventilating the room with the cool, unconditioned outdoor air. While opening the windows requires additional manual maintenance, mechanical operation of room ventilation systems requires additional energy input. The combination of these possible air-based PCM cooling methods (mechanically ventilated air gap, opening the windows, and mechanical ventilation) could present the optimal solution for the reference case of microclimate in a building in terms of energy use.

7.3.2. Result comparison to other studies

The results obtained in this study can be compared with some other relevant studies.

7.3.2.1. Thermal performance

For example, Diarce et al. studied a 2D model in ANSYS Fluent of macroencapsulated PCM (RT35; $T_m = 35\text{ °C}$) positioned in hollow aluminium profiles of the external layer (thickness 2 cm) for a seasonal application [136]. Heat transfer from the air gap to the PCM in the wall was enhanced by the short horizontal aluminium fins inclined toward the air gap. On the inner side of the 6 cm wide air gap, which was ventilated with an additional fan, there was an XPS insulation layer. To simulate the heat transfer in the air gap, a DO (Discrete Ordinates) radiation model was applied in the air gap between the PCM aluminium wall and the XPS layer, which improved the accuracy of the temperatures on the XPS wall according to the experimentally measured temperatures (without using the radiation model, the temperature difference of the XPS surface reached 2.6 °C). The airflow rate studied ranged from 97.2 m³/h to 277.2 m³/h with inlet temperatures between 0 °C and 10 °C and velocities up to 0.93 m/s.

Furthermore, Hu and Heiselberg used COMSOL Multiphysics to calculate a 2D model of a 10 cm wide heat exchanger with PCM plates ($T_m = 22\text{ °C}$) for summer cooling in Copenhagen, Denmark, placed in the glazed exterior wall with 60 PCM plates (5-20 mm thick, 10 mm thick is optimal in terms of cooling effect) separated by air gaps (5 mm wide) [145]. The tested velocities in the air gaps were between 0.74-1.78 m/s and 00:00-4:00 (4 h) at an air inlet temperature of 14 °C. The nighttime was shorter compared to the other studies because the system was tested in colder climates and therefore, the plates could consolidate sufficiently within the night cycle.

In addition, Kant et al. studied a PCM layer (4 cm; $T_m = 26.6\text{ °C}$; 28.2 °C and 32 °C) applied on the BiPV wall and separated from the concrete wall by an air gap (8 cm) and calculated it using the COMSOL Multiphysics 5.0 software tool [148]. The nightly cycle lasted 10 hours at an inlet temperature of 25 °C, as the PV system is preheated to temperatures of 60 °C or higher. Similar to Diarce et al. the model was simulated using the radiation model [136]. The PCM was also modelled using the solidification and melting model.

Similarly, Li et al. created a 2D model of a double-skin glazing façade (air gap width of 45 cm) with laminated composite blinds PCM (PX35; $T_m = 35\text{ °C}$; 15 cm wide and 0.3 cm

thick) using the ANSYS Fluent software tool [144]. The model was calculated using the $k-\varepsilon$ viscosity model and the DO radiation model. The inlet air temperatures varied between 25 °C and 27 °C at supply air velocities of 0.45 m/s. The ambient temperature varied between 26 and 40 °C. The surface temperature of the inner façade was reduced to about 2.9 °C (compared to the surface temperature of the external façade). The peak surface temperatures of the PCM layer reached at noon (12:00) were between 38 °C and 40 °C, and the temperature difference between inlet and outlet air varied between 3 °C and 3.5 °C. On average, the temperature difference in the cases investigated in this study reached 2 °C in all inlet temperature scenarios.

The previous cases of air gap walls in contact with PCM layers were tested as 2D models. In contrast, Faheem et al. tested the PCM for cooling (microencapsulated PCM, $T_m = 19^\circ\text{C}$ and 20 °C) in low thermal mass buildings with a 3D model in ANSYS Fluent 14 [119]. The inlet air temperature of 12 °C was lower compared to previous studies, and the PCM T_m are also lower. Nighttime ventilation was in operation between 18:00 and 6:00 (12 h). The effects of velocities were significant at PCM ($T_m = 20^\circ\text{C}$) and were less than 2 m/s, and at PCM ($T_m = 19^\circ\text{C}$) they reached 5 m/s. During the nighttime cycle at 0:00, average surface temperatures at the bottom of the slab dropped by 1.5 °C, while room air temperatures dropped by 4 °C. The model of the present study predicts that indoor cell temperatures drop by about 4 °C during the first 5 hours and by 2-2 °C between 5 and 20 hours.

Similarly, Yu et al. used ANSYS Fluent to calculate a 3D model of the shape-stabilised outer layer PCM of the ventilated roof (different summers $T_m = 34\text{-}38^\circ\text{C}$ and thicknesses between 2.5-3.5 cm) [120]. The best results were obtained with inlet air velocities between 1.9-2.5 m/s and inlet temperatures of 24-25°C. In two cases studied during the hot summer, the ventilation was conducted from 18:00 h for 13-15 h and from 19:00 h for 11-12 h to fully consolidate the PCM layer.

A concept very similar to the one proposed in this study was presented by Evola et al. using Energy Plus software to study a ventilated internal PCM (Micronal T23[®] - 60 % microencapsulated; peak $T_m = 26.7^\circ\text{C}$ and 2 cm thick) with a 3 cm air gap [126]. The air gap was ventilated with an airflow of 168 m³/h and a velocity of 0.65 m/s between 21:00-6:00 h (9 h) at an air inlet temperature of 20 °C, a wall surface temperature of 27 °C, and an air outlet temperature of 24.5 °C. The temperature difference between inlet and outlet air temperatures was smaller in the present study (2 °C) than in the presented study (up to 4.5 °C).

In addition, Weinländer et al. experimentally tested a ventilated chilled ceiling with PCM in a suspended ceiling (PCM DELTA[®]- COOL 24, $T_m = 24^\circ\text{C}$) [117]. With an airflow of 300 m³/h (the highest tested reached 600 m³/h) supplied between 21:00-5:00 (8 h) at an air inlet temperature of 16 °C, the surface temperatures measured on the back side of the PCM panels dropped below 24 °C after 8 h of the experiment. The solidification time is comparable to the results of this study, where the plates solidified in 7 h at an air inlet temperature of 15 °C.

The values tested in the present study are within the range of the other studies discussed. In fact, the studies have shown that the temperature differences tested between the inlet air temperatures and the melting temperatures of PCM range from 7 °C to 14 °C (7-9 °C in the

present study), so that the plates could solidify overnight. The airflow rates studied mostly varied between 97.2 m³/h and 600 m³/h (present study: 483 m³/h) with air gap velocities between 0.45 m/s and 5 m/s (present study: 0.8 m/s). The duration of the night cycle varied between 4 h and 15 h, but averaged between 8 h and 12 h (present study: 12 h; 7 - 12 h for complete solidifications). The temperature differences between the inlet and outlet air temperatures are smaller in the present study compared to the other studies, but still reasonable. Thus, the solidification time depends on the temperature difference between the inlet air temperatures and the PCM melting temperatures, the amount and heat storage capacity of the PCM, the type of encapsulation, and the characteristics of the airflow in the air gap (airflow rate and velocity).

7.3.2.2. Energy performance

Due to different methods of energy performance determination among the reviewed studies, the comparison of the results of the present study to them is limited. Moreover, many studies do not present the results of systems' energy performance, but only the temperature distribution [119], [120], [136], [144]. The energy performance of the systems was determined only, when PCM plates were not in the direct contact with the indoor space (room) because the heat flux could be monitored.

For example, Evola et al. used Energy Plus for the determination of daily energy use for cooling and concluded that the presence of ventilated air gap decreased the energy from 185.0 Wh/(m² day) to 107.3 Wh/(m² day) [126]. In present study the cooling effect of the plates to the room could not be assessed directly and therefore, neither the presence of the ventilated air gap. However, considering the floor area of the room to be 7.32 m² and the total theoretical cooling capacity of the plates 6.53 kWh, the cooling effect of the plates may contribute to 892.1 Wh/(m² day). The cooling capacity of the APS system in the present study is much larger than in the referenced one, since the value is theoretical and not based on the calculated room temperatures and the amount of PCM mass in this study is much larger (reference study: microencapsulated plates).

Furthermore, Hu and Heiselberg closed PCM into a ventilated wall (heat exchanger) and ventilated it over the day and over the night. Over the night, the 10 mm thick PCM discharged 3.55 MJ (0.981 kWh) and over the day charged 3.19 MJ (0.886 kWh) of heat [145]. The setup of the reference study has a different purpose compared to the present (the room is cooled by the outlet air and not by the PCM plates in contact of the room air directly) which results in the lower amount of energy needed for cooling. Also, the system is dimensioned for a cooler climate type with lower cooling demand. Nevertheless, as the study investigated a closed system of heat exchanger, the room wall boundary conditions didn't play a crucial role in the determination of PCM solidification which could be determined only based on the outlet temperatures. Similar conclusion based on the experimental setup is aligned with the experimental investigation by Osterman et al. where an active ventilated PCM heat storage for ventilation system was investigated with 30 PCM plates (1.361 kg of RT22HC with heat storage capacity of 181 kJ/kg per plate;) mounted into a rectangular EPS box. When the plates were preheated to 25 °C and ventilated with T_{ai} of 16 °C they released 5.1 MJ (1.42 kWh) of energy [168].

Weinläder et al. presented a case of ventilated PCM ceiling [117] and determined the total cooling power of the system by summing the cooling power of the air in the ventilated ceiling (based on the temperature difference between the inlet and outlet temperature measured in the air gap) and cooling power of the PCM through the plaster board ceiling (based on the temperature difference of temperatures measured on the front and on the back of the gypsum plate). They found that in the conference room, the total cooling power yields 7.50 kWh (theoretical 7.92 kWh) which is close to the total latent storage capacity of the PCM plates. Compared to APS system (the present study), the total latent storage capacity of the PCM plates is 6.53 kWh and similar to the compared case. However, in this case the total cooling power of the system cannot be calculated because the PCM plates are in direct contact with the air and the temperature difference on the front and on the back of the gypsum plate cannot be determined. In the comparing study, during the nighttime solidification cycle (duration: 8 h) the ventilation flow rates of 300 m³/s and 600 m³/s were established at fans operating power of 60 W and 150 W, respectively and consumed 1.68 kWh of electrical energy which is higher than the electrical energy consumed in the present study (0.57 kWh).

Navarro et al. experimentally investigated ventilated concrete slab filled with PCM modules (tubes) [113]. The system's operation (fan and heat pump together) consumed between 4 kWh/day and 1.2 kWh/day. Compared to this study, the fan operation present between 0.57 kWh/day (solidification time of 7 h and T_{ai} of 15 °C) and 0.98 kWh/day (solidification time of 12 h and T_{ai} of 17 °C) depending on the solidification time and inlet temperature.

Prabhakar et al., simulated and optimized the model of single-family house with PCM plates (optimised $T_m = 22-26$ °C depending on the location) in CSM cases integrated in the internal building elements (interior walls, internal partition walls and ceiling) without the presence of air gap with EnergyPlus and GenOpt v3.1.1 [56]. By using PCM, the maximum energy savings were determined in Ceduna, South Australia of 26.31 %. In the temperate climate conditions, by coupling a PCM passive system with night ventilation, the effectiveness of PCM was increased from 3.32 % to 25.62 % and was even more improved (to 40 %) when coupled with temperature-controlled ventilation. Within this study, the energy savings cannot be determined and compared, since our outdoor boundary conditions are limited to only one day scenario and nighttime solidification cycle. However, the results of this study stress the importance of the correctly applied ventilation on the effectiveness of PCM performance.

Similarly to the present study where the PCM plates were installed on the internal wall in contact with the room air, Gracia et al. experimentally tested a ventilated external walls with PCM plates located in its air gap [130]. In the experimental conditions in July and August the heat stored and released by the PCM was investigated. During the night, the PCM system stored 20.25 MJ (5.62 kWh) and 25.90 MJ (7.19 kWh) in July and August season, respectively. During the day, the PCM system released 2.20 MJ (0.61 kWh) and 0.10 MJ (0.03 kWh) in July and August season, respectively. Comparing the results from the present study to the reference, the released energy is comparable to the theoretical energy storage capacity of the plates.

Comparing energy performance of the APS system to air-conditioning (AC) devices with energy classes A+++ and G shows that the APS system consumes more energy compared to both AC devices. When comparing the three systems based on the operational costs the

performance of APS improves. AC devices cool during the daily cycles with higher electricity prices, while the APS system uses electricity over the night when the electricity tariffs are lower. It is shown that the operation costs of A+++ class AC device are lower compared to the APS system and that G class AC device has the highest costs. Therefore, based on the operation costs it is cheaper to renovate the building with APS system than inefficient AC device. However, the construction costs of the APS might be higher than of the AC device since the APS system is still a technology under the development.

However, it should be noted that simulating a parametric case of the proposed system in ANSYS Fluent is a challenging task due to an unknown boundary condition that significantly affects the results. Such an objective would be more likely to be achieved by using Energy Plus or TRNSYS software. However, these do not provide results with detailed temperature distribution along the studied model.

8. Conclusions

Within this PhD. project an active-passive system (APS) for overheating reduction in buildings was investigated. After reviewing the APS-relevant literature a series of preliminary investigations were performed, where not only the heat transfer between PCM and air was investigated but also the effect of PCM on indoor thermal environment. The potential of the APS was experimentally tested at National School of State Public Works (ENTPE) in Lyon, France. Afterwards, the system's properties were optimised with micro-scale numerical model in CFD. Finally, the energy saving potential of the system was assessed.

8.1. Hypotheses

The main objectives (O) of the research are:

- O1: to investigate the cooling effect of the APS (experiment)
- O2: to determine the effect of different air gap inlet air temperatures on the nighttime solidification of the PCM (experiment and numerical model)
- O3: to determine the highest air gap inlet air temperature for a complete PCM solidification in the selected nighttime period (12 h) (experiment and numerical model)
- O4: to evaluate the energy performance of the APS during the cooling season (experiment, numerical model and calculation model)

The hypotheses (H) of the research are:

H1: The PCM panels will fully solidify in the night cycle of discharge and completely melt in the daily charge cycle was obtained with O1 and O3. The complete melting and solidification of the PCM were determined based on the experimental and numerical results (cell air temperatures and temperature distribution along the PCM of the APS).

- The experimental results showed that in the daytime cycle the PCM in APS completely melted in 40 h, 25 h and 20 h in cases with set point air temperature in cell B (T_{set_B}) of 26 °C, 30 °C and 35 °C, respectively. Therefore, the PCM material didn't completely melt in the daytime cycle (12 h).

- The experimental (ex) and numerical (nu) results showed that the PCM in APS at air flowrate of 483 m³/h needed 5 h/7 h (ex/nu), 14 h/9 h (ex/nu) and 16 h/12 h (ex/nu) to completely solidify when ventilated with inlet air temperatures (T_{ai}) of 15 °C, 16 °C and 17 °C, respectively. Therefore, the PCM material can be completely solidified during the nighttime cycle (12 h). There are some differences between the experimental and numerical results. The inlet air temperature set point in the experiment couldn't be met instantly due to the temperature fluctuations of the laboratory air. Therefore, the set point in some cases ($T_{ai} = 15$ °C and 16 °C) wasn't met for hours and was higher than required. Such experimental conditions influence the results, and it can be assumed that with perfect T_{ai} conditions (numerical model) the PCM would solidify faster.

H2: The results of a parametric operation test show that optimal thermal comfort (local operative temperature) is provided with 2 cm thick panels, with a melting point of 24°C panels and a melting point of 25°C ceiling panels at a distance of 5 cm from the wall. The optimum direction of air ventilation is the wall-ceiling direction with a volumetric flow of 150 m³/h. The shape of the diffuser is mixing. The hypothesis was obtained with O1, O2 and O3.

- The configuration of the APS was designed based on the characteristics found during the literature review and preliminary investigation. It was further optimized and evaluated based on the experimental and numerical results. Based on the literature review and preliminary investigation, PCM with melting point of 24 °C and plate thickness of 1.5 mm was selected and investigated.
- Considering the possibilities of the experimental test cells, the air gap was 7 cm (PCM wall) and 10 cm (PCM ceiling) wide. Due to the high complexity of the system (ensuring airtightness, positioning the fans etc.) other ventilation possibilities than airflow direction wall-ceiling weren't tested.
- The final flow rate was finally higher much higher (483 m³/h) than assumed in H2 (150 m³/h). High amounts of airflow were needed to solidify the PCM in the nighttime cycle (12 h), whereas the air flowrate of 150 m³/h would be too low.
- The shape of the inlet diffuser was linear inlet diffuser to enable as equal distribution of the airflow along the entire PCM wall and ceiling as possible. In the initial plans, also the outlet diffuser was supposed to be linear, however this was not possible due to the test cell geometry and the outlet was in the shape of the circular duct. A mixing diffuser used as the inlet diffuser would perform poorly, because it wouldn't be able to distribute the air along the entire length of the PCM wall.

H3: The best local thermal comfort (the chosen criterion of thermal comfort) will be compared to the passive system, the ventilated wall without ceiling, the ventilated ceiling without a wall, the APS system. Obtained with O1.

The APS geometry configuration variations should be assessed based on the experimental results with measurements of the temperature fluctuations in the cells.

- The thermal comfort during the daytime cycles was assessed with global thermal comfort evaluation (PMV and PPD) and not local one. To ensure melting of the PCM in the test cell in the daytime cycles, the room fan was switched ON at all times. By mixing the room air temperatures were equalized along the entire test cell. Therefore, with the use of local thermal comfort assessment methods, there wouldn't be any new or different information gathered than with the global one. Also, the heat gains in the room were simulated with the electric heater (with approximate surface area of 1 m²) and its surface temperatures could reach up to 60 °C. This is not a realistic case in summer, as

the window glass temperatures are much lower. The temperatures from the electric heater would negatively affect the mean radiant temperature and consequently the required operative temperatures.

- Four APS geometry configuration variations should be experimentally investigated. Unfortunately, the two variations of the PCM wall without the ceiling and the PCM ceiling without the wall were not investigated, because it was not possible to modify the test cell in this way. The PCM plates were positioned in the wooden frame and carefully sealed with the aluminium tape to avoid air leakage from the air gap and to ensure sufficient solidification. To perform experiments without either PCM wall or PCM ceiling, the PCM plates should be unsealed and after the completed daytime cycle installed back. As it takes several hours to return the experiment in the previous state, the following nighttime solidification cycle couldn't be studied. Also, the plates were equipped with very sensitive surface temperatures sensors and their removal could harm them. Also, the problem couldn't be solved with the numerical model on the room-scale due to the high number of unknown conditions in the test cell (validation difficulties). However, it can be concluded, that by removing approximately one half of the PCM mass from the room (either PCM wall or PCM ceiling) would drastically deteriorate the cooling potential of the APS. The cooling effect of each variation (no PCM wall/no PCM ceiling) would be best visible without the use of room fan.

H4: Considering the local thermal comfort, the best thermal comfort (the lowest daily temperature in the room) will be symmetrically close to the PCM wall and will decrease depending on the radiation level of the radiation surface opposite the PCM wall. Obtained with O1. The local thermal comfort related to the location in cell with the APS should be assessed experimentally where measurements of the temperature fluctuations in the test cell. As discussed in H3, the local thermal comfort couldn't be assessed due to the presence of room fans and high temperatures of the electric heater's surface.

H5: The energy use for cooling of the APS with the selected heating, cooling and ventilation system will be lower than the energy use for cooling of passive system alone, where the panels are not ventilated at night. Obtained with O2 and O3. The cooling potential of the APS where PCM is nocturnally ventilated and compared to the regular passive system without nocturnally ventilated PCM should be assessed based on the amounts of solidified PCM in both cases after the nighttime solidification cycle. For such analysis, the unsteady state numerical model of the systems prepared for example in TRNSYS or EnergyPlus is required [40], [169]. Such numerical model of the systems wasn't performed due to the lack of time. However, the PCM may cool only with the amount of solidified material and therefore, the daily cooling effect depends on the % of solidified material in PCM.

H6: The energy use for cooling will be lower in the chosen heating, cooling and ventilation system in the APS (walls and ceiling), as in the case with ventilated single element - ventilated ceiling without ceiling or ventilated ceiling without wall. Obtained with O1 and O4. The cooling potential of the APS differs when the amount and location of the PCM material is changed.

- As previously stated in H3 the two geometrical variations of the PCM wall without the ceiling and the PCM ceiling without the wall were not possible to investigate. Also, the problem couldn't be solved with the numerical model on the room-scale due to the high number of unknown conditions in the test cell (validation difficulties).

- As stated in H5, the energy use for cooling under different variations need to be analysed by the unsteady state numerical model of the systems prepared for example in TRNSYS or EnergyPlus.
- However, instead of the energy use for cooling analysis based on the presence of ventilation or the amount and location of the PCM in APS, the energy performance and operation costs of the APS in one day are determined and compared to the results of two air-conditioning devices of the best and the worst energy efficiency classes (A+++ and G). The results showed that the proposed APS underperforms in comparison to class A+++ and G air conditioner from energy use point of view. To produce 6.34 kWh of cooling energy, the APS consumes 4.6 kWh, class G air conditioner 3.3 kWh and class A+++ air conditioner 1.2 kWh. Considering the daytime and nighttime cost of consumed electrical energy, one day operation costs 0.174 €/day for class A+++ air conditioner and 0.467 €/day and 0.462 €/day for class G air conditioner and APS system. Eventhought, at this stage the APS consumes the highest amount of energy, the operation costs show positive results. With future system improvements, the energy efficiency and overall technical potential of the APS could be increased.

8.2. Scientific contribution

The advantages of APS are lower renovation costs and increased energy efficiency of the system because the system is placed only offices with critical need for indoor thermal comfort improvement (overheating reduction) and the system's characteristics (e.g. melting point and thickness of the PCM plates) may be accurately optimised based on the individual office conditions and requirements. This PhD project obtained the following contributions to science:

- Holistic step-by-step design approach of the APS system that can be applied to other smart technologies towards increasing the energy efficiency and comfort.
- Investigating the APS with three different methods (full-scale numerical model, microscale numerical model and experiment).
- The investigated system combines a ventilated internal PCM wall and ceiling (APS).
- APS is investigated experimentally in controlled experimental conditions where APS is measured simultaneously with the reference cell without APS. Such experimental facilities enable APS investigation under constant thermal conditions, optional transient thermal conditions (selected day of the test reference year or summer heatwave scenarios) and adding ventilation for improving the indoor air quality in the test cells for building users. In this way, the effect of the individual influential parameter under investigation can be distinguished.
- The micro-scale numerical simulation is calculated and validated with geometry of the room-scale PCM ceiling and wall.
- Micro-scale numerical simulation in ANSYS Fluent considers the boundary condition of the temperature change in the test cell during the ventilation of the PCM curing air during the night (the effect of system's surrounding thermal environment). Considering such boundary conditions, a parametric analysis is performed based on changing the temperature of the inlet air in the air gap. The solidification time and the maximum inlet air temperature are determined for sufficient operation of the APS system – optimization of the system.

- Energy performance and operation cost calculated based on the results from micro-scale numerical model in ANSYS Fluent.

8.3. General conclusions

Within this research the following conclusions were obtained:

- Based on the literature review, it is safe to say that a great deal of research has been performed and yet the thermal characteristics of PCM (T_m) in a passive system are still difficult to determine.
- The system is appropriate for the renovation of lightweight office buildings because only a single unit (office) may be renovated and not necessarily the entire building. PCM were normally positioned in the external but more often in the internal layers of the building envelope.
- Following the results obtained with full-scale numerical model it can be concluded that melting temperature is the most important thermal characteristic of PCM for optimal performance and maximal cooling effect.
- With focus on the preliminary research, it was concluded that for a deeper understanding of the APS thermal behaviour, not only one method of work is sufficient. For example, full-scale models often aren't accurate enough to assess all relevant effects and micro-scale models do not enable holistic simulation with all influential parameters. Also, the experimental methods have their limitations. For example, limited equipment (fewer measuring points – less information), difficulties to perform many cases in parametric analysis and laboratory environment often doesn't provide the real-life conditions, so also the experiments do not often a holistic approach.
- The PCM material SP24E was selected based on its thermal characteristics. The melting temperature of PCM should be high enough to establish a sufficient temperature difference between the inlet air temperature and the PCM material melting point. Meanwhile, the melting temperature of PCM should be selected so, that the indoor operative temperatures don't exceed the recommended values for indoor thermal comfort.
- The experimental results show that the APS system cools the cell during the daytime cycles by lowering the cell air temperatures. At the lower cell air temperatures tested (26 °C), the APS system does not require an additional cooling source. However, in the other cases, it was able to independently cool the air temperatures down to the recommended levels for indoor thermal comfort in summer. The cooling effect of the system was most pronounced at the higher air temperatures of the cells tested (30 °C and 35 °C), where it decreased the indoor temperatures for up to 4.5 °C.
- The APS system was able to adequately reduce air temperatures on the hottest day of the test reference year in Rome (Italy), but not in Ljubljana neither during the test reference year nor the heat wave. This indicates that the system is adequate for Mediterranean summer conditions and not for continental (bordering on a subtropical humid climate) conditions or its summer heatwaves.
- The addition of active systems increases the power requirements for cooling, making the feasibility of using the APS system with nighttime power use at this stage questionable.

- With the micro-scale numerical model, the nighttime solidification was achieved by ventilating the air gap with a flow rate of 483 m³/h, and with the current configuration, the highest inlet temperature to the system (for full solidification during the night cycle - 12 h) must not exceed 17 °C.
- The study showed that solidification was completed within the nighttime cycle at inlet temperatures of 15 °C, 16 °C and 17 °C, making the inlet temperatures optimal among the cases studied. Other inlet temperatures of 18 °C, 19 °C and 20 °C were not low enough to fully prepare PCM for a new daily cycle.
- The solidification time of the PCM can be improved by increasing the airflow rates in the air gap or by combining the nighttime ventilation in the air gap simultaneously with the ventilation from the room side (natural - window opening or mechanical ventilation), so that the PCM plates are cooled from both sides.
- The results on energy performance and operating costs of the APS system under the static conditions investigated in the framework of this study show, that APS system has higher energy use and operational costs than A+++ class air-conditioning device and slightly lower operational costs than G label air-conditioning device.
- The economic feasibility of PCM application depends on the energy savings calculation, costs related to the PCM material, energy prices and discount rates. Even though the PCM prices significantly dropped in last 5 years, the studies evaluating the economic feasibility of PCM systems integrated in building still report their application to economically insufficient.

8.4. Advantages, disadvantages and limitations

8.4.1. Active passive system

The main advantage of APS is that in the daily cycle it provides cooling without additional energy required, which can reduce the energy demand peaks in large urban communities. In the nighttime cycle, the system can be solidified with the outdoor air. The system can be used in buildings with glass façade because it is installed on the internal walls and ceiling. However, its main disadvantages are that:

- the system cannot provide enough cooling to maintain the required indoor thermal conditions alone and it has to be combined with active cooling systems
- in the nighttime PCM needs to be ventilated with outdoor air at high velocities, which results in relatively large airflow rates and consequently high energy consumption for fan operation
- the prices of PCM are still relatively high which compromises the feasibility of their application.

The limitation of the system is that it can be only used for cooling application and not during the heating season.

8.4.2. Preliminary research

The advantage of the preliminary research was that the thermal behaviour of the PCM was investigated with different methods. In this way, the non-compliances between the methods were identified. Building level simulation showed the indoor temperatures obtained with PCM under different climate types. However, the detailed effect of PCM couldn't be distinguished. Also, the simulation tool cannot be used for simulation of ventilated air gaps.

The pre-experimental investigation showed the realistic thermal dynamics of PCM. However, the temperatures in the laboratory couldn't be controlled. Due to the small scale of the experimental set-up, the cooling effect of the PCM on the indoor environment couldn't be determined.

With validated pre-numerical model parametric study could be performed and the effect of different inlet temperatures and PCM melting temperatures and capacities could be investigated to determine the required thickness of the plates in the APS design process. However, the melting progress in the numerical model differed from the experimentally tested cases.

8.4.3. Experimental investigation

The advantages of the experimental investigation are to see the performance of the APS system on a realistic scale (room level). The investigation showed a direct cooling effect of the system and provided possibility to test the indoor conditions for different climate types. The results of the investigated cases could be directly compared in-between which makes the different influential parameters on cooling performance of the system clearly distinguishable. In the laboratory, the system can be measured in detailed as the measuring equipment is available on spot. Unfortunately, the laboratory environment cannot provide all factors present in the nature. Therefore, the performance of the system cannot be evaluated fully. In the experimental investigation, the thermal environment in the test cell was measured and not assessed by the perceived thermal comfort of the human subject during the investigated cases. Also, the heat was added to the cell with the electric heater which established a very hot surface in the room (e.g. 50 °C). Normally, in summer, the temperatures of the indoor surfaces are much lower (e.g. 28 °C). The limitation of the study is that only one geometric configuration could be tested. Reconstruction of the APS geometry could compromise the airtightness of the air gap.

8.4.4. Numerical model

With validated model it is possible to evaluate the performance of the system under various boundary conditions and parameters. The numerical model allowed to optimize the system's performance. However, then model couldn't show the cooling effect of PCM to the indoor environment. The limitation of the numerical model is the inability to calculate the energy performance of the system.

8.5. Future work

The presented research underlines the problem of PCM night-time solidification. Therefore, future research on PCM integrated into building elements should focus:

- The addition of active systems increases the power requirements for cooling, making the feasibility of using the APS system with nighttime power use questionable. Specifically, the power use for nighttime air gap ventilation may not be greater than the power use of active wraparound systems that independently cool the building during the day. Therefore, it needs to be investigated further with unsteady state building modelling tool with special attention given to mechanical components, such as TRNSYS.
- On the enhancement of heat transfer in PCM at low energy use rates. Such improvement may be reached by developing new PCM materials and combining them with metal structures. The cooling potential of the PCM application is drastically improved with addition of a second PCM layer embedded with water-pipes to the primary locally ventilated layer of PCM located on the external side of the building envelope.
- While the air supplied locally to the PCM affects the phase change better than the total volume ventilation, its practical implementation may be challenged due to demanding and in reality unapplicable complex composition. Thus, the future work should focus on simplicity of such systems.
- The overall performance of the PCM cooling systems is considerably improved when combined with appropriate and optimized control strategies and artificial intelligence. To assess the performance of TES application objectively, the melting temperature and thickness of the PCM layer should be optimised considering the individual climate type.
- As one of the major issues of the PCM system implantation is its economic feasibility, studies would benefit by providing such system analysis and evaluating the system with economic indicators.
- The PCM material, installation and maintenance costs including the recommended payback periods are mostly estimated. A review of common building integrated PCM in this aspect would be very valuable.
- Often life cycle assessment (LCA) analysis of PCM systems is neglected. Accordingly, such analysis should be of positive value.
- Even though many studies summarize PCM melting temperatures depending on the location in the building element, location of the PCM layer in it (external or internally layers of the envelope) and the climate type, there is no clear guidelines available for the selection of the PCM for cooling application in lightweight buildings.
- Further on, there is no specific requirements for the nighttime ventilation rates for the PCM solidification period and need to be provided.
- The requirements for the feasibility of PCM application with regard to minimal required indoor operative temperature reduction would be beneficial.

9. Literature

- [1] European Commission, “Renovation wave,” 2021. https://ec.europa.eu/energy/topics/energy-efficiency/energy-efficient-buildings/renovation-wave_en (accessed Feb. 01, 2021).
- [2] Eurostat, “Share of Population Living in a Dwelling Not Comfortably Cool during Summer Time by Income Quintile and Degree of Urbanization,” 2012. https://ec.europa.eu/eurostat/data/database?node_code=ilc_hcmp03 (accessed Apr. 04, 2019).
- [3] Intergovernmental Panel on Climate Change, “Global Warming of 1.5 °C,” 2018. Accessed: Apr. 04, 2019. [Online]. Available: <https://www.ipcc.ch/sr15/>
- [4] Statistical office of the European Union EUROSTAT, “Energy consumption in households,” 2020.
- [5] “The Future of Cooling – Analysis - IEA.” <https://www.iea.org/reports/the-future-of-cooling> (accessed Dec. 23, 2019).
- [6] M. Isaac and D. P. van Vuuren, “Modeling global residential sector energy demand for heating and air conditioning in the context of climate change,” *Energy Policy*, 2009, doi: 10.1016/j.enpol.2008.09.051.
- [7] F. Stazi, C. Bonfigli, E. Tomassoni, C. Di Perna, and P. Munafò, “The effect of high thermal insulation on high thermal mass: Is the dynamic behaviour of traditional envelopes in Mediterranean climates still possible?,” *Energy Build.*, vol. 88, pp. 367–383, Feb. 2015, doi: 10.1016/J.ENBUILD.2014.11.056.
- [8] “Heating & Cooling.” <https://www.irena.org/heatingcooling> (accessed Nov. 14, 2020).
- [9] EPBD 2010/31/EU, “Directive 2010/31/EU of the European Parliament and of the Council of 19 May 2010 on the energy performance of buildings,” 2010. Accessed: Apr. 04, 2019. [Online]. Available: <https://eur-lex.europa.eu/LexUriServ/LexUriServ.do?uri=OJ:L:2010:153:0013:0035:EN:PDF>
- [10] The Buildings Performance Institute Europe (BPIE), “» On the way to a climate-neutral Europe – Contributions from the building sector to a strengthened 2030 climate target BPIE - Buildings Performance Institute Europe,” 2020. <https://www.bpie.eu/publication/on-the-way-to-a-climate-neutral-europe-contributions-from-the-building-sector-to-a-strengthened-2030-target/> (accessed Feb. 01, 2021).
- [11] European Commission, “New rules for greener and smarter buildings will increase quality of life for all Europeans | European Commission,” 2019.

- https://ec.europa.eu/info/news/new-rules-greener-and-smarter-buildings-will-increase-quality-life-all-europeans-2019-apr-15_en (accessed Feb. 01, 2021).
- [12] European Commission, “A European Green Deal,” 2019. https://ec.europa.eu/info/strategy/priorities-2019-2024/european-green-deal_en (accessed Feb. 01, 2021).
- [13] Enerdata, “Addressing fuel poverty,” Nov. 05, 2019. <https://www.enerdata.net/publications/executive-briefing/fuel-poverty.html> (accessed Nov. 16, 2022).
- [14] CIBSE, “CIBSE - Overheating Position Statement,” 2020. <https://www.cibse.org/News-and-Policy/Policy/Overheating-Position-Statement> (accessed Jan. 30, 2021).
- [15] House of Commons - Environmental Audit Committee, “Heatwaves: adapting to climate change Ninth Report of Session 2017-19 Report, together with formal minutes relating to the report,” 2018.
- [16] World Health Organization WHO, “Heatwaves,” 2020. https://www.who.int/health-topics/heatwaves#tab=tab_1 (accessed Jan. 30, 2021).
- [17] Naumann G. *et al.*, “Global warming and human impacts of heat and cold extremes in the EU,” 2020. doi: 10.2760/47878.
- [18] S. Vardoulakis *et al.*, “Impact of climate change on the domestic indoor environment and associated health risks in the UK,” *Environ. Int.*, vol. 85, pp. 299–313, 2015, doi: 10.1016/j.envint.2015.09.010.
- [19] C. Brimicombe *et al.*, “Heatwaves: An invisible risk in UK policy and research,” *Environ. Sci. Policy*, vol. 116, pp. 1–7, Feb. 2021, doi: 10.1016/j.envsci.2020.10.021.
- [20] Chartered Institution of Building Services Engineers (CIBSE), “TM49: Design summer years for London,” 2014. <https://www.cibse.org/Knowledge/knowledge-items/detail?id=a0q20000008I6yFAAS> (accessed Jan. 30, 2021).
- [21] Chartered Institution of Building Services Engineers (CIBSE), “TM59: Design methodology for the assessment of overheating risk in homes,” 2017. <https://www.cibse.org/knowledge/knowledge-items/detail?id=a0q000000DVrTdQAL> (accessed Jan. 30, 2021).
- [22] M. Vega, N. Llantoy, M. Chafer, S. Ushak, and L. F. Cabeza, “Life cycle assessment of the inclusion of phase change materials in lightweight buildings,” *J. Energy Storage*, vol. 56, p. 105903, Dec. 2022, doi: 10.1016/j.est.2022.105903.
- [23] C. Dara, C. Hachem-Vermette, and G. Assefa, “Life cycle assessment and life cycle costing of container-based single-family housing in Canada: A case study,” *Build. Environ.*, vol. 163, p. 106332, Oct. 2019, doi: 10.1016/j.buildenv.2019.106332.
- [24] “Popularity of Timber Frame Construction.” <https://ukdiss.com/examples/increasing-popularity-surrounding-timber-frame-construction.php> (accessed Nov. 16, 2022).
- [25] A. Borgentorp, “The increase in timber construction is based on environmental concerns, competence and competitiveness.” <https://www.nordtreat.com/en/insights/the-increase-in-timber-construction-is-based-on-environmental-concerns-competence-and-competitiveness> (accessed Nov. 16, 2022).
- [26] M. Petruch and D. Walcher, “Timber for future? Attitudes towards timber construction by young millennials in Austria - Marketing implications from a representative study,” *J. Clean. Prod.*, vol. 294, p. 126324, Apr. 2021, doi: 10.1016/j.jclepro.2021.126324.

- [27] C. Liu, T. Kershaw, D. Fosas, A. P. Ramallo Gonzalez, S. Natarajan, and D. A. Coley, "High resolution mapping of overheating and mortality risk," *Build. Environ.*, vol. 122, pp. 1–14, 2017, doi: 10.1016/j.buildenv.2017.05.028.
- [28] K. J. Lomas and S. M. Porritt, "Overheating in buildings: lessons from research," *Build. Res. Inf.*, vol. 45, no. 1–2, pp. 1–18, 2017, doi: 10.1080/09613218.2017.1256136.
- [29] N. Bundle, E. O'Connell, N. O'Connor, and A. Bone, "A public health needs assessment for domestic indoor overheating," *Public Health*, pp. 9–15, 2018, doi: 10.1016/j.puhe.2017.12.016.
- [30] A. Krainer, "Passivhaus contra bioclimatic design," *Bauphysik*, vol. 30, no. 6, pp. 393–404, Dec. 2008, doi: 10.1002/bapi.200810051.
- [31] A. Blumenfeld, W. T. Thumm, and H. Phelps, "Passive Building Systems vs. Active Building Systems and the Return On Investment," *Building Innovation Conference and Expo*, 2014.
- [32] M. Dabaieh and A. Elbably, "Ventilated Trombe wall as a passive solar heating and cooling retrofitting approach; a low-tech design for off-grid settlements in semi-arid climates," *Sol. Energy*, vol. 122, pp. 820–833, Dec. 2015, doi: 10.1016/j.solener.2015.10.005.
- [33] B. Lamrani, K. Johannes, and F. Kuznik, "Phase change materials integrated into building walls: An updated review," *Renew. Sustain. Energy Rev.*, vol. 140, p. 110751, Apr. 2021, doi: 10.1016/j.rser.2021.110751.
- [34] J. M. P. Q. Delgado, J. C. Martinho, A. V. Sá, A. S. Guimarães, and V. Abrantes, *Thermal Energy Storage with Phase Change Materials A Literature Review of Applications for Buildings Materials*. Springer briefs in applied science and technology, 2019. Accessed: Apr. 13, 2021. [Online]. Available: <http://www.springer.com/series/8884>
- [35] International Standard Organisation (ISO), "ISO - ISO 6946:2017 - Building components and building elements — Thermal resistance and thermal transmittance — Calculation methods." <https://www.iso.org/standard/65708.html> (accessed May 31, 2021).
- [36] J. Guo, J. Dong, B. Zou, H. Wang, L. Zhu, and Y. Jiang, "Experimental investigation on the effects of phase change material and different ventilation modes on the thermal storage, space heating and energy consumption characteristics of ventilated mortar blocks," *J. Energy Storage*, vol. 41, p. 102817, Sep. 2021, doi: 10.1016/J.EST.2021.102817.
- [37] European Committee for Standardization CEN, "EN 16798-1:2019 (E) Energy performance of buildings - Ventilation for buildings - Part 1: Indoor environmental input parameters for design and assessment of energy performance of buildings addressing indoor air quality, thermal environment, lighting and acoustics - Module M1-6." European Committee for Standardization CEN, 2019.
- [38] S. Medved, *Gradbena fizika*. Univerza v Ljubljani, Fakulteta za arhitekturo, 2010.
- [39] DesignBuilder Software Ltd, "DesignBuilder Software Ltd - Home," 2017. <https://designbuilder.co.uk/> (accessed Apr. 25, 2019).
- [40] "EnergyPlus." <https://energyplus.net/> (accessed Nov. 17, 2022).
- [43] E. Osterman, "Doktorska naloga: Sistem z latentnim hranilnikom toplote za ogrevanje in hlajenje prostorov," Univerza v Ljubljani, Fakulteta za strojništvo, 2015.

- [44] A. Zastawna-Rumin, T. Kisilewicz, and U. Berardi, “Novel algorithm for modelling the hysteresis of Phase Change Materials,” *Energies*, vol. 13, Mar. 2020, doi: 10.3390/en13051200.
- [45] Rubitherm, “Data sheet Rubitherm RT24,” 2020. https://www.rubitherm.eu/media/products/datasheets/Techdata_RT24_EN_09102020.PDF (accessed Nov. 24, 2021).
- [46] F. M. White, *Fluid Mechanics*, 4th ed. McGraw-Hill College, 1998.
- [47] V. Antony Aroul Raj and R. Velraj, “Heat transfer and pressure drop studies on a PCM-heat exchanger module for free cooling applications,” *Int. J. Therm. Sci.*, vol. 50, no. 8, pp. 1573–1582, Aug. 2011, doi: 10.1016/j.ijthermalsci.2011.01.025.
- [48] B. R. Munson, A. P. Rothmayer, T. H. Okiishi, and W. W. Huebsch, *Fundamentals of Fluid Mechanics*, 7th ed. Wiley, 2012.
- [49] M. Rostamizadeh, M. Khanlarkhani, and S. Mojtaba Sadrameli, “Simulation of energy storage system with phase change material (PCM),” *Energy Build.*, vol. 49, pp. 419–422, Jun. 2012, doi: 10.1016/j.enbuild.2012.02.037.
- [50] A. Škerlavaj, “Numerična analiza toka tekočine v vtočnem bazenu vertikalnih črpalk,” Fakulteta za strojništvo, Univerza v Mariboru, 2011.
- [51] A. Bakker, “Lecture 5: Solution Methods. Applied Computational Fluid Dynamics.” 2002. [//ppt-online.org/648148](http://ppt-online.org/648148) (accessed Nov. 17, 2022).
- [52] J. H. Ferziger and M. Perić, *Computational Methods for Fluid Dynamics*, 3rd ed. Springer, 2001.
- [53] ANSYS, Inc., “ANSYS Fluent Theory Guide 14.0.” ANSYS, 2011.
- [54] M. Sinka, D. Bajare, A. Jakovics, J. Ratnieks, S. Gendelis, and J. Tihana, “Experimental testing of phase change materials in a warm-summer humid continental climate,” *Energy Build.*, vol. 195, pp. 205–215, Jul. 2019, doi: 10.1016/j.enbuild.2019.04.030.
- [55] S. Álvarez, L. F. Cabeza, A. Ruiz-Pardo, A. Castell, and J. A. Tenorio, “Building integration of PCM for natural cooling of buildings,” *Appl. Energy*, vol. 109, pp. 514–522, Sep. 2013, doi: 10.1016/j.apenergy.2013.01.080.
- [56] M. Prabhakar, M. Saffari, A. de Gracia, and L. F. Cabeza, “Improving the energy efficiency of passive PCM system using controlled natural ventilation,” *Energy Build.*, vol. 228, p. 110483, Dec. 2020, doi: 10.1016/j.enbuild.2020.110483.
- [57] Y. Pal and V. R. Kumar, “Thermal decomposition study of paraffin based hybrid rocket fuel containing Aluminum and Boron additives,” *Thermochim. Acta*, vol. 655, pp. 63–75, Sep. 2017, doi: 10.1016/j.tca.2017.06.002.
- [58] A. Alhusseny, N. Al-Zurfi, A. Nasser, A. Al-Fatlawi, and M. Aljanabi, “Impact of using a PCM-metal foam composite on charging/discharging process of bundled-tube LHTES units,” *Int. J. Heat Mass Transf.*, vol. 150, p. 119320, Apr. 2020, doi: 10.1016/j.ijheatmasstransfer.2020.119320.
- [59] J. M. Mahdi, H. I. Mohammed, E. T. Hashim, P. Talebizadehsardari, and E. C. Nsofor, “Solidification enhancement with multiple PCMs, cascaded metal foam and nanoparticles in the shell-and-tube energy storage system,” *Appl. Energy*, vol. 257, p. 113993, Jan. 2020, doi: 10.1016/j.apenergy.2019.113993.
- [60] L. Boussaba, G. Lefebvre, S. Makhlof, A. Grados, and L. Royon, “Investigation and properties of a novel composite bio-PCM to reduce summer energy consumptions in buildings of hot and dry climates,” *Sol. Energy*, vol. 214, pp. 119–130, Jan. 2021, doi: 10.1016/j.solener.2020.11.060.
- [61] L. Boussaba, A. Foufa, S. Makhlof, G. Lefebvre, and L. Royon, “Elaboration and properties of a composite bio-based PCM for an application in building envelopes,”

- Constr. Build. Mater.*, vol. 185, pp. 156–165, Oct. 2018, doi: 10.1016/j.conbuildmat.2018.07.098.
- [62] D. M. C. Shastry and U. C. Arunachala, “Thermal management of photovoltaic module with metal matrix embedded PCM,” *J. Energy Storage*, vol. 28, p. 101312, Apr. 2020, doi: 10.1016/j.est.2020.101312.
- [63] K. P. Venkataraj, S. Suresh, B. Praveen, and S. C. Nair, “Experimental heat transfer analysis of macro packed neopentylglycol with CuO nano additives for building cooling applications,” *J. Energy Storage*, vol. 17, pp. 1–10, Jun. 2018, doi: 10.1016/j.est.2018.02.005.
- [64] K. Biswas, J. Lu, P. Soroushian, and S. Shrestha, “Combined experimental and numerical evaluation of a prototype nano-PCM enhanced wallboard,” *Appl. Energy*, vol. 131, pp. 517–529, Oct. 2014, doi: 10.1016/j.apenergy.2014.02.047.
- [65] S. Lu, Y. Zhao, K. Fang, Y. Li, and P. Sun, “Establishment and experimental verification of TRNSYS model for PCM floor coupled with solar water heating system,” *Energy Build.*, vol. 140, pp. 245–260, Apr. 2017, doi: 10.1016/j.enbuild.2017.02.018.
- [66] S. Lu, J. Gao, H. Tong, S. Yin, X. Tang, and X. Jiang, “Model establishment and operation optimization of the casing PCM radiant floor heating system,” *Energy*, vol. 193, p. 116814, Feb. 2020, doi: 10.1016/j.energy.2019.116814.
- [67] W. Sun, Y. Zhang, Z. Ling, X. Fang, and Z. Zhang, “Experimental investigation on the thermal performance of double-layer PCM radiant floor system containing two types of inorganic composite PCMs,” *Energy Build.*, vol. 211, p. 109806, Mar. 2020, doi: 10.1016/j.enbuild.2020.109806.
- [68] H. Weinläder, F. Klinker, and M. Yasin, “PCM cooling ceilings in the Energy Efficiency Center – Regeneration behaviour of two different system designs,” *Energy Build.*, vol. 156, pp. 70–77, Dec. 2017, doi: 10.1016/j.enbuild.2017.09.010.
- [69] M. Yasin, E. Scheidemantel, F. Klinker, H. Weinläder, and S. Weismann, “Generation of a simulation model for chilled PCM ceilings in TRNSYS and validation with real scale building data,” *J. Build. Eng.*, vol. 22, pp. 372–382, Mar. 2019, doi: 10.1016/j.jobe.2019.01.004.
- [70] P. Arce, C. Castellón, A. Castell, and L. F. Cabeza, “Use of microencapsulated PCM in buildings and the effect of adding awnings,” *Energy Build.*, vol. 44, no. 1, pp. 88–93, Jan. 2012, doi: 10.1016/j.enbuild.2011.10.028.
- [71] U. Stritih *et al.*, “IEA ECES – Annex 31 investigation overview PCM Thermal Energy Storage in Solar Heating of Ventilation Air - Experimental and Numerical Investigations 1 . Introduction Content of presentation : • Research problem • Aims and objectives of the research • The,” 2017.
- [72] N. Soares, J. J. Costa, A. R. Gaspar, and P. Santos, “Review of passive PCM latent heat thermal energy storage systems towards buildings’ energy efficiency,” *Energy Build.*, vol. 59, pp. 82–103, Apr. 2013, doi: 10.1016/j.enbuild.2012.12.042.
- [73] H. Akeiber *et al.*, “A review on phase change material (PCM) for sustainable passive cooling in building envelopes,” *Renew. Sustain. Energy Rev.*, vol. 60, pp. 1470–1497, Jul. 2016, doi: 10.1016/j.rser.2016.03.036.
- [74] M. Saffari, A. de Gracia, S. Ushak, and L. F. Cabeza, “Passive cooling of buildings with phase change materials using whole-building energy simulation tools: A review,” *Renew. Sustain. Energy Rev.*, vol. 80, pp. 1239–1255, Dec. 2017, doi: 10.1016/j.rser.2017.05.139.

- [75] M. Iten, S. Liu, and A. Shukla, "A review on the air-PCM-TES application for free cooling and heating in the buildings," *Renew. Sustain. Energy Rev.*, vol. 61, pp. 175–186, Aug. 2016, doi: 10.1016/j.rser.2016.03.007.
- [76] E. Oró, A. de Gracia, A. Castell, M. M. Farid, and L. F. Cabeza, "Review on phase change materials (PCMs) for cold thermal energy storage applications," *Appl. Energy*, vol. 99, pp. 513–533, Nov. 2012, doi: 10.1016/j.apenergy.2012.03.058.
- [77] F. Souayfane, F. Fardoun, and P. H. Biwole, "Phase change materials (PCM) for cooling applications in buildings: A review," *Energy Build.*, vol. 129, pp. 396–431, Oct. 2016, doi: 10.1016/j.enbuild.2016.04.006.
- [78] E. Osterman, V. V. Tyagi, V. Butala, N. A. Rahim, and U. Stritih, "Review of PCM based cooling technologies for buildings," *Energy Build.*, vol. 49, pp. 37–49, 2012, doi: 10.1016/j.enbuild.2012.03.022.
- [79] M. Alizadeh and S. M. Sadrameli, "Development of free cooling based ventilation technology for buildings: Thermal energy storage (TES) unit, performance enhancement techniques and design considerations - A review," *Renew. Sustain. Energy Rev.*, vol. 58, pp. 619–645, May 2016, doi: 10.1016/j.rser.2015.12.168.
- [80] Y. Zhou, S. Zheng, and G. Zhang, "A review on cooling performance enhancement for phase change materials integrated systems—flexible design and smart control with machine learning applications," *Build. Environ.*, vol. 174, p. 106786, May 2020, doi: 10.1016/j.buildenv.2020.106786.
- [81] K. Faraj, M. Khaled, J. Faraj, F. Hachem, and C. Castelain, "Phase change material thermal energy storage systems for cooling applications in buildings: A review," *Renew. Sustain. Energy Rev.*, vol. 119, p. 109579, Mar. 2020, doi: 10.1016/j.rser.2019.109579.
- [82] C. Zhang, M. Pomianowski, P. K. Heiselberg, and T. Yu, "A review of integrated radiant heating/cooling with ventilation systems- Thermal comfort and indoor air quality," *Energy Build.*, vol. 223, p. 110094, Sep. 2020, doi: 10.1016/j.enbuild.2020.110094.
- [83] A. Bastani, F. Haghghat, and J. Kozinski, "Designing building envelope with PCM wallboards: Design tool development," *Renew. Sustain. Energy Rev.*, vol. 31, pp. 554–562, Mar. 2014, doi: 10.1016/j.rser.2013.12.031.
- [84] E. Solgi, Z. Hamedani, R. Fernando, H. Skates, and N. E. Orji, "A literature review of night ventilation strategies in buildings," *Energy Build.*, vol. 173, pp. 337–352, Aug. 2018, doi: 10.1016/j.enbuild.2018.05.052.
- [85] S. Memarian, B. M. Kari, R. Fayaz, and S. Asadi, "Single and combined phase change materials: Their effect on seasonal transition period," *Energy Build.*, vol. 169, pp. 453–472, 2018, doi: 10.1016/j.enbuild.2018.03.085.
- [86] C. Piselli, M. Prabhakar, A. de Gracia, M. Saffari, A. L. Pisello, and L. F. Cabeza, "Optimal control of natural ventilation as passive cooling strategy for improving the energy performance of building envelope with PCM integration," *Renew. Energy*, vol. 162, pp. 171–181, Dec. 2020, doi: 10.1016/j.renene.2020.07.043.
- [87] J. Liu, Y. Liu, L. Yang, T. Liu, C. Zhang, and H. Dong, "Climatic and seasonal suitability of phase change materials coupled with night ventilation for office buildings in Western China," *Renew. Energy*, vol. 147, pp. 356–373, Mar. 2020, doi: 10.1016/j.renene.2019.08.069.
- [88] I. Adilkhanova, S. A. Memon, J. Kim, and A. Sheriyev, "A novel approach to investigate the thermal comfort of the lightweight relocatable building integrated with PCM in different climates of Kazakhstan during summertime," *Energy*, vol. 217, p. 119390, Feb. 2021, doi: 10.1016/j.energy.2020.119390.

- [89] H. Jamil, M. Alam, J. Sanjayan, and J. Wilson, "Investigation of PCM as retrofitting option to enhance occupant thermal comfort in a modern residential building," *Energy Build.*, vol. 133, pp. 217–229, Dec. 2016, doi: 10.1016/j.enbuild.2016.09.064.
- [90] U. Berardi and S. Soudian, "Experimental investigation of latent heat thermal energy storage using PCMs with different melting temperatures for building retrofit," *Energy Build.*, vol. 185, pp. 180–195, Feb. 2019, doi: 10.1016/j.enbuild.2018.12.016.
- [91] L. Bai, J. Xie, M. M. Farid, W. Wang, and J. Liu, "Analytical model to study the heat storage of phase change material envelopes in lightweight passive buildings," *Build. Environ.*, vol. 169, p. 106531, Feb. 2020, doi: 10.1016/j.buildenv.2019.106531.
- [92] Y. Xiang and G. Zhou, "Thermal performance of a window-based cooling unit using phase change materials combined with night ventilation," *Energy Build.*, vol. 108, pp. 267–278, Dec. 2015, doi: 10.1016/j.enbuild.2015.09.030.
- [93] A. Mechouet, E. M. Oualim, and T. Mouhib, "Effect of mechanical ventilation on the improvement of the thermal performance of PCM-incorporated double external walls: A numerical investigation under different climatic conditions in Morocco," *J. Energy Storage*, vol. 38, p. 102495, Jun. 2021, doi: 10.1016/j.est.2021.102495.
- [94] R. Barzin, J. J. J. Chen, B. R. Young, and M. M. Farid, "Application of PCM energy storage in combination with night ventilation for space cooling," *Appl. Energy*, vol. 158, pp. 412–421, Nov. 2015, doi: 10.1016/j.apenergy.2015.08.088.
- [95] G. Evola, L. Marletta, and F. Sicurella, "A methodology for investigating the effectiveness of PCM wallboards for summer thermal comfort in buildings," *Build. Environ.*, vol. 59, pp. 517–527, Jan. 2013, doi: 10.1016/j.buildenv.2012.09.021.
- [96] V. Costanzo, G. Evola, L. Marletta, and F. Nocera, "The effectiveness of phase change materials in relation to summer thermal comfort in air-conditioned office buildings Article History", doi: 10.1007/s12273-018-0468-2.
- [97] L. Pajek, B. Hudobivnik, R. Kunič, and M. Košir, "Improving thermal response of lightweight timber building envelopes during cooling season in three European locations," *J. Clean. Prod.*, vol. 156, pp. 939–952, Jul. 2017, doi: 10.1016/j.jclepro.2017.04.098.
- [98] E. Solgi, R. Fayaz, and B. M. Kari, "Cooling load reduction in office buildings of hot-arid climate, combining phase change materials and night purge ventilation," *Renew. Energy*, vol. 85, pp. 725–731, 2016, doi: 10.1016/j.renene.2015.07.028.
- [99] F. Ascione, N. Bianco, R. F. De Masi, F. de' Rossi, and G. P. Vanoli, "Energy refurbishment of existing buildings through the use of phase change materials: Energy savings and indoor comfort in the cooling season," *Appl. Energy*, vol. 113, pp. 990–1007, Jan. 2014, doi: 10.1016/j.apenergy.2013.08.045.
- [100] A. Karaoulis, "Investigation of Energy Performance in Conventional and Lightweight Building Components with the use of Phase Change Materials (PCMS): Energy Savings in Summer Season," *Procedia Environ. Sci.*, vol. 38, pp. 796–803, Jan. 2017, doi: 10.1016/j.proenv.2017.03.164.
- [101] W. I. W. M. Nazi, Y. Wang, H. Chen, X. Zhang, and A. Paul Roskilly, "Passive Cooling Using Phase Change Material and Insulation for High-rise Office Building in Tropical Climate," in *Energy Procedia*, Dec. 2017, vol. 142, pp. 2295–2302. doi: 10.1016/j.egypro.2017.12.632.
- [102] G. Zhou, Y. Yang, X. Wang, and S. Zhou, "Numerical analysis of effect of shape-stabilized phase change material plates in a building combined with night

- ventilation,” *Appl. Energy*, vol. 86, no. 1, pp. 52–59, Jan. 2009, doi: 10.1016/j.apenergy.2008.03.020.
- [103] G. Zhou, Y. Yang, and H. Xu, “Energy performance of a hybrid space-cooling system in an office building using SSPCM thermal storage and night ventilation,” *Sol. Energy*, vol. 85, no. 3, pp. 477–485, Mar. 2011, doi: 10.1016/j.solener.2010.12.028.
- [104] S. Soudian and U. Berardi, “Assessing the effect of night ventilation on PCM performance in high-rise residential buildings,” *J. Build. Phys.*, vol. 43, no. 3, pp. 229–249, Nov. 2019, doi: 10.1177/1744259119848128.
- [105] Y.-B. Seong, J.-H. Lim, Y.-B. Seong, and J.-H. Lim, “Energy Saving Potentials of Phase Change Materials Applied to Lightweight Building Envelopes,” *Energies*, vol. 6, no. 10, pp. 5219–5230, Oct. 2013, doi: 10.3390/en6105219.
- [106] Y. Qu, D. Zhou, F. Xue, and L. Cui, “Multi-factor analysis on thermal comfort and energy saving potential for PCM-integrated buildings in summer,” *Energy Build.*, vol. 241, p. 110966, Jun. 2021, doi: 10.1016/j.enbuild.2021.110966.
- [107] Z. A. Al-Absi, M. I. Mohd Hafizal, M. Ismail, A. Mardiana, and A. Ghazali, “Peak indoor air temperature reduction for buildings in hot-humid climate using phase change materials,” *Case Stud. Therm. Eng.*, vol. 22, p. 100762, Dec. 2020, doi: 10.1016/j.csite.2020.100762.
- [108] M. Hou, X. Kong, H. Li, H. Yang, and W. Chen, “Experimental study on the thermal performance of composite phase change ventilated roof,” *J. Energy Storage*, vol. 33, p. 102060, Jan. 2021, doi: 10.1016/j.est.2020.102060.
- [109] H. Li, J. Li, C. Xi, W. Chen, and X. Kong, “Experimental and numerical study on the thermal performance of ventilated roof composed with multiple phase change material (VR-MPCM),” *Energy Convers. Manag.*, vol. 213, p. 112836, Jun. 2020, doi: 10.1016/j.enconman.2020.112836.
- [110] R. Stropnik and U. Stritih, “Increasing the efficiency of PV panel with the use of PCM,” *Renew. Energy*, vol. 97, pp. 671–679, 2016, doi: 10.1016/j.renene.2016.06.011.
- [111] W. Lin, Z. Ma, M. I. Sohel, and P. Cooper, “Development and evaluation of a ceiling ventilation system enhanced by solar photovoltaic thermal collectors and phase change materials,” *Energy Convers. Manag.*, vol. 88, pp. 218–230, Dec. 2014, doi: 10.1016/j.enconman.2014.08.019.
- [112] M. Alizadeh and S. M. Sadrameli, “Indoor thermal comfort assessment using PCM based storage system integrated with ceiling fan ventilation: Experimental design and response surface approach,” *Energy Build.*, vol. 188–189, pp. 297–313, Apr. 2019, doi: 10.1016/j.enbuild.2019.02.020.
- [113] L. Navarro, A. de Gracia, A. Castell, and L. F. Cabeza, “Experimental study of an active slab with PCM coupled to a solar air collector for heating purposes,” *Energy Build.*, vol. 128, pp. 12–21, Sep. 2016, doi: 10.1016/j.enbuild.2016.06.069.
- [114] K. Yanbing, J. Yi, and Z. Yinping, “Modeling and experimental study on an innovative passive cooling system - NVP system,” *Energy Build.*, vol. 35, no. 4, pp. 417–425, May 2003, doi: 10.1016/S0378-7788(02)00141-X.
- [115] J. R. Turnpenny, D. W. Etheridge, and D. A. Reay, “Novel ventilation cooling system for reducing air conditioning in buildings. Part I: Testing and theoretical modelling,” *Appl. Therm. Eng.*, vol. 20, no. 11, pp. 1019–1037, Aug. 2000, doi: 10.1016/S1359-4311(99)00068-X.
- [116] J. Lizana, M. de-Borja-Torrejón, A. Barrios-Padura, T. Auer, and R. Chacartegui, “Passive cooling through phase change materials in buildings. A critical study of

- implementation alternatives,” *Appl. Energy*, vol. 254, p. 113658, Nov. 2019, doi: 10.1016/j.apenergy.2019.113658.
- [117] H. Weinläder, W. Körner, and B. Strieder, “A ventilated cooling ceiling with integrated latent heat storage - Monitoring results,” *Energy Build.*, vol. 82, pp. 65–72, Oct. 2014, doi: 10.1016/j.enbuild.2014.07.013.
- [118] F. Jiao and P. Xu, “Simulation and Feasibility Analysis of PCM Based Passive Cooling Technique in Residential House,” in *Procedia Engineering*, Jan. 2015, vol. 121, pp. 1969–1976. doi: 10.1016/j.proeng.2015.09.189.
- [119] A. Faheem, G. Ranzi, F. Fiorito, and C. Lei, “A numerical study on the thermal performance of night ventilated hollow core slabs cast with micro-encapsulated PCM concrete,” *Energy Build.*, vol. 127, pp. 892–906, Sep. 2016, doi: 10.1016/j.enbuild.2016.06.014.
- [120] J. Yu *et al.*, “Study on thermal insulation characteristics and optimized design of pipe-embedded ventilation roof with outer-layer shape-stabilized PCM in different climate zones,” *Renew. Energy*, vol. 147, pp. 1609–1622, Mar. 2020, doi: 10.1016/j.renene.2019.09.115.
- [121] N. Morovat, A. K. Athienitis, J. A. Candanedo, and V. Dermardiros, “Simulation and performance analysis of an active PCM-heat exchanger intended for building operation optimization,” *Energy Build.*, vol. 199, pp. 47–61, Sep. 2019, doi: 10.1016/j.enbuild.2019.06.022.
- [122] T. Kodo and T. Ibamoto, “Research on using the PCM for ceiling board,” in *IEA ECESIA, 3rd workshop, Tokyo, Japan, 1–2 October 2002, Annex 17*.
- [123] M. Jaworski, “Thermal performance of building element containing phase change material (PCM) integrated with ventilation system - An experimental study,” *Appl. Therm. Eng.*, vol. 70, no. 1, pp. 665–674, Sep. 2014, doi: 10.1016/j.applthermaleng.2014.05.093.
- [124] K. Nagano, S. Takeda, T. Mochida, K. Shimakura, and T. Nakamura, “Study of a floor supply air conditioning system using granular phase change material to augment building mass thermal storage - Heat response in small scale experiments,” *Energy Build.*, vol. 38, no. 5, pp. 436–446, May 2006, doi: 10.1016/j.enbuild.2005.07.010.
- [125] F. J. Neila González, C. Acha Román, E. Higuera García, and C. Bedoya Frutos, “Phase Change Materials (PCMs) for energy storage in architecture. Use with the Magic Box prototype,” *Mater. Constr.*, vol. 58, no. 291, pp. 119–126, 2008.
- [126] G. Evola, L. Marletta, and F. Sicurella, “Simulation of a ventilated cavity to enhance the effectiveness of PCM wallboards for summer thermal comfort in buildings,” *Energy Build.*, vol. 70, pp. 480–489, Feb. 2014, doi: 10.1016/j.enbuild.2013.11.089.
- [127] V. Dermardiros, Y. Chen, and A. K. Athienitis, “Modelling of an active PCM thermal energy storage for control applications,” in *Energy Procedia*, Nov. 2015, vol. 78, pp. 1690–1695. doi: 10.1016/j.egypro.2015.11.261.
- [128] V. Dermardiros, “Modelling and Experimental Evaluation of an Active Thermal Energy Storage System with Phase-Change Materials for Model-Based Control,” 2015.
- [129] C. Wang, S. Deng, J. Niu, and E. Long, “A numerical study on optimizing the designs of applying PCMs to a disaster-relief prefabricated temporary-house (PTH) to improve its summer daytime indoor thermal environment,” *Energy*, vol. 181, pp. 239–249, Aug. 2019, doi: 10.1016/j.energy.2019.05.165.

- [130] A. De Gracia, L. Navarro, A. Castell, Á. Ruiz-Pardo, S. Álvarez, and L. F. Cabeza, “Thermal analysis of a ventilated facade with PCM for cooling applications,” *Energy Build.*, vol. 65, pp. 508–515, Oct. 2013, doi: 10.1016/j.enbuild.2013.06.032.
- [131] A. De Gracia, C. Fernández, A. Castell, C. Mateu, and L. F. Cabeza, “Control of a PCM ventilated facade using reinforcement learning techniques,” *Energy Build.*, vol. 106, pp. 234–242, Nov. 2015, doi: 10.1016/j.enbuild.2015.06.045.
- [132] A. de Gracia, L. Navarro, A. Castell, and L. F. Cabeza, “Energy performance of a ventilated double skin facade with PCM under different climates,” *Energy Build.*, vol. 91, pp. 37–42, Mar. 2015, doi: 10.1016/j.enbuild.2015.01.011.
- [133] A. de Gracia, R. Barzin, C. Fernández, M. M. Farid, and L. F. Cabeza, “Control strategies comparison of a ventilated facade with PCM – energy savings, cost reduction and CO₂ mitigation,” *Energy Build.*, vol. 130, pp. 821–828, Oct. 2016, doi: 10.1016/j.enbuild.2016.09.007.
- [134] A. Laaouatni, N. Martaj, R. Bennacer, M. Lachi, M. El Omari, and M. El Ganaoui, “Thermal building control using active ventilated block integrating phase change material,” *Energy Build.*, vol. 187, pp. 50–63, Mar. 2019, doi: 10.1016/j.enbuild.2019.01.024.
- [135] G. Diarce *et al.*, “Ventilated active façades with PCM,” *Appl. Energy*, vol. 109, pp. 530–537, Sep. 2013, doi: 10.1016/j.apenergy.2013.01.032.
- [136] G. Diarce, Á. Campos-Celador, K. Martin, A. Urresti, A. García-Romero, and J. M. Sala, “A comparative study of the CFD modeling of a ventilated active façade including phase change materials,” *Appl. Energy*, vol. 126, pp. 307–317, Aug. 2014, doi: 10.1016/j.apenergy.2014.03.080.
- [137] Y. Zhou, C. W. F. Yu, and G. Zhang, “Study on heat-transfer mechanism of wallboards containing active phase change material and parameter optimization with ventilation,” *Appl. Therm. Eng.*, vol. 144, pp. 1091–1108, Nov. 2018, doi: 10.1016/j.applthermaleng.2018.04.083.
- [138] Y. Zhou, S. Zheng, and G. Zhang, “Study on the energy performance enhancement of a new PCMs integrated hybrid system with the active cooling and hybrid ventilations,” *Energy*, vol. 179, pp. 111–128, Jul. 2019, doi: 10.1016/j.energy.2019.04.173.
- [139] Y. Zhou and S. Zheng, “Multi-level uncertainty optimisation on phase change materials integrated renewable systems with hybrid ventilations and active cooling,” *Energy*, vol. 202, p. 117747, Jul. 2020, doi: 10.1016/j.energy.2020.117747.
- [140] T. M. O. Diallo *et al.*, “Numerical investigation of the energy performance of an Opaque Ventilated Façade system employing a smart modular heat recovery unit and a latent heat thermal energy system,” *Appl. Energy*, vol. 205, pp. 130–152, Nov. 2017, doi: 10.1016/j.apenergy.2017.07.042.
- [141] C. Luo, L. Xu, J. Ji, M. Liao, and D. Sun, “Experimental study of a modified solar phase change material storage wall system,” *Energy*, vol. 128, pp. 224–231, Jun. 2017, doi: 10.1016/j.energy.2017.04.020.
- [142] N. Zhu, S. Li, P. Hu, F. Lei, and R. Deng, “Numerical investigations on performance of phase change material Trombe wall in building,” *Energy*, vol. 187, p. 116057, Nov. 2019, doi: 10.1016/j.energy.2019.116057.
- [143] U. Strith, “Heat transfer enhancement in latent heat thermal storage system for buildings,” *Energy Build.*, vol. 35, no. 11, pp. 1097–1104, Dec. 2003, doi: 10.1016/j.enbuild.2003.07.001.
- [144] Y. Li, J. Darkwa, G. Kokogiannakis, and W. Su, “Phase change material blind system for double skin façade integration: System development and thermal

- performance evaluation,” *Appl. Energy*, vol. 252, p. 113376, Oct. 2019, doi: 10.1016/j.apenergy.2019.113376.
- [145] Y. Hu and P. K. Heiselberg, “A new ventilated window with PCM heat exchanger—Performance analysis and design optimization,” *Energy Build.*, vol. 169, pp. 185–194, Jun. 2018, doi: 10.1016/j.enbuild.2018.03.060.
- [146] Y. Hu, R. Guo, and P. K. Heiselberg, “Performance and control strategy development of a PCM enhanced ventilated window system by a combined experimental and numerical study,” *Renew. Energy*, vol. 155, pp. 134–152, Aug. 2020, doi: 10.1016/j.renene.2020.03.137.
- [147] J. Čurpek and M. Čekon, “Climate response of a BiPV façade system enhanced with latent PCM-based thermal energy storage,” *Renew. Energy*, vol. 152, pp. 368–384, Jun. 2020, doi: 10.1016/j.renene.2020.01.070.
- [148] K. Kant, R. Pitchumani, A. Shukla, and A. Sharma, “Analysis and design of air ventilated building integrated photovoltaic (BIPV) system incorporating phase change materials,” *Energy Convers. Manag.*, vol. 196, pp. 149–164, Sep. 2019, doi: 10.1016/j.enconman.2019.05.073.
- [149] Ansys, Inc., “Ansys Fluent | Fluid Simulation Software.” <https://www.ansys.com/products/fluids/ansys-fluent> (accessed Nov. 17, 2022).
- [150] Phase Change, “BioPCM-Data-Sheet-Q23,” 2018.
- [151] Phase Change, “BioPCM-Data-Sheet-Q27,” 2018.
- [152] Phase Change, “BioPCM-Data-Sheet-Q25,” 2018.
- [153] Knauf, “Generic Heat Storage Capacity Knauf Comfortboard 23,” 2016.
- [154] Rubitherm, “Data sheet Rubitherm RT22HC,” 2020. https://www.rubitherm.eu/media/products/datasheets/Techdata_RT22HC_EN_09102020.PDF (accessed Nov. 24, 2021).
- [155] Rubitherm, “Data Sheet Rubitherm SP24E,” 2020. https://www.rubitherm.eu/media/products/datasheets/Techdata_SP24E_EN_09112020.PDF (accessed Nov. 24, 2021).
- [156] Rubitherm, “Data Sheet Rubitherm SP25E2,” 2020. https://www.rubitherm.eu/media/products/datasheets/Techdata_SP25E2_EN_09112020.PDF (accessed Nov. 24, 2021).
- [157] A. Beizaee, K. J. Lomas, and S. K. Firth, “National survey of summertime temperatures and overheating risk in English homes,” *Build. Environ.*, vol. 65, pp. 1–17, Jul. 2013, doi: 10.1016/j.buildenv.2013.03.011.
- [158] E. Zavrl, G. Zupan, U. Stritih, and M. Dovjak, “Overheating Reduction in Lightweight Framed Buildings with Application of Phase Change Materials,” *Stroj. Vestn.-J. Mech. Eng.*, vol. 66, pp. 3–14, 2020, doi: 10.5545/sv-jme.2019.6244.
- [159] A. R. S. Z. O. Ministrstvo za okolje in prostor, “Ocena podnebnih sprememb v Sloveniji do konca 21. stoletja: Priloga 1: spremembe temperature,” 2018.
- [160] H. Jamil, M. Alam, J. Sanjayan, and J. Wilson, “Investigation of PCM as retrofitting option to enhance occupant thermal comfort in a modern residential building,” *Energy Build.*, vol. 133, pp. 217–229, Dec. 2016, doi: 10.1016/j.enbuild.2016.09.064.
- [161] Y. Kharbouch, A. Mimet, M. El Ganaoui, and L. Ouhsaine, “Thermal energy and economic analysis of a PCM-enhanced household envelope considering different climate zones in Morocco,” *Int. J. Sustain. Energy*, vol. 37, no. 6, pp. 515–532, Jul. 2018, doi: 10.1080/14786451.2017.1365076.
- [162] F. Souayfane, P. Henry Biwole, F. Fardoun, and P. Achard, “Energy performance and economic analysis of a TIM-PCM wall under different climates,” 2018,

- Accessed: Jan. 27, 2022. [Online]. Available: <https://www.sciencedirect.com/science/article/pii/S0360544218324885>
- [163] D. Virk and M. Eames, “CIBSE Weather Files 2016 release: Technical Briefing and Testing,” 2016.
- [164] “Rubitherm GmbH.” <https://www.rubitherm.eu/en/productCategories.html> (accessed Nov. 21, 2021).
- [165] “Ventilateur Centrifuge mobile/chantier, mono/triphasé -Ventilation VIF.” <http://www.ventilation-vif.fr/ventilateur-de-chantier/56-ventilateur-centrifuge-mobile.html> (accessed Oct. 09, 2022).
- [166] European Council, “Regulation of the European Parliament and of the Council of 9 March 2011 laying down harmonised conditions for the marketing of construction products and repealing Council Directive 89/106/EECText with EEA relevance,” *Off. J. Eur. Union*, no. 305, pp. 43–88, 2011.
- [167] “Dokumenti in ceniki.” <https://www.elektro-energija.si/za-dom/dokumenti-in-ceniki> (accessed Oct. 09, 2022).
- [168] E. Osterman, K. Hagel, C. Rathgeber, V. Butala, and U. Stritih, “Parametrical analysis of latent heat and cold storage for heating and cooling of rooms,” *Appl. Therm. Eng.*, vol. 84, pp. 138–149, Jun. 2015, doi: 10.1016/j.applthermaleng.2015.02.081.
- [169] “Welcome | TRNSYS: Transient System Simulation Tool.” <https://www.trnsys.com/> (accessed Nov. 17, 2022).
- [170] X. Mi, R. Liu, H. Cui, S. A. Memon, F. Xing, and Y. Lo, “Energy and economic analysis of building integrated with PCM in different cities of China,” *Appl. Energy*, vol. 175, pp. 324–336, Aug. 2016, doi: 10.1016/J.APENERGY.2016.05.032.

Appendix A: Remaining literature review analysis

A.1 Ventilation rates and duration period of the nighttime ventilation cycle

Table 0.1 below presents the ventilation rates and duration period of the nighttime ventilation cycle. It shows that in majority of cases the period lasts between 6 and 12 h, normally starting between 19:00 and 21:00 and lasting until 6:00 and 8:00.

Table 0.1: Ventilation rates and duration period of the nighttime ventilation cycle.

#	FLOW RATE	VENTILATION PERIOD	REF	#	FLOW RATE	VENTILATION PERIOD	REF
NATURAL				MECHANICAL			
1	Depending on the wind pressures of each location	24:00-06:00	[56]	12	300 m ³ /h	21:00-07:00	[94]
2	0 ACH, 1 ACH, 3 ACH, 5 ACH, 7 ACH and 10 ACH	/	[85]	13	2-8 ACH	21:00-06:00	[95]
3	/	02:00-06:00	[86]	14	2-4 ACH	02:00-07:00	[96]
4	Depending on the location, PCM case and outdoor temperatures	/	[87]	15	Daytime: 0.7 ACH and Daytime and nighttime (when air temperature over 23 °C): 1.5 ACH, 3 ACH, 7 ACH, and 14 ACH	/	[97]
5	8 ACH	19:00-07:00	[88]	16	10, 20 and 30 ACH	24:00-07:00	[98]
6	/	19:00-07:00	[89]	17	Daily: 0.5 ACH and nighttime: 3 ACH	19:00-07:00	[99]
NATURAL AND MECHANICAL				18	1.5 ACH	18:00-08:00	[100]
7	0.76 ACH mechanical	Windows: 19:00-07:00	[54]	19	According to the set point	17:00-07:00	[101]
8	1 m ³ /s (2 ACH), 0.16 m ³ /s (3 ACH), 0.26 m ³ /s (5 ACH), 0.37 m ³ /s (7 ACH) and 0.53 m ³ /s (10 ACH)	00:00-07:00	[90]	20 and 21	During the day: 2 ACH and during the night: 0 ACH, 10 ACH, 20 ACH, 30 ACH and 40 ACH	Daytime: 8:00-18:00 and nighttime: 18:00-08:00	[102] and [103]
9	Natural: 2 ACH and 10 ACH and mechanical: 0 to 40 ACH	/	[91]	22	5 ACH to 10 ACH	Melting periods of 3 h, 5 h, 7 h and 9 h	[104]
10	Inlet wind direction are 0.5 m/s, 1 m/s, 2 m/s	21:00-04:00	[92]	23	Background ventilation rate: 6 m ³ /(m ² h)	00:00-07:00	[105]
11	Mechanical ventilation: 0.5 ACH, 1.5 ACH, 3 ACH and 6 ACH	Natural: 21:00-06:00 and mechanical 19:00-24:00	[93]	24	3 ACH	21:00-07:00	[106]
				25	8 ACH	/	[107]

* data not specified (/)

A.2 Discussion

The most important parameter of the PCM performance in building is the melting temperature of the material. It should be selected carefully with consideration of location and its climate conditions. Regarding this fact, a careful optimization of the PCM based on the location should be performed. A significant effect on the energy cooling demand is obtained when using natural or mechanical ventilation. In both cases, ventilation control

strategy (window opening schedule, temperature set point etc.) significantly affect the energy performance of the system. Due to high amount of PCM material in buildings, environmentally friendly and sustainable materials should be used.

The majority of the researched studies tested the PCM systems for cooling application in hot arid – mild climate types. In comparison to the total volume ventilation systems, the melting temperatures in local ventilation systems are generally lower.

A.2.1 Numerical simulation tools

Most of the total volume ventilation studies were performed with unsteady state building simulation EnergyPlus or DesignBuilder tools. Their application is suitable for the building level energy analysis and as a result determines the yearly energy use and indoor operative temperatures. While DesignBuilder with geometry modelling interface is more user-friendly compared to EnergyPlus tool alone, it has some limitations. For example, the previous versions couldn't calculate hysteresis in PCM and thus, the calculated results of the indoor operative temperatures and additional energy required for cooling were less accurate. TRNSYS is enabling a very accurate mechanical component calculation with accurately adaptable PCM properties. However, it is less practical for the calculation with the building geometry. Also, ANSYS Fluent and COMSOL allow a very accurate PCM properties input. The results of the temperature distribution are very detailed. However, their usage is more appropriate for a building element/component-level performance calculation since they don't directly calculate the energy performance of the building or system. GenOpt serves as an optimisation tool used for optimization of the selected parameter, such as melting temperature or thickness of the PCM. It may be coupled with EnergyPlus.

A.2.2 Economic analysis

The economic feasibility of PCM application depends on the energy savings calculation, costs related to the PCM material, energy prices and discount rates. Even though the PCM prices significantly dropped in last 5 years, the studies evaluating the economic feasibility of PCM systems integrated in building still report their application to economically insufficient.

For example, Kharbouch et al. investigated the economic feasibility with thermal energy potentials of a building integrated PCM family house coupled with air-conditioning system in different climate zones in Morocco [161]. Using EnergyPlus and GenOpt they obtained optimum design strategies and building energy use. Based on the optimized results of cost-effectiveness it was concluded, that the economic feasibility of PCM is stilling insufficient with regard to the actual PCM market. The payback period was estimated to 44-75 years, depending on the city.

Furthermore, Mi et al. determined the static and dynamic payback period, where they estimated the cost of purchasing and installing PCMs to 2 USD/m² for a 10 mm thick layer of PCM [170]. It was determined that the static payback period of PCM system located in Hong Kong was the shortest (52.91 years). Based on the calculated energy savings and assumed service life of PCM (35 years), the investment paid back only during the summer

operation. The rest of the cases located in other Chinese cities showed economically non-feasible results.

Moreover, Souayfane et al. under different climate types investigated a passive PCM system combining transparent insulation material and PCM (TIM-PCM wall) positioned on the envelope [162]. It was shown that in some climates, such as polar and subarctic climates, the payback of the system is adequate: 10.5 years and 7.8 years, respectively. However, in other climates (continental, Mediterranean or Humid continental climate) the investment was unfeasible. The estimations of prices of PCM and their installation largely vary depending on the material. The installation costs may be estimated to 4.36 €/m², while the material price normally variates between 0.22 USD/kg to 53.9 USD/kg (majority of the PCM for building application do not exceed 20 USD/kg).

Table 0.2 and Table 0.3 summarise the presented studies in Chapter 3 of this dissertation.

Table 0.2: The research summary of the nighttime ventilation studies.

#	PCM	Phase change temperature (T_{mp} , T_{ms} and T_r) [$^{\circ}\text{C}$] and enthalpy [kJ/kg]	PCM type	Location	Method	Author	Reference
1	Rubitherm RT24	$T_{mp} = 24^{\circ}\text{C}$ (21–25 $^{\circ}\text{C}$); 160 kJ/kg	organic	15 locations with arid or warm temperate climate	Numerical: Energy Plus v8.9 and Gen Opt v3.1.1	Prabhakar et al.	[56]
2	Experiment: DuPont Energain [®] and simulation: BioPCM [™]	DuPont Energain [®] : $T_{mp} = 21.7^{\circ}\text{C}$; 121 kJ/kg (plate: 70 kJ/kg) BioPCMs: $T_{mp} = 21^{\circ}\text{C}$, 23°C , 25°C , 27°C and 29°C ; 200 kJ/kg	organic and fatty-acid-based organic	Tehran, Iran	Simulation (Ecotect 2011 and EnergyPlus V.8.) and experiment (outdoor climatic and calorimetric box)	Memarian et al.	[85]
3	Knauf PCM SmartBoard	$T_{mp} = 23^{\circ}\text{C}$; 23°C – 26°C , 110 kJ/kg	organic	Palermo, Naples, Rome, and Milan, Italy	EnergyPlus v8.4	Piselli et al.	[86]
4	BioPCM [™] 19-33 $^{\circ}\text{C}$	$T_{mp} = 19^{\circ}\text{C}$, 21°C , 23°C , 25°C , 27°C , 29°C , 31°C and 33°C ; 219 kJ/kg	organic	Altay, Urumqi, Turpan, Xi'an, Chengdu, Chongqing, Guiyang, Kunming, Hechi, and Nanning, China	EnergyPlus 8.7	Liu et al.	[87]
5	Simulated fictive material: PCM 26, PCM 28, PCM 30 and PCM 32; Simulated commercial PCM: Rubitherm RT21, RT24, RT26, RT28 and RT31	$T_{mp} = 26^{\circ}\text{C}$, 28°C , 30°C , and 32°C ; 219 kJ/kg; 155 kJ/kg, 160 kJ/kg, 180 kJ/kg, 250 kJ/kg, 165 kJ/kg	organic	Nur Sultan, Karaganda, Kokshetau, Almaty, Aktobe, and Atyrau, Kazakhstan	Design Builder	Adilkhanova et al.	[88]
6	BioPCM [™] Q25	$T_{mp} = 25^{\circ}\text{C}$, 219 kJ/kg	fatty-acid-based organic	Melbourne, Australia	EnergyPlus V8.3.	Jamil et al.	[89]
7	DuPont Energain [®] and BioPCM [™] Q25 M51	DuPont Energain [®] : $T_{mp} = 21.7^{\circ}\text{C}$; 121 kJ/kg (plate: 70 kJ/kg) BioPCM [™] : $T_{mp} = 25^{\circ}\text{C}$, 200 kJ/kg	organic and fatty-acid-based organic	Riga, Latvia	Experiment and WUFI+ modelling program	Sinkaet al.	[54]
8	DuPont Energain [®] BioPCM [™] Q25	DuPont Energain [®] : $T_{mp} = 21.7^{\circ}\text{C}$; 121 kJ/kg (plate: 70 kJ/kg) BioPCM [™] Q25: 25°C , 200 kJ/kg	organic and fatty-acid-based organic	Toronto, Canada	Experiment and simulation	Berardi and Soudian	[90]

9	PureTemp PT20	$T_{mp} = 20\text{ }^{\circ}\text{C}$; 180 kJ/kg	fatty-acid-based organic	Auckland, New Zealand	mathematic model	Bai et al.	[91]
10	Self-prepared paraffin	$T_r = 22\text{--}24\text{ }^{\circ}\text{C}$; 189 kJ/kg	organic	Beijing, China	Meteorological Data Producer for HVAC Analysis and Designer's Simulation Toolkit	Xiang and Zhou	[92]
11	Infinite R™	$T_{mp} = 18\text{ }^{\circ}\text{C}$, 19 °C, 20 °C, 21 °C, 22 °C, 23 °C, 24 °C, 25 °C, 26 °C, 27 °C, 28 °C and 29 °C; 190 kJ/kg.	inorganic	Agadir, Marrakech, Tangier, Fes, Ifrane, and Errachidia, Morocco	Design Builder V6.1.6.005	Mechouet et al.	[93]
12	PCM-impregnated gypsum boards; Pure Temp PT20°C	$T_{mp} = 20\text{ }^{\circ}\text{C}$; 180 kJ/kg	fatty-acid-based organic	Auckland, New Zealand	Experiment	Barzin et al.	[94]
13	Aluminium honeycomb matrix containing 60 %wt Micronal T23®	Micronal®: $T_{mp} = 27.6\text{ }^{\circ}\text{C}$ (22-28.5 °C); Fictive: 23.6 °C, 24.6 °C, 25.6 °C, 26.6 °C and 28.6 °C	organic	Chambéry, France and Catania, Italy	EnergyPlus v7.0	Evola et al.	[95]
14	BioPCM™ Q23, Q25 and Q27; M27 and M51	$T_{mp} = 23\text{ }^{\circ}\text{C}$, 25 °C and 27 °C; 200 kJ/kg	organic and fatty-acid-based organic	Southern Europe (Rome, Italy), Continental Europe (Vienna, Austria) and Northern Europe (London, UK)	EnergyPlus	Costanzo et al.	[96]
15	Gypsum PCM board and clay PCM board	$T_{mp} = 23\text{ }^{\circ}\text{C}$, 25 °C and 27 °C; 12652 J/kg	/	Helsinki, Finland, Vienna, Austria, and Madrid, Spain	Energy Plus with finite element method	Pajek et al.	[97]
16	/	$T_{mp} = 19\text{ }^{\circ}\text{C}$, 20 °C, 21 °C, 22°C, 23 °C, 24 °C, 25°C, 26°C, 27°C, 28°C and 29 °C; n.a. enthalpy	/	Phoenix, Arizona, USA and Yazd, Iran	Simulation: EnergyPlus 8.1	Solgi et al.	[98]
17	PCM plaster	$T_{mp} = 26\text{ }^{\circ}\text{C}$, 27 °C, 28 °C and 29 °C; 110 kJ/kg	/	Ankara, Turkey, Athens, Greece, Naples, Italy, Marseille, France, and Seville, Spain.	Simulation: EnergyPlus 7.2.0	Ascione et al.	[99]
18	PCM29	$T_{mp} = 29\text{ }^{\circ}\text{C}$; /	/	Athens, Thessaloniki, and Heraklion, Greece	DesingBuilder 4.0	Karaoulis	[100]
19	BioPCM M182/Q29	$T_{mp} = 29\text{ }^{\circ}\text{C}$, 200 kJ/kg	fatty-acid-based organic	Putrajaya, Malaysia	DesingBuilder	Nazi et al.	[101]

20	/	$T_{mp} = 24\text{ }^{\circ}\text{C}$, 26 $^{\circ}\text{C}$ and 28 $^{\circ}\text{C}$; 100 kJ/kg, 120 kJ/kg, 140 kJ/kg 160 kJ/kg and 180 kJ/kg	/	Beijing, China	Mathematical model	Zhou et al.	[102]
21	/	$T_{mp} = 24\text{ }^{\circ}\text{C}$, 26 $^{\circ}\text{C}$ and 28 $^{\circ}\text{C}$; 100 kJ/kg, 120 kJ/kg, 140 kJ/kg 160 kJ/kg and 180 kJ/kg	/	Beijing, China	Mathematical model	Zhou et al.	[103]
22	DuPont Energain Bio PCMQ25	DuPont Energain [®] : $T_{mp} = 21.7\text{ }^{\circ}\text{C}$; 121 kJ/kg (plate: 70 kJ/kg) BioPCM [™] : $T_{mp} = 25\text{ }^{\circ}\text{C}$, 200 kJ/kg	organic and fatty-acid-based organic	Toronto, Canada and New York, U.S.A.	EnergyPlus	Soudian and Berardi	[104]
23	Hexadecane, Heptadecane, Dodecanol and Octadecane	Hx: $T_{mp} = 20\text{ }^{\circ}\text{C}$; 281 kJ/kg, Hp: $T_{mp} = 21\text{ }^{\circ}\text{C}$; 230 kJ/kg, Do: $T_{mp} = 24\text{ }^{\circ}\text{C}$; 235 kJ/kg and Oc: $T_{mp} = 29\text{ }^{\circ}\text{C}$; 267 kJ/kg	organic	Seoul, South Korea	EnergyPlus 6.0	Seong et al.	[105]
24	DuPont Energain, BioPCM [™] 23, Natural TCM Energy Saver [®] and Paraffin/LDPE/EVA	$T_{ms} = 21.7\text{ }^{\circ}\text{C}$; 121 kJ/kg (plate: 70 kJ/kg), $T_{mp} = 23\text{ }^{\circ}\text{C}$; 182.5 kJ/kg, $T_r = 15\text{-}31\text{ }^{\circ}\text{C}$; 107.3 kJ/kg and $T_{ms} = 19\text{ }^{\circ}\text{C}$; 45 kJ/kg	organic, fatty-acid-based organic and organic	Lijiang, Weifang, Wuhan, Hohhot, Yan'an, and Guangzhou, China	EnergyPlus v8.7	Qu et al.	[106]
25	Infinite-R [™] 29	$T_{mp} = 29\text{ }^{\circ}\text{C}$; 200 kJ/kg and fictive: 30 $^{\circ}\text{C}$, 28 $^{\circ}\text{C}$ and 27 $^{\circ}\text{C}$	inorganic	Penang Island, Malaysia	DesignBuilder v6.1	Al-Absi et al.	[107]

Table 0.3: The research summary of the ventilated building element studies.

#	PCM	Phase change temperature (T_{mp} , T_{ms} and T_r) [$^{\circ}$ C] and enthalpy [kJ/kg]	PCM type	Location	Method	Active/passive	Author	Reference
PCM improved ventilated Roofs								
1	PCM 1: 48.23wt %: 51.77wt % Composite: expanded vermiculite + PCM = PCM particles; PCM particles + acrylate copolymer emulsion; PCM 2: eutectic mixture of TD and MA	PCM 1: $T_{mp} = 32^{\circ}$ C; 131.43 kJ/kg PCM 2: $T_{mp} = 24^{\circ}$ C; 167.571 kJ/kg	eutectic	Tianjin (China)	Experimental and numerical	Passive/active	Hou et al and Li et al.	[108], [109]
2	Lab test: PlusICE TM S22 Numerical: Rubitherm SP24E	S22: $T_{mp} = 22^{\circ}$ C; 215 kJ/kg SP24E $T_r = 21-25^{\circ}$ C; 190 kJ/kg	inorganic	Sydney (Australia)	Numerical TRNSYS and test for validation	External ventilated layer: passive Internal ventilated layer: active	Lin et al.	[111]
PCM improved ventilated Ceilings								
3	PlusICE TM S27	$T_{mp} = 27^{\circ}$ C; 185 kJ/kg	inorganic	Tehran (Iran)	Experiment and validation with DesignExpert [®] 7.0.0 for determination of optimum conditions	Active/passive	Alizadeh and Sadrameli	[112]
4	Rubitherm RT21	$T_{mp} = 21^{\circ}$ C; 134 kJ/kg	organic	Lleida (Spain)	Numerical: ‘Design builder’	Active	Navarro et al.	[113]
5	Self-developed fatty acid	$T_{mp} = 25^{\circ}$ C (22-26 $^{\circ}$ C); 190 kJ/kg	organic	Beijing (China)	Experiment and mathematical model	Passive day, active night	Yanbig et al.	[114]
6	Salt Na ₂ SO ₄ ·10H ₂ O, with added borax nucleating agent (1.5 %)	$T_{mp} = 21^{\circ}$ C, 198 kJ/kg	inorganic	Nottingham (UK)	Experimental results and model predictions	Active	Turnpenny et al.	[115]
7	SP26E (and fictive melting temperature peaks 30 $^{\circ}$ C, 28 $^{\circ}$ C, 26 $^{\circ}$ C and 24 $^{\circ}$ C)	$T_{mp} = 26^{\circ}$ C; 140 to 180 kJ/m ² for a layer of 15 mm	inorganic	Seville (Spain)	Validated with experiment TRNSYS v18	Passive/active	Lizana et al.	[116]
8	CSM DELTA [®] -COOL 24 (plastic - DELTA [®] -COOL board and metal CSM cases)	$T_{mp} = 24^{\circ}$ C (22-28 $^{\circ}$ C); 158 kJ/kg	inorganic	Munich (Germany)	Experiment	Active/passive daytime	Weinläder et al.	[117]
9	/	$T_{mp} = 25^{\circ}$ C, 26 $^{\circ}$ C, 27 $^{\circ}$ C and 28 $^{\circ}$ C; 200 kJ/kg	/	Shanghai (China)	Energy Plus	Passive and active	Jiao and Xu	[118]

10	Pure Temp 23 (PT23); pure mPCMs with TPC of 18 °C, 19 °C, 20 °C and 21 °C	$T_{mp} = 23$ °C; 227 kJ/kg (and 18 °C, 19°C, 20 °C and 21 °C)	Organic fatty acid-based	Sydney (Australia)	Validated numerical model ANSYS Fluent	Active	Faheem et al.	[119]
11	Paraffin wax and high-density polyethylene	$T_i = 31-33$ °C, 34–36 °C, 36–38 °C, 34–36 °C and 29–31 °C; 200 kJ/kg	organic	Five representative climate regions of China: Harbin, Beijing, Wuhan, Guangzhou and Kunming	ANSYS Fluent	Passive - day; active fan - nights	Yu et al.	[120]
12	DuPont Energain™	DuPont Energain®: $T_{ms} = 21.7$ °C; 121 kJ/kg (plate: 70 kJ/kg)	organic	Montreal (Canada)	Simulation EnergyPlus	active	Morovat et al.	[121]
13	Rock wool board with addition of microcapsulated PCM	$T_{mp} = 24.5$ °C; 174.4 kJ/kg	/	Tokyo (Japan)	Experiment	Active/passive by day	Kodo and Ibamoto	[122]
14	Gypsum-PCM composite mixed with BASF Micronal DS-5008, 30 % wt of PCM	$T_{mp} = 23.5$ °C; 102.6 kJ/kg (gypsum)	organic	Central Poland	Experimental	active	Jaworski	[123]
PCM improved ventilated Floor								
15	Foamed glass beads and granulated paraffin waxes: hexadecane and octadecane	$T_{mp} = 20$ °C; 201, 202 and 121 kJ/kg Mixed, sample 1 and sample 2 in ratio s1:s2=3:7	Organic eutectic	Tokyo (Japan)	active	experimental	Nagano et al.	[124]
16	Eutectic mixture of saturated hydrocarbon derivatives (paraffinic hydrocarbon or paraffin, C_nH_{2n+2}) with anticorrosive additives, preservatives and colourants	$T_{mp} = 23$ °C; 188 kJ/kg	eutectic	Madrid (Spain), Washington (U.S.) and Beijing (China)	passive	experimental	González et al.	[125]
PCM improved ventilated Internal Walls								
17	Micronal T23® in thin wallboards; 60 % of	Micronal®: $T_{mp} = 27.6$ °C (22-28.5 °C); 100 kJ/kg (PCM)	organic	Catania (Italy)	simulations performed with EnergyPlus 7.0	Active/passive	Evola et al.	[126]
18	DuPont Energain	DuPont Energain®: $T_{ms} = 21.7$ °C; 121 kJ/kg (plate: 70 kJ/kg)	paraffin	-	Experimental and numerical study	Active	Dermadimos et al.	[127], [128]
PCM improved ventilated Façades								

19	/	$T_r = 18-26$ °C; 216 kJ/kg	inorganic	Chengdu (China)	passive	EnergyPlus	Wang et al.	[129]
20	Rubitherm SP22	$T_{mp} = 22$ °C; 150 kJ/kg	Inorganic	Puigverd de Lleida (Spain)	Experiment and numerical model	Active/passive; night free cooling; ventilated wall	de Gracia et al.	[130]
21	Rubitherm SP22	$T_{mp} = 22$ °C; 150 kJ/kg	inorganic	21 locations around the world covering A- D climate classes	Simulation and experiment	Active; ventilated facade	de Gracia et al.	[132]
22	Rubitherm SP22	$T_p = 22$ °C; 150 kJ/kg	inorganic	21 locations around the world covering A- D climate classes	Simulation and experiment	Active; ventilated facade	de Gracia et al.	[133]
23	Paraffin and styrene- type polymer	$T_{mp} = 27$ °C; 179 kJ/kg (after adding it 15 % polymer 110 kJ/kg)	organic	-	Experiment and numerical study with COMSOL Multiphysics, thermal modelling by electrical analogy and Matlab Simscape tool	Passive -day; active fan - night	Laaouatni et al.	[134]
24	Rubitherm RT35	$T_{mp} = 35$ °C; 135 kJ/kg	organic	Vitoria- Gasteiz (Spain)	Experiment in PASILINK facility and Design Builder simulation	active	Diarce et al.	[135]
25	Rubitherm RT35	$T_{mp} = 35$ °C; 135 kJ/kg	organic	Vitoria- Gasteiz, Basque Country, (Spain)	ANSYS Fluent	active	Diarce et al.	[136]
26	CaCl ₂ ·6H ₂ O	$T_{mp} = 22$ °C; 26°C; 176 kJ/kg	inorganic	Changsha (China)	Mathematical model	Active	Zhou et al.	[137]
27	CaCl ₂ ·6H ₂ O	$T_{mp} = 22$ °C; 26°C; 176 kJ/kg	inorganic	Changsha (China)	Mathematical model	Active	Zhou et al.	[138]
28	CaCl ₂ ·6H ₂ O	$T_{mp} = 22$ °C; 26°C; 176 kJ/kg	inorganic	Changsha (China)	Mathematic model	active	Zhou et Zheng	[139]

29	/	$T_{mp} = 24\text{ }^{\circ}\text{C}$ (+-2 $^{\circ}\text{C}$); 218 kJ/kg	/	Athens (Greece), Madrid (Spain), Paris (France), Gdansk (Poland) and Stockholm (Sweden)	TRNSYS and Matlab	Active	Diallo et al.	[140]
30	Crystalline hydrate and organic PCM	$T_{mp} = 25^{\circ}\text{C}$; 160 kJ/kg	Eutectic	Hefei City (China)	Experiment	Passive	Luo et al.	[141]
31	PCM wallboard	$T_{mp} = 30\text{ }^{\circ}\text{C}$ and 18 $^{\circ}\text{C}$, 200 kJ/kg and 190 kJ/kg	/	Wuhan (China)	TRNSYS	passive	Zhu et al.	[142]
PCM improved ventilated Glazing Elements								
32	Rubitherm PX35 powder mixed with epoxy resin material; mixing ratio of 75 wt % PCM and inorganic carrier matrix	$T_{mp} = 35\text{ }^{\circ}\text{C}$ (26–40 $^{\circ}\text{C}$); 100 kJ/kg (composite: 77.8 kJ/kg)	Eutectic (organic and inorganic)	Ningbo (China)	ANSYS Fluent and experiment	Passive/active	Li et al.	[144]
33	Mixture of fiber (50 %) and paraffin wax (50 %)	$T_{mp} = 22\text{ }^{\circ}\text{C}$; 115.2 kJ/kg	organic	Copenhagen (Denmark)	Experiment and Comsol	active	Hu and Heiselberg	[145]
34	Mixture of fiber (50 %) and paraffin wax (50 %)	$T_{mp} = 21.5\text{ }^{\circ}\text{C}$; 115.2 kJ/kg	organic	Alborg (Denmark)	full-scale experiment and EnergyPlus	active	Hu et al.	[146]
35	RUBITHERM RT30	$T_r = 25\text{--}30\text{ }^{\circ}\text{C}$; n.a.	organic	Ljubljana (Slovenia)	Fortran	passive	Stritih	[143]
PCM improved ventilated walls with BiPV								
36	Rubitherm RT27	$T_{mp} = 26.5^{\circ}\text{C}$; 189 kJ/kg	organic	Brno (Czech Republic)	experiment	passive	Čurpek and Čekon	[147]
37	Rubitherm RT25, n-octadecane and capric acid	RT25: $T_{mp} = 26.6\text{ }^{\circ}\text{C}$; 232 kJ/kg n-oc.: $T_{mp} = 28.2\text{ }^{\circ}\text{C}$; 245 kJ/kg ca. ac.: $T_{mp} = 32\text{ }^{\circ}\text{C}$; 152.7 kJ/kg	organic	Arlington (Virginia, USA)	COMSOL Multiphysics 5.0 software	-	Kent et al.	[148]

Appendix B: Remaining full-scale numerical model results

Figure 0.1 shows the results obtained with PCM with melting temperature of 23 °C.

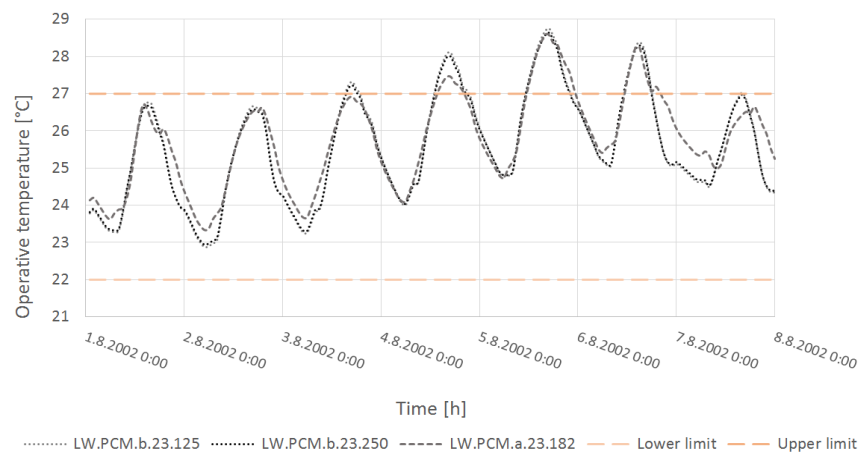


Figure 0.1: PCM with melting temperature of 23 °C.

Figure 0.2 shows the results obtained with PCM with melting temperature of 25 °C.

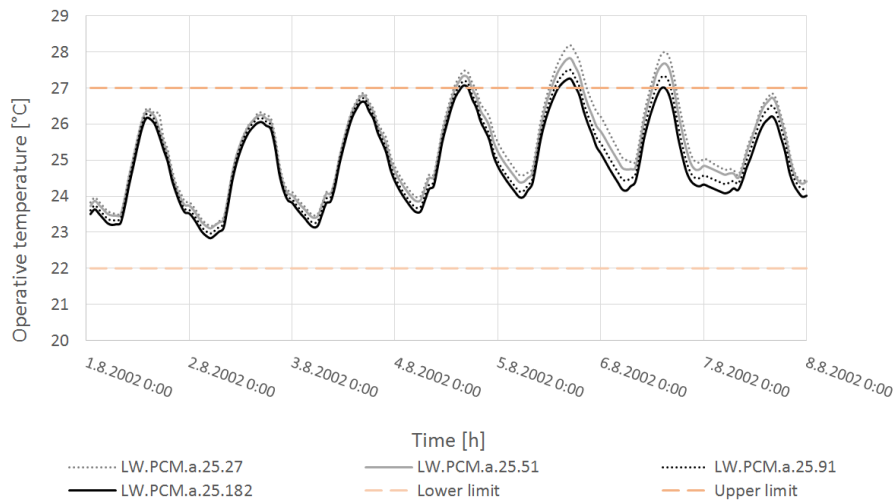


Figure 0.2: PCM with melting temperature of 25 °C.

Figure 0.3 shows the Average daily temperatures subtracted from the upper limit of thermal comfort 26 °C. The green cells present the overheated days.

DATE (13 - 17 h)	LW	LW.PCM	LW.PCM	LW.PCM	LW.PCM	LW.PCM	LW.PCM	LW.PCM	LW.PCM	LW.PCM	LW.PCM	LW.PCM	LW.PCM	LW.PCM	LW.PCM	LW.PCM
		b.23.125	b.23.250	b.25.125	b.25.250	a.23.182	a.24.27	a.24.51	a.24.91	a.24.182	a.25.27	a.25.51	a.25.91	a.25.182	a.26.182	a.27.182
01-Aug	-0.5	-0.6	-0.5	-0.4	-0.4	-0.6	0.0	0.2	0.4	0.4	-0.5	-0.4	-0.3	-0.2	-0.3	-0.5
02-Aug	-0.4	-0.4	-0.4	-0.3	-0.3	-0.3	0.0	0.2	0.3	0.4	-0.4	-0.4	-0.3	-0.2	-0.2	-0.5
03-Aug	-0.4	-0.4	-0.4	-0.3	-0.3	-0.5	0.0	0.3	0.4	0.5	-0.3	-0.3	-0.2	-0.1	-0.1	-0.4
04-Aug	-0.7	-0.7	-0.7	-0.4	-0.5	-0.5	0.1	0.4	0.5	0.6	-0.4	-0.3	-0.2	-0.1	0.1	-0.5
05-Aug	-1.0	-1.0	-1.0	-0.6	-0.8	-0.9	0.0	0.4	0.8	0.9	-0.6	-0.4	-0.1	0.0	0.2	-0.6
06-Aug	-0.9	-0.9	-0.9	-0.5	-0.7	-0.8	0.0	0.6	1.0	1.2	-0.6	-0.4	0.0	0.2	0.9	-0.4
07-Aug	-0.2	-0.2	-0.2	-0.3	-0.2	0.2	0.2	0.6	1.0	1.1	-0.2	-0.1	0.1	0.3	0.6	-0.3

Figure 0.3: Average daily temperatures subtracted from the upper limit of thermal comfort 26 °C.

Appendix C: Detailed sketch of pre-experimental set-up

Figure 0.4 shows the detailed sketch of pre-experimental set-up.

Appendix D: ANSYS Fluent calculation parameters

PRELIMINARY NUMERICAL MODEL (DESCRIBED IN CHAPTER 5.3)

Fluent

Version: 2d, dp, pbns, lam, transient (2d, double precision, pressure-based, laminar, transient)

Release: 19.1.0

Title:

Models

Model	Settings
Space	2D
Time	Unsteady, 1st-Order Implicit
Viscous	Laminar
Heat Transfer	Enabled
Solidification and Melting	Disabled
Radiation	None
Species	Disabled
Coupled Dispersed Phase	Disabled
NOx Pollutants	Disabled
SOx Pollutants	Disabled
Soot	Disabled
Mercury Pollutants	Disabled

Material Properties

Material: pcm-rt24-solid (solid)

Property	Units	Method	Value(s)
----------	-------	--------	----------

 Density kg/m3 constant 800
 Cp (Specific Heat) j/kg-k polynomial (278 6000) (289 8000) (290 9000) (291
 10000) (292 13000) (293 16000) (294 19000) (295 31000) (296 36000) (297 2000) (298
 2000) (318 2000)
 Thermal Conductivity w/m-k constant 0.2

Material: pcm-sp252e-solid (solid)

Property	Units	Method	Value(s)
----------	-------	--------	----------

 Density kg/m3 constant 1500
 Cp (Specific Heat) j/kg-k polynomial (278 3000) (289 3000) (290 4000) (291
 5000) (292 7000) (293 8000) (294 9000) (295 22000) (296 71000) (297 41000) (298 3000)
 (299 3000) (318 3000)
 Thermal Conductivity w/m-k constant 0.5

Material: pcm-solid-sp24e-plus (solid)

Property	Units	Method	Value(s)
----------	-------	--------	----------

 Density kg/m3 constant 1450
 Cp (Specific Heat) j/kg-k polynomial (280 2000) (291 2000) (291.5 2500) (292
 3000) (292.5 4500) (293 6000) (293.5 10000) (294 14000) (294.5 29000) (295 44000)
 (295.5 80500) (296 117000) (296.5 59500) (297 2000) (297.5 2000) (298 2000) (310
 2000)
 Thermal Conductivity w/m-k constant 0.5

Material: pcm-rt22hc-solid-plus (solid)

Property	Units	Method	Value(s)
----------	-------	--------	----------

 Density kg/m3 constant 730
 Cp (Specific Heat) j/kg-k polynomial (270 300) (287 5000) (288 5000) (289 6000)
 (290 9000) (291 13000) (292 15000) (293 23000) (294 29000) (295 46000) (296 42000)
 (296.5 22500) (297 3000) (298 3000) (299 2000) (310 2000)
 Thermal Conductivity w/m-k constant 0.2

Material: pcm-rt22hc-solid (solid)

Property	Units	Method	Value(s)
----------	-------	--------	----------

Density kg/m3 constant 730
 Cp (Specific Heat) j/kg-k polynomial (287 5000) (288 5000) (289 6000) (290 9000) (291 13000) (292 15000) (293 23000) (294 29000) (295 46000) (296 42000) (297 3000) (298 2000) (299 2000) (300 2000)
 Thermal Conductivity w/m-k constant 0.2

Material: pcm-rt22hc-solid-and-melt (solid)

Property	Units	Method	Value(s)
----------	-------	--------	----------

Density	kg/m3	constant	730
Cp (Specific Heat)	j/kg-k	polynomial	(287 5000) (288 4000) (289 5500) (290 8500) (291 11000) (292 15500) (293 22500) (294 33000) (295 48500) (296 30000) (297 4500)
Thermal Conductivity	w/m-k	constant	0.2

Material: air (fluid)

Property	Units	Method	Value(s)
----------	-------	--------	----------

Density	kg/m3	boussinesq	1.1799999
Cp (Specific Heat)	j/kg-k	constant	1006.43
Thermal Conductivity	w/m-k	constant	0.0242
Viscosity	kg/m-s	constant	1.7894001e-05
Molecular Weight	kg/kmol	constant	28.966
Thermal Expansion Coefficient	1/k	constant	0.0035999999
Speed of Sound	m/s	none	#f

Material: aluminum (solid)

Property	Units	Method	Value(s)
----------	-------	--------	----------

Density	kg/m3	constant	2719
Cp (Specific Heat)	j/kg-k	constant	871
Thermal Conductivity	w/m-k	constant	202.4

Cell Zone Conditions

Zones

name	id	type
part_2_mesh_5_mm_-surface_body_mesh_5_mm_	3	solid
fluid-part_2_mesh_5_mm_-surface_body_mesh_5_mm_	4	fluid

Setup Conditions

part_2_mesh_5_mm_-surface_body_mesh_5_mm_

Condition Value

Material Name pcm-sp252e-solid

Frame Motion? no

Mesh Motion? no

fluid-part_2_mesh_5_mm_-surface_body_mesh_5_mm_

Condition Value

Frame Motion? no

Mesh Motion? no

Boundary Conditions

Zones

name	id	type
outlet_mesh_5_mm_	8	outflow
inlet_mesh_5_mm_	7	velocity-inlet
wall-part_2_mesh_5_mm_-surface_body_mesh_5_mm_	9	wall
wall-part_2_mesh_5_mm_-surface_body_mesh_5_mm_.1	10	wall
wall-part_2_mesh_5_mm_-surface_body_mesh_5_mm_.2	11	wall
wall-part_2_mesh_5_mm_-surface_body_mesh_5_mm_.1-shadow	6	wall

Setup Conditions

outlet_mesh_5_mm_

Condition Value

inlet_mesh_5_mm_

Condition Value

Velocity Magnitude (m/s) 0.1

Temperature (profile udf unsteady_temperature)

wall-part_2_mesh_5_mm_-surface_body_mesh_5_mm_

Condition Value

Thermal BC Type 1

wall-part_2_mesh_5_mm_-surface_body_mesh_5_mm_.1

Condition	Value

Thermal BC Type	3

wall-part_2_mesh_5_mm_-surface_body_mesh_5_mm_.2

Condition	Value

Thermal BC Type	1
Wall Motion	0
Shear Boundary Condition	0

wall-part_2_mesh_5_mm_-surface_body_mesh_5_mm_.1-shadow

Condition	Value

Thermal BC Type	3
Wall Motion	0
Shear Boundary Condition	0

Solver Settings

Equations

Equation	Solved

Flow	yes
Energy	yes

Numerics

Numeric	Enabled

Absolute Velocity Formulation	yes

Unsteady Calculation Parameters

Time Step (s)	120
Max. Iterations Per Time Step	400

Relaxation

Variable	Relaxation Factor

Pressure 0.3
 Density 1
 Body Forces 1
 Momentum 0.7
 Energy 1

Linear Solver

Variable	Solver Type	Termination Criterion	Residual Reduction Tolerance
Pressure	V-Cycle	0.1	
X-Momentum	Flexible	0.1	0.7
Y-Momentum	Flexible	0.1	0.7
Energy	F-Cycle	0.1	

Pressure-Velocity Coupling

Parameter	Value
Type	SIMPLE

Discretization Scheme

Variable	Scheme
Pressure	Second Order
Momentum	Second Order Upwind
Energy	Second Order Upwind

Solution Limits

Quantity	Limit
Minimum Absolute Pressure	1
Maximum Absolute Pressure	5e+10
Minimum Temperature	1
Maximum Temperature	5000

NUMERICAL MODEL (DESCRIBED IN CHAPTER 7)

Fluent

Version: 2d, dp, pbns, skw, transient (2d, double precision, pressure-based, standard k-omega, transient)

Release: 19.1.0

Title:

Models

Model	Settings
Space	2D
Time	Unsteady, 1st-Order Implicit
Viscous	Standard k-omega turbulence model
Heat Transfer	Enabled
Solidification and Melting	Disabled
Radiation	None
Species	Disabled
Coupled Dispersed Phase	Disabled
NOx Pollutants	Disabled
SOx Pollutants	Disabled
Soot	Disabled
Mercury Pollutants	Disabled

Material Properties

Material: pcm-solid-sp24e-plus-new-red-density (solid)

Property	Units	Method	Value(s)
Density	kg/m3	constant	816
Cp (Specific Heat)	j/kg-k	polynomial	(280 2000) (291 2000) (291.5 2500) (292 3000) (292.5 4500) (293 6000) (293.5 10000) (294 14000) (294.5 29000) (295 44000) (295.5 80500) (296 117000) (296.5 59500) (297 2000) (297.5 2000) (298 2000) (310 2000)
Thermal Conductivity	w/m-k	constant	0.5

Material: pcm-solid-sp24e-plus-new (solid)

Property	Units	Method	Value(s)
Density	kg/m3	constant	1450

Cp (Specific Heat) j/kg-k polynomial (280 2000) (291 2000) (291.5 2500) (292 3000) (292.5 4500) (293 6000) (293.5 10000) (294 14000) (294.5 29000) (295 44000) (295.5 80500) (296 117000) (296.5 59500) (297 2000) (297.5 2000) (298 2000) (310 2000)

Thermal Conductivity w/m-k constant 0.5

Material: pcm-solid-sp24e-melting (solid)

Property	Units	Method	Value(s)
Density	kg/m3	constant	1400
Cp (Specific Heat)	j/kg-k	polynomial	(294 7000) (295 9000) (296 18000) (297 150000) (298 6000)
Thermal Conductivity	w/m-k	constant	0.5

Material: pcm-solid-sp24e (solid)

Property	Units	Method	Value(s)
Density	kg/m3	constant	1500
Cp (Specific Heat)	j/kg-k	polynomial	(293 6000) (294 14000) (295 44000) (296 117000) (297 2000)
Thermal Conductivity	w/m-k	constant	0.5

Material: air (fluid)

Property	Units	Method	Value(s)
Density	kg/m3	boussinesq	1.1799999
Cp (Specific Heat)	j/kg-k	constant	1006.43
Thermal Conductivity	w/m-k	constant	0.0242
Viscosity	kg/m-s	constant	1.7894001e-05
Molecular Weight	kg/kmol	constant	28.966
Thermal Expansion Coefficient	1/k	constant	0.00336
Speed of Sound	m/s	none	#f

Material: aluminum (solid)

Property	Units	Method	Value(s)
Density	kg/m3	constant	2719
Cp (Specific Heat)	j/kg-k	constant	871
Thermal Conductivity	w/m-k	constant	202.4

Cell Zone Conditions

Zones

name	id	type
part_2-surface_body	3	fluid
solid-part_2-surface_body	4	solid

Setup Conditions

part_2-surface_body

Condition	Value
Frame Motion?	no
Mesh Motion?	no

solid-part_2-surface_body

Condition	Value
Frame Motion?	no
Mesh Motion?	no

Boundary Conditions

Zones

name	id	type
outlet	8	outflow
inlet	7	velocity-inlet
wall-part_2-surface_body	9	wall
wall-part_2-surface_body.1	10	wall
wall-part_2-surface_body.2	11	wall
wall-part_2-surface_body.1-shadow	6	wall

Setup Conditions

outlet

Condition	Value
-----------	-------

inlet

Condition	Value
Velocity Magnitude (m/s)	0.8
Temperature (k)	285

wall-part_2-surface_body

Condition	Value
Material Name	aluminum
Thermal BC Type	1
Wall Motion	0
Shear Boundary Condition	0

wall-part_2-surface_body.1

Condition	Value
Material Name	pcm-solid-sp24e-melting
Thermal BC Type	3
Wall Motion	0
Shear Boundary Condition	0

wall-part_2-surface_body.2

Condition	Value
Material Name	aluminum
Thermal BC Type	0
Temperature	(profile udf unsteady_temperature_wall)

wall-part_2-surface_body.1-shadow

Condition	Value
Material Name	pcm-solid-sp24e-melting
Thermal BC Type	3

Solver Settings

Equations

Equation	Solved
Flow	yes
Turbulence	yes
Energy	yes

Numerics

Numeric	Enabled
Absolute Velocity Formulation	yes

Unsteady Calculation Parameters

```

-----
Time Step (s)          30
Max. Iterations Per Time Step 400

```

Relaxation

Variable	Relaxation Factor
Pressure	0.3
Density	1
Body Forces	1
Momentum	0.7
Turbulent Kinetic Energy	0.8
Specific Dissipation Rate	0.8
Turbulent Viscosity	1
Energy	1

Linear Solver

Variable	Solver Type	Termination Criterion	Residual Reduction Tolerance
Pressure	V-Cycle	0.1	
X-Momentum	Flexible	0.1	0.7
Y-Momentum	Flexible	0.1	0.7
Turbulent Kinetic Energy	Flexible	0.1	0.7
Specific Dissipation Rate	Flexible	0.1	0.7
Energy	F-Cycle	0.1	

Pressure-Velocity Coupling

Parameter	Value
Type	SIMPLE

Discretization Scheme

Variable	Scheme
Pressure	Second Order
Momentum	Second Order Upwind
Turbulent Kinetic Energy	First Order Upwind
Specific Dissipation Rate	First Order Upwind
Energy	Second Order Upwind

Solution Limits

Quantity	Limit
Minimum Absolute Pressure	1
Maximum Absolute Pressure	5e+10
Minimum Temperature	1
Maximum Temperature	5000
Minimum Turb. Kinetic Energy	1e-14
Minimum Spec. Dissipation Rate	1e-20
Maximum Turb. Viscosity Ratio	100000

Curriculum Vitae



Assist. Eva Zavrl, eva.zavrl@fs.uni-lj.si

EDUCATION

2017 present	– University of Ljubljana – Faculty of Mechanical Engineering – Interdisciplinary Doctoral Degree in Environmental Protection	SLO
2020-2021	National School of State Public Works (ENTPE), University of Lyon – Guest PhD student	FR
2015 – 2017	DTU (Denmark's Technical University) – Master program in Architectural Engineering – Following study line: Energy design. Thesis title: <i>Control of airflow interaction in the micro-environment around human body for improved thermal comfort and reduction of indoor exposure to bioeffluents</i> . Grade 12/12 (A).	DK
2016	NTU (Nanyang Technological University, Singapore) – Exchange student in Postgraduate program in spring semester 2016 School of Civil and Environmental Engineering and School of Mechanical and Aerospace and Engineering	SG
2014 -	University of Ljubljana – Faculty of Civil and Geodetic Engineering – Master program of Architectural Engineering	SLO
2010 – 2014	University of Ljubljana – Faculty of Civil and Geodetic Engineering – graduated from Bachelor in Civil Engineering in Department of Structures and Structural Complexes. Thesis title: <i>Thermal flux through structural complex-comparison of one-dimensional and two-dimensional calculation</i> . Grade 10/10 (A).	SLO
2014	DTU (Technical University of Denmark) – Exchange student in Bachelor program in spring 2014	DK
2005 – 2010	Gymnasium Jože Plečnik Ljubljana	SLO
1998 – 2005	Elementary school Danila Kumar Ljubljana	SLO

WORKING EXPERIENCES

Field of studies:	<ul style="list-style-type: none"> • HORIZON 2020 PROJECT (2022): CrossCert; Institute for Research and Innovation of University of Ljubljana (IRI) • HORIZON 2020 PROJECT (2022): reMODULEES; Institute for Research and Innovation of University of Ljubljana (IRI) • Horizon 2020 PROJECT (2022): U-CERT; Institute for Research and Innovation of University of Ljubljana (IRI) • HORIZON 2020 PROJECT HEART (2017-2022): Holistic Energy and Architectural Retrofit Toolkit (HEART); Faculty of Mechanical Engineering, University of Ljubljana • DTU, COWI and Logstore – supervisor: prof. dr. Bjarne W. Olesen and dr. Ongun Berk Kazanci – Heat Transfer in pipe systems • International Centre for Indoor Environment and Energy, Department of Indoor Climate DTU 402 – Special Course, help with experiment and research – Angela Simone and Arsen Krikor Melikov • University of Ljubljana – assisted the researches in the Department for Testing of Materials and Structures, help with the research and practical work • The Housing Fund of the Republic of Slovenia, Public Fund, administrative work • Translation of civil engineering documentation from Slovene to English
Data analyses:	<ul style="list-style-type: none"> • Questionnaires and working reports SAGITA 17 • Interviews and public surveys SAGITA 17
Promotions:	<ul style="list-style-type: none"> • Promotions of hardware, software and other products such as Prestigio, HTC, Smart Guru, Ecological food products Dana, HYPO Bank, Colgate etc. ADECCO
Administration:	<ul style="list-style-type: none"> • Institute of Civil and Commercial Law

Microsoft Office™ tools	Linux	Sketch Up	Velux Visualizer, Daysim	CFD: Flovent, ANSYS
AutoCAD	3ds Max	REVIT, Dynamo, Solibri (Model Checker)	Visual Basic.net	IDA ICE, ESBO
Thermis	Korado	HOBO Logger	iButtons	TRNSYS
ID Design Builder				

SCIENTIFIC PUBLICATIONS

- 1 OSTERMAN, Eneja, STRITIH, Uroš, DOVJAK, Mateja, VAUPOTIČ, Janja, VERBAJS, Tomaž, MLAKAR, Urška, **ZAVRL, Eva**. Analysis of educational building's ventilation suitability to prevent the spread of coronavirus (SARS-CoV-2). *Strojniški vestnik*. Apr. 2022, vol. 68, no. 4, str. 233-239, ilustr. ISSN 0039-2480. <https://www.sv-jme.eu/sl/article/analysis-of-ventilation-suitability-to-prevent-the-spread-of-coronavirus-sars-cov-2/>, DOI: [10.5545/sv-jme.2022.68](https://doi.org/10.5545/sv-jme.2022.68).
- 2 **ZAVRL, Eva**, EL MANKIBI, Mohamed, DOVJAK, Mateja, STRITIH, Uroš. Experimental investigation of air-based active-passive system for cooling application in buildings. *Sustainable cities and society*. [Spletna izd.]. Oct. 2022, vol. 85, str. 1-13, ilustr. ISSN 2210-6715. <https://www.sciencedirect.com/science/article/pii/S2210670722003511>, DOI: [10.1016/j.scs.2022.104031](https://doi.org/10.1016/j.scs.2022.104031).
- 3 KOŽELJ, Rok, MLAKAR, Urška, **ZAVRL, Eva**, STRITIH, Uroš, STROPNIK, Rok. An experimental and numerical analysis of an improved thermal storagetank with encapsulated PCM for use in retrofitted buildings for heating. *Energy and buildings*. [Print ed.]. Oct. 2021, vol. 248, str. 1-13, ilustr. ISSN 0378-7788. <https://www.sciencedirect.com/science/article/pii/S0378778821004801>, DOI: [10.1016/j.enbuild.2021.111196](https://doi.org/10.1016/j.enbuild.2021.111196).
- 4 **ZAVRL, Eva**, ZUPANC, Gašper, STRITIH, Uroš, DOVJAK, Mateja. Overheating reduction in lightweight framed buildings with application of phase change materials. *Strojniški vestnik*. Jan. 2020, vol. 66, no. 1, str. 3-14, si 3, ilustr. ISSN 0039-2480. <https://www.sv-jme.eu/article/overheating-reduction-in-lightweight-framed-buildings-with-application-of-phase-change-materials/>, DOI: [10.5545/sv-jme.2019.6244](https://doi.org/10.5545/sv-jme.2019.6244).
- 5 LAAROUSI, Yousra, BAHRAR, Myriam, **ZAVRL, Eva**, EL MANKIBI, Mohamed, STRITIH, Uroš. New qualitative approach based on data analysis of European building stock and retrofit market. *Sustainable cities and society*. [Spletna izd.]. Dec. 2020, vol. 63, f. 1-23, ilustr. ISSN 2210-6715. <https://www.sciencedirect.com/science/article/pii/S2210670720306727?via%3Dihub>, DOI: [10.1016/j.scs.2020.102452](https://doi.org/10.1016/j.scs.2020.102452).
- 6 STRITIH, Uroš, **ZAVRL, Eva**, PAKSOY, Halime. Energy analysis and carbon saving potential of a complex heating system with solar assisted heat pump and phase change material (PCM) thermal storage in different climatic conditions. *European journal of sustainable development research*. 2019, vol. 3, iss. 1., f. 1-17, ilustr. ISSN 2542-4742. <http://www.lectitopublishing.nl/download/energy-analysis-and-carbon-saving-potential-of-a-complex-heating-system-with-solar-assisted-heat-3930.pdf>, DOI: [10.20897/ejosdr/3930](https://doi.org/10.20897/ejosdr/3930).
- 7 STROPNIK, Rok, KOŽELJ, Rok, **ZAVRL, Eva**, STRITIH, Uroš. Improved thermal energy storage for nearly zero energy buildings with PCM integration. *Solar energy*. [Print ed.]. Sep. 2019, vol. 190, str. 420-426, ilustr. ISSN 0038-092X. <https://www.sciencedirect.com/science/article/pii/S0038092X19308229>, DOI: [10.1016/j.solener.2019.08.041](https://doi.org/10.1016/j.solener.2019.08.041).
- 8 KIERAT, Wojciech, BIVOLAROVA, Mariya, **ZAVRL, Eva**, POPIOLEK, Zbigniew, MELIKOV, Arsen K. Accurate assessment of exposure using tracer gas measurements. *Building and environment*. [Print ed.]. Mar. 2018, vol. 131, str. 163-173, ilustr. ISSN 0360-1323. <https://www.sciencedirect.com/science/article/pii/S0360132318300234>, DOI: [10.1016/j.buildenv.2018.01.017](https://doi.org/10.1016/j.buildenv.2018.01.017).
- 9 BIVOLAROVA, Mariya, KIERAT, Wojciech, **ZAVRL, Eva**, POPIOLEK, Zbigniew, MELIKOV, Arsen K. Effect of airflow interaction in the breathing zone on exposure to bioeffluents. *Building and environment*. [Print ed.]. Nov. 2017, vol. 125, str. 216-226, ilustr. ISSN 0360-1323. <https://www.sciencedirect.com/science/article/pii/S0360132317303967?via%3Dihub#!>, DOI: [10.1016/j.buildenv.2017.08.043](https://doi.org/10.1016/j.buildenv.2017.08.043).
- 10 **ZAVRL, Eva**, EL MANKIBI, Mohamed, DOVJAK, Mateja, STRITIH, Uroš. Enhancing performance of building elements with phase change materials for cooling with air-based systems. *Journal of energy storage*. [Print ed.]. Jul. 2022, vol. 51, str. 1-32, ilustr. ISSN 2352-152X. <https://www.sciencedirect.com/science/article/pii/S2352152X22004832>, DOI: [10.1016/j.est.2022.104461](https://doi.org/10.1016/j.est.2022.104461).
- 11 KOŽELJ, Rok, OSTERMAN, Eneja, LEONFORTE, Fabrizio, DEL PERO, Claudio, MIGLIOLI, Alessandro, **ZAVRL, Eva**, STROPNIK, Rok, ASTE, Niccolò, STRITIH, Uroš. Phase-change materials in hydronic heating and cooling systems : a literature review. *Materials*. Jul. 2020, vol. 13, iss. 13, f. 1-22, ilustr. ISSN 1996-1944. <https://www.mdpi.com/1996-1944/13/13/2971#cite>, DOI: [10.3390/ma13132971](https://doi.org/10.3390/ma13132971).

<https://cris.cobiss.net/ecris/si/sl/researcher/50578>

10. Povzetek v slovenščini

10.1 UVOD

Stavbni sektor predstavlja 40 % končne energije porabljene za ogrevanje in hlajenje. V Evropi je ta sektor eden največjih porabnikov energije, saj proizvede več kot tretjino emisij toplogrednih plinov v EU [8].

Eurostat in Medvladni panel za podnebne spremembe (IPCC) sta potrdila, da je ena od posledic globalnega segrevanja povišana temperatura zunanjega zraka v poletnem času [9,10]. Po analizi Eurostata 2020 ostaja ogrevanje prostorov največja energetska potratna dejavnost, zlasti v stanovanjskem sektorju (evropsko povprečje 68 %) [11]. Vendar se povpraševanje po energiji za hlajenje povečuje. Mednarodna agencija za energijo (IEA) ocenjuje, da se približno 20 % celotne električne energije v stavbah porabi za hlajenje in da se je povpraševanje po električni energiji med letoma 1990 in 2018 potrojilo [12]. Projekcije kažejo, da bo povpraševanje po energiji za ogrevanje do leta 2030 naraščalo in se nato ustalilo. Prav tako kažejo, da bo do leta 2060 potreba po energiji za hlajenje prehitela potrebo po energiji za ogrevanje [13]. V zadnjih 10 letih se je v Evropi število ogrevalnih dni v stavbah zmanjšalo za 13 % [14]. Ocenjuje se, da se bo do leta 2030 raba energije za hlajenje povečala za 72 %. Hkrati se bo raba energije za ogrevanje zmanjšala za 30 % [15]. Naraščajoča raba energije za hlajenje je povezana s splošno povišanimi zunanji temperaturami skozi vse leto (1,5 °C globalno segrevanje), spremembami v dinamiki dnevnih vročinskih valov (zelo nenadni in nepredvidljivi vrhovi) in večjimi zahtevami po toplotnem ugodju v prostorih.

Danes so lahke montažne stavbe (skeletalna konstrukcija in toplotna izolacija nizke gostote kot prevladujoči material v sestavi sten) in stavbe z visokim deležem površine oken priljubljeni načini gradnje. V ogrevalni sezoni so notranji prostori topli zaradi velike količine toplotne izolacije v ovoju stavbe. V zadnjih letih se je zaradi energetskih prenov stavb raba energije za ogrevanje zmanjšala. Vendar pa je pri energetski učinkovitosti ogrevalnih sistemov v stavbah še vedno nekaj prostora za izboljšave. V hladilni sezoni se lahke montažne stavbe zlahka pregrejejo, saj ima stavbe zaradi nizke toplotne akumulacije visok toploten odziv. Tako je za učinkovito zagotavljanje toplotnega ugodja v bivalnih prostorih stavbe potrebno ohladiti hitro [24–26]. Stavbe z visokim toplotnim odzivom je potrebno prenoviti, da bodo poleti v njih zagotovljene zadostno nizke notranje temperature (tj. znotraj območij toplotnega ugodja).

Stavbe lahko ogrevamo ali hladimo z bioklimatsko arhitekturno zasnovo in pasivnimi ali aktivnimi stavbnimi sistemi [27]. Pasivni stavbni sistemi so sistemi, ki za svoje delovanje ne potrebujejo pogonske moči, gibljivih delov in krmilnikov ter zahtevajo relativno malo vzdrževanja [28]. Aktivni stavbni sistemi predstavljajo mehanske sisteme za ogrevanje, hlajenje in prezračevanje (HVAC), razsvetljavo in nadzorne sisteme.

Toploto lahko hranimo fizično ali kemično. Fizični sistemi imajo visoko sposobnost akumulacije toplote in shranjujejo odvečno toploto s spreminjanjem svoje temperature (občutna toplota) ali spreminjanjem faze (latentna toplota). Ampak, senzibilni hranilniki toplote zavzamejo veliko prostora, vplivajo na videz stavbe, niso primerni za poslovne stavbe in se običajno ne uporabljajo za prenavo posamezne enote (sobe/pisarne/cone) v stavbi.

Fazno spremenljivi material (PCM) ima visoko sposobnost shranjevanja toplote pri izbrani temperaturi spreminjanja faze. PCM se lahko integrira v enote mehanskih hladilnih sistemov za izboljšanje njihove energetske učinkovitosti, kot so hranilniki toplote na vodni osnovi, toplotni izmenjevalniki PCM itd. (aktivni sistemi), lahko pa predstavlja plast v strukturnem kompleksu gradbene komponente. (stena, strop, tla itd.; pasivni sistemi): PCM integriran v zgradbo.

V nasprotju z aktivnimi sistemi pasivni sistemi (npr. PCM) za svoje delovanje ne porabljajo električne energije. PCM služi kot alternativa za hladilni sistem in se lahko implementira v aktivne stavbne sisteme ali v gradbene komponente, kjer hladijo stavbe pasivno.

V zadnjih letih so raziskave pokazale, da imajo PCM podnevi visok hladilni potencial. V Ponoči pa se težko popolnoma strdijo zaradi majhne gostote materiala (material se izolira po debelini svoje plasti) in oddajanja toplote materiala v zaprte notranje prostore stavbe. Zato je treba PCM strditi s pomočjo aktivnih sistemov (npr. z izboljšanjem prenosa toplote z zrakom).

V okviru te doktorske disertacije je aktivno-pasivni sistem (APS) zasnovan za pasivno hlajenje notranjih prostorov zgradbe in aktivno regeneracijo ponoči. Sistem je eksperimentalno in numerično optimiziran, da zagotovi optimalno delovanje poleti v podnebnih razmerah jugovzhodne Evrope. Energetska učinkovitost sistema in obratovalni stroški so primerjani s konvencionalnimi hladilnimi sistemi.

10.2 HIPOTEZE, CILJI IN DOPRINOS ZNANOSTI

Po opravljenem pregledu literature je bila predlagana je bila zasnova APS. Spodaj so predstavljene raziskovalne hipoteze in cilji.

Raziskovalne hipoteze:

- H1: plošče PCM se bodo v nočnem ciklu popolnoma strdile strjevanja in v dnevnem ciklu popolnoma stalile.
- H2: Rezultati parametrične analize bodo pokazali, da je optimalno toplotno ugodje (lokalna operativna temperatura) zagotovljeno s PCM ploščami debeline 2 cm in tališčem 24 °C na steni in 25 °C na stropu 5 cm od stene. Optimalna smer

prezračevanja zraka je smer stena-strop z volumskim pretokom $150 \text{ m}^3/\text{h}$. Oblika difuzorja je mešalna.

- H3: Najboljše lokalno toplotno ugodje (izbrani kriterij toplotnega ugodja) bomo primerjali s pasivnim sistemom brez prezračevanja, prezračevano steno brez stropa, prezračevanim stropom brez stene, sistemom APS.
- H4: Z upoštevanjem lokalnega toplotnega ugodja bo najboljše toplotno ugodje (najnižja dnevna temperatura zraka v prostoru) simetrično blizu stene PCM in se bo znižalo glede na stopnjo sevanja površine nasproti stene PCM.
- H5: Raba energije za hlajenje bo z APS in izbranim sistemom ogrevanja, hlajenja in prezračevanja nižja kot pri pasivnem sistemu, kjer se paneli ponoči ne prezračujejo.
- H6: Raba energije za hlajenje bo z APS (stena+strop) in izbranim sistemom ogrevanja, hlajenja in prezračevanja nižja, kot pri prezračevanem sistemu s samo stropom ali s samo steno.

Glavni cilji raziskave so:

- O1: raziskati učinek hlajenja APS,
- O2: raziskati učinek različnih temperatur vstopnega zraka v zračno rego na strjevanje PCM plošč v nočnem ciklu,
- O3: določiti najvišjo temperaturo vstopnega zraka v zračno rego za popolno strjevanje plošč PCM v nočnem ciklu (12 h) in
- O4: oceniti energijsko učinkovitost APS v sezoni hlajenja.

Na podlagi ugotovljenih vrzeli v znanju so novosti in znanstveni doprinos te raziskave:

- Preiskovani sistem preučuje kombinacijo prezračevane notranje PCM stene in stropa (APS) in ne le enega stavbnega PCM elementa.
- APS je raziskan eksperimentalno v kontroliranih eksperimentalnih pogojih, kjer je delovanje APS z merjenjem ugotovljeno sočasno z merjenjem razmer v referenčni testni celici brez APS. Uporabljena eksperimentalna oprema omogočajo raziskavo delovanja APS pri stacionarnih toplotnih pogojih, tranzientnih prehodnih toplotnih pogojih (izbran dan referenčnega leta testa ali scenariji poletnega vročinskega vala) in dodajanje prezračevanja v testnih celicah za določanje vpliva prezračevanja na delovanje APS. S tovrstno opremo je mogoče poiskati in določiti učinek posameznega preiskovanega vplivnega parametra.
- Numerična simulacija na mikro skali je izračunana in validirana s celotno geometrijo stropa in stene PCM.
- Numerična simulacija na mikro skali upošteva robni pogoj spremembe temperature v testni celici ob prezračevanju zračne rege za strjevanje PCM v nočnem času. Z upoštevanjem teh robnih pogojev je izvedena izvedbo parametrična analiza na podlagi spreminjanja temperature vstopnega zraka v zračno rego. Ugotavljan je čas strjevanja in določena je najvišja temperatura vstopnega zraka za zadostno delovanje APS sistema – optimizacija sistema APS.

10.3 PRELIMINARNE RAZISKAVE

Preliminarne raziskave so osnova za izbiro karakteristik PCM materiala in vrste izdelka. Preliminarne raziskave so sestavljene iz štirih delov od katerih vsak predstavlja svoj tip posamezne raziskave:

- numerični model na nivoju stavbe,
- eksperimentalna raziskava,
- numerični model na mikro skali in
- razprava ter analiza sistematičnega pregleda literature.

V tem delu je predstavljena pot do izbire izdelka PCM za nadaljnje eksperimentalne meritve in numerično modeliranje. Temperatura taljenja PCM (T_m) in izbira mase morata izpolnjevati zahteve in optimalno delovanje v vsakem ciklu, pasivno delovanje – dnevni cikel, kjer T_m ne sme preseči zahtev glede notranje temperature, in aktivno delovanje – nočni cikel, kjer mora T_m ostati dovolj visoka, da zagotovi popolno strjevanje. Vsaka predhodna raziskava je pomembno prispevala k odločitvi:

- numerični model na nivoju stavbe:

Preiskava z orodjem za nestacionarno analizo energetske učinkovitosti stavbe v DesignBuilderju je pokazala, da je bila optimalna temperatura taljenja v preiskovanih mediteranskih in celinskih podnebnih razmerah 24 °C. Rezultati so pokazali še, da mikrokapsulirani PCM nima dovolj kapacitete za učinkovito hlajenje notranjih prostorov.

- eksperimentalna raziskava:

Rezultati so pokazali pomembnost dovolj nizkih temperatur za doseganje strjevanja v nočnem ciklu. Prav tako je za določanje trendov toplotnega odziva PCM plošč pomembna stabilna temperatura zraka na vstopu zračne rege, saj le tako lahko jasno razločimo vpliv posamezne temperature na delovanje sistema. Rezultati raziskave so zaradi neustreznih testnih pogojev (nestabilne temperature zraka na vstopu zračne rege in prekratek čas izvedbe meritev) služili kot orodje za validacijo numeričnega modela na mikro skali – analizo z ANSYS Fluent.

- numerični model na mikro skali:

Na podlagi simuliranih rezultatov je mogoče sklepati, da imata SP24E in SP252E velik potencial za popolno strjevanje pri višjih vstopnih temperaturah (npr. 17 ali 18 °C), ker pri temperaturi 21 °C ali nižji ne moreta shranjevati energije (nimata toplotne kapacitete). Da ne shranjujeta toplote pri nižjih temperaturah od tališča je pomembno v vročih poletnih nočeh, ko se zunanje temperature ponoči ne znižajo dovolj in tako ne bi mogle ustrezno pripomoči k strjevanju PCM.

- Pregled literature:

Rezultati povzeti iz sistematičnega pregleda literature kažejo na širok nabor PCM z različnimi temperaturami taljenja in različnimi načini uporabe v elementih stavbe (stena, strop, tla ali streha). Vendar je mogoče opaziti, da premajhne količine PCM (npr. mikrokapsulacija) nimajo močnega hladilnega učinka. Pretežno se zdi, da notranje površine prekrite s PCM niso presegle 24 °C (v raziskavah uporabljen tudi PCM s precej nižjimi temperaturami taljenja).

Končno temperature v bivalnih prostorih stavbe ne smejo preseči priporočenih standardnih vrednosti (PCM s $T_m = 25$ °C). Hkrati mora biti T_m dovolj visoka, da se lahko vzpostavi zadostna temperaturna razlika med temperaturo vstopnega zraka in tališčem materiala PCM. Zdi se, da bi se s pretoki višjimi od tistih iz simulacije PCM linije SP lahko strdil v

12-urnem nočnem ciklu. Tudi pri raziskovani debelini PCM plošče. Na tem mestu je pomembno poudariti dejstvo, da predlagani APS hladi prostor pasivno. Zato plošče PCM niso v tesnem prezračevanem stiku z vstopnim zrakom, kot so na primer v zaprtem izmenjevalniku toplote. Plošče PCM ne smejo biti pretanke – s premajhno vsebnostjo PCM materiala, saj bi se lahko v dnevnem ciklu prehitro stalile in tako bi bil njihov učinek hlajenja nezadosten.

Na podlagi predstavljenih zaključkov preliminarnih raziskav so bile za nadaljnje eksperimentalne in numerične raziskave izbrane plošče PCM iz podjetja Rubitherm tip SP24E, makrokapsulirane v aluminijastih ohišjih CSM z 2 kg PCM na ploščo in debeline 1 cm.

10.4 EKSPERIMENTALNA RAZISKAVA

Namen eksperimentalne raziskave je ugotavljanje učinka hlajenja APS sistema v dnevnem ciklu in čas strjevanja ob različnih temperaturah vpihanega zraka v nočnem ciklu.

Raziskava je bila izvedena v testnih prostorih šole ENTPE v Lyonu (Francija) v testnih celicah z imenom Hybcell. Gre za dve enaki preizkusni celici, v celico A je bil vgrajen APS (strop in stena iz PCM) in celica B je bila prazna (referenčna). Celici imata eno zunanjo steno, ostale površine so notranje.

S preliminarno raziskavo izbrane PCM plošče Rubitherm SP24E (dimenzije: 40x30x15 mm in teža: 2 kg) so bile nameščene v podkonstrukcijo iz lesenega okvirja na notranjo steno (29 plošč) in strop (38 plošč). Podkonstrukcija tvori s primarno steno celice zrakotesno zračno rego. Material ima temperaturo taljenja (T_m) pri 24 °C in lahko shrani do 180 kJ/kg toplote ter temperaturo strjevanja pri 22 °C in 23 °C, pri katerih lahko shrani 118 kJ/kg in 42 kJ/kg toplote.

V celici se zrak dovaja preko ovalnega vstopnega linearne difuzorja (širine 5 cm) z linearno odprtino debeline 1 cm. Zrak se odvaja skozi okrogel izpust (\varnothing 16 cm), ki se nahaja na sredini stropa in je od zunanje stene oddaljen 117 cm. Zračna rega je razdeljena na 5 enakih kanalov v širini PCM plošč (45 cm). Za zagotavljanje želene vstopne temperature zraka, je bil vstopni zrak pred vstopom v kabino kondicioniran (ohlajen s ali ogret). Vsaka celica je bila opremljena z vstopnim in izstopnim ventilatorjem (volumski pretok 483 m³/h). Za raziskovanje delovanja APS v dnevnem ciklu sta bili obe testni celici opremljeni z enakim sobnim grelnikom (2000 W) nameščenimi pred zunanjo steno vsake celice. Tekom eksperimenta je bil zrak v celicah mešan s sobnim ventilatorjem.

s

Med poskusom so bili spremljani naslednji parametri: temperatura zraka v vstopnem kanalu, v zračni regi, pred odvodnim ventilatorjem in v središču celice (T_a), povprečna temperatura sevanja (T_{mr}), izmerjena površinska temperatura na sprednji strani plošče PCM (T_{PCM_back}), temperaturo površine izmerjeno na zadnji strani plošče PCM (T_{PCM_front}) in hitrost zraka (v).

Raziskana sta bila dva sklopa raziskav. Namen prvega sklopa je oceniti učinek hlajenja APS (s ploščami PCM) tekom dnevnega cikla taljenja. Izbrana temperatura zraka v celici B (T_{set_B}) je bila vzpostavljena in vzdrževana preko PID krmiljenega grelnika B. Grelnik v

celici A je sledil ukazom grelnika B. Tako je bila v celico A istočasno dovedena popolnoma enaka količina toplote kot v celico B. Učinek hlajenja APS je bil določen na podlagi temperaturne razlike zraka T_a izmerjenega v središču celice A in B. Preizkušeni so bili trije primeri, kjer je bila T_{set_B} stacionarna ($T_{set_B} = 26\text{ °C}$, 30 °C in 35 °C), kjer so bile pred začetkom poskusa plošče ohlajene na 20 °C . Primer je bil zaključen (PCM staljen), ko je T_{a_A} dosegel T_{a_B} . Stacionarnem primeru $T_{set_B} = 30\text{ °C}$ je bilo tekom preiskave v dnevnem ciklu dodano prezračevanje v celici, ki zadošča pretoku potrebnemu za 2-3 osebe ($T_{set_B} = 30\text{ °C}$, $T_{ai} = 21\text{ °C}$). Preizkušeni so bili še trije primeri, kjer je bila T_{set_B} tranzientna, njen namen pa je bil simulacija temperatur zraka v prostoru montažne stavbe tekom najbolj vročega dneva v testnem referenčnem letu (TRY) v Ljubljani in Rimu ter tekom dneva, ko je v Ljubljani nastopil vročinski val ($T_{set_B} = \text{TRY LJ, TRY RO and OH LJ}$).

Cilj drugega sklopa raziskav je ugotavljanje časa potrebnega za popolno strditev PCM plošč tekom nočnega cikla. Zrak s tremi različnimi temperaturami vstopnega zraka ($T_{ai} = 15\text{ °C}$, 16 °C in 17 °C) je bil vpihan v zračno rego. Plošče so bile segrete na 28 °C . Primer se je zaključil, ko je povprečna površinska temperatura plošč padla na $20,5\text{ °C}$. Izbrane temperature so v skladu z notranjimi in zunanji temperaturami hladilne sezone v srednji Evropi.

V dnevnem ciklu so rezultati so pokazali jasno viden učinek hlajenja APS. V primerih, kjer je bila T_{set_B} stacionarna so temperaturne razlike med T_{CELL_A} in T_{CELL_B} v prvih 12ih urah eksperimenta znašale 1 °C pri $T_{set_B} = 26\text{ °C}$, 2 °C pri $T_{set_B} = 30\text{ °C}$, $3,5\text{ °C}$ pri $T_{set_B} = 30\text{ °C}$ s prezračevanjem in $4,5\text{ °C}$ pri $T_{set_B} = 35\text{ °C}$. V primerih, kjer je bila T_{set_B} tranzientna so temperaturne razlike med T_{CELL_A} in T_{CELL_B} v prvih 12ih urah eksperimenta znašale med 1 °C in $1,5\text{ °C}$ v vseh testiranih primerih ($T_{set_B} = \text{TRY LJ, TRY RO and OH LJ}$).

Rezultati so pokazali, da se v danih testiranih pogojih v nočnem ciklu PCM lahko popolnoma strdi. Ob upoštevanju, da se izbrani material PCM popolnoma strdi pri 21 °C in da je porazdelitev temperature vzdolž stene in stropa PCM neenakomerna ($\pm 0,5\text{ °C}$), je konec fazne spremembe določen, ko povprečna temperatura PCM plošč merjena na strani plošč v kontaktu s celico doseže $20,5\text{ °C}$. S tremi raziskanimi primeri, ki so se razlikovali po temperaturah vstopnega zraka, so rezultati eksperimenta pokazali, da se plošče PCM strdijo v 5 h pri $T_{ai} = 15\text{ °C}$, v 14 h pri $T_{ai} = 16\text{ °C}$ in v 16 h pri $T_{ai} = 17\text{ °C}$.

10.5 NUMERIČNO MODELIRANJE

Namen numerike je ob upoštevanju robnih pogojev temperature okolice delovanje APS optimizirati in določiti najvišjo temperaturo pri kateri se PCM v nočnem ciklu lahko popolnoma strdi. Na podlagi numeričnih rezultatov je bila izračunana tudi raba energije in stroški obratovanja APS v primerjavi z najbolj in najmanj učinkovito klimatsko napravo.

Rezultati numeričnega modela so bili primerjani z eksperimentalnimi rezultati. Pokazali so dobro ujemanje in tako je bil model validiran. Občutljivost modela je bila preverjena s spreminjanjem časovnega koraka ter velikosti mreže v simulaciji.

Model je bil poenostavljen in simuliran kot 2D model z uporabo ANSYS Fluent v19.1. Sestavljen je bil iz dveh površin, zračno rego (območje tekočine) in PCM (območje trdnine). Nestacionarni model je bil izračunan z uporabo „energijske enačbe“, pretok zraka

v zračni regi pa s turbulentnim modelom „k- ω “, ki je primeren za izračun tokov, omejenih na steno.

Model je bil sestavljen iz vstopne in izstopne odprtine za hitrost. V modelu je imela primarna stena adiabatni robni pogoj, stena PCM v stiku z notranjim prostorom (zunanja stena PCM) pa temperaturo vneseno s pomočjo uporabniško-definirane funkcije UDF, kjer je bil vnos odvisen od simulirane primera v parametrični analizi (za vsak primer drugačen vnos). Vhodna hitrost je bila nastavljena na 0,8 m/s in začetna temperatura PCM na 28 °C, kot je bila izmerjena med eksperimentalnim referenčnim primerom. Zrak tekočega materiala ima Boussinesqovo gostoto 1,18 kg/m³ in koeficient toplotne razteznosti 0,00336 1/°C.

Debelina PCM plošč v aluminijastem ovoju izbranih v okviru preliminarnih raziskav (Rubitherm SP24E, 2 kg) je 0,65 mm (višina določena glede na maso in gostoto materiala v plošči). Toplotne karakteristike plošč (temperatura v odvisnosti od delne entalpije) so bile v model vnesene kot nov material. PCM je bil simuliran kot trden material (spreminjane kapacitete v odvisnosti od temperature), ker je stena PCM tanka v primerjavi z velikostjo sistema in se sklepa, da je konvekcija v ploščah zanemarljiva. Takšna poenostavitev znatno zmanjša čas računanja v primerjavi z modelom, kjer PCM menja agregatna stanja. Ker je bil simulirano samo nočni cikel PCM – strjevanje, je bila histereza ob vnosu toplotnih karakteristik PCM popolnoma upoštevana.

V izogib nepotrebnih geometrijski zapletenosti in računskim težavam, je bil 3D model stene in stropa na sredini prerezan s simetrično ravnino. Prerez 3D modela je določil geometrijo 2D modela. Izstop zraka je nameščen na koncu zračne rege. Zaradi kompleksne konfiguracije laboratorijske testne celice tam tega ni bilo mogoče uresničiti.

Parametrično analizo je preučen učinek posameznega vplivnega parametra (vstopne temperature zunanjega zraka - T_{ai}). Na podlagi nočnih zunanjih temperatur zraka v južni in srednji Evropi je bilo izvedenih šest različnih primerov preizkusov z različnimi T_{ai} (15 °C, 16 °C, 17 °C, 18 °C, 19 °C in 20 °C).

V začetku nočnega cikla je zrak v celici še vedno segret in njegov vpliv na izračun ni zanemarljiv. Uporabljena je bila predpostavka za temperature na meji PCM zraka v celici ($T_{PCM_front, avg}$). Ker je sprednja stran PCM plošč ($T_{PCM_front, avg}$), v stalnem stiku z notranjim okoljem celice, to pomembno vpliva na proces strjevanja PCM plošč. Vpliv stika PCM plošč z notranjim okoljem celice je bil izmerjen v eksperimentalnih študijah, ko je bil PCM strjen po cikličnih segrevanja (taljenja). Temperatura zraka je bila merjena v središču celice ($T_{a, cell}$), kjer je bil zrak med vsakim poskusom mešan s sobnimi ventilatorji. Eksperimentalno določena dinamika temperatur v celici med strjevanjem tekom različnih eksperimentalnih primerov je bila analiziran. Na podlagi slednjih primerov je bila ocenjena $T_{a, cell}$ za UDF za vsakega od primerov pripravljenih za parametrično analizo ($T_{ai} = 15$ °C, 16 °C, 17 °C, 18 °C, 19 °C in 20 °C).

V treh primerih parametrične analize z različnimi temperaturami vstopnega zraka, so numerični rezultati pokazali, da se plošče PCM strdijo v 7 h pri $T_{ai} = 15$ °C, v 9 h pri $T_{ai} = 16$ °C in v 12 h pri $T_{ai} = 17$ °C. Pri višjih temperaturah vstopnega zraka se plošče ne strdijo v času nočnega cikla (12 h).

Znotraj enega dneva ima APS (4,62 kWh) večjo rabo energije za obratovanje kot klimatska naprava razreda A+++ (1,3 kWh) in klimatska napravo razreda G (3,4 kWh). Enako velja za stroške obratovanja izračunane na podlagi rabe energije ter dnevnih in nočnih tarif cene električne energije. Obratovalni stroški so najnižji za klimatsko napravo razreda A+++ (0,174 €/dan), višji za APS (0,462 €/dan) ter najvišji za klimatsko napravo razreda G (0,467 €/dan).

10.6 ZAKLJUČKI IN NADALJNJE DELO

V okviru doktorske disertacije je bil raziskan aktivno-pasivni sistem (APS) za zmanjševanje pregrevanja stavb z lahko nosilno konstrukcijo. Po pregledu literature je bila izvedena vrsta preliminarnih raziskav. Delovanje APS je bilo eksperimentalno preizkušeno v Lyonu v Franciji. Nato je bila izvedena parametrična analiza in optimizacija z numeričnim modelom na mikro skali (CFD). Na koncu sta bili izračunani še raba energije in stroški obratovanja APS in primerjani z delovanjem dveh klimatskih naprav (najvišja (razred A+++)) in najnižja (razred G) energetska učinkovitost).

- Na podlagi sistematičnega pregleda literature je bilo ugotovljeno, da je bilo opravljenih že veliko sorodnih raziskav, vendar je optimalne toplotne karakteristike PCM (T_m) za posamezni primer pasivnega sistema še vedno težko določiti, saj zato potrebujemo več različnih pristopov k raziskavam.
- Sistem je primeren za prenovo poslovnih stavb skeletne gradnje (lahke endoskelete nosilne konstrukcije) z visokim deležem zasteklitve in že prisotnim prezračevalnim sistemom za izboljšanje kakovostni zraka v prostoru. APS je primeren za prenovo že obstoječih objektov, saj se lahko z njegovo aplikacijo prenove le ena posamezna enota (pisarna) s kritično lego v objektu in tako ni potrebno prenavljati celotne stavbe. S pregledom literature je bilo moč ugotoviti, da so PCM uporabljeni v sorodnih raziskavah običajno nameščeni v zunanjih še pogosteje pa v notranjih plasteh stavbnega ovoja.
- Rezultati numeričnega modela so s simuliranjem celotne stene in stropa iz PCM plošč v APS sistemu pokazali, da je temperatura taljenja najpomembnejša toplotna karakteristika PCM in je bistvena za njegovo optimalno delovanje in doseganje najvišjega učinka hlajenja.
- S poudarkom na preliminarnih raziskavah je bilo ugotovljeno, da za globlje razumevanje toplotnega obnašanja APS ne zadostuje le ena metoda dela (en znanstveni pristop). Na primer modeli, ki simulirajo sisteme v polnem merilu, pogosto niso dovolj natančni za eksaktno določanje vpliva posameznega parametra. Modeli na mikro skali pa ne omogočajo celostne simulacije delovanja izbranega sistema z vsemi vplivnimi parametri iz okolice. Poleg tega imajo tudi eksperimentalne metode svoje omejitve. Na primer uporabljena merilna oprema ne more biti nameščena v vsaki točki sistema (manj merilnih točk – manj informacij). Zaradi časovnih omejitev je težko izvesti veliko število primerov s spreminjanjem vplivnih parametrov in tako je parametrična analiza manj obširna. Prav tako v laboratorijskem okolju ni mogoče zagotoviti želenih testnih pogojev poleg tega pa je sisteme težko izmeriti celostno (kot na dejanskem objektu).
- V okviru preliminarnih raziskav je bil na podlagi toplotnih karakteristik izbran PCM material SP24E. Temperatura taljenja PCM je morala biti dovolj visoka, da se lahko vzpostavi zadostna temperaturna razlika med temperaturo vstopnega zraka in tališčem materiala PCM. Hkrati je bilo potrebno temperaturo taljenja PCM izbrati tako, da

temperature v prostorih stavbe ne bi presegle priporočenih standardnih vrednosti toplotnega ugodja v prostoru.

- Eksperimentalni rezultati kažejo, da v dnevnem ciklu sistem APS zniža temperature zraka v testni celici in tako pripomore k hlajenju. Pri raziskanih temperaturah zraka nastavljenih v referenčni testni celici B ($T_{\text{set}_B} = 26 \text{ °C}$) sistem APS ni potreboval dodatnega vira hlajenja, saj je s svojim delovanjem znižal temperature v prostoru za 1 °C in na priporočene vrednosti notranjih temperature za doseganje ustreznega toplotnega ugodja v prostoru. V ostalih primerih bi APS v dnevnem ciklu morali dodati dodaten vir hlajenja. Učinek hlajenja APS je bil najbolj izrazit pri višjih raziskanih temperaturah zraka nastavljenih v referenčni testni celici B ($T_{\text{set}_B} = 30 \text{ °C}$ in 35 °C), kjer je APS znižal notranjo temperaturo tudi do $4,5 \text{ °C}$.
- Sistem APS je uspel ustrezno znižati temperaturo zraka na najtoplejši dan testnega referenčnega leta v Rimu (Italija), ampak ne v Ljubljani ne v testnem referenčnem letu ne v času vročinskega vala. To pomeni, da je sistem raziskan pri izbranih lastnostih primeren za sredozemske poletne razmere in ne za vroča poletja v celinskem podnebjju ali njihove poletne vročinske valove.
- Pri numeričnem modelu na mikro skali je bilo nočno strjevanje doseženo s prezračevanjem zračne rege s pretokom $483 \text{ m}^3/\text{h}$. Pri raziskani konfiguraciji je bilo ugotovljeno, da najvišja vstopna temperatura zraka vpihanega v zračno rego s katero je bilo moč v času nočnega cikla (12) še popolnoma strditi PCM ne sme presegati 17 °C .
- Preostale testirane temperature vstopnega zraka višje od 17 °C (18 °C , 19 °C in 20 °C) so bile previsoke, da bi PCM v celoti strdile in ga pripravile za najboljše delovanje v prihajajočem dnevnem ciklu.
- Čas strjevanja PCM je mogoče izboljšati s povečanjem pretoka zraka v zračni regi ali pa s kombinacijo nočnega prezračevanja v zračni regi združenim s sočasnim prezračevanjem prostora (testne celice) – nočno prezračevanje. To lahko dosežemo z odpiranjem oken ali pa mehanskim prezračevanjem, saj so na tak način PCM plošče hlajene sočasno z obeh strani.
- APS v nočnem ciklu za prezračevanje zračne rege z namenom izboljšanja strjevanja PCM porablja električno energijo. Rezultati izračuna rabe energije in stroškov obratovanja APS v statičnih pogojih kažejo, da ima sistem APS višjo rabo energije in obratovalne stroške kot klimatska naprava razreda A+++ in nižje obratovalne stroške od klimatske naprave razreda G.
- Z ekonomskega vidika je smotrnost uporabe PCM odvisna od izračuna prihranka energije, cene materiala PCM in cen električne energije. Čeprav so se cene PCM v zadnjih 5 letih znatno znižale, raziskave, ki ocenjujejo ekonomsko smotrnost uporabe PCM vgrajenih v stavbe, še vedno poročajo, da je njihova cena previsoka.

Predstavljena raziskava poudarja problem strjevanja PCM ponoči. Prihodnje raziskave PCM integriranih v elemente stavbe bi se morale osredotočiti:

- Aktivni del APS viša stroške rabe energije v stavbi za hlajenje, kar predstavlja vprašljivo smotrnost aplikacije in uporabe APS. Natančneje, raba energije za prezračevanje zračne rege v nočnem ciklu ne sme biti večja od rabe energije konvencionalnih aktivnih sistemov za hlajenje stavb podnevi. Delovanje APS je potrebno nadaljnje raziskati z orodjem za nestacionarno modeliranje (programsko orodje TRNSYS) sistemov s poudarkom na preostalih potrebnih mehanskih komponentah stavbnega sistema za ogrevanje, hlajenje in prezračevanje prisotnih v stavbi.

- Raziskave na temo izboljšanja prenosa toplote s PCM pri nizki rabi energije. Takšno izboljšanje je mogoče doseči z razvojem novih PCM materialov in dodajanjem kovinskih struktur v material. V pregledane literature je bilo pokazano, da se je hladilni učinek PCM drastično izboljšal z dodajanjem druge plasti PCM, v katero so bile vgrajene vodne cevi (talno gretje ali stropno hlajenje), k primarni lokalno prezračevani plasti PCM, ki se je nahajala na zunanji strani stavbnega ovoja.
- Ko zrak dodajamo lokalno direktno na plošče PCM, hitreje dosežemo fazno spremembo kot če prezračujemo celoten volumen sobe. A žal, so sistemi za lokalno prezračevanje PCM geometrijsko kompleksni in zato zahtevnejši za izgradnjo. Zato je s prihodnjimi raziskavami potrebno poiskati sistem s preprostejšo geometrijo.
- Hladilna zmogljivost sistemov s PCM je znatno izboljšana v kombinaciji z ustreznimi in optimiziranimi strategijami nadzora nočnega prezračevanja in umetno inteligenco. Da bi objektivno ocenili učinkovitost uporabe TES, je treba temperaturo taljenja in debelino plasti PCM optimizirati glede na obravnavani tip podnebja.
- Ker je eno od glavnih vprašanj vgradnje sistema PCM vidik ekonomske smotnosti, bi nadaljnje raziskave lahko preučile ekonomski vidik uporabe PCM z ekonomskimi kazalniki ustreznosti sistema.
- V pregledu literature je bilo ugotovljeno, da le redke citirane raziskave analizirajo ceno PCM materiala, stroške njegove vgradnje in vzdrževanja vključno z vračilnimi dobami. Zato je v prihodnosti potrebno izvesti še več raziskav na omenjeno temo in spremljati gibanje cen PCM skozi čas.
- Le malo raziskav obravnava analizo ocene življenjskega cikla (LCA) sistemov s PCM, zato bi imele raziskave s takšno v prihodnosti visoko vrednost.
- Čeprav je v številnih raziskavah temperatura taljenja PCM izbrana na podlagi stavbnega elementa v katerem je PCM, lokacijo PCM v konstrukcijskem sklopu (zunanji ali notranji sloji ovoja) in tip podnebja, ni na voljo jasnih smernic za izbiro PCM za hlajenje v stavbah z lahko endoskeletno nosilno konstrukcijo.
- Poleg tega s pregledom literature ni bilo mogoče najti posebnih zahtev za stopnjo nočnega prezračevanja za strjevanje PCM in bi jih bilo v prihodnosti potrebno določiti.
- V prihodnje bi bilo potrebno določiti še minimalne zahteve za znižanje temperatur v stavbi s PCM, da je njihova namestitev v prenovi stavbe še smotna.